
# 49èmes Journées des Actinides

# 14 – 18 April 2019, Erice, Italy

Organized by

Joint Research Centre, European Commission

Programme and abstracts

# Foreword

On behalf of the local Organizing Committee and the Joint Research Centre of the European Commission, we would like to warmly welcome you at the Ettore Majorana Foundation and Centre for Scientific Culture in Erice, for the 49èmes Journées des Actinides.

In a context of increasing difficulties for actinide research in many countries, due to reinforced regulations, infrastructure or experimental issues and the concurrence of new, attractive, or easier fields of research for young scientists, it is important to continue the tradition of this informal conference where scientists from all generations and different disciplines in the field can present their latest results, meet, discuss and initiate collaborations, in a friendly atmosphere. It is therefore a positive signal to welcome more than 90 participants, from all over the world, to the 49ème edition of this conference.

We hope that you will enjoy these 49èmes Journées des Actinides and we wish you a pleasant stay in Erice, fruitful discussions and interesting presentations!

Roberto & Eric

# Erice

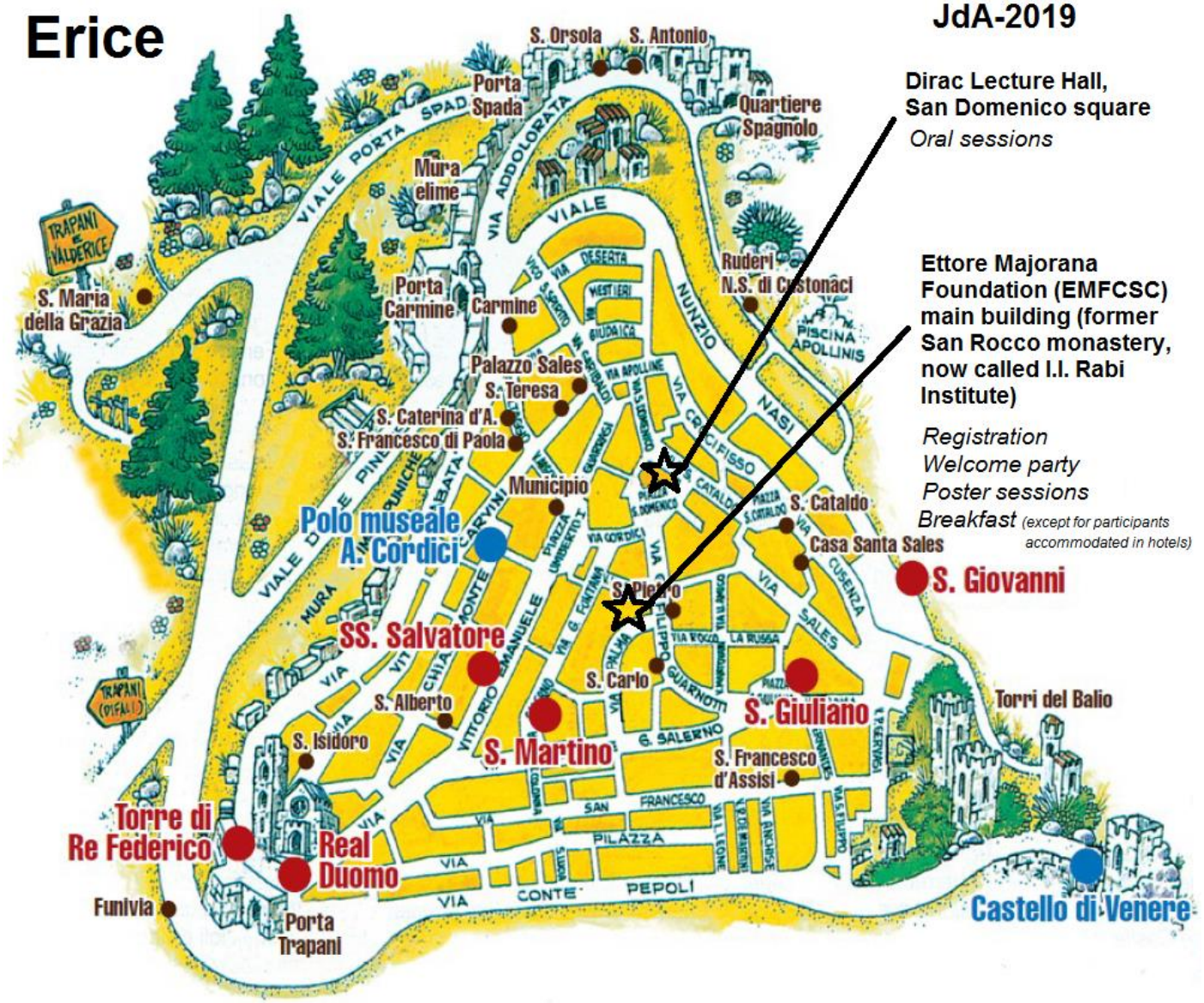
JdA-2019
Dirac Lecture Hall, San Domenico square
Oral sessions
Ettore Majorana Foundation (EMFCSC) main building (former San Rocco monastery, now called I.I. Rabi Institute)
Registration
Welcome party
Poster sessions
Breakfast (except for participants accommodated in hotels)
S. Orsola
S. Antonio
Porta Spada
Quartiere Spagnolo
Mura elime
Ruderi N.S. di Custonaci
Porta Carmine
Carmine
S. Maria della Grazia
Palazzo Sales
S. Teresa
S. Caterina d'A.
S. Francesco di Paola
Municipio
Polo museale A. Cordici
S. Cataldo
Casa Santa Sales
S. Giovanni
S. Pietro
SS. Salvatore
S. Carlo
S. Alberto
S. Martino
S. Giuliano
Torri del Balio
S. Isidoro
S. Francesco d'Assisi
Torre di Re Federico
Real Duomo
Funivia
Porta Trapani
Castello di Venere
VIALE PORTA SPADA
VIA ADDOLORATA
VIALE
VIA DESERTA
VIA MESTIERI
VIA GIUDAICA
NUNZIO NASI
PISCINA APOLLINIS
VIA APOLLINE
VIA CROCIFISSO
VIA CATALDO
PIAZZA S. CATALDO
VIA CUSENZA
VIA SALES
VIA LA RUSSA
VIA ROCCO GUARNOTTI
VIA G. FONTANA
VIA PALMA
VIA FILIPPO
VIA G. SALERNO
VIA SAN FRANCESCO
PIAZZA
VIA CONTE PEPOLI
VIA LEONE
VIA S. FILIPPO
VIA BANCHINE
VIA MURA
VIA VITTORIO EMANUELE
VIA CHIARAMONTE
VIA PUNICHE
VIA PINETE
VIA CARVINI
VIA GORDICI
PIAZZA UMBERTO I
TRAPANI E VALDERICE
TRAPANI (DIFALI)

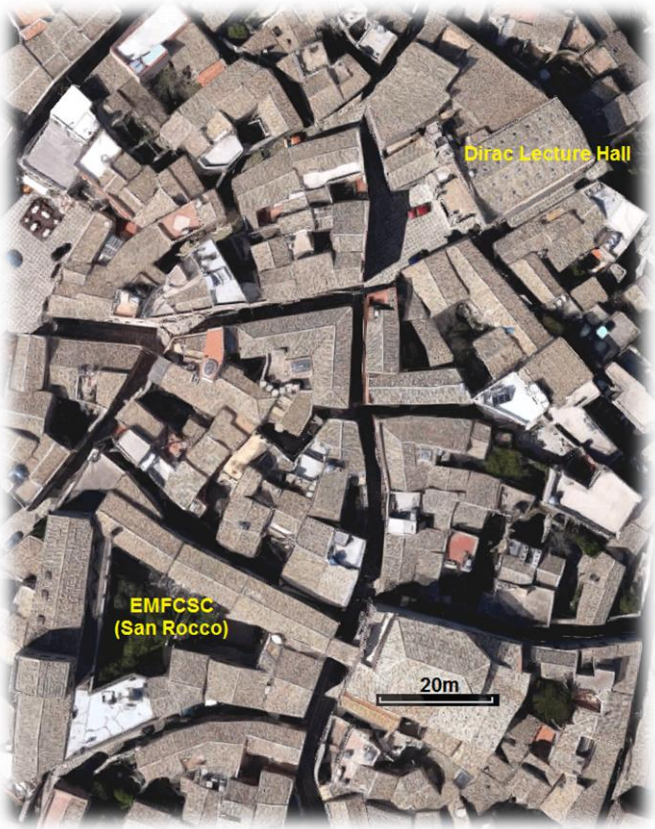
Dirac Lecture Hall
EMFCSC
(San Rocco)
20m

# Scope

The 49èmes Journées des Actinides (JdA-2019) will be held in Erice (Italy) on 14-18 April 2019, hosted by the "Ettore Majorana Foundation and Centre for Scientific Culture" (EMFCSC) (http://www.ccsem.infn.it).

The Journées des Actinides is a conference series providing an informal annual forum for the discussion of current research on the physical and chemical properties of actinide elements, their alloys and compounds. Following the editions held in Praia de Porto Novo (Portugal, 2018), Karpacz (Poland, 2017), and Alpe d'Huez (France, 2016), JdA-2019 will include discussion of

- strongly correlated systems, superconductivity, and quantum criticality
- inorganic and organometallic chemistry
- materials and nanomaterials
- theory and band structure
- safety of the nuclear fuel cycle
- nuclear safeguards and security
- actinide production and handling
- radiation protection
- environment contamination, remediation, and decommissioning

JdA-2019 encourages open discussion on different topics, in a mixture of oral presentations and poster sessions. Scientists, engineers, and students from universities, national laboratories, and the nuclear industry are invited to participate and make technical contributions.

# Journées des Actinides Committees

## Conference chairpersons:

Roberto Caciuffo (JRC Karlsruhe, Germany)
Eric Colineau (JRC Karlsruhe, Germany)

## International Advisory Committee:

- Jean Aupiais (CEA, Arpajon, France)
- Éric Colineau (JRC Karlsruhe, Germany)
- Nicolas Dacheux (ICSM, Montpellier, France)
- David Geeson (AWE, Reading, UK)
- Antonio Pereira Gonçalves (IST Sacavém, Portugal)
- Itzhak Halevy (NRCN, Be'er Sheva, Israel)
- Ladislav Havela (Charles University, Prague, Czech Republic)
- Dariusz Kaczorowski (INTIBS PAN, Wrocław, Poland)
- Thomas Scott (University of Bristol, UK)

## Local Organizing Committee:

- Roberto Caciuffo, co-chairman (JRC Karlsruhe)
- Éric Colineau, co-chairman (JRC Karlsruhe)
- Rachel Eloirdi, scientific programme (JRC Karlsruhe)
- Jean-Christophe Griveau, scientific program (JRC Karlsruhe)
- Laura Martel, scientific programme (JRC Karlsruhe)
- Štěpán Sechovský, web site (Charles University, Prague)
- Krisztina Varga, secretary (JRC Karlsruhe)
- Olaf Walter, scientific programme (JRC Karlsruhe)

# Venue

JdA-2019 will be held in Erice (Italy), an ancient town located at around 750 metres above sea level, on top of a mount overlooking the city of Trapani, on Sicily's north-western coast. Funded by the Elymians, Erice was later Hellenised by the Phoenicians and flourished under the Romans until its destruction by the Carthaginians in the First Punic War. During the early and high middle ages, Erice was conquered first by the Arabs and then by the Normans, whose magnificent buildings give to Erice the stunning medieval character that survived until today.

The conference will be hosted by the *Ettore Majorana Foundation and Centre for Scientific Culture (EMFCSC)*. Formally established in 1962 by John Bell, Patrick Blackett, Victor Weisskopf, Isidor Rabi and Antonino Zichichi (its president), the Foundation is home to 128 international schools on various branches of science. It occupies three restored ancient monasteries, known today as the Wigner Institute with the "Enrico Fermi" Lecture Hall, the Blackett Institute with the "Paul A.M. Dirac" Lecture Hall, and the Rabi Institute with the "Richard P. Feynman" Lecture Hall. There are living quarters in all three Institutes for people attending the courses of the Centre.

# Accommodation

Accommodation of participants will be organized by the EMFCSC on the basis of the indications provided by the Organizing Committee and by participants in the Travel Form.
Special requests should be addressed to the Conference Secretariat at the email address:

JRC-JdA2019@ec.europa.eu.

**Check-in.** On your arrival at the reception desk you shall fill the registration form, receive your room keys, your folder and your conference badge. The reception desk is located at the EMFCSC main building (former San Rocco monastery, now called I.I. Rabi Institute).

The locations of all housing facilities (Centre, Institutes, and Hotels) are shown on the Erice map, included in the documents you will receive upon registration. There is a "coffee room" in the I.I. Rabi Institute where coffee, tea, mineral water and snacks are available at any time. This "coffee room" is also used for breakfast. There is a "piano room" with a keg of complimentary Marsala wine. This "piano room" can also be used for working parties. The "piano room" will close at midnight. A computer room is available at the I.I. Rabi Institute. Free Wi-Fi is available on the premises of the Foundation.

**Breakfast** is served at San Rocco coffee area to all participants accommodated in the EMFCSC premises, whereas participants in hotels may have their breakfast there or at San Rocco.

**Restaurants.** At the restaurants associated with EMFSCS meals are free – you just have to show your badge and sign a list provided by the restaurant. Beverages and meals that are not included in the EMFCSC menu are extras and should be paid for. The choice among the associated restaurants is free. Thus, if you need a special food (vegetarian, kosher, etc.) you should negotiate directly with the restaurant (the EMFSCS secretary will be glad to offer his assistance). Coffee, tea, sandwiches, fresh fruits, mineral water, and Sicilian sweets are freely available 24 hours in the San Rocco coffee area and in the coffee-break area at San Domenico.

**Badge.** You are requested to have always your badge on, inside the EMFCSC as well as outside, especially at restaurants, during excursions, and social events.

**Technical facilities.** Moderate Xerox-copying is free. A limited number of PC's and internet terminals are available to participants at San Rocco (room of the 16$^{th}$ Century Madonna). Free wireless connection is available in various areas of the Majorana Centre.

# Further Information

**Get-together (Welcome Party)**
You are kindly invited to the after-dinner get-together which is due at 9.30 p.m. on the arrival day at the Marsala Room in San Rocco. You should do your best to reach Erice before 5 p.m. in order to have enough time to get in touch with the environment and to have a quiet dinner. No problem, however, if you cannot reach Erice but late at night: somebody will be waiting for you at the arrival place anyway.

**General information.** After registration you should carefully read: (1) the material in the folder concerning the regulations of the EMFCSC, meals, the location of restaurants associated with EMFCSC, etc.; (2) the specific information about JdA-2019 posted in the entrance hall of San Rocco (location and starting time of lectures, program, social events, etc.).

**Smoking** is forbidden inside all the facilities of the EMFCSC (San Rocco, San Domenico, San Francesco), including rooms. Restaurants in Erice are all no-smoking.

**Dress.** Erice is at about 750 m above sea level, on top of a mountain next to the sea. Weather in Erice may be chill and, occasionally, foggy or/and windy. Do not forget to bring a good pull-over and a rain-coat. The streets paving is slippery and not suitable for stiletto heels or shoes with smooth sole.

**EMFCSC Personnel.** The EMFCSC relies on a local staff, reduced in number but very efficient, ready to solve all problems that may arise (travel ticket & reservation changes, PC facilities, visa, medical care, police, etc.).

**Water** Although water from the tap is drinkable, you are advised to use mineral water, freely available in breakfast and coffee rooms at the EMFCSC.

---

**Social programme.** On the afternoon of Tuesday 16$^{th}$ April, we will visit the archaeological site of Segesta, This was one of the major cities of the Elymians, an ancient people who inhabited the western part of Sicily during the Bronze Age. Its foundation is ascribed to a band of Trojan settlers, fugitives from the destruction of their city after the Trojan war (1260–1180 BC).

Accompanying persons can enjoy the cable car that links Erice to the city of Trapani, along a 3099-meters slant height (42 cabins for 8 people each and 12 minute drive). The plant is equipped with night lighting to be operated in the dark as well as with special cabins for people with disabilities and for bikes. Frequent passenger ferry and hydrofoils services connect Trapani to the Aegadian Islands, Favignana, Levanzo, and Marettimo (about 1 hour trip, each way).

# Guidelines for presentations

## ORALS

All oral presentations will have **15 minutes, including 3 minutes of discussion**. Authors and session chair persons are asked to strictly follow these time limits. You are expected to notify the session chair person of your presence just before the start of the session so that she/he knows you are present.

Presentations must be made in Electronic Form (PowerPoint, PDF). Computerized projection facilities will be offered for oral presentations, including an LCD projector, a computer and a screen.

All speakers are required to submit an electronic version of their presentation by 8:00 pm of the day prior to their presentation. Presentations must be submitted in Microsoft Power Point format (but may be saved as a PDF). It is strongly recommended that speakers save their Power Point presentations with True Type fonts attached. All presentations will be scanned for viruses and subsequently loaded on the main projector computer for the following day presentations. Authors are strongly encouraged to bring an additional electronic copy for added security against unanticipated software/hardware anomalies.

Presentations prepared on platforms other than Windows (Mac, etc.) should be checked by the Author for compatibility with the Windows Platform prior to the presentation. Animations and movies in Microsoft Windows Media file (wmf) and DivX format will be possible.

## POSTERS

All posters are required to conform to Portrait Orientation. Failure to follow this requirement will mean that the poster will not fit on the allotted board.

Poster Board dimensions are 0.90 m wide x 1.10-1.30 m high. If printing on a single page, use size A0 PORTRAIT ORIENTATION (0.84 x 1.19 m). Alternatively, a number of smaller sheets can be used to create a larger collage, but do not go beyond a maximum 'layout' height of 1.1m. The Organization will provide boards and materials to fix your poster.

Poster Authors will have the opportunity to give a **short oral presentation (2 minutes)** about the content of their poster. Poster Authors are kindly asked to prepare one or two summary slides to be presented

# Excellent research awards

The main goal of Best Young Researcher Awards is to appreciate and acknowledge young researchers who made an excellent achievement in their early career.

There are researchers who have been contributing to our community for few decades. We would like to express our appreciation to them by awarding them with the Life-Time Research Award.

The committee will consider the abstract, the presentation and the impact on our community.

Before the poster session begins, authors of poster contributions are asked to give a 2 minutes oral presentation on their work.

1. Best Young Researcher's Oral presentation
2. Best Young Researcher's Poster
3. Best Young/Mid Career Research Award
4. Life-Time Research Award

| | Sunday 14.04 | Monday 15.04 | Tuesday 16.04 | Wednesday 17.04 | Thursday 18.04 |
|---|---|---|---|---|---|
| | | *Breakfast* | *Breakfast* | *Breakfast* | *Breakfast* |
| **8:40** | | **Opening Session**<br>Welcome Address | | | |
| **9:00** | | **Physics-I**<br>In memoriam Robert Troć<br>Chair: D. Kaczorowski | **Physics-III**<br>Chair: L. Havela | **Chemistry-III**<br>Chair: O. Walter | **Physics-VI**<br>Chair: A. Shick |
| | | O.Mo1 F. Gatti | O.Tu1 H. Amitsuka | O.We1 J. März | O.Th1 A. Castellano |
| 9:15 | | O.Mo2 S. Maskova | O.Tu2 L. Luo | O.We2 J. Farnaby | O.Th2 J. Kolorenc |
| 9:30 | | O.Mo3 L. Amidani | O.Tu3 Tereshina-Chitrova | O.We3 S. Schöne | O.Th3 D. Legut |
| 9:45 | | O.Mo4 T. Vitova | O.Tu4 L. Paolasini | O.We4 L. Köhler | **Physics-VII**<br>Chair: L. Paolasini<br>O.Th4 E. Lawrence Bright |
| 10:00 | | O.Mo5 G. Lander | O.Tu5 V. Mineev | O.We5 M. Zegke | O.Th5 D. Braithwaite |
| 10:15 | | O.Mo6 D. Chaney | O.Tu6 E. Svanidze | O.We6 E. Re | O.Th6 O. Koloskova |
| **10:30** | | *Coffee break* | *Coffee break* | *Coffee break* | *Coffee break* |
| **11:00** | | **Chemistry-I**<br>Chair: M. Pasturel | **Fuel Cycle – Decommissioning**<br>Chair: T. Vitova | **Physics-IV**<br>Chair: I. Halevy | **Closing Session** |
| | | O.Mo7 J. Lin | O.Tu7 A. Holdsworth | O.We7 D. Gnida | JdA Awards |
| 11:15 | | O.Mo8 R. Kloditz | O.Tu8 L. Soldi | O.We8 A. Pikul | Physics: I. Halevy |
| 11:30 | | O.Mo9 F. Joly | O.Tu9 H. Im | O.We9 G. Murphy | Chemistry : T. Vitova |
| 11:45 | | O.Mo10 N. Hibert | O.Tu10 F. Virot | O.We10 M. Virot | Concluding Remarks |
| 12:00 | | O.Mo11 M. Maiwald | O.Tu11 Y. Zhao | O.We11 J. Wąsik | |
| 12:15 | | O.Mo12 N. Chen | O.Tu12 L. Pourcelot | O.We12 F. Wilhelm | |
| 12:30 | | | ***Conference Picture*** | O.We13 P. Bagus | |
| **12:45** | | *Lunch* | *Lunch* | *Lunch* | *Lunch* |
| **14:30** | | **Physics-II**<br>Chair: J. Kolorenc | Excursion<br>to Segesta archaeological site | **Chemistry-IV**<br>Chair: H. Lu | Departure<br>Information about your transport time from Erice to the airport will be displayed in the entrance hall of the Rabi Institute (San Rocco) the day before your departure. |
| | | O.Mo13 A. Shick | | O.We14 S. Corradetti | |
| 14:45 | | O.Mo14 B. Amadon | | O.We15 I. Izosimov | |
| 15:00 | | O.Mo15 H. Yu | | O.We16 M. Schmidt | |
| 15:15 | | O.Mo16 R. Zeng | | O.We17 H. Oher | |
| 15:30 | | O.Mo17 A. Karavaev | | O.We18 R. Morales Martinez | |
| 15:45 | | O.Mo18 H. Lu | | O.We19 M. Leblanc | |
| **16:00** | | *Coffee break* | | *Coffee break* | |
| **16:30** | | **Chemistry-II**<br>Chair: A. P. Gonçalves | | **Physics-V**<br>Chair: G. Lander | |
| | | O.Mo19 H. Huang | | O.We20 A. P. Gonçalves | |
| 16:45 | Registration | O.Mo20 S. O'Sullivan | | O.We21 Y. Zhang | |
| 17:00 | | O.Mo21 T. Dumas | | O.We22 D. Kaczorowski | |
| 17:15 | EMFCSC | O.Mo22 L. Bonato | | O.We23 I. Halevy | |
| 17:30 | Main building | O.Mo23 R. Ben David | | O.We24 T. Gouder | |
| 17:45 | (San Rocco) | O.Mo24 O. Tougait | | O.We25 L. Havela | |
| **18:00** | | **Posters-I**<br>Chair: L. Martel | **Posters-II**<br>Chair: L. Martel | Announcement of next JdA | |
| | | Posters 2' oral presentations<br>P.Mo1-P.Mo10 | Posters 2' oral presentations<br>P.Tu1-P.Tu10 | *Free time* | |
| **18:20** | | *Free time*<br>***Meeting of the International Advisory Committee*** | *Free time* | | |
| **20:00** | *Dinner* | *Dinner* | *Dinner* | *Banquet* | |
| **21:30**<br>23:00 | *Welcome Party*<br>Marsala Room in San Rocco | **Poster Session**<br>P.Mo1-P.Mo10 | **Poster Session**<br>P.Tu1-P.Tu10 | | |

| Posters-I | | Posters-II | |
|---|---|---|---|
| P.Mo1 | A. Andreev | P.Tu1 | M. Giovannini |
| P.Mo2 | A. Shestakov | P.Tu2 | K. Park |
| P.Mo3 | A. Makarov | P.Tu3 | E. Tereshina-Chitrova |
| P.Mo4 | N.T.H. Kim-Ngan | P.Tu4 | F. Joly |
| P.Mo5 | C. Sala | P.Tu5 | C. Tabata |
| P.Mo6 | M. Dopita | P.Tu6 | V. Buturlim |
| P.Mo7 | M. Pasturel | P.Tu7 | S. Fryars |
| P.Mo8 | L. Horák | P.Tu8 | D. Belyaev |
| P.Mo9 | O. Walter | P.Tu9 | F. Kon |
| P.Mo10 | E. Colineau | P.Tu10 | H. Shamoradifar |

Posters will be displayed in the San Rocco building:


*Entrance door of the Ettore Majorana Foundation (former San Rocco Monastery)*

Oral sessions will be held in the Dirac lecture hall, San Domenico square:

*Entrance of Dirac lecture hall*

*Dirac lecture hall*

# SCIENTIFIC PROGRAMME

## Sunday, 14th April 2019

Arrival from Palermo or Trapani airports by limousine or bus provided by the EMFCSC according to travel forms.

**Participants should register upon arrival**

**at the EMFCSC Secretariat (I.I. Rabi Institute / San Rocco).**

17:00-19:00

Registration

EMFCSC Secretariat (I.I. Rabi Institute / San Rocco)

20:00

Dinner

Free choice among restaurants associated with EMFSCS meals (list provided at registration). Badge and signature requested. *Beverages and meals not included in the EMFCSC menu are extras and should be paid for.*

21:30

After-dinner get-together

Marsala Room in San Rocco

# Monday, 15th April 2019

Dirac lecture hall, San Domenico square

08:40-09:00 **Opening Session**

Welcome Address

09:00-10:30 **Physics-I**

**Chair: Dariusz Kaczorowski**

In memoriam Robert Troć

9:00-09:15 **O.Mo1**

Prospects of Direct Search for Low Energy Nuclear Isomeric Transition of Th229 with Low Temperature Detectors.
*F. Gatti, M. Biasotti, R. Caciuffo, G. Gallucci, L. Ferrari Barusso2, M. Giovannini, M. Osipenko, M. Ripani, B. Siri, M. Taiuti*

9:15-09:30 **O.Mo2**

$U_2Ni_2Sn$: two-ion magnetic anisotropy
*S. Mašková, A.V. Andreev, Y. Skourski, S. Yasin, S. Zherlitsyn, H. Nakotte, K. Kothapalli, F. Nasreen, C. Cupp, H. B. Cao, D.I. Gorbunov, A. Kolomiets, L. Sandratski, L. Havela*

9:30-09:45 **O.Mo3**

Modeling XANES of $U^{5+}$ and $U^{6+}$ in different local coordination geometries
Lucia Amidani, Ivan Pidchenko, Kristina Kvashnina

9:45-10:00 **O.Mo4**

Exploring the electronic structure and speciation of aqueous and colloidal Pu with high energy resolution XANES and computations
*Tonya Vitova, Aron Beck, Agost Tasi, David Fellhauer, Ivan Pidchenko, Paul S. Bagus, Yves Joly, Kathy Dardenne, Jörg Rothe, Marcus Altmaier, Horst Geckeis*

10:00-10:15 **O.Mo5**

Measurements related to the magnetism of curium metal
*G. H. Lander, J-C. Griveau, R. Eloirdi, N. Magnani, E. Colineau, F. Wilhelm, S. D. Brown, D. Wermeille, A. Rogalev, R. G. Haire, and R. Caciuffo*

10:15-10:30 **O.Mo6**

Exploring the phonon dispersion of γ-(UMo) with grazing incidence IXS
*Daniel Chaney, Sophie Rennie, Luigi Paolasini, Alexei Bosak, Gerard Lander, Ross Springell*

10:30-11:00 **Coffee Break**

11:00-12:45 **Chemistry-I**

**Chair: Mathieu Pasturel**

11:00-11:15 **O.Mo7**

Influence of Acidity, Temperature, and Countercation Hydration Enthalpies on Hydrolysis, Nucleation, and Condensation of Tetravalent Actinide Ions
*Jian Lin, Zenghui Yue, Jian-Qiang Wang*

11:15-11:30 **O.Mo8**

Comprehensive real space bonding analysis of tetravalent f-element complexes with Schiff-base ligands
*Roger Kloditz, Thomas Radoske, Michael Patzschke, Thorsten Stumpf*

11:30-11:45 **O.Mo9**

[Bumim][PF6] ionic liquid as reactant for uranium (IV) oxide fluorination
*Florian Joly, Mehdi Arab, Bertrand Morel, Christophe Volkringer*

11:45-12:00 **O.Mo10**

Investigation of Plutonium(IV) peroxide-based complexes, syntheses and structural characterization
*Nicolas Hibert, Murielle Rivenet, Olivier Tougait, Bénédicte Arab-Chapelet, Laurent Venault*

12:00-12:15 **O.Mo11**

Complexation of Np(V) with OH functionalized carboxylates: structures and thermodynamics
*M. M. Maiwald, D. R. Fröhlich, K. Dardenne, J. Rothe, A. Skerencak-Frech, P. J. Panak*

12:15-12:30 **O.Mo12**

Actinide Endohedral Fullerenes: Molecular Structures and Unique bindings
*Ning Chen,Yaofeng Wang , Xingxing Zhang , Luis Echegoyen, Lai Feng, Shuao Wang, Josep M. Poblet, Antonio RodrÃguez-Fortea ,Jun Li, Eugen Schwarz*

12:30-14:30 **Lunch**

14:30-16:00 **Physics-II**

**Chair: Jindrich Kolorenc**

14:30-14:45 **O.Mo13**

The orbital to spin moment ratio in $UGe_2$ under pressure: part 2 Theory
*A. B. Shick, J.-P. Sanchez, F. Wilhelm*

14:45-15:00 **O.Mo14**

First principles DFT+DMFT and DFT+U calculations of structural properties of actinides
*B. Amadon, J.B. Morée and B. Dorado*

15:00-15:15 **O.Mo15**

Strong and weak adsorption of $CO_2$ on $PuO_2$(110) surfaces from first principles calculations
*Huilong Yu, Xiaodi Deng, Gan Li, Daqiao Meng*

15:15-15:30 **O.Mo16**

Study of atomic structure and electron structure of uranium oxide and nitride
*R.G. Zeng, Y.W. Zhao, T. Fa, Y. Hu, B. Bai, K.Z. Liu and H. Tian*

15:30-15:45 **O.Mo17**

Radioactive strengthening and nanopolycrystalline structure interplay in model Pu-Ga alloys: atomistic simulations
*Alexey V. Karavaev, Vladimir V. Dremov, Philippe A. Sapozhnikov*

15:45-16:00 **O.Mo18**

Boron coordination tuned electronic structure of plutonium borides
*Haiyan Lu, Bingyun Ao, Li Huang*

16:00-16:30 **Coffee Break**

16:30-18:00 **Chemistry-II**

**Chair: Antonio Pereira Gonçalves**

16:30-16:45 **O.Mo19**

Machine Learning Prediction of Novel Uranium-based High Entropy Alloy
*He Huang, Yawen Zhao, Xin Wang, Tao Fa*

16:45-17:00 **O.Mo20**

Ammonolysis of Uranium Oxides
*S.E. O'Sullivan, S.K. Sun, M.C. Stennett, N.C. Hyatt*

17:00-17:15 **O.Mo21**

Electronic structure of f-element Prussian blue analogs by soft X-ray absorption spectroscopy
*Thomas Dumas, Christophe Den Auwer, Clara Fillaux, Dominique Guillaumont, Philippe Moisy, Tolek Tyliszczak, David Shuh*

17:15-17:30 **O.Mo22**

Partial sonochemical conversion of nanostructured $ThO_2$ into 1D Th(IV) peroxo sulfate
*Laura Bonato, Matthieu Virot, Thomas Dumas, Adel Mesbah, Damien Prieur, Philippe Moisy, Sergey I. Nikitenko*

17:30-17:45 **O.Mo23**

Thermal decomposition of β-$UH_3$ powder: Kinetics and mechanism
*Roey Ben David, Noa Bitton, Fredi Simca, Shmuel Samuha, Dvir Fadel, Tzachi Eretz-Kedosha, Natalie Kostirya, Genadi Agronov, Albert Danon, Yacov Finkelstein*

17:45-18:00 **O.Mo24**

Use of Uranyl Nanoclusters containing Rare-Earth Cations as an Innovative Route for the Preparation of Mixed-Oxides Pellets.
*PP-H. Imbert, F. Abraham, J. Nos, M.O.J.Y. Hunault, A. Addad, O. Tougait*

18:00-18:20 **Posters-I (Oral presentation)**

**Chair: Laura Martel**

| | | |
|---|---|---|
| 18:00-18:02 | **P-Mo1** | *Alexander V. Andreev* |
| 18:02-18:04 | **P-Mo2** | *Alexander Shestakov* |
| 18:04-18:06 | **P-Mo3** | *Artem Makarov* |
| 18:06-18:08 | **P-Mo4** | *Nhu-Tarnawska Hoa Kim-Ngan* |
| 18:08-18:10 | **P-Mo5** | *Chris Sala* |
| 18:10-18:12 | **P-Mo6** | *Milan Dopita* |
| 18:12-18:14 | **P-Mo7** | *WITHDRAWN* |
| 18:14-18:16 | **P-Mo8** | *Lukáš Horák* |
| 18:16-18:18 | **P-Mo9** | *Olaf Walter* |
| 18:18-18:20 | **P-Mo10** | *Eric Colineau* |

20:00-21:30 **Dinner**

21:30-23:00 **Posters-I (Poster presentation)**

**Chair: Laura Martel**

EMFCSC building (I.I. Rabi Institute / San Rocco)

**P-Mo1**
Magnetism of $Nd_{1-x}U_xRu_4Al_{12}$ intermetallic compounds
*Alexander V. Andreev, Denis I. Gorbunov, Josef Šebek*

**P-Mo2**
X-ray diffraction study of dislocations in uranium
*A.E. Shestakov, I.V. Artamonov*

**P-Mo3**
Experimental separation of americium-241 from aged MOX-fuel
*A.O. Makarov, A.S. Kornilov, O.S. Dmitrieva., K.O. Scherbakova*

**P-Mo4**
Influence of Mo and B doping on the structure and properties of $U_6Fe$-based alloys prepared by splat cooling
*N.-T.H. Kim-Ngan, M. Paukov, V. Buturlim, L. Havela*

**P-Mo5**
Coordination of Uranyl Ions by Hydroxybisphosphonates
*Chris H. Sala, Gerrit Scharper, Felix Hennersdorf, Giuseppe Zanoni, Jan J. Weigand*

**P-Mo6**
Structure and Properties of Reactively Deposited Uranium Hydride Coatings Studied by the X-ray Scattering Methods
*Milan Dopita, Lukáš Horák, Mykhaylo Paukov, Evgenia Tereshina-Chitrova, Ladislav Havela*

**P-Mo7**
WITHDRAWN

**P-Mo8**
Epitaxial layers of $UO_2$ studied by x-ray scattering methods
*L. Horák, E. A. Tereshina-Chitrova, Z. Bao, L. Havela, T. Gouder, R. Caciuffo*

**P-Mo9**
Actinide dioxide nanocrystals via low temperature oxalate decomposition in hot compressed water
*Olaf Walter, Karin Popa, Marco Cologna, Oliver Dieste*

**P.Tu10**
The Actinide User Laboratory: JRC Open Access in Karlsruhe
*Eric Colineau, Roberto Caciuffo*

# Tuesday, 16th April 2019

Dirac lecture hall, San Domenico square

09:00-10:30 **Physics-III**

**Chair: Ladislav Havela**

09:00-09:15 **O.Tu1**

Search for Odd-Parity Augmented Multipoles and Cross-Correlation Phenomena in Antiferromagnetic Metals
*Hiroshi Amitsuka, Akinari Koriki, Nana Shikanai, Masataka Yamamoto, Yusuke Suzuki, Fusako Kon, Hiroyuki Hidaka, Tatsuya Yanagisawa, Hiraku Saito, Chihiro Tabata, Hironori Nakao, Hiroshi Tanida, Takeshi Matsumura, and Masafumi Sera*

09:15-09:30 **O.Tu2**

Comparison of oxidation behaviors of $UN_{0.68}$ and $UN_{1.66}$ by XPS
*Lizhu Luo, Yin Hu,Kezhao Liu,Xiaolin Wang*

09:30-09:45 **O.Tu3**

Magnetic anisotropy of $UO_2$ studied on $UO_2/Fe_3O_4$ thin films
*E. A. Tereshina-Chitrova, Z. Bao, L. Havela, S. Daniš, L. Horak, A. Mackova, P. Malinsky, L. V. Pourovskii, S. Khmelevskyi, T. Gouder, R. Caciuffo*

09:45-10:00 **O.Tu4**

Examination of excitation spectra of $UO_2$ with inelastic X-ray spectroscopy
*L. Paolasini, D. Chaney, G. H. Lander, R. Caciuffo*

10:00-10:15 **O.Tu5**

Theory of type-II superconductivity in ferromagnetic metals with triplet pairing
*V.P.Mineev*

10:15-10:30 **O.Tu6**

Crystal structure and physical properties of the novel complex intermetallic compounds $R_8Pt_{32}Be_{66}$ (R = Y, La-Nd, Sm-Lu)
*E. Svanidze, A. Amon, Yu. Prots, M. Avdeev, A. Leithe-Jasper, Yu. Grin*

10:30-11:00 **Coffee Break**

11:00-12:30 **Fuel Cycle - Decommissioning**

**Chair: Tonya Vitova**

11:00-11:15 **O.Tu7**

The Effects of Gamma Irradiation on the Physiochemical and Ion Exchange Properties of Caesium-Selective Porous AMP-PAN Composites
*Alistair F. Holdsworth, Daniel Rowbotham, Harry Eccles, Gary Bond, Parthiv Kavi and Ruth Edge*

11:15-11:30 **O.Tu8**

Study on the interaction between U-containing metallic alloys and oxidic liquid for the vitrification processes of contaminated waste
*Luca Soldi, Stéphane Gossé, Christophe Bonnet, Adrien Morellec, Annabelle Laplace, Mathieu Roskosz*

11:30-11:45 **O.Tu9**

Study of Reactor Pressure Vessel Dismantling scenario in Nuclear Power Plant
*Han-sol Im, Kwang-soo Park, Gyu-ho Jang, Hae-woong Kim, Sang-cheol Lee, Jong-hwan Lee*

11:45-12:00 **O.Tu10**

ALAMBIC, a simulation tool to assess the red-oils hazards in reprocessing facilities
*F. Virot, F. Réal, M. Saab, V. Vallet, M. Philippe*

12:00-12:15 **O.Tu11**

Microstructural evolution of adiabatic shear band in U-5.7Nb alloy impacted by Slip Hopkinson Pressure Bar
*Yawen Zhao, Dawu Xiao, Li Zhang, Xian'e Tang, Lidong Zou, Lifeng He, Kezhao Liu*

12:15-12:30 **O.Tu12**

The sources of plutonium around nuclear facilities in the South of France
*Laurent Pourcelot, Béatrice Boulet*

12:30-12:45 **Conference Picture**

12:45-14:30 **Lunch**

14:30-18:00 **Social excursion to Segesta archeological site**

18:00-18:20 **Posters-II (Oral presentation)**

**Chair: Laura Martel**

| | | |
|---|---|---|
| 18:00-18:02 | **P-Tu1** | *Mauro Giovannini* |
| 18:02-18:04 | **P-Tu2** | *Kwang-soo Park* |
| 18:04-18:06 | **P-Tu3** | *Evgenia Tereshina-Chitrova* |
| 18:06-18:08 | **P-Tu4** | *Florian Joly* |
| 18:08-18:10 | **P-Tu5** | *Chihiro Tabata* |
| 18:10-18:12 | **P-Tu6** | *Volodymyr Buturlim* |
| 18:12-18:14 | **P-Tu7** | *Stéphanie Fryars* |
| 18:14-18:16 | **P-Tu8** | *Dmitry Belyaev* |
| 18:16-18:18 | **P-Tu9** | *Fusako Kon* |
| 18:18-18:20 | **P-Tu10** | *Hadi Shamoradifar* |

20:00-21:30 **Dinner**

21:30-23:00 **Posters-I (Poster presentation)**

**Chair: Laura Martel**

EMFCSC building (I.I. Rabi Institute / San Rocco)

**P.Tu1**
$YbPd_2In$: a promising metallic material for adiabatic demagnetization cooling
*Mauro Giovannini, Federica Gastaldo, Andrea Džubinska, Marian Reiffers, Slavo Gabani, Gabriel Pristas, Ivan Čurlik, J.G. Sereni*

**P.Tu2**
Development of In-situ Remote Dismantling System For Reactor Vessel (RV) in Nuclear Power Plant
*Kwang-soo Park, Hae-woong Kim, Hee-dong Sohn, Han-sol Im, Chang-sig Kong*

**P.Tu3**
Crystal structure, magnetism and electrical resistivity of the β-$UH_3$ and fcc $UH_2$ thin films
*E. A. Tereshina-Chitrova, L. Havela, M. Paukov, L. Horak, M. Dopita, T. Gouder, A. Seibert, F. Huber*

**P.Tu4**
Study of uranium oxides fluorination using aqueous hydrofluoric acid in ionic liquid [Emim][$NTf_2$]
*Florian Joly, Mehdi Arab, Bertrand Morel, Christophe Volkringer*

**P.Tu5**
Single Crystal X-ray Structure Analysis of $UNi_4B$
*Chihiro Tabata, Hajime Sagayama, Hiraku Saito, Hironori Nakao, and Hiroshi Amitsuka*

**P.Tu6**
Large enhancement of the electron mass in the U-Ti hydrides
*Volodymyr Buturlim, Ladislav Havela, Oleksandra Koloskova, Daria Drozdenko, Milan Dopita, Peter Minarik, Silvie Mašková, Michal Falkowski*

**P.Tu7**
Novel phase and phase equilibria at 1000 K in the U-Ag-Ge ternary system
*Stéphanie Fryars, Francis Gouttefangeas, Thierry Guizouarn, Mathieu Pasturel*

**P.Tu8**
Hardness and damage of the U-Fe-Ge alloy sphere under explosive loading
*D.A.Belyaev, A.S.Aleksandrov. Yu.N.Zuev, E.A.Kozlov, S.A.Lekomtsev, A.S.Nedosviti, I.L.Svyatov, E.A.Levi*

**P.Tu9**
Low-Temperature Electronic and Magnetic Properties of $UIr_2Ge_2$ Single Crystal
*Fusako Kon, Yusuke Suzuki, Akinari Koriki, Masataka Yamamoto, Ryoya Murata, Hiroyuki Hidaka, Tatsuya Yanagisawa, Hiroshi Amitsuka, Chihiro Tabata, Hironori Nakao, Yusei Shimizu, Yoshiya Homma, Fuminori Honda, and Dai Aoki*

**P.Tu10**
Neutronic Parameters and CPS (Control and Protection System) Worth Calculation of Thermal Research Reactor Using MCNPX code
*Hadi Shamoradifar , Behzad Teimuri, Parviz. Parvaresh, Saeed mohammadi.*

# Wednesday, 17th April 2019

Dirac lecture hall, San Domenico square

09:00-10:30 **Chemistry-III**

**Chair: Olaf Walter**

09:00-09:15 **O.We1**

A series of tetravalent Pu, Np, U and Th complexes of a salen type ligand
*Thomas Radoske, Peter Kaden, Olaf Walter, Roger Kloditz, Michael Patzschke, Thorsten Stumpf, Juliane März*

09:15-09:30 **O.We2**

Controlled synthesis of actinide and mixed-metal f-element materials from organometallic precursors
*Joy H. Farnaby, James R. Hickson, Samuel J. Horsewill, Bradley Wilson, Jake McGuire, Claire Wilson and Stephen Sproules*

09:30-09:45 **O.We3**

Enantiopure Tetravalent Actinide Amidinates - Synthesis and Reactivity
*Sebastian Schöne, Roger Kloditz, Juliane März, Peter Kaden, Michael Patzschke, Peter W. Roesky, Thorsten Stumpf*

09:45-10:00 **O.We4**

The Inverse Trans Influence in U(IV/V) complexes
*Luisa Köhler, Michael Patzschke, Juliane März, Thorsten Stumpf*

10:00-10:15 **O.We5**

Mechanochemistry of low valent uranium
*Markus Zegke, Sophia Eimermacher, Khan Lê and Mathias Wickleder*

10:15-10:30 **O.We6**

Synthesis of actinides-based hybrids nanomaterials using bottom up approach
*Elisa Re, Jérôme Maynadie, Daniel Meyer, Xavier Le Goff*

10:30-11:00 **Coffee Break**

11:00-12:45 **Physics-IV**

**Chair: Itzhak Halevy**

11:00-11:15 **O.We7**

Anisotropic low-temperature thermodynamic and magnetotransport properties of single crystalline $UCoSi_2$
*Daniel Gnida, Maria Szlawska, Piotr Wiśniewski, Dariusz Kaczorowski*

11:15-11:30 **O.We8**

Magnetic and related properties of the ternary germanides $UT_{1-x}Ge_2$ (T = Fe, Ni, Os)
*Mathieu Pasturel, Maria Szlawska, Adam P. Pikul, Antonio P. Gonçalves, H. Noël, Dariusz Kaczorowski*

11:30-11:45 **O.We9**

New Insights into Actinide High Pressure Science: Unravelling Pressured Induced Bond Expansion and Implications for Structural Chemistry
*Gabriel L. Murphy, Evgeny V. Alekseev, Philip Kegler, Brendan J. Kennedy, Zhaoming Zhang and Helen Maynard-Casely*

11:45-12:00 **O.We10**

Particle Size vs. Local Environment Relationship for $ThO_2$ and $PuO_2$
*Laura Bonato, Matthieu Virot, Elodie Dalodière, Thomas Dumas, Adel Mesbah, Oliver Dieste Blanco, Thierry Wiss, Damien Prieur, André Rossberg, Laurent Venault, Philippe Moisy, Sergey I. Nikitenko*

12:00-12:15 **O.We11**

In situ X-ray diffraction studies of $UO_2$ oxidation and phase transition into $U_3O_8$
*Jacek Wąsik, Joseph Sutcliffe, Neil Fox, Ross Springell*

12:15-12:30 **O.We12**

The orbital to spin moment ratio in $UGe_2$ under pressure:
*F. Wilhelm, J.-P. Sanchez, D. Braithwaite, J.-P. Brison, D. Aoki, A. B. Shick and A. Rogalev*

12:30-12:45 **O.We13**

Broadening of the XPS Spectra in Heavy Metal Oxides
*Paul S. Bagus, Connie J. Nelin, Sophie Rennie, Gerry H. Lander and Ross Springell*

12:45-14:30 **Lunch**

14:30-16:00 **Chemistry-IV**

**Chair: Haiyan Lu**

14:30-14:45 **O.We14**

Graphene derived uranium carbide for isotopes production targets
*Stefano Corradetti, Lisa Biasetto, Sara Carturan, Rachel Eloirdi, Pedro Amador-Celdran, Dragos Staicu, Oliver Dieste Blanco, Alberto Andrighetto*

14:45-15:00 **O.We15**

Detection of Actinides/Lanthanides in Solutions by Time Resolved Laser Spectroscopy
*Igor Izosimov*

15:00-15:15 **O.We16**

Effect of background electrolyte composition on the formation of Th(IV) nanoparticles on the muscovite (001) basal plane
*Moritz Schmidt, Canrong Qiu, Stefan Hellebrandt, Peter J. Eng, S. Skanthakumar, Michael Steppert, and L. Soderholm*

15:15-15:30 **O.We17**

Exploring excited state potential energy profile and luminescence properties of uranyl complexes by TRLFS and ab initio methods
*Hanna Oher, Florent Real, Thomas Vercouter, Valerie Vallet*

15:30-15:45 **O.We18**

Thorium and Uranium Endohedral Metallofullerenes: Theoretical Characterization of Oxidation States and Interactions Inside Fullerenes
*Roser Morales-Martínez, Antonio Rodríguez-Fortea, Ning Chen, Luis Echegoyen, Josep M. Poblet*

15:45-16:00 **O.We19**

$U_{1-x}Pu_xO_{2\pm\delta}$ fuel precursor synthesis through advanced thermal denitration in presence of organic additive
*Martin Leblanc, Gilles Leturcq, Eléonore Welcomme, Xavier Deschanels and Thibaud Delahaye*

16:00-16:30 **Coffee Break**

16:30-18:00 **Physics-V**

**Chair: Gerry Lander**

16:30-16:45 **O.We20**

Peculiarities of the U-Fe-Sb system
*M.S. Henriques, I.C. Santos, L.C.J. Pereira, E.B. Lopes, J.C. Waerenborgh, N. Zahurakova, V. Kontuľ, A. Džubinská, S. Iľkovič, I. Curlik, M. Reiffers, J. Rusz, A.P. Gonçalves*

16:45-17:00 **O.We21**

Investigation of structure and oxidation kinetics of uranium surface after pulsed laser nitriding
*Yanzhi Zhang, Jianwei Qin, Yongbin Zhang, Zhilei Chen, Yin Hu, Kezhao Liu*

17:00-17:15 **O.We22**

Iridium 5d-electron driven superconductivity in $ThIr_3$
*Debarchan Das, Karolina Górnicka, Konrad Wochowski, Sylwia Gołąb, Bartłomiej Więdlocha, Tomasz Klimczuk, Dariusz Kaczorowski*

17:15-17:30 **O.We23**

Preliminary resistivity results on $U_2Ni_2Sn$ single crystals
*I. Halevy, A. Kolomiets, S. Mašková, A. V. Andreev, L. Havela*

17:30-17:45 **O.We24**

Spectroscopy Study of the Intermediate Surface Oxide $U_2O_5$
*Thomas Gouder, Rachel Eloirdi and Roberto Caciuffo*

17:45-18:00 **O.We25**

Electron spectroscopy study and magnetism of $UH_3$ and $UH_2$ thin films
*Ladislav Havela, E. Tereshina-Chitrova, Mykhaylo Paukov, Milan Dopita, Lukas Horak, Martin Divis, Ilja Turek, Dominik Legut, Lukáš Kývala, Thomas Gouder, Alice Seibert, Frank Huber*

18:00-18:10 **Announcement of next JdA**

20:00 **Banquet**

# Thursday, 18th April 2019

Dirac lecture hall, San Domenico square

09:00-09:45 **Physics-VI**

**Chair: Alexander Shick**

09:00-09:15 **O.Th1**

Thermodynamic properties of UMo alloys from first-principles
*Aloïs Castellano, Johann Bouchet, François Bottin, Boris Dorado*

09:15-09:30 **O.Th2**

Electronic Structure and Magnetism of $UGa_2$ Using LDA+DMFT Method
*Banhi Chatterjee, Jindrich Kolorenc*

09:30-09:45 **O.Th3**

Lattice dynamics and thermodynamic stability of $UH_2$ and $UH_3$ from first principles
*L. Kývala , L. Havela, D. Legut*

09:45-10:30 **Physics-VII**

**Chair: Luigi Paolasini**

09:45-10:00 **O.Th4**

Resonant x-ray diffraction of uranium nitride epitaxial films
*E. Lawrence Bright, R. Springell, D. G. Porter, G. H. Lander*

10:00-10:15 **O.Th5**

Tuning the uranium ferromagnetic superconductors with hydrostatic and uniaxial pressure
*Daniel Braithwaite, Dai Aoki, Jean-Pascal Brison, Jacques Flouquet, Georg Knebel, Ai Nakamura, Alexandre Pourret*

10:15-10:30 **O.Th6**

Structure and magnetic properties of uranium-vanadium hydrides
*Oleksandra Koloskova, Volodymyr Buturlim, Peter Minárik, Mykhaylo Paukov, Ladislav Havela*

10:30-11:00 **Coffee Break**

11:00-12:00 **Closing Session**

11:00-11:15 **JdA Awards**

11:15-11:30 **Conference Summary (Physics)** *Itzhak Halevy*

11:30-11:45 **Conference Summary (Chemistry)** *Tonya Vitova*

11:45-12:00 **Concluding Remarks**

12:45-14:30 **Lunch**

14:30 **Departure**

Transfer to Palermo or Trapani airports by the EMFCSC

Information about your transport time from Erice to the airport will be displayed in the entrance hall of the Rabi Institute (San Rocco) the day before your departure.

# Oral Presentations

# Prospects of Direct Search for Low Energy Nuclear Isomeric Transition of Th229 with Low Temperature Detectors.

**F. Gatti[1,2], M. Biasotti[1,2], R. Caciuffo[3], G. Gallucci[1], L. Ferrari Barusso[2], M. Giovannini [1,4], M. Osipenko[1], M. Ripani[1], B. Siri[1,2], M. Taiuti [1,2].**

[1] *INFN-Genova, Via Dodecaneso 33, 16146-Genova, Italy, e-mail: Flavio.Gatti@ge.infn.it*
[2] *Dipartimento di Fisica, Università di Genova, Via Dodecaneso 33, 16146-Genova, Italy.*
[3] *European Commission, Joint Research Centre (JRC), Karlsruhe, D-76125, Germany*
[4] *Dipartimento di Chimica, Università di Genova, Via Dodecaneso 31, 16146-Genova, Italy.*

Precise knowledge of the energy and lifetime of Th-229m isomeric state has a great importance for technological development. Indeed, this state was proposed to be used as a basis for a nuclear clock [1]. Such clock would be capable to extend precision on the oscillator frequency by up to four orders of magnitude [2]. However, the technique proposed for the clock requires that the isomeric state energy being accessible with existing laser systems. Previous indirect measurement [3] placed this state at 7.6 eV (160 nm), in the Vacuum Ultra Violet (VUV) range of the electromagnetic spectrum, within the reach of contemporary laser systems. However, a direct excitation measurement in the range around 8 eV at synchrotron radiation facility gave negative results [4,5]. Therefore, a direct measurement of the energy of this state is necessary to determine whether nuclear clock can be made using existing laser technology.

Within TORIO-229 experiment of INFN we are developing a cryogenic micro-calorimeter to measure the energy and lifetime of Th-229m isomeric state directly. The micro-calorimeter will use a U-233 source deposited on the active surface of a silicon detector, whose alpha-decay will populate Th-229m isomeric state with 2% probability. The subsequent decay of Th-229m will be measured on Transition Edge Sensor (TES) with less than 1 eV resolution [5]. Such technique will allow to observe all possible types of decays of Th-229m in the range of energy from 3 to 50 eV and lifetimes greater than 5 microseconds. Indeed, these TES have high resolving power combined with high efficiency in the whole VUV energy band. The detectors are equally sensitive to pure EM emissions as well as to Auger electrons with the same efficiency. The first prototype of TES based on Au-Ti bilayer film 90 nm thick was tested with pulsed blue laser and demonstrated 1.1 eV energy resolution and 40 microsecond signal recovery time. Second prototype based on Ir film is now being tested. Details of dedicated cryogenic TES will be presented along with prospects of the final measurement campaign on Th-229m.

[1] E. Peik and M. Okhapkin, Nuclear clocks based on resonant excitation of gamma-transitions. C. R. Phys. 16 (5), 516, (2015).
[2] E. Peik and C. Tamm., Nuclear laser spectroscopy of the 3.5 eV transition in Th-229. Europhys. Lett. 61(2), 181 (2003).
[3] B. Beck et. al., Energy Splitting of the Ground-State Doublet in the Nucleus 229Th, Phys. Rev. Lett. 98, 142501 (2007).
[4] J.Jeet et. al., Results of a Direct Search Using Synchrotron Radiation for the Low-Energy 229Th Nuclear Isomeric Transition, Phys. Rev. Lett. 114, 253001 (2015).
[5] S. Stellmer et. al., Attempt to optically excite the nuclear isomer in 229Th, Phys. Rev. A **97**, 062506 (2018).
[6] D. Bagliani et. al., Ir TES Electron-Phonon Thermal Conductance and Single Photon Detection, J. Low. Temp. Phys. 151, 234 (2008).

# $U_2Ni_2Sn$: two-ion magnetic anisotropy

**S. Mašková[1], A.V. Andreev[2], Y. Skourski[3], S. Yasin[3,4], S. Zherlitsyn[3], H. Nakotte[5], K. Kothapalli[5,6], F. Nasreen[7], C. Cupp[6], H. B. Cao[8], D.I. Gorbunov[3], A. Kolomiets[1], L. Sandratski[9], L. Havela[1]**

*[1]Department of Condensed Matter Physics, Charles University, Prague, The Czech Republic, e-mail:maskova@mag.mff.cuni.cz*
*[2]Institute of Physics, Academy of Sciences, Prague, The Czech Republic*
*[3]Hochfeld-Magnetlabor, FZ Dresden-Rossendorf, Dresden, Germany*
*[4]American University of the Middle East, College of Engineering and Technology, Egaila, Kuwait*
*[5]Department of Physics, New Mexico State University, Las Cruces, NM, USA*
*[6]College of Arts and Sciences, King University, Bristol, Tennessee, USA*
*[7]High Pressure Science and Engineering Center (HiPSEC) and Department of Physics and Astronomy, University of Nevada, Las Vegas, Nevada, USA*
*[8]Neutron Scattering Division, Oak Ridge National Laboratory, Oak Ridge, Tennessee, USA*
*[9]Max-Planck-Institute of Microstructure Physics, Weinberg 2, Halle, Germany*

$U_2Ni_2Sn$ represents an important case for considerations the origin of magnetic anisotropy in U intermetallics. Majority of $U_2T_2X$ compounds, crystallizing in the tetragonal $Mo_2FeB_2$-type structure (Fig. 1), have the closest U-U spacing along the *c*-axis. Magnetic moments are, as a rule, in the basal plane. In $U_2Ni_2Sn$, the U-U spacing in the basal plane is smaller than along *c*. Existing reports on magnetic structure are contradictory.

A powder neutron diffraction experiment led to a conclusion that the known antiferromagnetic order ($T_N$ = 26 K) has a propagation vector $\boldsymbol{q}$ = (0,0,1/2) and AF coupling also within each unit cell [1]. The magnetic structure should be collinear with basal-plane orientation of the U-moments ($\mu_U$ = 1.05 $\mu_B$). Later and never published neutron diffraction data on allegedly single crystalline sample probably pointed to *c*-axis orientation [2].

We have successfully prepared a single-crystal of $U_2Ni_2Sn$ by the Czochralski method and studied anisotropy of bulk magnetic properties as well as neutron diffraction. The temperature dependence of the crystal structure parameters was studied by means of X-ray diffraction. The results of the refinement show that the *a*-parameter increases with increasing temperature (Fig. 2-left). On the contrary, the *c*-parameter of $U_2Ni_2Sn$ is surprisingly decreasing within the whole *T*-range. For $U_2Ni_2Sn$, the shortest U-U links perpendicular to the *c*-axis ($d^{\perp}_{U-U}$) are considerably shorter than the corresponding shortest U-U links along the *c*-axis (Fig. 2-right) ($d^{\perp}_{U-U}$ = 3.61 Å, $d^{\parallel}_{U-U}$ = 3.69 Å at room temperature). Contrary to expectations from usual thermal-expansion behavior, the $d^{\parallel}_{U-U}$ increases with decreasing temperature, while $d^{\perp}_{U-U}$ decreases with decreasing temperature.

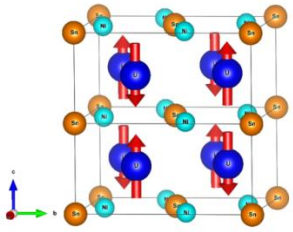

Fig. 1. The crystal structure of $U_2Ni_2Sn$ (right) with arrows showing directions of U moments (two crystallographic unit-cells are shown).

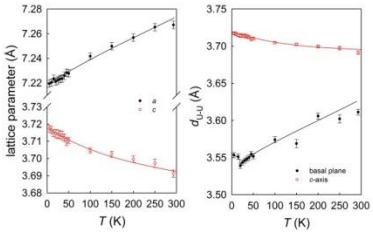


Fig. 2. Temperature dependence of the lattice parameters *a* and *c* (left) and of shortest inter-atomic distances (right) in $U_2Ni_2Sn$ obtained from X-ray diffraction analysis.

The temperature dependence of magnetic susceptibility was measured with field along the *c*-

axis and in the basal plane (Fig. 3). It reveals that the *c*-axis is an easy axis of magnetization, i.e. indeed perpendicular to the shortest U-U links. $\chi(T)$ can be approximated by the Curie-Weiss law with an effective moment $\mu_{eff} = 3.8\ \mu_B$/mol f.u. and paramagnetic Curie temperature $\theta_p = -75$ K for the susceptibility measured along the [001] direction and $\theta_p = -248$ K in the basal plane. The difference of the $\theta_p$ values, $\Delta\theta_p \approx 170$ K, gives an estimate of the magnetic anisotropy energy per U atom, $E_a = 1.1$ mRy. The measured paramagnetic moment $\mu_{eff} = 2.68\ \mu_B$/U atom is far below the expected value for the localized $5f^3$ ($U^{3+}$ – 3.62 $\mu_B$) or $5f^2$ ($U^{4+}$ – 3.58 $\mu_B$) state. The field dependence of magnetization shows 3 metamagnetic transitions at approx. 30, 39 and 50 T (Fig. 4). The magnetization does not show any tendency to saturation in the highest possible fields.

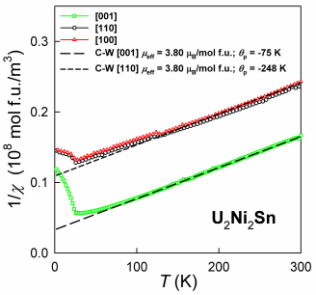


Fig. 3. Temperature dependence of inverse magnetic susceptibility in fields 3 T and 6 T applied along the main axes of the $U_2Ni_2Sn$ single crystal. The dashed lines are C-W fits with parameters shown in the legend.

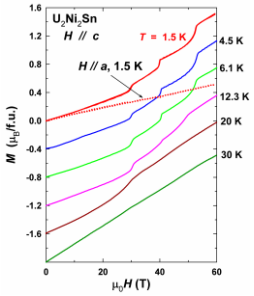


Fig. 4. High-field magnetization curves with magnetic field along the main crystallographic directions of the $U_2Ni_2Sn$ single crystal at various temperatures.

A low-temperature neutron diffraction experiment at ORNL, USA was performed in order to determine the magnetic structure. Our data indicate a clear preference for a collinear antiferromagnetic structure with *c*-axis direction of the U moments with alternating orientation within each unit cell and propagation vector $k = (0,0,1/2)$. No Ni moments were considered. It is interesting to point out that the U magnetic moment (0.87 $\mu_B$) in $U_2Ni_2Sn$ is very close to the value obtained for the deuteride (0.8(3) $\mu_B$), which has, however, different magnetic structure [3] as a result of an anisotropic lattice expansion. The magnetic structure of $U_2Ni_2Sn$ (Fig. 2) is fully compatible with the 5*f*-5*f* two-ion anisotropy model dominant in most of U band systems.

Ab-initio fully relativistic calculations performed with ASW method in the generalized gradient approximation (GGA) found the experimental magnetic structure as the state with the lowest energy among all types tested, and yield indeed the *c*-axis orientation as the moments direction. Preserving the type of coupling and rotating the moments to (100) gives the energy increase by 1.7 mRy per U atom, which is in a quite good agreement with experimentally observed anisotropy energy.

*This work was supported by the Czech Science Foundation under the grant No. 18-02344S.*

## References

[1] F. Bourée, B. Chevalier, L. Fournès, F. Mirambet, T. Roisnel, V.H. Tran, and Z. Zolnierek, *J. Magn. Magn. Mater.* **138**, 307 (1994).
[2] D. Laffargue, B. Chevalier, S.F. Matar, and F. Bourée, 1996, private communication.
[3] K. Miliyanchuk, L. Havela, L.C.J. Pereira, A.P. Gonçalves, and K. Prokeš, *J. Magn. Magn. Mater.* **310**, 945 (2007).

# Modeling XANES of $U^{5+}$ and $U^{6+}$ in different local coordination geometries

**Lucia Amidani,[1,2] Ivan Pidchenko[1,2], Kristina Kvashnina[1,2]**

[1] *Helmholtz-Zentrum Dresden-Rossendorf, ROBL, Bautzner Landstraße 400, 01328 Dresden, e-mail: lucia.amidani@esrf.fr*
[2] *Rossendorf Beamline at ESRF – The European Synchrotron, CS40220, 38043 Grenoble Cedex 9, France*

X-ray Absorption Spectroscopy (XAS) is an invaluable tool in nuclear material research, allowing to probe the oxidation state and the local coordination of selected atomic species. The first part of the spectrum, the X-ray Near Edge Structure (XANES), is less exploited than the Extended X-ray Absorption Fine Structure (EXAFS). However XANES conceals a wealth of information on the electronic structure and on the local geometry around the absorber. What prevents XANES to become a more common technique is the complexity of its analysis, which still gives more qualitative than quantitative information. Nowadays important progresses in the interpretation of XANES have been made thanks to i) the development of dedicated ab-initio codes using powerful computational resources and ii) the use of High Energy Fluorescence Detected (HERFD) XANES, which boosted spectral resolution especially in the case of actinides. These recent developments make the systematic studies based on XANES simulations an invaluable tool to strengthen our understanding of XANES.

In this regards we present a detailed investigation on how the local coordination of $U^{5+}$ and $U^{6+}$ affects the U $L_3$ edge HERFD XANES. By simulating a large number of structures containing $U^{5+}$ and/or $U^{6+}$ in different local coordination geometries we found systematic trends, especially correlated with the presence of longer or shorter U – O bonds. It is well established that the presence of the short uranyl bond shows up in U $L_3$ edge XANES by the presence of a characteristic post-edge feature [1]. Interestingly, some experimental investigations reported that the uranyl post-edge feature shifts to lower energy when going from the uranyl to the uranate coordination, i.e. identical U – O distances [2,3]. Our systematic investigation confirms that this behavior correlates with the presence of U coordinated with 6 oxygen atoms in a regular octahedron and it is a consequence of the splitting of U 6d Density of States (DOS) induced by the crystal field. The possibility to detect the presence of $U^{5+}$ in systems with both $U^{5+}$ and $U^{6+}$ by HERFD XANES will be discussed on the bases of our systematic investigation.

## References

[1] M. A. Hudson et al., *Phys. Rev. B* **54**, 156 (1996).
[2] P. G. Allen *et al.*, *Radiochim. Acta* **75**, 47 (1996).
[3] S. Van den Berghe et al., *J. Solid State Chem.* **166**, 320 (2002).

# Exploring the electronic structure and speciation of aqueous and colloidal Pu with high energy resolution XANES and computations

**T. Vitova,[1] A. Beck,[1] A. Tasi,[1] D. Fellhauer, [1] I. Pidchenko, [1] P.S. Bagus,[2] Y. Joly,[3,4] K. Dardenne, [1] J. Rothe, [1] M. Altmaier, [1] H. Geckeis[1]**

*[1] Karlsruhe Institute of Technology (KIT), Institute for Nuclear Waste Disposal (INE), P.O. 3640, D-76021 Karlsruhe, Germany, e-mail: Tonya.Vitova@kit.edu*
*[2] Department of Chemistry, University of North Texas, Denton, Texas 76203-5017, USA*
*[3] University Grenoble Alpes, Inst NEEL, F-38042 Grenoble, France*
*[4] CNRS, Inst NEEL, F-38042 Grenoble, France*

Plutonium (Pu) is one of the elements with an exceptionally complex chemistry and the ability to coexist in four different oxidation states in aqueous solution. To predict Pu chemistry under environmentally relevant conditions, detailed understanding of Pu redox properties and intrinsic colloid formation processes is essential. It is well known that Pu(IV) has a high tendency towards hydrolysis, polymerization and subsequent colloid formation depending on pH and Pu concentration. Even though such species may have a significant impact on Pu solubility and mobility in the environment, their structure is still not well understood and remains controversial. There is evidence that Pu colloids may contain oxidic and more amorphous domains and also feature different Pu redox states, inter alia Pu(V), depending on Eh and pH.[1–3]

Pu $L_3$ and $M_5$ X-ray absorption near edge structure (XANES) and high resolution XANES (HR-XANES) spectra of Pu(III), Pu(IV), Pu(V), Pu(VI) in aqueous solution, colloidal Pu(IV), amorphous/nano-crystalline and crystalline $PuO_2$ have been measured at the INE-Beamline and the CAT-ACT beamline at the Karlsruhe research accelerator (KARA), Karlsruhe, Germany (previous ANKA).[4-6] The HR-XANES spectra have reduced spectral broadening resulting in better energy resolved features. Our experimental results corroborated by theory (FEFF9 code) give evidence that the Pu 6d states condense and are split by the cubic crystal field when going from molecular to colloidal Pu(IV) species. This appears to be the main reason for reduction of the main peak intensity of the Pu $L_3$ edge XANES/HR-XANES spectra.[6] The Pu $M_5$ HR-XANES technique is valuable for speciation investigations as it provides increased sensitivity to minor contributions of Pu oxidation states in samples containing mixtures, compared to Pu $L_3$ edge HR-XANES. The method can serve as an extremely valuable tool e.g. for the experimental verification of Pu(V) fractions existing in $PuO_2$ solids in presence of different oxygen levels. We observed X-ray induced formation of colloidal Pu(IV) species, which will be reported. Presence of Pu(V)/Pu(VI) oxidation states (plutonate), Pu–OH/Pu–$H_2O$ bonds and/or O vacancies onto the surface of the particles/colloids might have contributions and will be discussed.

The HR-XANES spectra measure relative energies within Pu 5f ($M_5$) and 6d ($L_3$) as well as between Pu 5f and 6d ($L_3$ edge) unoccupied valence states. This information can help to benchmark and drive improvement in theoretical approaches for calculations of Pu electronic structures.[4,6] We will compare and discuss experimental with computed spectra; FDMNES and FEFF9 codes as well as multiplet calculations are applied. [4,6] We will also show that the enhanced resolution allows using the Pu $L_3$ HR-XANES spectra for the estimation of An(V)/An(VI)–Oax bond lengths for actinyl cations. This can be a valuable tool for studies of systems with Pu concentrations below the limit for extended X-ray absorption fine structure (EXAFS) measurements.[6]

## References

[1] M. Altmaier et al., *Chem. Rev*. **113**, 901–943 (2013).
[2] C. Walther and M. A. Denecke, *Chem. Rev*. **113**, 995–1015 (2013).
[3] V. Neck et al., *J. Alloys Compd.* **444**, 464–469 (2007).
[4] T. Vitova et al., *Nat. Commun.* **8**, 1-9 (2017).
[5] S. Bahl et al., *Inorg. Chem.* **56**, 13982-13990 (2017).
[6] T. Vitova et al., *Chem. Commun.* **54**, 12824 (2018).

# Measurements related to the magnetism of curium metal

**G. H. Lander,[1] J-C. Griveau[1], R. Eloirdi[1], N. Magnani[1*], E. Colineau[1], F. Wilhelm[2], S. D. Brown[3], D. Wermeille[3], A. Rogalev[2], R. G. Haire[4], and R. Caciuffo[1]**

*[1]European Commission, Joint Research Centre, Postfach 2340, D-76125 Karlsruhe, Germany*
*[2]European Synchrotron Radiation Facility (ESRF), BP 220, F-38043 Grenoble, France*
*[3]XMaS, European Synchrotron Radiation Facility, BP220, F-38043 Grenoble, France*
*[4]Oak Ridge National Laboratory, Oak Ridge, TN 37831, USA*

*e-mail:lander@ill.fr*

We report a series of measurements on a < 1 mg sample of $^{248}$Cm metal. Magnetization measurements are similar to those reported earlier. X-ray absorption and magnetic circular dichroism (XMCD) measurements at the ESRF synchrotron at the $M_{4,5}$ absorption edges show that the element has an orbital moment of ~ 6% of the spin moment, and the two are parallel. This confirms the predictions of intermediate coupling, which has been suggested for Cm by other spectroscopies. In an XMCD measurement 2.5 years later, a field of 17 T was found to induce a larger induced signal (by a factor of ~ 2) than that found earlier, indicating a change in the sample. We attribute this to the gradual loss of crystallinity with time since preparation, as a result of the damaged caused by fission fragments from the spontaneous fission within the sample itself. The final measurements aimed to determine the antiferromagnetic structure with resonant X-rays were unable to observe any diffraction peaks from the sample. The ground-state antiferromagnetic structure remains unresolved.

# Exploring the phonon dispersion of γ-(UMo) with grazing incidence IXS

**D. Chaney[1, 2], S. Rennie[1], L. Paolasini[2], A. Bosak[2], G. H. Lander[3] and R. Springell[1]**

[1] *University of Bristol, Tyndall Avenue, Bristol, BS8 1TL, UK, email: daniel.chaney@bristol.ac.uk*
[2] *European Synchrotron Radiation Facility, BP 220, F-38043 Grenoble, France*
[3] *Institut Laue-Langevin, 71 Avenue des Martyrs, 38000, Grenoble, France*

The U-Mo system has been studied for at least 50 years since it was identified as potential low enriched fuel for research reactors, which require a high flux, avoiding the use of high-enriched $^{235}$U and the associated proliferation risk. The phase diagram suggests that for compositions between 15 at.% and ~30 at.% Mo the *bcc* structure (which for pure U is stable only above 775°C) may be stabilized at room temperature [1]. However due to the lack of single crystal samples, and perhaps also the complexity of the system, there has been little recent work on the fundamental character of the system.

Building on previous work [2], epitaxial films have been grown and characterized at Bristol, utilizing a Nb buffer deposited on A-plane sapphire to provide the required epitaxial match. Thicknesses between 75 and 300 nm for compositions of 22, 23, 29 and 35 at.% Mo have been synthesized with the epitaxial relationship $(110)_{\mathrm{Nb}}||(110)_{\mathrm{U-Mo}}\ [110]_{\mathrm{Nb}}||[110]_{\mathrm{U-Mo}}$.

These films have been part of three different synchrotron experiments. The first was a study of the *diffuse x-ray scattering* to determine the correct crystallographic structure. In agreement with Yakel [3] the structure between 22 and 30 at% Mo is a modification of the γ (*bcc*) structure denoted $\gamma^s$. Importantly, in this structure, there is *short-range disorder* with the structure described by doubling the original γ (*bcc*) unit cell and allowing some atoms to be displaced an amount δ from their special positions. The resulting *average structure* is based on the $I\bar{4}3m$ space group. The diffuse signal arises due to deviations from the ideal structure and is a factor of ~100 weaker compared to the ideal *bcc* reflections, and thus often missed using conventional x-ray scattering techniques.

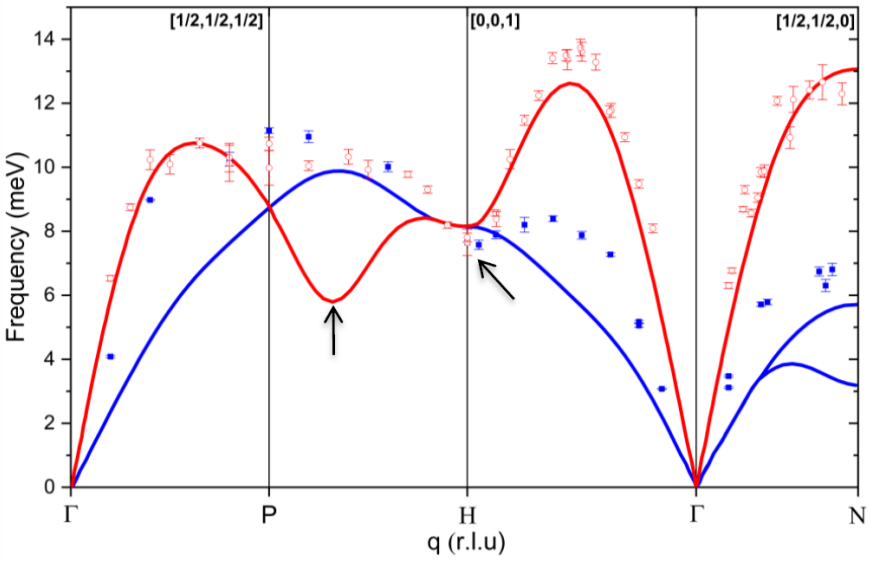


Fig.1. Theoretical dispersion shown as solid lines, experimental points as open red circles and filled blue squares for LA and TA modes respectively. Arrows are discussed in text.

Subsequently inelastic x-ray scattering studies have been performed at the ID28 beamline to explore the phonon dispersion in the 29 at.% Mo film using grazing-incidence techniques [4]. All major symmetry directions have been explored for both the longitudinal (LA) and transverse (TA) acoustic branches and generally compare well with first-principle calculations [5]. Notable differences (indicated by arrows) include the presence/absence of softening at the H and 2/3[1,1,1] positions respectively. Both provide an insight into the underlying electronic structure of the system. A strong variation in linewidth is also reported and is attributed to the short-range disorder. The IXS studies will form the basis of the current presentation with results discussed in the context of the first study.

## References

[1] A. E. Dwight, *J. Nuc. Mater.* **2**, 81 (1960).
[2] A.M. Adamska, R. Springell, & T.B. Scott, *Thin Solid Films* **550**, 319 (2014).
[3] H. R. Yakel, *J. Nucl. Mater.* **33**, 286 (1969).
[4] S. Rennie *et al*, *Phys. Rev. B* **97**, 224303 (2018).
[5] B. Dorado, private communication.

# Influence of Acidity, Temperature, and Countercation Hydration Enthalpies on Hydrolysis, Nucleation, and Condensation of Tetravalent Actinide Ions

**Jian Lin, Zenghui Yue, Jian-Qiang Wang**

*Shanghai Institute of Applied Physics, Chinese Academy of Sciences, 2019 Jia Luo Road, Shanghai 201800, China, e-mail: linjian@sinap.ac.cn*

As the softest tetravalent ions with high charge densities and large ionic radii, hydrolysis, nucleation, and condensation reactions are prevalent in aqueous chemistry of Th(IV) and U(IV), leading to the formation of oxo-hydroxo clusters, colloids, as well as oxide species. These actinide moieties play an important role in separation processes used in the nuclear industry and their significant discrepancies in solubility largely could affect the distribution and fate of thorium and uranium in the environment. Variables including temperature, relative concentration, and pH value can play critical roles in influencing the formation of oligomers. Furthermore, in addition to function as innocent charge-balancing species, the counterions also influence the thermodynamics and electrochemical properties that eventually affect the composition and local coordination of metal-ligand coordination polymers. Despite a handful of thorium or uranium oligomers that have been isolated from aqueous solutions, an in-depth understanding of formation processes including hydrolysis, nucleation, and condensation, remains relatively underexplored. In an effort to explore how the systematic changes in acidity, temperature, and countercation hydration enthalpies affect the mechanisms of cluster formation and the nature of resulting species, herein we report the synthesis and structure elucidation of four families of $Th^{IV}$ and $U^{IV}$ oxo/hydroxo oxoanion coordination polymers.

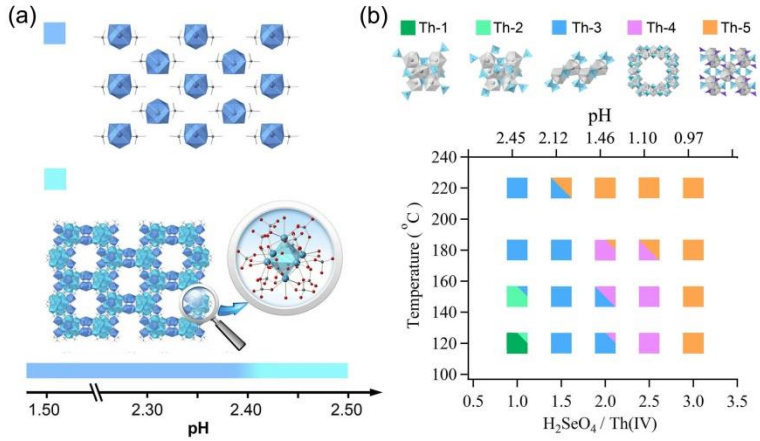


Figure 1. (a) Composition diagram of the $Th^{IV}$–$SO_4^{2-}$ system as functions of the pH. (b) Composition diagram of the $Th^{IV}$–$SeO_4^{2-}$ system as functions of the temperature and the pH.

By systematic control the pH in $Th^{IV}$-sulfate system, a $Th^{IV}$ oxohydroxosulfate $Th_3[Th_6(OH)_4O_4(H_2O)_6](SO_4)_{12}(H_2O)_{13}$ with hexameric cores was isolated from the solution under relatively high pH, while higher acidity result in a monomeric $Th^{IV}$ species was $Th(SO_4)_2(H_2O)_7\cdot(H_2O)_2$ (Figure 1a).[1] In $Th^{IV}$ selenate system, high pH or low temperature gives rise to the formation of octameric $[Th_8(\mu_3\text{-}O)_4(\mu_2\text{-}OH)_8]^{16+}$ cores in Th-1/Th-2 and infinite $[Th(\mu_2\text{-}OH)_2H_2O]^{2+}$ chains in Th-3, respectively, as shown in Figure 2b.[2] Decreasing the pH or elevating the temperature generates a microporous (11.3 Å voids) open-framework Th-4, a monomeric thorium species without oxo/hydroxyl ligands, and a three-dimensional

thorium structure Th-5. These results indicate that increasing acidity limits the deprotonation of water molecules and formation of nucleophilic hydroxo/oxo-aquo Th species, and high temperature appears to suppress the olation/oxolation hydrolysis reactions, which in both ways limit the formation of the thorium oligomers.

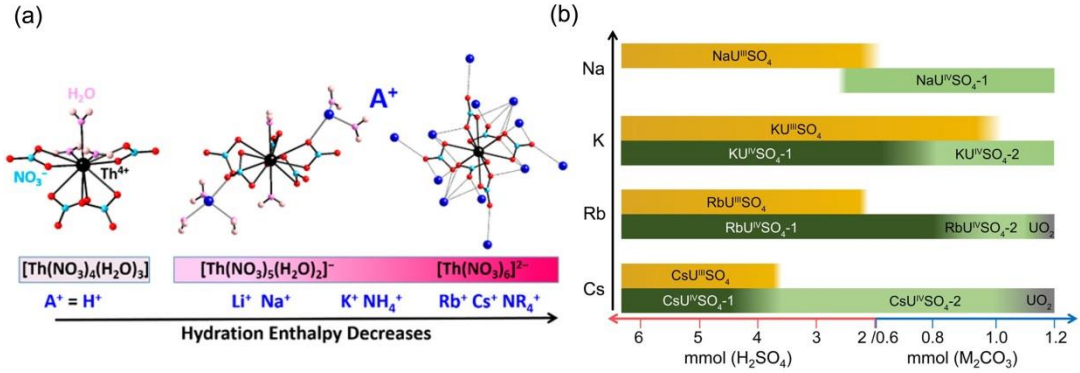


Figure 2. (a) Monomeric Th−nitrato complexes, isolated in solids by evaporating aqueous solutions, shown as a function of counteraction hydration enthalpies. (b) Composition diagram of the $A^+$–$U^{IV}$–$SO_4^{2-}$ system (A = Na, K, Rb, and Cs).

Furthermore, a correlation between the composition and condensation of metal-ligand complexes and hydration enthalpies of countercation ($A^+$) was established by two systems $A^+$–$Th^{IV}$–nitrate and A–U–sulfate. Analyses of the chemical compositions and solid-state structures of $A^+$–$Th^{IV}$–nitrate compounds demonstrate that $A^+$ not only affects the overall solid-state packing of the Th−nitrato complexes but also influences the composition of the Th−nitrato monomeric anions themselves (Figure 2a).[3] Trends in composition and structure are found to correlate with $A^+$ hydration enthalpies, such that the $A^+$ with smaller hydration enthalpies associate with less hydrated and more anionic Th−nitrato complexes. In the A–U–sulfate system, we also explore how the variation of alkali-metals affects the formation of uranium coordination polymers with the presence of zinc amalgam.[4] The alkali metals with smaller ionic radius tend to push uranium toward lower oxidation state and stabilize the $U^{IV}$ polynuclear species with high number of U cores (Figure 2b). These perspectives, broader than the general assumption of size and charge as the dominant influence of $An^+$, open a new avenue for the design and synthesis of targeted metal−ligand complexes.

## References

[1] J. Lin, G.B. Jin, L. Soderholm, *Inorg. Chem.* ***55***, 10098-10101 (2016).
[2] J. Lin, M. Qie, L. Zhang, X. Wang, Y. Lin,W. Liu, H. Bao, J. Wang, *Inorg. Chem.* ***56***, 14198-14205 (2017).
[3] G.B. Jin, J. Lin, S.L. Estes, S. Skanthakumar, L. Soderholm, *J. Am. Chem. Soc.* ***139***, 18003-18008 (2017).
[4] J. Lin, Z. Yue, M.A. Silver, M. Qie, X.Wang, W. Liu, X. Lin, H.-L. Bao, L.-J. Zhang, S. Wang, J.-Q. Wang, *Inorg. Chem.* ***57***, 6753-6761 (2018).

# Comprehensive real space bonding analysis of tetravalent *f*-element complexes with *Schiff*-base ligands

**Roger Kloditz, Thomas Radoske, Michael Patzschke, Thorsten Stumpf**

*Helmholtz-Zentrum Dresden-Rossendorf, Institute of Resource Ecology, Bautzner Landstraße 400, 01328 Dresden, Germany, e-mail: r.kloditz@hzdr.de*

The contribution of the *f*-orbitals to chemical bonding leads to the rich chemistry of the actinides. [1] This is in contrast to the lanthanides, where it is known that this contribution is less important. Of special interest is the influence of these orbitals on the bonding character of actinides and lanthanides with organic ligands reflecting natural binding motifs.
This study compares the different bonding behavior of tetravalent actinides and lanthanides with the *Schiff* base salen (see Fig. 1, left) by means of real-space bonding analysis. Our approach makes use of the quantum theory of atoms in molecules (QTAIM), plots of the non-covalent interactions (NCI)[2] and density differences complemented by natural population analysis (NPA). Especially the local properties at the bond critical points (Fig. 1, right), for instance charge, density, ellipticity and others, can be used to characterize a bond's order, strength, and covalent contribution. In addition, thermodynamic calculations on the stability of these complexes are presented since the difference in stability is a direct consequence of the different interaction strengths of the *f*-elements.
First results reveal a strong interaction of the actinides, i.e. Th to Pu, with the oxygen of salen characterized by a high electron density concentration between the atoms. In contrast, the interaction between the actinides and the nitrogen of salen is much weaker. The delocalization index, density and Laplacian reveal a significant increase of covalency for Pa to Pu compared to Th and Ce being an indicator of the contribution of the *f*-electrons. Tetravalent Ce as a lanthanide analogue of Th is expected to show a similar bonding behavior, but, surprisingly, this is not the case for all investigated bonding properties.
Such a detailed analysis of the electronic properties of actinide compounds will help to improve understanding of their behavior in the environment as well as in technical processes and leads to the possibility to predict properties of unknown complexes.

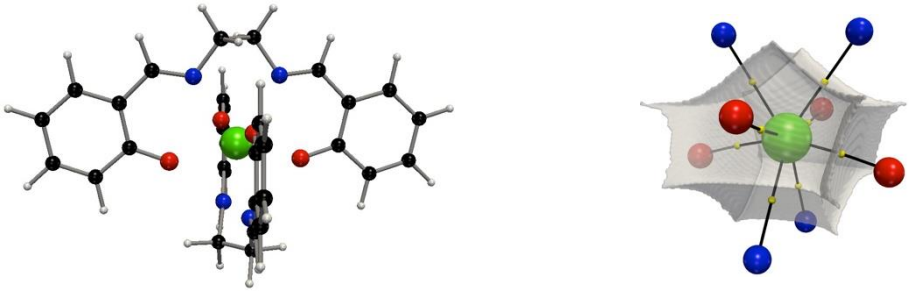

Fig. 1. Left: Molecular structure of the $[U(salen)_2]$ complex (U green, O red, N blue, C black, H white). Right: QTAIM-based uranium atom with bond paths to N,O-donor atoms and bond critical points (yellow).

## References

[1] J.-P. Dognon, *Coord. Chem. Rev.* ***266–267***, 110–122 (2014).
[2] J. Contreras-Garcia et. al., *J. Chem. Theory Comput.* ***7***, 625–632 (2011).

# [Bumim][$PF_6$] ionic liquid as reactant for uranium (IV) oxide fluorination

**Florian Joly,[1] Mehdi Arab[3], Bertrand Morel,[3] Christophe Volkringer[1,2]**

[1] *UCCS UMR 8181, Cité scientifique, 59655 Villeneuve d'Ascq, FRANCE, e-mail: florian.joly@univ-lille.fr, christophe.volkringer@univ-lille.fr*
[2] *Institut Universitaire de France, 75005 Paris, FRANCE*
[3] *Orano, Place Jean Millier, 92400 Courbevoie, FRANCE*

Ionic liquids have met an increasing interest over the last twenty years. These salts which have a melting point below 100°C are often presented as alternative for classical solvents because of their low vapor pressure and adaptable properties through the cation and anion choice.
Some fluorinated ionic liquids are known to decompose and liberate fluoride anion F- *in-situ* [1]. Then, this ion can be used to achieve fluorination of uranium as well as other metals using the ionic liquid as both reactant and solvent [2,3]. This fluorination pathway allows for synthesis of metals fluorides without handling dangerous fluorinated reactants.
To our knowledge, only two works have reported the synthesis of uranium fluorides using [Emim][$F(HF)_{2.3}$] as ionic liquid: one from $UF_5$ [4], the other from uranium oxides ($UO_2$ or $UO_3$) [5]. However, synthesis of this ionic liquid requires the use of anhydrous HF which is highly corrosive and not commonly available in laboratories.
This work studied the synthesis of uranium tetrafluoride $UF_4$ from $UO_2$ using a commercial ionic liquid: [Bumim][$PF_6$] [3,6,7].
Synthesis of uranium fluoride was studied *ex-situ* using UV-visible, PXRD, SEM and NMR ($^{1}H$, $^{13}C$, $^{15}N$, $^{19}F$, $^{31}P$) and ICP-OES. Results shows that $UF_4$ can be observed by PXRD for reaction time as low as 7 hours and temperature above 150°C. After cooling down uranium could not be observed in the ionic liquid by UV-visible which is confirmed by ICP-OES measurement of uranium concentration. No deterioration of the cation $[Bumim]^+$ is observable on NMR spectra. However, some new peaks appeared on $^{19}F$ and $^{31}P$ NMR spectra giving insight on the degradation product of the hexafluorophosphate anion. Only $[PO_2F_2]^-$ could be identified as a degradation product which indicates lost of more than one fluorine atom from $[PF_6]^-$.

## References

[1] R.P. Swatloski et al., *Green Chemistry* **5**, *361* (2003).
[2] D.S. Jacob et al., *Chemistry of Materials* **18**, *3162* (2006).
[3] J. Olchowka et al., *Chemistry - A European Journal* **6**, *12092* (2017).
[4] T. Kanatani et al., *Chemistry Letters* **38**, *714* (2009).
[5] C.A. Zarzana et al., *Journal of the American Society for Mass Spectrometry* **29**, *1963* (2018).
[6] Y. Song et al., *Journal of Colloid and Interface Science* **487**, *281* (2017).
[7] J.-S. Xu et al., *CrystEngComm* **14**, *2630* (2012).

# Investigation of Plutonium(IV) peroxide-based complexes, syntheses and structural characterization

**Nicolas Hibert[1], Murielle Rivenet[2], Olivier Tougait[2], Bénédicte Arab-Chapelet[1], Laurent Venault[1]**

*[1]Laboratoire d'études des Procédés de Conversion des Actinides – LPCA – CEA Marcoule, CEA ; Nuclear Energy Division, Research Department on Mining and Fuel Recycling Processes Service – DEN\DMRC\SMFA\LPCA – F30207 Bagnols-sur-Cèze, France*
*e-mail: nicolas.hibert@cea.fr*
*[2] Unité de Catalyse et Chimie du Solide – UCCS – UMR 8181, Univ. Lille, CNRS, Centrale Lille, ENSCL, Univ. Artois, F-59000 Lille, France*

In order to tackle the optimization of 2nd and 3rd GEN reactor nuclear fuel properties, new conversion processes are being investigated. On the long run, tomorrow's nuclear fuels should also be designed to be operated in 4th GEN reactor nuclear plant. Thus, today's nuclear fuel process development research must take into account not only the latest highest quality standards but also the MOX nuclear fuel waste recovery input. The hydrogen peroxide conversion process, which had already been applied to the plutonium metal production at an industrial scale in the 60's at Savannah Rivers [1], represents a lot of interest in the Pu conversion process R&D area. The peroxide route has been the focus of our attention regarding its ability to precipitate Pu in its targeted oxidation number (+IV) and as a carbon-free precursor of oxides, which prevent any $CO_{(g)}$ and $CO_{2(g)}$ emissions during thermal treatment. Promising results have been acquired for single metallic systems with Pu and Th and they will be introduced in this present contribution.

From a state-of-the-art literature assessment, three plutonium peroxide-complexes have been identified and targeted for our synthesis experiments. Two of them readily form at equimolar and 2:1 molar ratio in favor of peroxide as already outlined [2] and further confirmed by our experimental investigation. Their molar extinction coefficients were established in nitric acid 1M thanks to the calculation of their UV-Vis spectroscopic spectra. The third Pu peroxide, which forms starting at $H_2O_2$:Pu molar ratio of 3:1, is insoluble, and should be regarded as a salt. It crystallizes as a colloidal-like solid in nitric acid below 2M while a well-filterable better-crystallized precipitate takes shape above 2M [2]. The solid has been the subject of extensive characterizations carried out by Raman and Infrared spectroscopies, powder XRD, DSC-TG and SEM. Our analyses confirm the nature of the salt which is a plutonium nitrate-peroxide with chemical formulas $Pu_2(OO)_{3.30}(NO_3)_{1.39}\cdot 2.5H_2O$ and $Pu_2(OO)_{3.43}(NO_3)_{1.11}\cdot 3.4H_2O$, calculated from the thermogravimetric analysis.

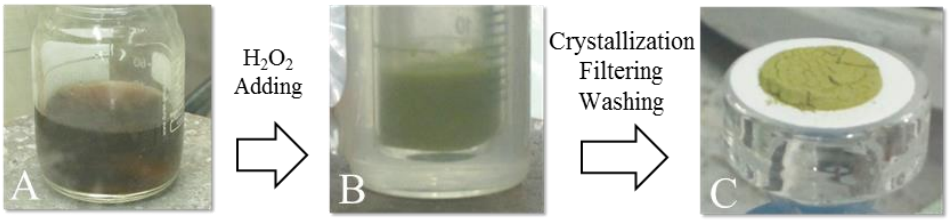


Figure 1 _ A) Pu(IV) initial solution in nitric acid 2M. B) Mixture of hydrogen peroxide and Pu(IV) in nitric acid 3M, molar ratio $H_2O_2$ : Pu = 50 : 1. C) Filtrated Pu nitrate-peroxide cake after washing.

The first Pu peroxide synthesis experiments ended up with low-crystallized precipitates whose powder X-ray diffraction (PXRD) diagrams remained unknown from the JCPDS-International Centre Diffraction Data while using Bruker's EVA pattern-matching software with a 2018 PDF 4+ license. Several experimental parameters such as the rate of hydrogen peroxide addition to the Pu(IV) solution, the aging time, the washing solution (ethanol : water ratio), the drying time and the temperature have been varied in order to assess their influence on the precipitate crystallinity. When comparing the X-ray powder diffraction diagrams, it was found that all patterns show a low state of crystallization. Consequently, the studied parameters don't have a significant impact on the precipitate crystallinity. However, without washing the precipitate, the Pu peroxide XRD pattern shows thin peaks with high intensities. Oddly, the powder-like texture is completely lost and the precipitate turns rapidly into a sticky gelatinous-like solid probably due to radiolysis.

In order to put aside the redox reaction which can arise upon mixing hydrogen peroxide with plutonium ions, additional syntheses were carried out using thorium ions, Th(IV), in place of Pu(IV). As previously mentioned in literature the two systems show similar PXRD diagrams [3]. Several attempts to grow single-crystal of thorium peroxide salt have been carried out. They have turned out fruitless so far but this part of the work is still ongoing.

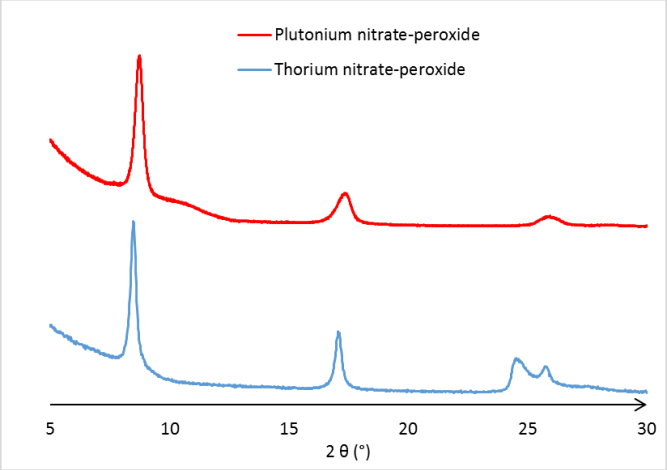


Figure 2. Comparison of Pu nitrate-peroxide and Th nitrate-peroxide PXRD diagrams

An *in-situ* PXRD study of the thorium peroxide compound was carried out under argon flow to follow the phase transformations up to $ThO_2$. It revealed that thorium oxide begins to form at 400 °C, which is a relatively low temperature compared to other oxide precursors. This temperature compares well the one determined for $PuO_2$ formation from Pu-peroxide by means of thermogravimetric analysis.

## References

[1] El. W. Mainland, D. A. Orth, E. L. Field, and J. H. Radke, "Production of Plutonium Metal," *Savannah River Plant*, **vol. 53, no. 9**, pp. 685–694 (1961).
[2] J. A. Leary, "Studies on the preparation, properties and composition of plutonium peroxide," Los Alamos Sci. Lab. Univ. Calif., **no. 39** (1954).
[3] D. E. Koshland, J. C. Kroner, and L. Spector, "Peroxide Of Plutonium And Thorium," *Transuranium Elem.*, vol. **Paper 6.6** (1949).

# Complexation of Np(V) with OH functionalized carboxylates: structures and thermodynamics

**M. M. Maiwald,[1,2] D. R. Fröhlich[1], K. Dardenne[2], J. Rothe[2], A. Skerencak-Frech[2], P. J. Panak[1,2]**

[1] *Ruprecht Karls Universität Heidelberg, Physikalisch-Chemisches Institut, Im Neuenheimer Feld 253, D-69120 Heidelberg, m.maiwald@pci.uni-heidelberg.de*
[2] *Karlsruher Institut für Technologie (KIT), Institut für Nukleare Entsorgung (INE), Hermann-von-Helmholtz Platz 1, D-76344 Eggenstein-Leopoldshafen*

## Introduction

The complexation of actinides with organic ligands is an important topic in terms of nuclear waste disposal. These organic molecules can originate from different sources: They can either be naturally occurring as macromolecular compounds and small organic ligands in pore waters of clay rock formations or are of anthropogenic origin such as polycarboxylate based cement additives and their degradation products.[1-3] These compounds may serve as complexing agents towards actinides and thus influence their migration behavior considerably. Therefore, a detailed thermodynamic description of these complexation reactions in the aqueous phase is of high importance for the safety case of a nuclear waste repository. In the past, the majority of conducted studies were focused on the complexation of actinides with simple mono- and dicarboxylic acids. Only limited data is available on the interaction of actinides with defined poly-functionalized organic ligands. In particular, systematic studies on the effect of α-OH groups in carboxylic acids on the complex stabilities and thermodynamics of An(V) complexes are rare. Furthermore, most of the so-far available data is valid only at 25 °C and/or fixed ionic strength. Due to the radioactive decay, elevated temperatures are expected in the near field of a repository. This will considerably alter the (geo)chemical reactions of the actinides. For a comprehensive model to describe the migration behavior of actinides thermodynamic data (log $\beta^0_i(T)$, $\Delta_R H^0_{m,i}$, $\Delta_R S^0_{m,i}$) at ambient conditions as well as at increased temperatures are required.

## Results and Discussion

In this work the complexation of Np(V) with lactate ($Lac^-$), malate ($Maa^{2-}$) and tartrate ($Tart^{2-}$) is studied as a function of the temperature (20 – 85 °C) and ionic strength ($I_m$(NaCl or $NaClO_4$) = 0.5 – 4.0 mol $kg^{-1}$) using near infrared absorption spectroscopy (NIR). The structure of the formed complexes is investigated by extended x-ray absorption fine structure spectroscopy (EXAFS) and quantum chemical calculations. The formation of the complex species $NpO_2(L)_n^{1-mn}$ (n = 1, 2) is determined for all ligands ($L^{m-}$ = $Lac^-$, $Maa^{2-}$, $Tart^{2-}$) by principle component analyses of the absorption spectra. Application of the specific ion interaction theory (SIT) and the integrated Van´t Hoff equation yields the thermodynamic functions (log $\beta^0_i(T)$, $\Delta_R H^0_{m,i}$, $\Delta_R S^0_{m,i}$) and the SIT-specific binary ion-ion-interaction coefficients ($\varepsilon_T(j,k)$) for the different complexation reactions. The results show similar log $\beta^0_i(25°C)$ values for all studied ligand metal complexes, which are independent of the alkyl chain length, number of $COO^-$ and OH groups of the ligand. More pronounced differences are observable regarding the reaction enthalpies. The $\Delta_R H^0_{m,i}$ shifts from exothermic ($Lac^-$) to endothermic ($Maa^{2-}$, $Tart^{2-}$) values with increasing alkyl chain length of the ligand, with $Maa^-$ showing the highest enthalpy. The EXAFS data reveal that the coordination modes of the ligands are different in the 1:1- and 1:2-complexes. In case of the 1:1-complexes all studied

ligands coordinate in an end-on fashion to the metal ion via one $COO^-$ group. For the 1:2-complexes the formation of chelate rings is found. The ligands coordinate via the $COO^-$ and OH-group to the Np(V) center. This is confirmed by quantum chemical calculations. The results show that the end-on coordination is thermodynamically favored in case of the 1:1-complex, whereas for the 1:2-complex the formation of chelate complexes is energetically preferred.

The present work provides detailed insights into the complexation of Np(V) with different OH functionalized carboxylates in aqueous solution at T > 25 °C. The data highlight the effect OH groups on the complex stability and thermodynamic behavior. The results add to a better understanding of the (geo)chemistry of actinides at repository conditions where macromolecular and small organic molecules may be present. Furthermore, the derived thermodynamic data improve the scientific basis to describe disposal scenarios at elevated temperature conditions.

**References**

[1] A. Courdouan et al., *Appl. Geochem.*, **22,** 1537 (2007).
[2] A. Courdouan et al., *Appl. Geochem.*, **22,** 2926 (2007).
[3] L. Ferrari et al., *Cem. Concr. Res.*, **41,** 1058 (2011).

# Actinide Endohedral Fullerenes: Molecular Structures and Unique bindings

**Ning Chen,[1] Yaofeng Wang [1], Xingxing Zhang [1], Luis Echegoyen[2], Lai Feng,[3] Shuao Wang,[4] Josep M. Poblet,[5] Antonio Rodríguez-Fortea ,[5] Jun Li, [6] Eugen Schwarz [6]**

*[1] College of Chemistry, Chemical Engineering and Materials Science, Soochow University, Jiangsu 215123, Suzhou, China, e-mail: chenning@suda.edu.cn*
*[2] Department of Chemistry, University of Texas at El Paso, 500 West University Avenue, El Paso, Texas 79968, United States.*
*[3] Soochow Institute for Energy and Materials InnovationS (SIEMIS), College of Physics, Optoelectronics and Energy & Collaborative, Soochow University, Suzhou, Jiangsu, 215006, China.*
*[4] School of Radiological and Interdisciplinary Sciences & Collaborative Innovation Center of Radiation Medicine of Jiangsu, Higher Education Institutions, Soochow University, Jiangsu 215123, China.*
*[5] Departament de Química Física i Inorgànica, Universitat Rovira i Virgili, c/Marcel·lí Domingo 1, 43007 Tarragona, Spain*
*[6] Department of Chemistry and Key Laboratory of Organic Optoelectronics & Molecular Engineering of the Ministry of Education, Tsinghua University, Beijing 100084, China.*

The hollow internal cavity of fullerene buckyballs, e.g. $C_{2n}$, has been known to able to encapsulate novel metallic units, especially those otherwise very reactive or virtually impossible to prepare clusters. In this talk, we will present our recent studies of a novel family of fullerenes, actinide endohedral fullerenes. The synthesis of Th@$C_{82}$, U@$C_{2n}$, $U_2$@$C_{80}$, $Th_2$@$C_{80}$ and $U_2C$@$C_{80}$ and their unique electronic properties will be discussed. We found that these endohedral fullerenes are unique for not only fullerene chemistry but also to actinide chemistry. Th@$C_{82}$ shows a unique four electron metal-to-cage electron transfer and U@$C_{82}$ isomers represent the first pair where the oxidation state of the encapsulated ion depends on the isomeric cage structure.[1,2] The structural and computational studies of $U_2$@$C_{80}$ revealed a weak U-U bonding interaction inside fullerene cage.[2] The crystallographic and computational studies of UCU@$I_h$-$C_{80}$ reveal reveals a cage-stabilized, carbide-bridged, bent UCU cluster with unprecedentedly short uranium-carbon distances (2.03 Å) of U=C double-bond character.[3] The isolation of $U_2C$@$C_{80}$ gives an unprecedented look into a long sought after but heretofore unknown U=C bond which lacks heteroatom support, allowing for detailed structural and electronic insights. This study suggests that actinide endohedral fullerenes not only demonstrate substantially different bond motif and cage structures from those lanthanide fullerenes and also reveal unique actinide bonds which have never been discovered in the conventional actinide compound reported previously.

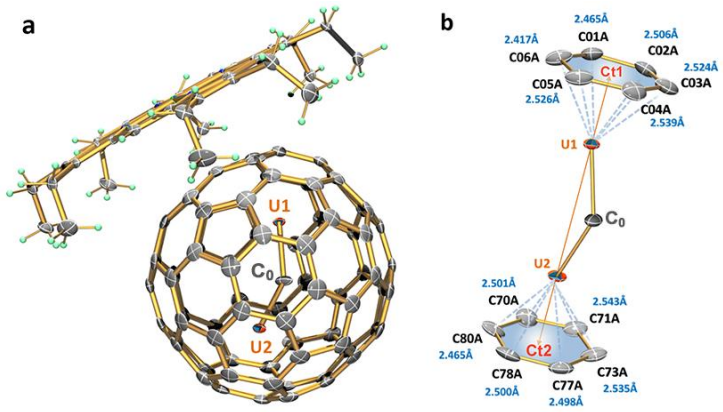


Fig. 1. ORTEP drawing of UCU@$I_h$(7)-$C_{80}$·[$Ni^{II}$-OEP] with 40 % probability ellipsoids. **a** UCU@$I_h$(7)-$C_{80}$·[$Ni^{II}$-OEP] structure showing the relationship between the fullerene cage and the [$Ni^{II}$-OEP] ligands. **b** Fragment view showing the interaction of the major U1-$C_0$-U2 cluster with the closest aromatic ring fragments of the cage with centers Ct1 and Ct2. The orange line connects Ct1-U1−U2-Ct2.

## Reference

[1] Wang, Y.; Morales-Martínez, R.; Zhang, X.; Yang, W.; Wang, Y.; Rodríguez-Fortea, A.; Poblet, J. M.; Feng, L.; Wang, S.; Chen, N., *J. Am. Chem. Soc.* **139**,5110 (2017).
[2] Cai, W.; Morales-Martinez, R.; Zhang, X.; Najera, D.; Romero, E. L.; Metta-Magana, A.; Rodriguez-Fortea, A.; Fortier, S.; Chen, N.; Poblet, J. M.; Echegoyen, L., *Chem. Sci.* **8,** 5282 (2017).
[3] Zhang, X.; Wang, Y.; Morales-Martínez, R.; Zhong, J.; de Graaf, C.; Rodríguez-Fortea, A.; Poblet, J. M.; Echegoyen, L.; Feng, L.; Chen, N., *J. Am. Chem. Soc.* **140**, 3907 (2018**)**.
[4] Zhang, X.; Li, W.; Feng, L.; Chen, X.; Hansen, A.; Grimme, S.; Fortier, S.; Sergentu, D.-C.; Duignan, T. J.; Autschbach, J.; Wang, S.; Wang, Y.; Velkos, G.; Popov, A. A.; Aghdassi, N.; Duhm, S.; Li, X.; Li, J.; Echegoyen, L.; Schwarz, W. H. E.; Chen, N., *Nature Commun.* **9**, 2753 (2018**)**.

# The orbital to spin moment ratio in $UGe_2$ under pressure

**A. B. Shick,[1] J.-P. Sanchez[2], F. Wilhelm[3]**

[1] *Institute of Physics CAS, Na Slovance 2, CZ-18221 Prague, Czech Republic, e-mail:shick@fzu.cz*
[2] *University of Grenoble Alpes, CEA, INAC- PHELIQS, F- 38000 Grenoble, France*
[3] *European Synchrotron Facility (ESRF), B.P. 220, F- 38043 Grenoble cedex, France*

$UGe_2$ shows a coexistence of unconventional superconductivity with ferromagnetism [1]. It crystallizes in an orthorhombic structure of $ZrGa_2$ type and orders ferromagnetically at $T_C$ = 52 K. Below 35 K down to 20 K one observes a cross-over from a weakly polarized FM1 phase to a low temperature strongly polarized ferromagnetic phase FM2. The superconductivity domain appears to exist only for pressures close to 12 kbar up to 15 kbar with a maximum of $T_{sc} \approx 0.7$ K.

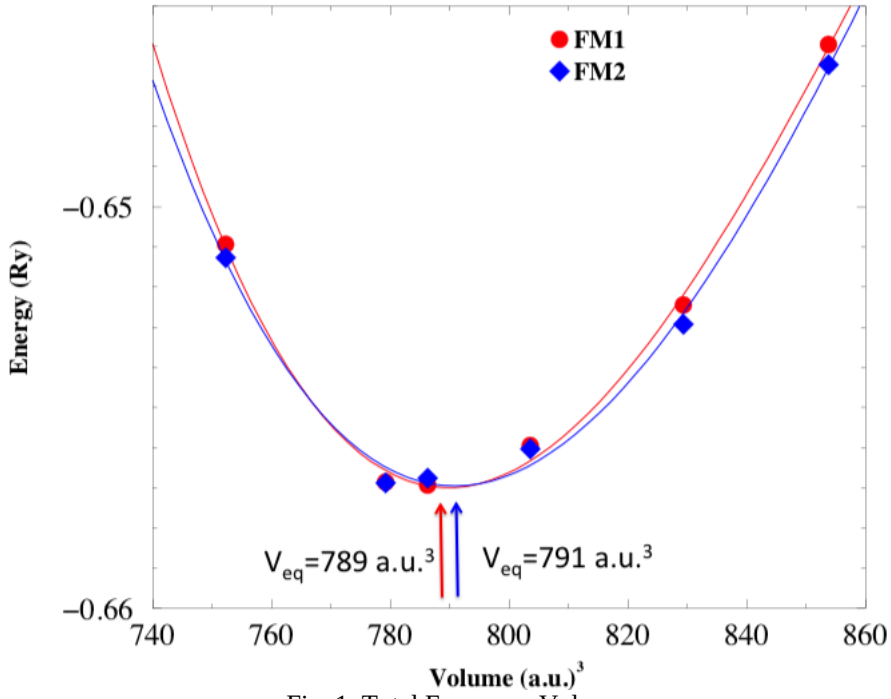


Fig. 1. Total Energy vs Volume.

We examine theoretically the electronic structure and magnetic properties of $UGe_2$ making use of a combination of density functional theory with Hubbard+$U$ (DFT+U). The total energy vs volume dependence is shown in Fig. 1 for $U$=1 eV and $J$=0.51 eV. These values of $U$ and $J$ are in the ballpark of the parameters commonly used in the calculations of the uranium intermetallics. We find two nearly degenerate DFT+U solutions, similar to those reported in Ref. [2], as strong candidates for the FM1 and FM2 states. The calculated equilibrium volume $V_{eq}$ = 789 (a.u.)$^3$ for FM1 and $V_{eq}$ = 791 (a.u.)$^3$ for FM2 are in reasonable agreement with experiment [3]. Nevertheless, the U-atom magnetic momen $\mu_{tot}$ of 1.6 $\mu_B$ (FM1) and 1.9 $\mu_B$ (FM2) at equilibrium volume differ substantially from the experimental values of 0.9 and 1.5 $\mu_B$ , respectively [4].

In order to improve description of the magnetic properties, we select Hubbard-$U$ (= $F_0$) equal to the value of $J$. With this artificial choice of $U$, all spherically-symmetric terms in the

«+*U*» part of the rotationally invariant DFT+U functional are set to zero, and remaining spin and orbitally dependent DFT+U terms include the orbital polarization (OP) and spin-flips beyond that given by DFT. This (*U=J*) approximation can be regarded as the OP-limit of DFT+U. It gives the $V_{eq}$ = 790 (a.u.)$^3$ for both the FM1 and FM2. The FM2 state is a ground state, and the FM1 solution has 0.15 mRy higher total energy, and lower magnetic moment $\mu_{tot}$ . We find good correspondence of the calculated spin, orbital, and total magnetic moments (see Table I.) for FM2 state to the experimental XMCD results [5], and the results of polarized neutron scattering [3]. The difference between strongly magnetically polarized FM2 and weakly polarized FM1 states is found to stem from the difference in $|j, m_j>$-resolved densities of 5f-states.

Table I. Spin ($\mu_S$), orbital ($\mu_L$), magnetic dipole moment ($\mu_D$), the ratio $R_{LS}$ ( $-\mu_L/\mu_S$ ) , and total magnetic moment $\mu_{tot}$ ($\mu_S + \mu_L$) in $\mu_B$ units for the 5f-shell of U atom, calculated in the limit OP-limit.

| P = 0 kbar | $\mu_S$ | $\mu_L$ | $\mu_D$ | $R_{LS}$ | $\mu_{tot}$ |
|---|---|---|---|---|---|
| FM1 | -1.35 | 2.75 | -2.03 | 2.03 | 1.40 |
| FM2 | -1.34 | 2.92 | -2.33 | 2.18 | 1.58 |

In order to analyse the effect of pressure, we used the experimental data for the pressure dependence of the volume $V/V_0$, lattice constants $a/a_0$ and $c/c_0$ [6]. The OP-limit calculations show that the orbital differentiation of nearly degenerate the FM2 and FM1 solutions remains unchanged. This difference in $|j, m_j>$ spin-orbital occupations of the FM2 and FM1 leads to the 0.2 $\mu_B$ difference in the total magnetic moment $\mu_{tot}$ , and can explain the experimentally observed 0.6 $\mu_B$ change in the magnetization under pressure [4]. The DFT+U in the OP-limit results suggest the change of the orbital-to-spin moments ratio $R_{LS}$ = 2.2-2.3 (FM2) > $R_{LS}$ = 2.0 (FM1) in good quantitative agreement with experimental XMCD data [5].

Financial support was provided by Operational Programme Research, Development and Education financed by European Structural and Investment Funds and the Czech Ministry of Education, Youth and Sports (Project No. SOLID21 – CZ.02.1.01/0.0/ 0.0/16_019/0000760).

## References

[1] S. S. Saxena *et al*., Nature (London) **406**, 587 (2000).
[2] A. B. Shick, V. Janiš, V. Drchal, W. E. Pickett, Phys. Rev. B **70**, 134506 (2004).
[3] N. Kernavanois, B. Grenier, A. Huxley, E. Ressouche, J.-P. Sanchez, J. Flouquet, Phys. Rev. B **64**, 174509 (2001).
[4] C. Pfleiderer and A. D. Huxley, Phys. Rev. Lett. **89**, 147005 (2002).
[5] F. Wilhelm, J.–P. Sanchez *et al*., unpublished (2018).
[6] G. Oomi, M. Ohashi, K. Nishimura, and Y. Ōnuki, J. of Nucl. Sci. and Techn. **39**, sup3, 90 (2002).

# First principles DFT+DMFT and DFT+U calculations of structural properties of actinides

**B. Amadon, J.B Morée, B. Dorado**

*CEA DAM DIF F-91297 Arpajon, France, e-mail:bernard.amadon@cea.fr*

We first use an ab initio calculation of effective Coulomb interactions to show that effective direct Coulomb interactions in plutonium and americium are much smaller than usually expected. Then we use DFT+U and DFT+DMFT calculation to compute the structural properties of pure actinides and phase of plutonium[1][2]. We emphasize the key role of spin orbit coupling and Hund's exchange in these calculations. With these calculations, we reproduce the experimental transition from low volume early actinides (uranium, neptunium, α-plutonium) to high-volume late actinides (δ-plutonium, americium, and curium) and a good agreement of volume of phases of plutonium with experiment. We also discuss phonons spectra of plutonium, and we discuss values of effective interactions U in the light of recent calculations [3].

## References

[1] B. Amadon Phys. Rev. B **94**, 115148 (2016), Phys. Rev. B 97, 039903 (2018).
[2] B. Amadon and B. Dorado J. Phys.: Condens. Matter **30** 405603 (2018).
[3] J.B. Morée and B. Amadon Phys. Rev. B 98, 205101 (2018).

# Strong and weak adsorption of $CO_2$ on $PuO_2$(110) surfaces from first principles calculations

**Huilong Yu,[1] Xiaodi Deng[2], Gan Li[1], Daqiao Meng[1]**

*[1] Insititute of Materials China Academy of Engineering Physics, Mianyang City Sichuan Province,China, 621907, e-mail: yuhuilong2002@126.com*
*[2] Department of Engineering Physics, Tsinghua University, Beijing 100084, China*

Plutonium is an important nuclear material in some nuclear reactors as a source of energy, which is generated in an operating nuclear reactor due to transmutation of uranium. In dry air, metallic plutonium behaves much like other active metals, the plutonium dioxide ($PuO_2$) layer is formed and a thin layer of plutonium sesquioxide ($Pu_2O_3$) is followed on plutonium surfaces [1-2]. $PuO_2$ may be exposed to carbon dioxide in $CO_2$-cooled nuclear reactors and other applications, a knowledge of the adsorption mechanism of this gas on $PuO_2$ is necessary to understand subsequent oxidation of this metal in $CO_2$ [3].

The $CO_2$ adsorption on Plutonium dioxide ($PuO_2$) (110) surface was studied using projector-augmented wave (PAW) method based on density-functional theory corrected for onsite Coulombic interactions (GGA+U). It is found that $CO_2$ has several different adsorption features on $PuO_2$ (110) surface. Both weak and strong adsorptions exist between $CO_2$ and the $PuO_2$ (110) surface. Further investigation of partial density of states (PDOS) and charge density difference on two typical absorption sites reveal that electrostatic interactions were involved in the weak interactions, while covalent bonding was developed in the strong adsorptions.

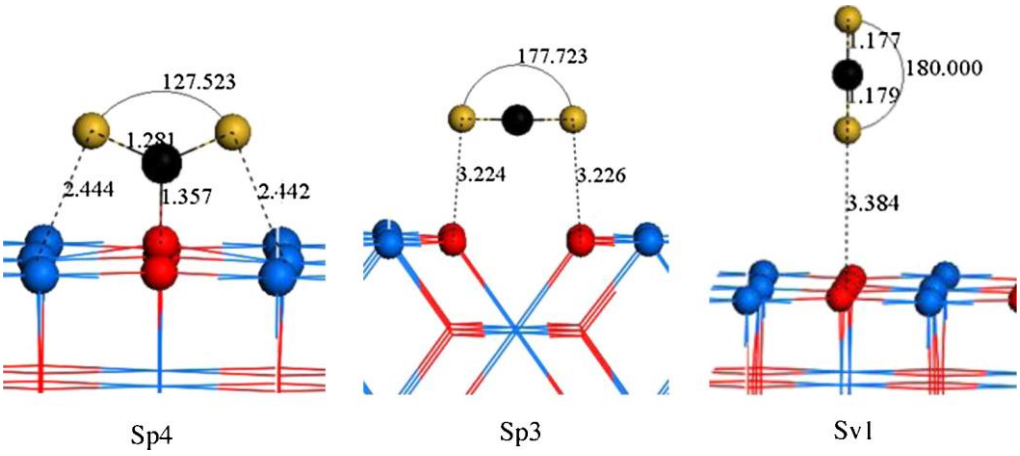


Fig. 1. $CO_2$ adsorption on $PuO_2$ (110) in the configurations of Sp4, Sp3 and Sv1.

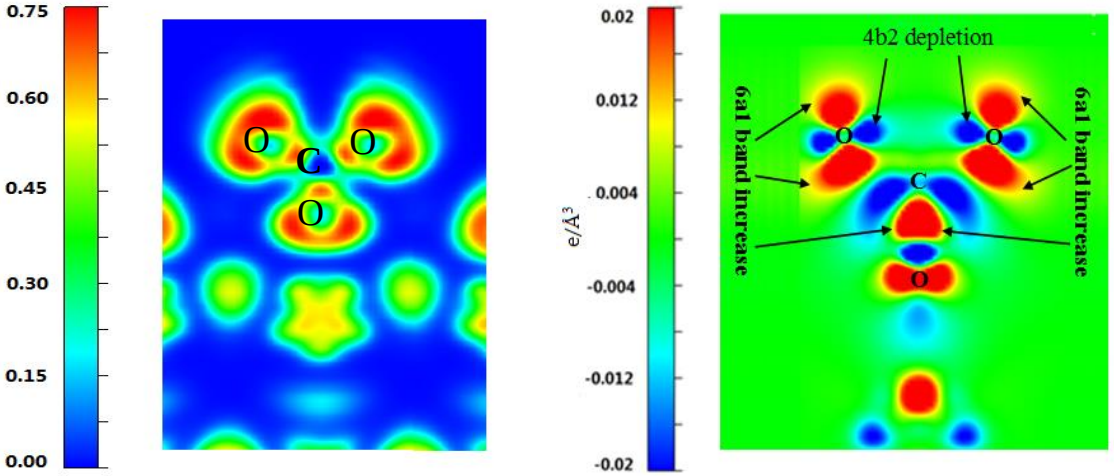


(a) (b)

Fig. 2. Bonding of $CO_2$ on the $PuO_2$ (110) for strong adsorption, (a) contours for the ELF in a tilted plane passing through $CO_2$ ; (b) contours for the CDD in the same plane.

## References

[1] D.H. Templeton, Carol H. Dauben, University of California Radiation Laboratory Report July 1952, Report No.UCRL-1886.
[2] J.M. Haschke, T.H. Allen, L.A. Morales, Surface and corrosion chemistry of plutonium, Los Alamos Sci. 252-273, 26 (2000 .
[3] C.A. Colmenares, K. Terada, The adsorption of carbon dioxide on uranium and plutonium oxides, J. Nucl. Mater. 336 -356, 58 (1975).

# Study of atomic structure and electron structure of uranium oxide and nitride

**R.G. Zeng[1,2], Y.W. Zhao[1], T. Fa[1], Y. Hu[1], B. Bai[1], K.Z. Liu[1] and H. Tian[2]**

*[1]Institute of Materials, China Academy of Engineering Physics, Mianyang, Sichuan 621907, China, e-mail: zengrongguang@caep.cn*
*[2]Center of Electron Microscopy, Zhejiang University, Hangzhou 310027, China*

The actinides are of great interest to the physics and chemistry communities due to the intriguing and unique physical and chemical properties they exhibit as a result of the complicated electronic structure of 5f states [1]. In this study, we aim to explore the electronic structure of complex 5f state of uranium in uranium-based materials. The atomic resolution aberration corrected scanning transmission electron microscopy combined with electron energy loss spectroscopy (STEM-EELS) has been employed to investigate the local atomic and electronic structure for uranium and uranium alloys and oxides at the sub-angstrom scale. How these 5f states evolve with the change in crystal structure, alloying and oxidation state are studied. Through comparison with the first principles calculations and simulation results, the characteristics of 5f electronic structure will allow to explain its unique physical and chemical properties.

Uranium dioxide is the most widely used nuclear fuel for the generation of electrical power. A detailed knowledge of the electronic structure of uranium dioxide is crucial for the benchmarking of the theoretical modelling because of their importance in the pursuit of safety within nuclear power generation. Hence, uranium and uranium dioxide have been studied for many decades with an immense variety of theoretical models and electron spectroscopic techniques. With the use of aberration corrected atomic resolution STEM-EELS technique, we have studied the local atomic and electronic structure of $UO_2$ at sub-angstrom scale, and hence to explore how the atomic structure and 5f states evolve with oxidation state. The atomic resolution ADF-STEM image of $UO_2$ is obtained for the first time, as shown by Fig. 1. The atomic number ratio, $Z_U/Z_O$, is as large as 11.5, it is hard to observe the oxygen atoms [2] in STEM image of $UO_2$. Combined with the simulation, we have confirmed the oxygen atomic site occupation in the ADF-STEM image.

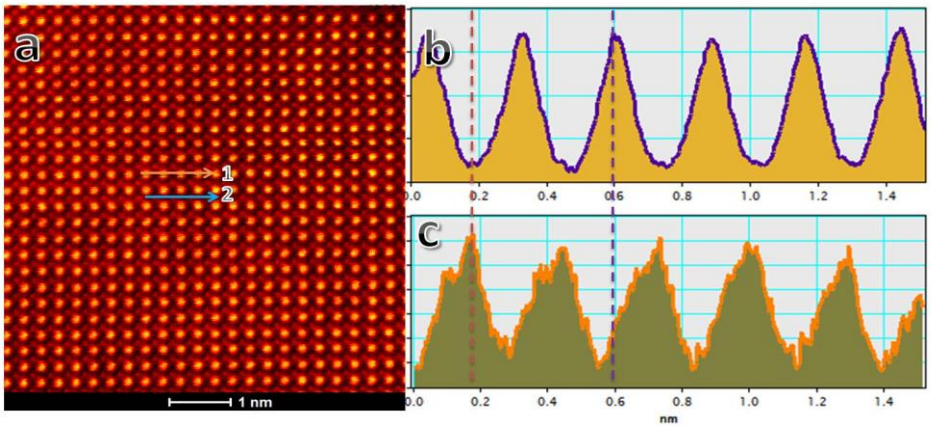


Fig. 1 (a) Experimental ADF-STEM image of $UO_2$ (001) face, whose line profiles along arrows 1 & 2 indicate respectively the (b) uranium and (c) oxygen atomic sites.

EELS is used to characterize changes in the bulk electronic structure. To investigate the 5f states of actinide elements the transitions from d core states are considered because they

directly probe the f states by the electric-dipole transitions $\Delta l = \pm 1$; the core 4d states can only be excited to specific 5f final states. Experimental O4,5 and N4,5 EELS spectra of UO2 are measured to discern fundamental aspects of the electronic structure of the 5f states, whose peak intensity gives information about occupation of the 5f states. We present the branching ratio of N4,5 edge of UO2, which is due to dipole selection rules.

Uranium nitrides are also important to nuclear industry. An oxide layer will be formed on the surface of nitrogen-rich uranium nitride (UN2-x) after a long-term exposure to air [3]. The surface composition, electronic structure and microstructure of the oxide layer are studied by using X-ray photoelectron spectroscopy (XPS), Auger electron spectroscopy (AES), and STEM-EELS. XPS and AES studies show that the oxide layer is a kind of ternary compound uranium oxynitride (UNxOy) with nanometer-scale thickness. The high-angle annular dark-field (HAADF) images combined with the EELS signals indicate the UNxOy layer covered on the single grain of UN2-x is not existed in an amorphous state and is coherently related to the UN2-x matrix. The lattice spacing of UNxOy matches well with the cubic UN2 phase. The work provides a microscopic insight into UNxOy crystal structure and is promising for exploring the oxidation mechanism of uranium nitride.

**Acknowledgements**
This work was supported by the National Natural Science Foundation of China Grant (Nos. 51701192 and U1630250).

**References**

[1] S.G. Minasian, J.M. Keith, E.R. Batista, K.S. Boland, D.L. Clark, S.A. Kozimor, R.L. Martin, D.K. Shuh, T. Tyliszczak, *Chem. Sci.* **5**, 351-359 (2014).
[2] H. Yang, R.N. Rutte, L. Jones, M. Simson, R. Sagawa, H. Ryll, M. Huth, T.J. Pennycook, M.L.H. Green, H. Soltau, Y. Kondo, *Nature Commun*. **7** 12532 (2016).
[3] L. Lu, F. Li, Y. Hu, H. Xiao, B. Bai, Y. Zhang, L. Luo, J. Liu, K. Liu, *J. Nucl. Mater*. **480** 189 (2016).

# Radioactive strengthening and nanopolycrystalline structure interplay in model Pu-Ga alloys: atomistic simulations

**A.V. Karavaev, V.V. Dremov, F.A. Sapozhnikov**

*Russian Federal Nuclear Center – Zababakhin Institute of Technical Physics (RFNC-VNIITF), 13 Vasiliev St., Snezhinsk, Chelyabinsk Region 456770, Russia, e-mail: a.v.karavayev@vniitf.ru*

It is well known that the mechanical properties of nanocrystalline materials differ dramatically from those of conventional ones [1]. In particular, the yield strength noticeably grows as grain size decreases. For many materials in the range of grain sizes larger than ~100 *nm* this effect can be described by the well-known empirical Hall-Petch (HP) relation $\sigma_y=\sigma_0+\kappa/d^{1/2}$, where $\sigma_y$ is the yield stress, $\sigma_0$ and $\kappa$ are empirical material constants, and $d$ is the average grain size. When the grain size gets smaller there is an increasing deviation from the HP relation [1]. On the other hand, the grain size is not the only factor affecting the yield stress. The in-grain extended defects such as dislocations and stacking faults also contribute to the shear strength of materials. For irradiated or self-irradiated materials like plutonium and its alloys radiation defects are another factor affecting the mechanical properties.

Modification of the mechanical properties of plutonium and its alloys via grain refinement is of interest because of their use in civil and military nuclear technologies, for example, as a component of metallic nuclear fuel. In the present work the atomistic simulation approach is applied to directly calculate the mechanical properties of nanocrystalline face centered cubic (fcc) δ-phase Pu-Ga alloys, in particular, the quasi-static yield stress dependence on the grain size and extended defects concentration. The range of grain sizes studied is 40-200 *nm*. A deviation from the HP relation is demonstrated. The effect of alloying addition redistribution inside grains as well as between the grains is also evaluated.

Present work demonstrates modern capabilities of large-scale classical molecular dynamics simulations (MD) in modeling the strength properties of real materials. These simulations are based on the model of interatomic interactions only and provide for the reliable results if it is properly parameterized. The technique of simulations developed in [2,3] allows to directly model elastic-plastic response of nanocrystalline materials to quasi-static loadings and calculation of the yield stress.

There are two techniques used to generate the samples for the MD simulations. The first one is to divide a box $L_x \times L_y \times L_z$ into a given number of Voronoi cells and then fill them with Pu and Ga atoms arranged in the fcc lattice with respect to a given Ga concentration and a random Ga distribution as disordered substitution solution. The mutual spatial orientation of the fcc lattices in the cells may be chosen as a random. The algorithm of the nanocrystalline sample construction provides for the samples under periodic boundary conditions. An advantage of this option is the construction of nanopolycrystallines free of defects in the bulk of the grains. One also has an a priori opportunity to choose the number of grains and their average size. The samples prepared with this technique are designated hereafter as V-samples.

The second option to construct nanopolycrystalline samples is to perform MD simulations of the crystallization from the liquid state. First, the molten state is equilibrated at temperature above the melting point and ambient pressure in *NPT*-ensemble. Then the temperature gradually decreases down to the δ-phase stability range, and then we have to wait for the crystal structure nucleation. At this point it is difficult to control the number of nanocrystalline nuclei and the number of grains after full crystallization. However, following increase of the system temperature and further modeling of the sample annealing leads to recrystallization and grain coarsening. Finally, the samples are gradually cooled down to

ambient temperature and equilibrated at zero stress tensor. To control the average grain size in this sample preparation technique one can cool the samples down to ambient temperature from different recrystallization process instances. An advantage of this technique is that one gets nanopolycrystallines with non-artificial grain shapes and boundaries between them. A disadvantage is a rather complicated and long CMD simulation needed to get the samples with the required average grain size. The main feature of such samples is a high concentration of extended defects (dislocations and stacking faults) in the bulk of the grains due to the natural process of crystallization. During the annealing stage the number of in-grain defects significantly decreases but stays nevertheless at a rather high level. The samples prepared with this technique are designated hereafter as M-samples.

Obtained for the δ-phase Pu-Ga nanocrystalline alloys results (see Fig. 1) evidence that there is no universal HP dependence for the material. Shear strength is determined not only by the average grain size but also by the material origin and processing history. Annealing of the defects in M-samples would gradually lead to approaching of their yield stress to that of V-samples. However, the annealing of the defects is accompanied by the grain coarsening. So one may consider the data obtained for M and V-samples as upper and lower limits for the yield stress of δ-phase Pu-Ga alloy with a given Ga concentration, while re-distribution of Ga atoms in the grains has little effect on the yield stress. The results of the MD simulations evidence that the radioactive strengthening effect due to accumulation of radiogenic nm-sized He bubbles [2] in nanopolycrystalline fcc Pu-Ga alloys is leveled down by the interaction of dislocations and stacking faults with the developed grain boundaries.

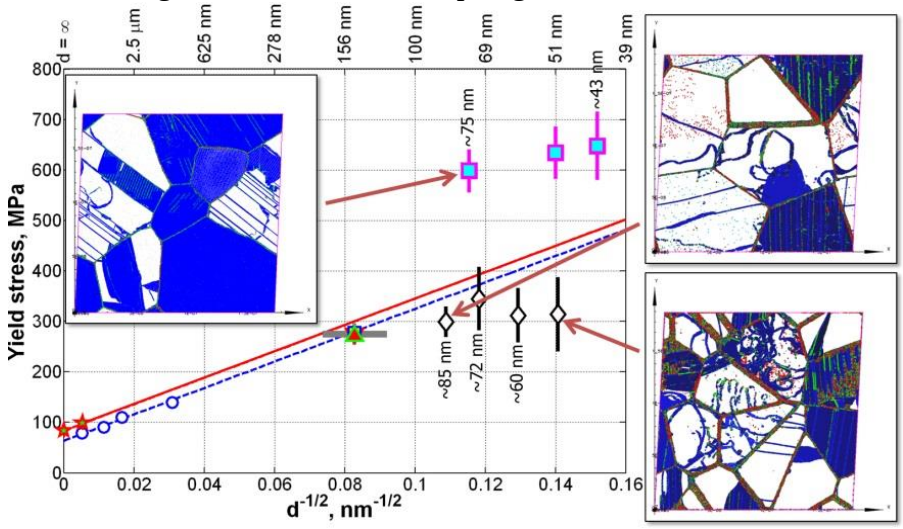


Fig. 1. The yield stress of fcc δ-phase Pu-Ga alloys *vs.* the grain size. Blue circles and blue dashed line represent experimental measurements and the HP relation for Pu-1 wt. % Ga [4]. Red pentagrams represent MD results for Pu-4 at. % Ga [2]. To get the value of the shear strength for the average grain size 35 μm using MD we calculated $Y_\infty$ [2] and then $Y_{35\mu m}$ using the HP relation [4]. Red solid line is for the HP relation for Pu-4 at. % Ga. Symbols with horizontal confidence bands represent results of the MD simulations for the V-samples with various Ga distributions in the grains: uniform Ga distribution, Ga distribution imitating the micro-liquation effect, samples with uneven distribution of Ga atoms among the grains. Black diamonds and magenta squares represent MD results for the samples with low and high initial in-grain defect concentrations: V-samples and M-samples, correspondingly. Insets show defect structure of the samples at the end of the simulations. One can see grain boundaries, dislocations and stacking faults. No fcc structure atoms are shown.

## References

[1] M.A. Mayers *et al.*, *Progr. Mat. Sci.* **51**, 427 (2006).
[2] A.V. Karavaev *et al.*, *EPJ Web of Conf.* **4**, 04007 (2015).
[3] A.V. Karavaev *et al.*, *J. Nucl. Mater.* **496**, 85 (2017).
[4] A.D. Wheeler *et al.*, in: W. Miner (Ed.), *Plutonium 1970 and Other Actinides*, Metallurgical Society of AIME, New York, 437 (1971).

# Boron coordination tuned electronic structure of plutonium borides

**Haiyan Lu, Bingyun Ao, Li Huang**

*Institute of Materials, China Academy of Engineering Physics, 621908, Jiangyou, China,*
*e-mail: hyluphys@163.com*

The detailed electronic structure and localized-itinerant dual nature of Pu-5*f* valence electrons for four plutonium borides (PuB, $PuB_2$, $PuB_6$, $PuB_{12}$) are investigated by using the combination of density functional theory and single-site dynamical mean-field theory. The momentum-resolved spectral functions and density of states consistently display metallic behavior except that $PuB_6$ exhibits topological feature. Particularly, the orbital-selective 5*f* states indicate the metallic $5f_{5/2}$ and insulating $5f_{7/2}$ electrons. Besides, the typical quasiparticle multiplets appear around the Fermi level, accompanied by significant valence fluctuations, revealing the mixed-valence nature. The charge redistribution and 5*f* occupancy tuned by boron chemical composition lead to the fantastic Pu-B bonding behavior, so as to modulate localized to itinerant crossover of 5*f* states. Consequently, the understanding of electronic structure and related crystal structure stability shall shed light on exploring novel 5*f* electrons states and ongoing experiment.

# Machine Learning Prediction of Novel Uranium-based High Entropy Alloys

**He Huang,[1,2] Yawen Zhao[1], Xin Wang[1], Tao Fa[1]**

[1] *China Academy of Engineering Physics, Mianyang 621900, PR Chin, e-mail:hehua@kth.se*
[2] *Applied Materials Physics, Department of Materials Science and Engineering, Royal Institute of Technology, Stockholm SE-10044, Sweden*

Uranium-based high entropy alloys can be used as an important candidate for fission fuels in future. Three uranium-based solid solution alloys with bcc structure and five elements were successfully predicted by machine learning and verified by experiments. The calculation results show, electronic structure is the characteristic variable which influences the formation of solid solution phase. The compressed yield strength of the alloy with double bcc structures is about 1.2 GPa and higher than that of other two alloys with single bcc structure. The reason for differences of compression property among these alloys is furtherly analyzed by various characterizations, such as SEM, TEM and EBSD.

# Ammonolysis of Uranium Oxides

**S.E. O'Sullivan,[1] S.K. Sun[1], M.C. Stennett[1], N.C.Hyatt[1]**

*[1] Department of Materials Science & Engineering, University of Sheffield, Sir Robert Hadfield Building, Mappin Street, Sheffield, S1 3JD, UK, e-mail: seosullivan1@sheffield.ac.uk*

Reactions of uranium compounds with ammonia are frequently reported in the field of nitride synthesis. However these preferentially use uranium halides, carbides or metal as a starting reactant [1-4]. The reaction of uranium oxide compounds with ammonia is more scarcely reported [5, 6] and is aided by carbothermal reduction additives. Here we present the results of the direct ammonolysis of uranium oxides without reducing agents.

In this work, reactions of powder $UO_2$, crystalline and amorphous $UO_3$,, and $U_3O_8$ with flowing ammonia gas (ammonolysis) have been undertaken, investigating the effects of the three principal variables: temperatures between 600 and 1100ºC, $NH_3$ flow rates between 75 and 300ml/min and reaction durations of 2 to 16 hours. Reaction of $UO_2$ under 300ml/min $NH_3$ for 16h at 1100ºC shows the most interesting results. A distinct colour change is observed from black to dark orange, a colour more often associated with treatment of urania under oxidising conditions. This orange colour is not reported in previous literature of high nitrogen content $UO_2$ [6] and is also not seen in the simple reduction of $UO_{2+x}$ to $UO_2$. Therefore, the colour attributed to nitridation of the samples by the $NH_3$ atmosphere. The colour change has been quantified using image analysis techniques to extract RGB histogram values (fig. 1).

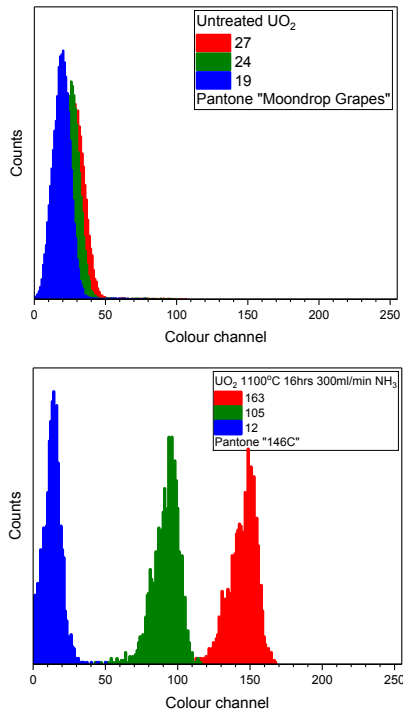


Figure 1. Comparison of RGB colour measurements between untreated $UO_2$ (upper) and product of 1100ºC, 16h, 300ml/min $NH_3$ $UO_2$ ammonolysis (lower) with average RGB values and corresponding Pantone colour name.

X-ray diffraction of the product indicates a consistent fluorite structure of the $UO_2$ but with an increased cell volume post ammonolysis. A calculated lattice parameter of 5.4711 +/- 0.0002 Å ($R_{wp}$ = 10.846, goodness of fit = 2.85) represents a marked expansion from the starting material. This is achieved with minimal changes to the powder morphology as seen in SEM characterisation.

The results presented will discuss additional characterisation of the compounds, including TG-MS and XPS measurements. Further to this, expansion of the project to the ammonolysis of higher order uranium oxides, such as alkali earth uranates, will also be discussed.

## References

[1] C.B Yeamans, et al., *Journal of Nuclear Materials* **374,** 75 (2008).
[2] T. Ogawa et al., *Journal of Nuclear Materials* **247,** 151 (1997).
[3] T. Nakagawa et al., *Journal of Nuclear Materials* **247,** 127 (1997).
[4] M. Katsura, H. Serizawa, *Journal of Alloys and Compounds* **187,** 389 (1992).
[5] T. Moromura, H. Tagawa, *Journal of Nuclear Materials* **71,** 65 (1977).
[6] P. Balakrishna et al., *Nuclear Technology* **150:2,** 189 (2005).

# Electronic structure of f-element Prussian blue analogs by soft X-ray absorption spectroscopy

**Thomas Dumas,[1] Christophe Den Auwer[1], Clara Fillaux[1], Dominique Guillaumont[1], Philippe Moisy[1], Tolek Tyliszczak[2], David Shuh[2]**

*[1]CEA, Nuclear Energy Division, Radiochemistry Process Department, SCPS/LILA F-30207 Bagnols sur Cèze, France,*
*e-mail: thomas.dumas@cea.fr*
*[2] Chemical Sciences Division, Berkeley Lab, 1 Cyclotron Rd MS6R2100 Berkeley, CA 94720, EU*

Bimetallic cyanide molecular solids derived from prussian blue are well known as building blocks with long-range magnetic ordering and itervalence charge transfer (IVTC) occurring through unoccupied cyano π* orbitals. Structurally speaking, these 3d transition metal Prussian Blue Analogs (PBA) derivatives generally form cubic phases. For the trivalent lanthanides PBA, both hexagonal and orthorhombic phases have been described (Figure 1.a). In the case of tetravalent actinides analogs (Th to Pu), EXAFS and XRD have been used to show that An(IV)-PBA are isomorphous to the early lanthanide (La-Nd) PBA [1, 2, 3]. Interestingly, the optical spectra of uranium, neptunium and plutonium compounds show intense IVTC bands similar to the transition metal PBA whereas the lanthanides PBA are not (Figure 1b). Moreover FTIR indicates a modification in the cyano bonds elongation energy as a function of the actinide electronic configuration that is not observed in the lanthanide cases (Figure 1c). These results are indirect evidence of a change in the cyano/metal bonding modes from the trivalent lanthanide to the tetravalent actinides.

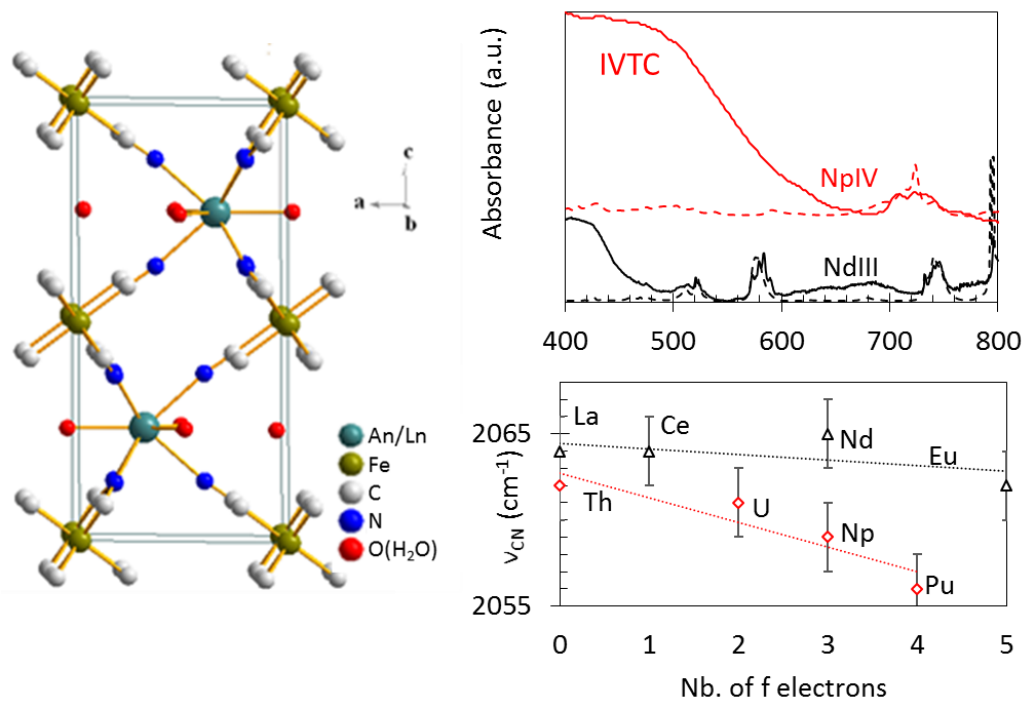


Fig. 1 (a) An/Ln-PBA structure. (b) UV-Vis absorption spectra of Nd(III) and Np(IV) in aqueous solutions (black and red dotted lines respectively) and the reflectance spectra of Nd-PBA and Np-PBA (black and red full lines). Spectra are rescaled and offset vertically for clarity. (c) νCN stretching frequencies for the An-PBAs and Ln-PBAs as a function of the number of f electrons.

To probe directly the valence molecular orbitals, we used soft X-ray spectroscopy. It brings essential information about the cyano and iron molecular orbitals using complementary nitrogen

and carbon K edges and iron $L_3$ edges to probe both the cyano and the iron LUMO orbitals. Overall, the soft X-ray absorption spectra highlight the strong An(IV) ability to modify the ferrocyanide electronic structure. In contrast, le trivalent lanthanide weakly interact and the ferrocyanide electronic structure remains unaltered. (Figure 2a.b.) [4, 5]

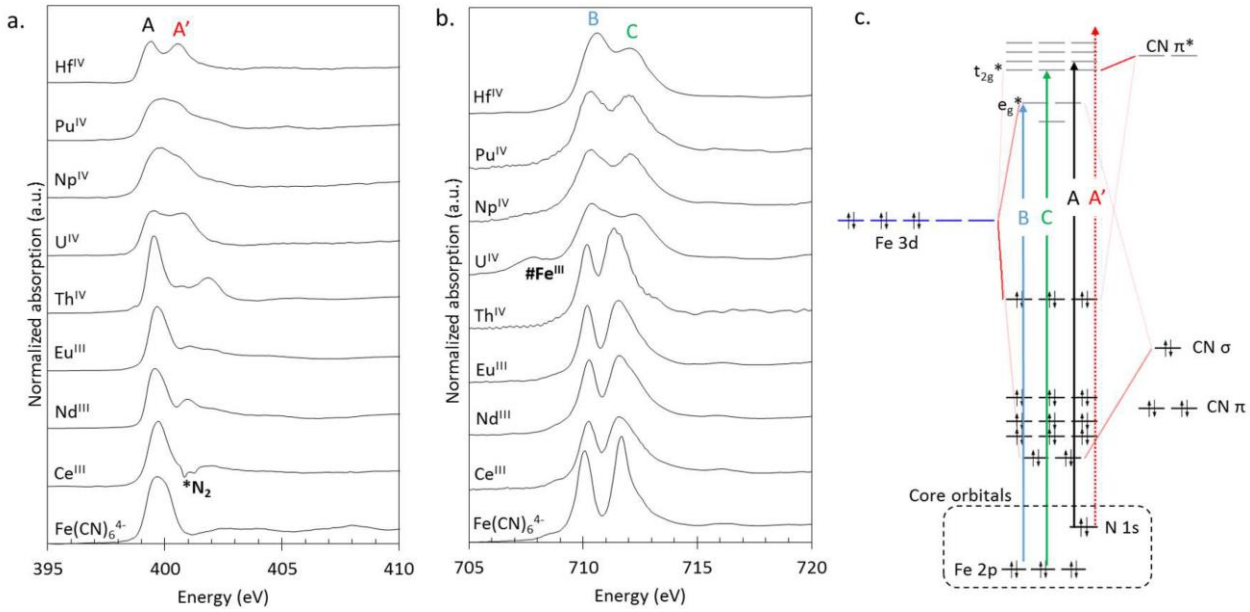


Fig. 2 N K edge (a.) and Fe L3 edge (b.) spectra for 5f and 4f PBAs, along with K4[Fe(CN)6] and Hf PBA reference spectra. *N2 indicates spurious spectral features due to molecular nitrogen contamination and #FeIII a ferricyanide contamination in the air sensitive UIV-PBA (transition to the eg orbital in FeIII complexes). c. Molecular orbital diagrams calculated by DFT calculation in a fixed geometry for K4[Fe(CN)6] (interactions between Fe2+ and CN- fragments also showing unoccupied MO's and the core hole orbital involved in the XAS process).

Theoretical chemical calculations were used to assign the nitrogen and carbon K edge spectra features in the ferrocyanide and in the Th(IV)-PBA compound.[4] It indicates that both Th 6d and 5f orbitals are in interaction with the cyano π* orbitals which are split as experimentally observed. Covalency versus ionicity, charge transfer and back-bonding effects are discussed in view of theoretical results and analogous soft X-ray studies on actinides and lanthanides chloride complexes [6, 7].

## References

[1] I. Bonnoure et al., *Can.J.Chem* 1305-1317, (2000)
[2] G. Dupouy et al., *Eur. J. Inorg. Chem*, 1560–1569, (2011).
[3] T. Dumas et al., *New J. Chem.*, **37**, 3003–3016, (2013).
[4] T. Dumas et al., *Phys. Chem. Chem. Phys.*, **18**, 2887–2895, (2016).
[5] T. Dumas et al., *Chem. Commun.*, **54**, 12206–12209, (2018).
[6] M. W. Löble et al. *J. Am. Chem*. Soc. **137**, 2506−2523 (2015)
[7] J. Su et al. *J. Am. Chem. Soc.* **140**, 17977−17984 (2018)

# Partial sonochemical conversion of nanostructured $ThO_2$ into 1D Th(IV) peroxo sulfate

**L. Bonato,[1] M. Virot[1], T. Dumas[2], A. Mesbah[1], D. Prieur[3], P. Moisy[2], S. I. Nikitenko[1]**

*[1] Institut de Chimie Séparative de Marcoule (ICSM) – UMR5257, CNRS/CEA/UM/ENSCM, Site de Marcoule, 30207 Bagnols sur Cèze, France, e-mail: laura.bonato@cea.fr*
*[2] CEA/DEN/MAR/DMRC, Nuclear Energy Division, Radiochemistry and Process Department, 30207 Bagnols sur Cèze, France*
*[3] European Commission, Joint Research Centre (JRC), Postfach 2340, 76125 Karlsruhe, Germany*

Nanostructured materials can be defined as materials with a microstructure the characteristic length scale of which is on the order of a few (typically 1-10) nanometers [1]. Nanostructured materials is an important subject of study because of their interesting physical and chemical properties potentially optimized through their size, morphology and structure. The nanoscale particles that compose these materials have a large surface-to-volume ratio and provide a greater amount of active sites compared to bulk materials. Therefore, nanostructured materials may find applications in catalysis, biomedical, synthesis of luminescent materials, etc. Nanostructuring of actinide oxides and their subsequent reactivity is scarcely reported in the literature [2]. Recent studies however demonstrate that nanostructuration of plutonium oxide appears to play a key role in the sonochemical formation of Pu colloids in aqueous solutions [3].

The sonochemical behavior of nanostructured thorium oxides prepared by oxalic route is investigated in this work. After characterization, the 20 kHz sonochemical reactivity of these oxides was studied in dilute aqueous solutions under Ar/20%$O_2$ bubbling. The effects of cavitation on solid materials were studied with Raman spectroscopy, XRD, SEM and HR-TEM, while the liquid medium was characterized by UV-vis and ICP-AES spectroscopies. Despite its very refractive behavior, a significant amount of $ThO_2$ was found to dissolve in sonicated 0.5 M $H_2SO_4$ solution. In more dilute acidic conditions, a lower dissolution rate of $ThO_2$ was observed. In these media, the sonicated nanostructured $ThO_2$ can be partly converted into a new crystalline phase which can be attributed to the physical and chemical effects driven by the acoustic cavitation phenomenon which allows: (i) the oxide particle fragmentation and size reduction, and (ii) the sonochemical generation of $H_2O_2$. This compound was then prepared in homogeneous solution in the absence of ultrasound via precipitation technique. Thermogravimetric analysis, Raman and FTIR spectroscopies coupled to synchrotron X-Ray Diffraction and EXAFS spectroscopy evidenced the formation of a thorium peroxo sulfate (Fig. 1), poorly referenced in the literature and for which a structure has never been reported. Computer simulation of the X-Ray and EXAFS data allowed to propose a 1D crystal structure of obtained $Th(O_2)SO_4(H_2O)_2$ complex in agreement with other analytical results.

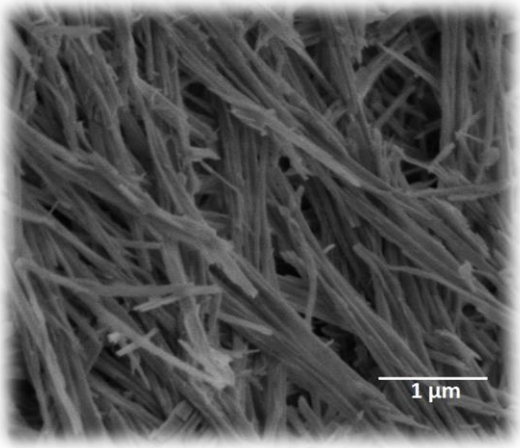


Fig. 1. SEM image obtained for the Th peroxo sulfate.

## References

[1] H. Gleiter et al., *Acta Materialia* **48**, 1-29 (2000).
[2] V. Tyrpekl et al., *Journal of Nuclear Materials* **460**, 200-208 (2015).
[3] E. Dalodiere et al., *Scientific Reports* **7:43514**, 1-10 (2017).

# Thermal decomposition of β-$UH_3$ powder: Kinetics and mechanism

**Roey Ben David[1], Noa Bitton[2], Fredi Simca[2], Shmuel Samuha[2], Dvir Fadel[1], Tzachi Eretz-Kedosha[2], Natalie Kostirya[2], Genadi Agronov[2], Albert Danon[2], Yacov Finkelstein[2]**

*[1] Israel Atomic Energy Commission (IAEC), Tel-Aviv, 61070, Israel, e-mail: Roeybd@gmail.com*
*[2] Nuclear Research Center Negev (NRCN), Beer-Sheva, 84190, Israel*

The kinetics and mechanism of uranium hydride ($UH_3$) formation and decomposition (dehydrogenation) are of considerable interest in the nuclear industry regarding the fields of uranium corrosion, solid-state hydrogen storage and safety of uranium fuels and uranium nuclear waste storage. While the hydrogenation reaction of uranium was extensively studied in the literature, relatively limited information exists regarding the counter process, i.e. the dehydrogenation reaction, including its kinetics and underlying mechanism [1].

In the current work, hydrogen desorption kinetics from β-$UH_3$ powder was investigated by means of temperature programmed desorption – mass spectrometry (TPD-MS) under a flow of He carrier gas, and at either isothermal or non-isothermal conditions [2]. The studied β-$UH_3$ powder was prepared by reacting a raw α-U sample with $H_2$ gas (gas-solid hydrogenation) via four consecutive hydrogenation-dehydrogenation cycles. The as synthesized powder was systematically characterized in terms of hydride phase (XRD), particles size and morphology (SEM). The resulting isothermal and non-isothermal hydrogen desorption profiles indicate unambiguously that dehydrogenation process of β-$UH_3$ follows a zero-order kinetics with an activation energy of 102-104 kJ/(mol $H_2$). By accounting for the observed kinetics and comparing the activation energy against reported density functional theory (DFT) values [3-4], a surface controlled mechanism, limited by surface recombination of hydrogen atoms, is proposed.

## References

[1] A. Banos, N.J. Harker, T.B. Scott, *Corros. Sci* .**136**, 129 (2018).
[2] R. Ben David et al., *J. Nucl. Mater.* **510**, 484 (2018).
[3] C.D. Taylor, R.S. Lillard, *Acta Mater.* **57**, 4707 (2009).
[4] J.L. Nie, H.Y. Xiao, X.T. Zu, F. Gao, *J. Phys.: Condens. Matter* **20**, 1 (2008).

# Use of Uranyl Nanoclusters containing Rare-Earth Cations as an Innovative Route for the Preparation of Mixed-Oxides Pellets.

**P-H. Imbert[1], F. Abraham[1], J. Nos[2], M.O.J.Y. Hunault[3], A. Addad[4], O. Tougait[1]**

*[1] Univ. Lille, CNRS, Centrale Lille, ENSCL, Univ. Artois, UMR 8181 - UCCS - Unité de Catalyse et Chimie du Solide, F-59000 Lille, France., e-mail: olivier.tougait@univ-lille.fr*
*[2] Orano, 1 Place Jean Millier, 92084 Paris La Défense, France*
*[3] Synchrotron SOLEIL, L'Orme des Merisiers Saint-Aubin, 91192 Gif-sur-Yvette, France*
*[4] Université Lille, CNRS, ENSCL, UMR 8207 - Unité Matériaux Et Transformations (UMET), F-59000 Lille, France*

Mixed $U^{6+}/Pu^{4+}$ solid compounds precipitated from aqueous solutions are regarded as possible precursors for MOX nuclear fuel, consisting of a $(U,Pu)O_2$ solid solution with fluorine type of structure. To this respect, the recent advances in the synthesis by cationic exchange within uranyl peroxide nanoclusters of ammonium ions by trivalent rare-earth ($Nd^{3+}$, $Ce^{3+}$) or tetravalent thorium ($Th^{4+}$) ions, used as transuranium surrogates, afford the opportunity of an innovative route for pellet manufacturing [1]. The uranyl peroxide nanoclusters $(NH_4)_{40}[(UO_2)_{32}(O_2)_{40}(OH)_{24}].nH_2O$ [2] was selected for this aim. It instantaneously precipitates with high yield and selectivity from an uranyl aqueous solution in presence of hydrogen peroxide and ammonia. The cationic substitution of the monovalent cation by a tri or tetravalent one steadily takes place driven by ionic force, when the peroxide powder is soaked into a *f*-metals ionic solution [3]. The resulting powder, recovered by filtering or centrifugation, provides one of the few examples of solid precursors containing both uranyl and rare-earth ions [4].

The objective of our study is to evaluate the ability of these precursor powders as suitable materials to obtain simulated pellets of nuclear fuel, after calcination and proper sintering. To this aim, our experimental investigation comprises two parts, the study of the thermal decomposition pathways of the substituted uranyl nanoclusters by rare-earth up to a single oxide phase with the fluorine structure and the powder densification by pressureless sintering of uniaxial pressing of green bodies.

The presentation will focus on both of these stages, depicting, (*i*) the stepwise thermal decomposition of the precursors which was investigated by *in-situ* powder XRD, DTA-TG for various atmospheres, *ex-situ* XANES and EXAFS experiments for intermediate phases covering a wide temperature range, and (*ii*) the microstructural characterisation of the pellets carried out by OM, SEM-EDS and TEM, mainly.

## References

[1] F. Blanchard, F. Abraham, M. Rivenet, S. Grandjean, N. Vigier, I. Hablot, Patent FR3015453, WO2015091753, (2015).
[2] G.E. Sigmon, P.C. Burns, *J. Am. Chem. Soc*., **133** (2011), 9137.
B. Morel, S. Grandjean, F. Abraham, *Chem. Comm.*, **52**, (2016) 3947-3950.
[4] P-H. Imbert, O. Tougait, P. Devaux, N. Henry, M. Ellart, F. Abraham, J. Nos, *Prog. Nucl. Sci. Tech*. **5**, 144 (2018).

# Search for Odd-Parity Augmented Multipoles and Cross-Correlation Phenomena in Antiferromagnetic Metals

**Hiroshi Amitsuka,[1] Akinari Koriki[1], Nana Shikanai[1], Masataka Yamamoto[1], Yusuke Suzuki[1], Fusako Kon[1], Hiroyuki Hidaka[1], Tatsuya Yanagisawa[1], Hiraku Saito[2], Chihiro Tabata[3], Hironori Nakao[4], Hiroshi Tanida[5], Takeshi Matsumura[6], and Masafumi Sera[6]**

*[1]Graduate School of Science, Hokkaido University, N10W8 Kita-ku, Sapporo 080-0810, Japan*
*e-mail: amiami@phys.sci.hokudai.ac.jp*
*[2]IMSS KENS, KEK, 2-4 Shirane Shirakata, Tokai, Naka-gun, Ibaraki 319-1195, Japan*
*[3]Institute for Integrated Radiation and Nuclear Science, Kyoto University, 2 Asashiro-Nishi, Kumatori, Sennan-gun, Osaka 590-0494, Japan*
*[4]IMSS CMRC, KEK, 1-1 Oho, Tsukuba, Ibaraki 305-0801, Japan,*
*[5]Graduate School of Engineering, Toyama Prefecture University, 5180 Kurokawa, Imizu, Toyama 939-0398, Japan*
*[6]Graduate School of Advanced Sciences of Matter, Hiroshima University, 1-3-1 Kagamiyama, Higashi-Hiroshima, Hiroshima 739-8530, Japan*

We present our recent efforts to explore emergence of odd-parity augmented multipoles, such as magnetic monopole, quadrupole, and toroidal dipole, and their causing new types of cross-correlation phenomena in antiferromagnetic (AF) metals. The present experimental study is based on the recent theoretical developments on the extension of multipole concepts to describe general aspects of electronic states in solids on the basis of symmetry considerations [1,2]. One of the most interesting and accessible phenomena predicted by the theories would be an induction of uniform magnetization under the AF order that may accompany a uniform order of the toroidal dipole $\boldsymbol{t}$ [3,4]. We have thus far investigated three such candidates, $UNi_4B$ ($T_N$ = 20.4 K) [5], $CeRh_2Si_2$ (35 K and 24 K) [6], and $CeRu_2Al_{10}$ (27 K) [7,8], and found that all of them show such an electromagnetic effect in their AF states [9,10]. Common characteristics among observed behaviors are (i) the current-induced magnetization $\Delta\boldsymbol{M}$ is perpendicular to the direction of electric currents $\boldsymbol{I}$, (ii) $\Delta\boldsymbol{M}$ is directly proportional to $\boldsymbol{I}$, and (iii) the rate of induction of $\Delta\boldsymbol{M}$ is on the order of ~ $10^{-7}$ – $10^{-9}$ $\mu_B$/(U or Ce) per unit current density (in units of kA/m$^2$). The obtained experimental results have confirmed that a uniform magnetization component can be induced by applying electric currents in AF metals, and its magnitude and direction are closely coupled with the magnetic structure. This feature is basically consistent with the theoretical predictions; however, we also observed some inconsistencies that may suggest the presence of unknown lowering symmetry in the crystal and/or magnetic structures of those compounds. We will also present our preliminary studies on other candidates, $UCu_5In$ and $UIr_2Ge_2$, which may possess the augmented magnetic monopole in their AF states.

## References

[1] S. Hayami *et al*., Phys. Rev. B **98**, 165110 (2018).
[2] H. Watanabe and Y. Yanase, Phys. Rev. B **98**, 245129 (2018).
[3] S. Hayami, H. Kusunose, and Y. Motome, Phys. Rev. B **90**, 024432 (2014).
[4] S. Hayami, H. Kusunose, and Y. Motome, J. Phys. Soc. Jpn. **84**, 064717 (2015).
[5] S. Mentink *et al*., Phys. Rev. Lett. **73**, 1031 (1994).
[6] B. H. Grier *et al*., Phys. Rev. B **29**, 2664 (1984).
[7] T. Nishioka *et al*., J. Phys. Soc. Jpn. **78**, 123705 (2009).
[8] T. Matsumura *et al*., J. Phys. Soc. Jpn. **78**, 123713 (2009).
[9] H. Saito *et al*., J. Phys. Soc. Jpn. **87**, 033702 (2018).
[10] A. Koriki, *to be submitted*.

# Comparison of oxidation behaviors of UN0.68 and UN1.66 by XPS

**Lizhu Luo,[1] Yin Hu,[1] Kezhao Liu,[1] Xiaolin Wang[2]**

[1]*Institute of Materials, China Academy of Engineering Physics, Mianyang, 621908, China*
[2]*China Academy of Engineering Physics, Mianyang, 621900, China*

Uranium nitride is regarded as a proposed nuclear fuel for the generation IV nuclear reactor, and has been extensively studied experimentally since the 1960s. However, the properties of uranium nitride are less studied than for carbide and oxide fuel. Owing to the large variety of available valence states of uranium, the oxidation process of uranium-contained system is very complex as known, among which the oxidation behaviors of uranium nitride under various conditions are not sufficiently investigated.

$UN_{0.68}$ and $UN_{1.66}$ thin film was fabricated by radio frequency (RF) magnetron sputtering method on silicon substrate in mixed $Ar/N_2$ atmosphere, and the N/U ratio is derived from the peak to peak intensity ratio by Auger Electron spectroscopy (AES) analysis. The electronic structure and surface oxidation behavior is carefully characterized by XPS.

The variations of U4f spectra as function of oxygen exposure are presented for further understanding of the oxidation behaviors of $UN_{0.68}$ and $UN_{1.66}$, which are achieved by subtraction of normalized U4f spectra in cases of corresponding oxygen exposure, as shown in Fig. 1 and 2 respectively.

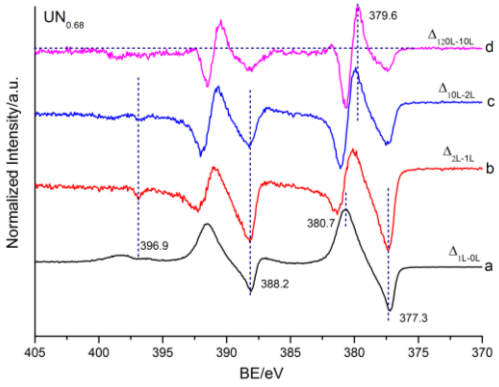


Fig. 1. The variations of U4f spectra of $UN_{0.68}$ under different oxygen exposures, which are denoted as the subscripts of Δ.

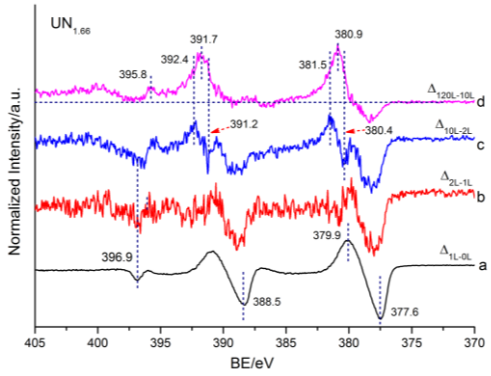


Fig. 2. The variations of U4f spectra of $UN_{1.66}$ under different oxygen exposures, which are denoted as the subscripts of Δ.

As shown in Fig. 1, $UN_{0.68}$ is easily oxidized, and prominent signals at 380.7 eV and 391.5 eV for $U4f_{7/2}$ and $U4f_{5/2}$ emerge even in case of 1 L $O_2$ exposure, which are about 0.2 eV lower than the as-oxidised U under similar condition. Valuable information related to the complicated oxidation behavior can be extracted from Fig. 2. Based on the spectrum variation of "b" and "c", the formation of U-contained species with $U4f_{7/2}$ peak at 380.4 eV is identified in case of 2 L oxygen exposure, which is further oxidized to higher states with U4f peaks at 380.9 eV or/and 381.5 eV. From spectrum "d" in Fig. 2, a broad increment of U4f signal is acquired by subtraction the U4f spectra in case of 120L and 10L, and can be attributed to the overlap of several components. At least three components with $U4f_{7/2}$ peak locating at 380.4 eV, 380.9 eV and 381.5 eV can be roughly defined. Furthermore, the incremental signals at 395.8 eV and in range of 398~400 eV could be induced by the satellite of $U4f_{5/2}$ peaks, assuming no increment for N1s signal during oxidation. Based on the previous reports [1-3], the three components on the oxidized $UN_{1.66}$ surface can be assigned to $UO_{2+x}$, $U_4O_9$ and a mixture of $UO_3$ with some uranium oxidation states lower than +6, where the as-generated U-N-O ternary compounds in the first contact with oxygen are further oxidized by complete displacement of O to N. However, the influence of N during progressive oxidation cannot be excluded, which cannot be correctly evaluated via this work.

## Summary

Significant difference among the corresponding spectra of $UN_{0.68}$ and $UN_{1.66}$ during oxidation reveals the distinctive properties of each own. The coexistence of UN and metallic U in $UN_{0.68}$ is revealed, where the oxidation process of $UN_{0.68}$ is not the simple combination of two independent oxidation behaviors, but an interactive association. The nitrogen species generated by interaction of UN with $O_2$ should be trapped by the oxygen vacancies in the $UO_{2-x}$, the oxidation product of uranium metal. The coexistence of $UO_{2-x}$, nitrogen trapped $UO_{2-x}$ ($UO_{2-x}.N_y$) and $UO_2$ results in the unique spectral variation around the XPS energy scale with gradually increasing oxygen. Ternary U-N-O compounds with symmetrical U4f peaks at 379.9 eV and 390.8 eV are formed on $UN_{1.66}$ surface, and the broadening of U4f peaks to higher energy side indicates the further oxidation of the U-N-O system with increasing oxygen exposure. A multistage mechanism is proposed for the oxidation of UN1.66, where a specific U:N:O ratio is corresponding to each stage for chemical equilibrium.

## References

[1] G. C. Allen, P. M. Tucker and J. W. Tyler, Oxidation of uranium dioxide at 298K studied by using X-ray photoelectron spectroscopy, *J. Phys. Chem.* **86**, 224-228 (1982).
[2] G. C. Allen, P. M. Tucker and J. W. Tyler, The behaviour of uranium oxides in low partial pressure of $O_2$ studied using X-ray photoelectron spectroscopy, *Vacuum* **32**, 481-486 (1982).
[3] G. C. Allen, J. A. Crofts, M. T. Curtis et al, X-ray photoelectron spectroscopy of some uranium oxide phases, *J. C. S. Dalton* **0**, 1296-1301 (1974).

# Magnetic anisotropy of $UO_2$ studied on $UO_2/Fe_3O_4$ thin films

**E. A. Tereshina-Chitrova[1,2], Z. Bao[3], L. Havela[1], S. Daniš[1], L. Horak[1], A. Mackova[4,5], P. Malinsky[4,5], L. V. Pourovskii[6,7], S. Khmelevskyi[8], T. Gouder[3], R. Caciuffo[3]**

[1]*Faculty of Mathematics and Physics, Charles University, 12116 Prague, Czech Republic*
[2]*Institute of Physics, Czech Academy of Sciences, 18121 Prague, Czech Republic, e-mail: teresh@fzu.cz*
[3]*European Commission, Joint Research Centre (JRC), Postfach 2340, DE-76125 Karlsruhe, Germany*
[4]*Nuclear Physics Institute CAS, Department of Neutron Physics, CZ-25068 Řež, Czech Republic*
[5]*Department of Physics, Faculty of Science, J. E. Purkinje University, Ceske Mladeze 8, 400 96 Usti nad Labem, Czech Republic*
[6]*CPHT, Ecole Polytechnique, CNRS, Université Paris-Saclay, Route de Saclay, 91128 Palaiseau, France*
[7]*Collège de France, 11 place Marcelin Berthelot, 75005 Paris, France*
[8]*Center for Computational Materials Science, IAP, Vienna University of Technology, Vienna, Austria*

Large magnetic anisotropy (MA) of the material is a keystone to the high-density magnetic storage. It defines the easy magnetization direction and ensures information storage by preventing the magnetization from switching. Magnetic anisotropy in thin film samples can be manipulated by varying deposition conditions (e.g. by inducing strain, deposition in a magnetic field, etc.). In bilayers, MA can also be controlled via pinning of a ferromagnetic (F) layer by an antiferromagnet (AF) in the exchange bias (EB) [1] systems [2].

In this work we aim at evaluating the anisotropy constant in the antiferromagnetic uranium dioxide by making use of exchange bias effect study in the $UO_2/Fe_3O_4$ bilayers deposited on various substrates. The shift of the magnetic hysteresis curve along the field direction (Fig. 1) of the magnetic bilayer field-cooled below the Néel temperature ($T_N$) of the antiferromagnet is related to its anisotropy constant $K_{AF}$ [3,4] via the critical thickness of the AF layer, above which the antiferromagnet is strong enough to pin the magnetization of a ferromagnet.

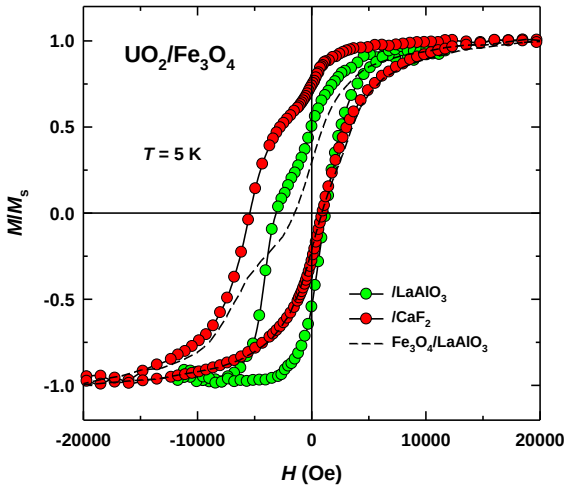


Fig. 1. Comparison of the *H-M* magnetization loops at 5 K for the $UO_2/Fe_3O_4$ bilayers on different substrates after field cooling in the 10 kOe field. For $UO_2$ and $Fe_3O_4$ the thicknesses are 271 and 282 Å ($CaF_2$ substrate) and 285 and 284 Å (LAO substrate), respectively. Data for a single layer of $Fe_3O_4$ (270 Å) (broken line) is shown for comparison.

Using reactive sputtering from metallic U and Fe targets, we prepared sets of the $UO_2/Fe_3O_4$ samples with the varied thickness of $UO_2$ (50-300 Å) and with a constant thickness of magnetite (~270±20 Å). We employed two types of substrates, $LaAlO_3$ (001) and $CaF_2$ (001), which both have a lattice parameter very close to that of $UO_2$ ($CaF_2$ has an identical crystal structure with $UO_2$). The bilayers of $UO_2/Fe_3O_4$ prepared using $LaAlO_3$ substrates have previously shown large EB of the order of several kOe [5].

The stoichiometry of each deposited layer was controlled by X-ray Photoelectron Spectroscopy (XPS). The samples were further characterized by Rutherford Back-Scattering Spectrometry (RBS) and x-ray diffraction (XRD). The $UO_2/Fe_3O_4$ bilayers

were examined using a SQUID magnetometer with the Reciprocating Sample Option installed to improve sensitivity and PPMS installation equipped with a Vibrating Sample Magnetometer (both by Quantum Design, USA).
Magnetization study revealed a large EB in the samples. Moreover, effect is stronger in the $CaF_2$ samples (see Fig. 1). Using the approach of Ref. [4] and the critical thickness of the antiferromagnetic $UO_2$ layer for appearance of EB in $UO_2/Fe_3O_4$ ~50 Å, we find the anisotropy constants of $UO_2$ in both systems ~0.1-0.3 MJ/m$^3$. However, the drastic difference in the exchange bias values for the two samples in Fig. 1 is probably attributed to the differences in the morphology of the deposited magnetic layers [6]. For instance, the substrate-induced tetragonality of the $UO_2$ layer deposited on $LaAlO_3$ ($UO_2$ is in compression of -1.9% with respect to the substrate in-plane spacing) in Ref. [6] was shown to be responsible for the appearance of a magnetically dead layer adjacent to the substrate. This was not the case of the $CaF_2$-based $UO_2$ film (in-plane strain is only -0.3%), which ordered magnetically throughout the film thickness [6].
The experimental results were compared with those obtained theoretically using a first-principles density-functional+dynamical-mean-field-theory (DFT+DMFT) method [7] in conjunction with a quasi-atomic (Hubbard-I) treatment of U 5*f* states. The LDA self-interaction error contribution to the crystal-field splitting was suppressed using the approach of Ref. [8]. For cubic $UO_2$ our calculations predict the $\Gamma_5$ crystal-field ground state with 3 densely-spaced excited crystal-field levels in the range from 190 to 210 meV, in a good agreement with experiment [9]. We predict a strong easy-axis anisotropy (single-ion anisotropy coefficient $K_1$= 3.3 MJ/m$^3$) to originate from the substrate-induced in-plain tetragonal compression by 1.5% of the $UO_2$ layer. It results in splitting of the $\Gamma_5$ triplet into a ground-state doublet and an excited singlet located 1.8 meV higher in energy.
*The samples were prepared in the framework of the TALISMAN project of the European Commission Joint Research Centre, ITU Karlsruhe. RBS measurements have been carried out at the CANAM (Centre of Accelerators and Nuclear Analytical Methods) infrastructure LM 2015056 and supported by OP RDE, MEYS, Czech Republic under the project CANAM OP, CZ.02.1.01/0.0/0.0/16_013/0001812 and by the Czech Science Foundation (GACR No. 18-03346S). We also acknowledge support of Czech Science Foundation, project #18-02344S. Part of the work was supported by "Nano-materials Centre for Advanced Applications," Project No.CZ.02.1.01/0.0/0.0/15_003/0000485, financed by ERDF.*

## References

[1] W. H. Meiklejohn and C. P. Bean, *Phys. Rev. B* **102** 1413 (1956).
[2] S. van Dijken *et al., J. Appl. Phys.* **97** 063907 (2005).
[3] D. Mauri *et al., J. Appl. Phys.* **57**, 3047 (1987).
[4] Ch. Binek *et al., J. Magn. Magn. Mater.* **234**, 353 (2001).
[5] E. A. Tereshina *et al., Appl. Phys. Lett.* **105** 122405 (2014).
[6] Z. Bao *et al., Phys. Rev. B* **88** (2013) 134426.
[7] M. Aichhorn *et al. Comp. Phys. Comm.* **204**, 200 (2016).
[8] P. Delange *et al., Phys. Rev. B* **96** 155132 (2017).
[9] G. Amoretti *et al., Phys. Rev. B* **40**, 1856 (1989).

# Examination of excitation spectra of $UO_2$ with inelastic X-ray spectroscopy

**L. Paolasini[1], D. Chaney[1,2], G. H. Lander[3], R. Caciuffo[3]**

*[1]European Synchrotron Radiation Facility, B.P.220, F-38043 Grenoble, France*
*[2]School of Physics, University of Bristol, Tyndall Avenue, Bristol, BS8 1TL, UK*
*[3]European Commission, Joint Research Centre, Postfach 2340, D-76125 Karlsruhe, Germany*

The low temperature excitation spectra of $UO_2$ are extremely complicated given that one can observe lattice vibrations, magnons, and potentially higher-order excitations due to multipolar excitations, as well as mixing between these modes [1]. Such complications have already been observed by inelastic neutron scattering [2]. However, a precise observation of the acoustic quadrupolar waves is still lacking, whereas the optical quadrupolar contribution has been identified because of strong mixing with the optical spin wave. In fact, this latter contribution was already observed in the early work on $UO_2$ [3], although not correctly identified.

Inelastic X-ray scattering measurements have been performed at the ID28 spectrometer at the ESRF with a resolution of 1.5 meV. The experiment was focused on the transverse acoustic (TA) mode in the [100] direction, where extensive work has already been reported using neutron scattering [2, 3]. Neither the magnetic scattering nor the excitations from higher multipoles can be observed directly with X-rays; the technique is sensitive to only vibrational excitations and others modes that *mix with such excitations.*

So far, there is little evidence for the quadrupolar acoustic (QA) waves. We observe mixing of the transverse acoustic phonons (TA) with the spin acoustic (SA) mode at low energy of ~ 6 meV, which is expected, but also a strong mixing of the TA phonon with the quadrupolar optic (QO) around 11 meV and the spin optic (SO) modes, which has been predicted but not observed previously. The QO mode is observed in neutron scattering spectra because it mixes with the spin optic (SO) mode through quadrupolar interactions that in large part have a vibrational origin. It is therefore to expect that the mixed mode at high energy has also a vibrational component, and it is this part that we observe with X-rays. The temperature dependence of the TA mode shows finite lifetime in the [100] direction well above the AF transition, demonstrating that the low temperature anomalous anisotropic thermal conductivity in $UO_2$ is mediated by this strong magnon-phonon coupling [4].

[1] P. Santini *et al.*, Rev. Mod. Phys. **81**, 807 (2009)
[2] R. Caciuffo *et al.* Phys. Rev. B **84**, 104409 (2011)
[3] R. A. Cowley and G. Dolling, Phys. Rev. **167**, 464 (1968)
[4] K. Gofryk et al., Nature Comm. **5**, 4551 (2014)

# Theory of type-II superconductivity in ferromagnetic metals with triplet pairing

**V.P.Mineev**[1,2]

[1] *Universite Grenoble Alpes, CEA, INAC, PHELIQS, GT, F-38000 Grenoble, France*
[2]*Landau Institute for Theoretical Physics, 142432 Chernogolovka, Russia*
*e-mail:vladimir.mineev@cea.fr*

Usually ferromagnetic ordering suppresses the superconducting state because the exchange field exceeds the paramagnetic limit field and aligns the electron spins directed oppositely in the Cooper pairs. Nevertheless, singlet superconductivity can coexist with ferromagnetism when the critical temperature of the transition to the superconducting state is greater than the Curie temperature, as is the case with ternary compounds investigated in the 1980-s. The coexistence occurs in a form of crypto-ferromagnetic superconducting state characterized by appearance a periodic magnetic structure with period larger than the interatomic distance, but smaller than the superconducting coherence length, which weakens the depairing effect of the exchange field.

The superconductivity in recently discovered uranium compounds $UGe_2$, URhGe and UCoGe exhibits quite different properties (for review see [1]). Here the superconducting states exist at temperatures far below the Curie temperature and in the magnetic fields strongly exceeding the paramagnetic limit indicating that we deal with the triplet pairing. Similar to the superfluid $^3$He the pairing interaction is caused by the magnetic fluctuations. The theory based on this mechanism and on the symmetry considerations allows explain many specific properties of these materials [2].

All the uranium superconductors are related to the type-II superconducting materials. The internal magnetic fields in all of them exceed the corresponding lower critical fields. Hence, at temperature decrease the phase transition from the ferromagnetic to the ferromagnetic superconducting state occurs to the mixed state characterized by the emergence of Abrikosov vortices. Accordingly, the proper desciption of this phase transition must be formulated in frame Ginzburg-Landau-Abrikosov theory of type-II superconductivity. Here, I present the recently developed theory of type-II superconductivity for equal spin pairing triplet superconducting state in a two band ferromagnetic metal [3]. First, I describe the phase transition from ferromagnetic to superconducting ferromagnetic state. Then I consider the solution for isolated vortex in such type superconductors and the transition from the Meissner to the mixed superconducting state which is realized in UCoGe.

## References

[1] D. Aoki and J. Flouquet, *J. Phys .Soc. Jpn.* **83**, 061011 (2014).
[2] V. P. Mineev, *Usp.Fizich.Nauk* **187**, 129 (2017) [*Physics-Uspekhi.* **60**, 121 (2017)].
[3] V. P. Mineev, *Low Temp.Physics* **44**, 663 (2018).

# Crystal structure and physical properties of the novel complex intermetallic compounds $R_8Pt_{32}Be_{66}$ (R = Y, La-Nd, Sm-Lu)

**E. Svanidze,[1] A. Amon,[1] Yu. Prots,[1] M. Avdeev,[2] A. Leithe-Jasper,[1] Yu. Grin[1]**

[1] *Max-Planck-Institut für Chemische Physik fester Stoffe, Nöthnitzer Straße 40, Dresden 01187, Germany*

[2] *Australian Nuclear Science and Technology Organization, Sydney, NSW 2232, Australia*

Crystallographically complex compounds often possess peculiar physical properties, the evolution of which can be tracked by changing one of the constituent elements at a time. We report the discovery and synthesis of a $R_8Pt_{32}Be_{66}$ (R = Y, La-Nd, Sm-Lu) series of compounds. These materials crystallize in the same cubic structure type (space group $I\bar{4}3d$) with lattice parameters ranging from $a$ = 13.4366(3) Å (R = Lu) to $a$ = 13.6682(4) Å (R = La). $R_8Pt_{32}Be_{66}$ compounds exhibit a wide range of physical properties - from superconductors (R = Y, La, and Lu) to ferromagnets (R = Ce, Gd-Ho), antiferromagnets (R = Pr and Eu), and paramagnets (R = Nd, Sm, Er, Tm, and Yb). These diverse properties can likely be attributed to the level of hybridization of *4f* orbitals with the *5d* conduction electrons of Pt, which, in turn, is driven by the complex crystal structure of these compounds -- in each case, R atoms are coordinated by 8 Pt atoms and 12 Be atoms.

# The Effects of Gamma Irradiation on the Physiochemical and Ion Exchange Properties of Caesium-Selective Porous AMP-PAN Composites

**Alistair F. Holdsworth,[1] Daniel Rowbotham,[2] Harry Eccles,[2] Gary Bond,[2] Parthiv Kavi,[2] and Ruth Edge.[3]**

*[1] University of Manchester, Manchester, UK, M13 9PL, e-mail: alistair.holdsworth@manchester.ac.uk*
*[2] University of Central Lancashire, Preston, UK, PR1 2HE*
*[3] Dalton Cumbrian Facility, Whitehaven, UK, CA24 3HA*

Nuclear energy will be key in securing our energy supplies for a low-carbon future. The management and safe disposal of the multitudinous and variable wastes produced by the nuclear fuel cycle, however, is a challenging prospect. [1,2] Caesium is one of the most chemically problematic elements produced during nuclear fission due to its environmental mobility [3] and the radioactivity of the $^{137}Cs$ isotope, a common fission product (FP). [4] While a great many natural and synthetic ion exchange materials can sequester $Cs^+$ ions from neutral or basic aqueous solutions,[5-7] few function effectively in acidic conditions with the exception of ammonium phosphomolybdate (AMP). [8] AMP is commonly implemented as a composite in a porous matrix of polyacrylonitrile (PAN) to facilitate column use. [9] Both AMP and PAN are acid- and radiation resistant, and the effects of both β [9] and γ [10] radiation have been explored to varying degrees, little work has analysed in-depth the effect of irradiation on the physiochemical properties of AMP-PAN composites, or their performance in spent fuel recycling, as proposed by Eccles *et al*. [1] With this in mind, we investigated the effect of 100 kGy γ irradiation on both AMP and a 70 wt% AMP-PAN composite with respect to $Cs^+$ ion exchange performance, and performed an in-depth physiochemical investigation including thermal analysis, XPS, EPR, surface area measurements, and an initial study into the high-temperature degradation of AMP. The samples were irradiated dry, in sealed vials at a rate of *c.a.*, 20 kGy/h at the Dalton Cumbrian Facility, Whitehaven, UK.

The most apparent visual effect of irradiation on AMP and AMP-PAN is a distinct colour change (**Fig 1**), hypothesized to result from radiolytic reduction on the $Mo^{VI}$ centres in AMP to $Mo^{V}$, [9] though this is reversible upon immersion in 3 M $HNO_3$. [10] XPS analysis presents contrary evidence, however: the virgin samples contain higher levels of $Mo^{V}$ than the irradiated ones.

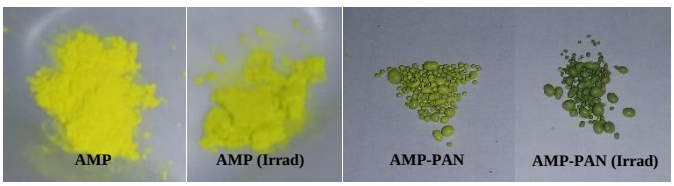


**Figure 2:** Optical images of virgin and irradiated AMP powder and AMP-PAN.

No changes are observed in the crystal structure or crystal morphology of AMP upon irradiation, though the porous structure of the AMP-PAN composite exhibits an internal collapse (**Fig 2**), confirmed by a reduction in BET surface area from 21.6 to 7.6 $m^2/g$ and increase in internal pore diameter from 5.2 to 13.4 nm. Despite this, no change in rate of $Cs^+$ ion uptake, ion exchange capacity, or mechanism of uptake was observed, as outlined below.

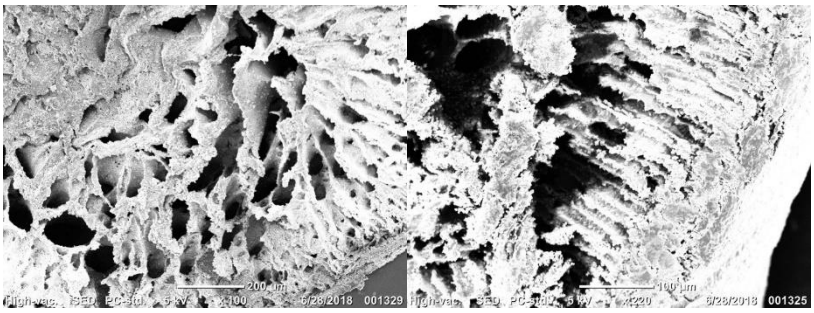

**Fig 2:** SEM micrographs of virgin (left) and irradiated (right) AMP-PAN composite.

The thermal degradation of AMP is largely unaffected by 100 kGy γ irradiation under 800 °C, while that of AMP-PAN is significantly affected by irradiation, showing sensitised mass loss (**Fig 3**) and a shift in degradation mechanism between 150 and 300 °C, and above 600 °C. This has significant implications for post-$Cs^+$ absorption storage and processing of the composite, but would have no effect on performance under absorption conditions.

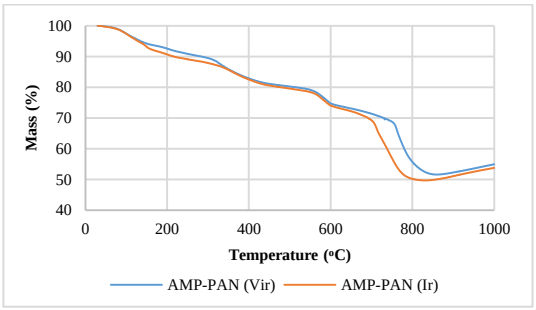


**Fig 3:** TGA of virgin (blue) and irradiated (orange) AMP-PAN composite under nitrogen.

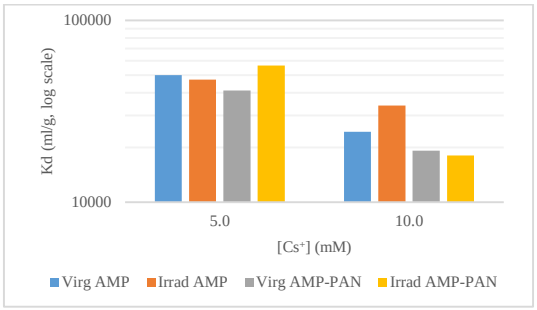


**Fig 4:** Distribution coefficients ($K_d$) of $Cs^+$ uptake onto AMP and AMP-PAN pre- and post-irradiation.

The ion exchange performance with respect to capacity and rate of uptake of both AMP and AMP-PAN is unaffected by 100 kGy γ irradiation, all samples completely absorb 10 mM $Cs^+$ from 3 M $HNO_3$ ($K_d$ values in **Fig 4**, [$Cs^+$] and [$H^+$] found in spent fuel recycling), via the Langmuir isotherm, as previously reported. [2] Prior research noted an increase in the $Cs^+$ capacity of AMP upon β irradiation, [10] but we did not observe this.

In conclusion, 100 kGy of γ irradiation has no negative effect on the ion exchange properties of AMP or AMP-PAN composites under conditions that would be used operationally in spent fuel recycling. [11] The sensitised degradation of the PAN matrix and the changes to the high-temperature degradation of AMP upon irradiation will have implications for the recycling, or vitrification and long-term disposal of these materials, however, and require further study.

## References

[1] H. Eccles et al, *J. Chromatog. Separat. Techniq.*, **8**, 1 (2017).
[2] G. Bond et al, *J. Chromatog. Separat. Techniq.*, in press (2019).
[3] F. R. Livens et al, *Soil Use & Manag.*, **4**, 5, 69 (1988).
[4] C. C. Busby, *Int. J. Envir. Res. Pub. Health*, **6**, 12, 3105 (2009).
[5] A. Dyer et al, *J. Mater. Chem.*, **9**, 2481-2481 (1999).
[6] C. B. Amphlett et al, *J. Inorg. Nucl. Chem.*, **2**, 403 (1956).
[7] A. Nilchi et al, *Appl. Rad. Isoptop.*, **70**, 369 (2012).
[8] J. van R. Smit et al, *J. Inorg. Nucl. Chem.*, **12**, 95 and 104 (1959).
[9] F. Sebesta et al, *SAND'95 Report* (1995).
[10] K. L. Narasimharao et al, *J. Chem. Soc. Faraday Trans.*, **94**, 11, 1641 (1998).
[11] G. Bond et al, *J. Chem. Eng.*, in press (2019).

# Study on the interaction between U-containing metallic alloys and oxidic liquid for the vitrification processes of contaminated waste

**Luca Soldi,[1] Stéphane Gossé[1], Christophe Bonnet[1], Adrien Morellec[2], Annabelle Laplace[3], Mathieu Roskosz[4]**

*[1] DEN-Service de la Corrosion et du Comportement des Matériaux dans leur Environnement (SCCME), CEA, Université Paris Saclay, F-91191, Gif sur Yvette, France, e-mail: luca.soldi@cea.fr*
*2 DEN – Service de Recherche en Métallurgie Physique (SRMP), CEA, Université Paris Saclay, F-91191, Gif sur Yvette, France*
*[3] DEN-Service d'Etudes de Vitrification et et procédés hautes Températures (SEVT), CEA Marcoule, D765, 30200 Chusclan, France*
*[4] Institute of Mineralogy, Physics of Materials and Cosmochemistry, National Museum of Natural History, 57 Rue Cuvier, 75005 Paris, France*

Several metallic devices and tools are implemented in gloveboxes where MOx fuel pellets are produced. These items are partially contaminated by the presence of actinide oxides, typically $UO_2$. This metallic waste is classified as Long-Lived Intermediate-Level (II-IL) nuclear waste and needs dedicated treatments before the definitive disposal. An interesting way to fulfill such goal is to melt the metallic contaminated tools and merge them in an oxide bath, in order to confine U and other actinides in a stable glass matrix. Given the nature of the technological waste to treat and the chemical interactions between the oxide and metallic liquids, the prediction of the high temperature interactions of uranium in such a complex vitrification process is challenging.
After having considered key sub-systems representative of the metallic waste from a thermodynamic point of view, the study will focus on the interaction between U-containing metallic alloys and $Na_2O$-$SiO_2$ prototypic glasses. Scanning Electronic Microscope images on laboratory scale samples will provide insight on the speciation of U and on the phases that may appear during the vitrification. The obtained data will be discussed and compared with the thermodynamic calculations.

# Study of Reactor Pressure Vessel Dismantling Scenario in Nuclear Power Plant

**Han-sol Im,[1] Kwang-soo Park[1], Gyu-ho Jang[1], Hae-woong Kim[1], Sang-cheol Lee[1], Jong-hwan Lee[2]**

*[1]Doosan Heavy Industries & Construction, 22 Doosan-Volvo-ro Seongsan-gu, 51711 Changwon, republic of Korea, hansol.im@doosan.com*
*[2] KAERI, 989-11 Daedeuk-daero Yuseong-gu, 305-353, Daejeon, Republic of Korea*

Out of the 454 nuclear power plants currently in existence, 309 power plants have been in operation for more than 30 years, accounting for about 70% of the total, while 169 permanently shut down account for about 37%. Similarly, Kori Unit 1 was permanently shut down in 2017 after it had been operated for 40 years. Kori Unit 1 is the Korean first nuclear power plant which will be decommissioned. This study is the one about RPV dismantling scenario using thermal and mechanical cutting method, analyzing worker's radiation exposure and working time for each scenario.

In order to develop the optimized scenario of RPV dismantling, three steps should be prepared. The first one is to design of cutting plan on the basis of activation evaluation and the size of container. The second one is to develop the scenario of RPV dismantling on the base of two kinds of cutting method. The last is to review the developed scenario using the Doosan Virtual Dismantling Simulator(DVDS).

When developing RPV dismantling scenario, we set two assumptions. First, RPV is dismantled in the air environment condition. Second, dismantling is performed while raising the RPV using lifting rig system. The reason why those assumptions are applied is that RPV is low level waste based on the activation evaluation and previously dismantled case in U.S. [1] and Germany [2]. The scenario using thermal method starts from the pre-cut process cutting the stainless steel cladding on the flange of RPV by mechanical cutting method. And then, nozzle cutting of RPV is performed using the mechanical cutting method. Once the preparations for lifting the RPV are completed, dismantling of RPV shell is performed using the thermal cutting method. When the RPV shell dismantling is finished, the rigging tool is disassembled and the RPV bottom head is dismantle. Another scenario is using mechanical method instead of thermal method and processed similar to the scenario above but no pre-cut process, so it starts from the cutting nozzles.

After reviewing scenarios using the DVDS, it is obtained that applying the thermal method is better than the mechanical cutting method because of working time, worker exposure, etc.

Table. 1. Review result using DVDS

| Methods | Working time(hr) | Worker exposure(man·mSv/h) |
|---|---|---|
| Thermal | 110.4 | 3285.7 |
| Mechanical | 2208.3 | 3457 |

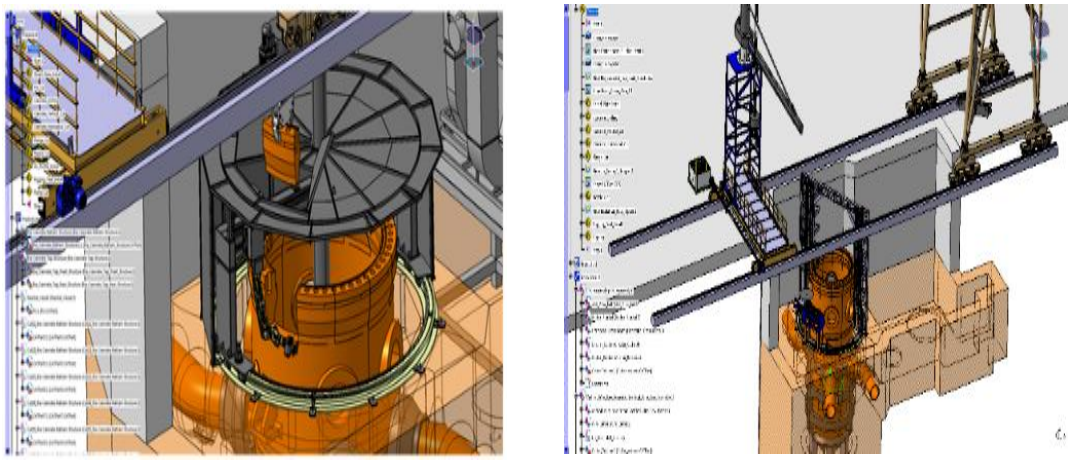

Thermal Cutting Scenario Mechanical Cutting Scenario

Fig. 1. RV Dismantling Scenario

## References

[1] A. Loeb, D. Stanke., "Decommissioning of the reactor pressure vessels by remote controlled thermal cutting segmentation facilities of the Zion nuclear plant at Zion"., WM2016 conference, (2016)

[2] A. Loeb, D. Stanke , "Decommissioning of the reactor pressure vessel and its peripheral facilities of the nuclear power plant in Stade "., WM2011 conference, (2011)

## Acknowledgement

This work was supported by the National Research Foundation of Korea (NRF) granted financial resource from the Ministry of Science and ICT, Republic of Korea (NRF-2017M2A8A5041777).

# ALAMBIC, a simulation tool to assess the red-oils hazards in reprocessing facilities

**F. Virot,[1] F. Réal[2], M. Saab[1], V. Vallet[2], M. Philippe[3]**

*[1] Institut de Radioprotection et de Sûreté Nucléaire (IRSN, PSN-RES/SAG), 13115 Saint Paul lez Durance, France, e-mail: francois.virot@irsn.fr*
*[2] Université de Lille, CNRS, UMR 8523 –PhLAM – Physique des Lasers Atomes et Molécules, 59000 Lille, France*
*[3] Institut de Radioprotection et de Sûreté Nucléaire (IRSN, PSN-EXP/SSTC),92262 Fontenay-aux-Roses Cedex, France*

In the French nuclear industry, the reprocessing of spent nuclear fuel is based on the PUREX aqueous process ("Plutonium Uranium Refining by EXtraction"). The main involved compounds are an organic mixture of hydrocarbon diluted tri-n-butyl phosphate (TBP) as well as a nitric acid solution used to dissolve the spent fuel. Even if the neat TBP is thermally stable, an extended contact with an acid solution (nitric acid and extractable heavy metal nitrates) forms a mixture called red-oils due to reaction at elevated temperature between involved species. These complex reactions and the formation of unstable by-products can lead to a thermal runaway in the plants' evaporators potentially followed by an explosion, a containment failure and a radioactive release into the environment [1]. In the past, these phenomena have been responsible of several significant accidents such as, two accidents in the United States at Savannah River plant (1953 and 1975) and more recently one accident in Russia at Tomsk (1993). This raises the question of exothermicity of reactions involving extractant TBP, its diluent (hydrogenated tetra-propylene, HTP) and their by-products and calls for a better knowledge of underlying thermochemical phenomena.

In the context of safety reviews regarding the French reprocessing plants at La Hague, one of the important risks concerning the evaporators is the explosion risk due to the red-oils compounds formation. Therefore, in order to simulate the behaviour of reactant solutions in evaporators during an accidental transient due to a thermal runaway, a simulation tool, ALAMBIC, is being developed at IRSN to support, in the next future, safety analyses. Its aim will be to simulate the thermal degradation of TBP in contact with nitric acid/uranyl nitrate solution and thus investigate the conditions leading to violent thermal runaways. This tool is built from modules of the ASTEC software package (Accident Source Term Evaluation Code) [2], one able to simulate the thermal-hydraulic behaviour coupled with another one to calculate the chemical evolution. For the latter, several key data are mandatory as the thermodynamic properties of species in aqueous and organic liquids or the kinetics rate laws of TBP and by-products degradations. Before addressing the chemical kinetics, a study based on quantum chemical methods has been started to fill the lack of knowledge regarding the standard heat of formation of n-butyl phosphate species [3]. Similarly, efforts have been recently continued towards the uranyl nitrate complex because the potential by-products are not as evident as TBP-nitric acid system.

We will first introduce the safety controls useful for safety reviews applied to evaporators in reprocessing facilities. Then, a highlight will be made on the recent theoretical results obtained about the reaction pathways of uranyl nitrate complexes. Finally the state of progress of ALAMBIC simulation tool will be presented.

## References

[1] V.N. Usachev *et al.*, *Radiochemistry* **45**, 1 (2003).
[2] L. Chailan *et al.*, *Overview of ASTEC code and models for Evaluation of Severe Accidents in Water Cooled Reactors*, IAEA Technical Meeting, Vienna (Austria), October, 9-12 (2017).
[3] M. Saab *et al.*, *J. Chem. Phys.* **146**, 244312 (2017).

# Microstructural evolution of adiabatic shear band in U-5.7Nb alloy impacted by Slip Hopkinson Pressure Bar

**Yawen Zhao, Dawu Xiao, Li Zhang, Xian'e Tang, Lidong Zou, Lifeng He, Kezhao Liu**

*China Academy of Engineering Physics, P.O.Box 919-71,Mianyang,621900,Sichuan,China ， e-mail ： jackiazhao@163.com*

Adiabatic shear localization inU-5.7Nb alloy was examined through a forced shear technique using a split Hopkinson pressure bar and hat-shaped specimens. The microstructure evolution of adiabatic shear band(ASB) was investigated to get in sight to the process and mechanisms of shear localization. The experiment results indicate that microcracks and nano-sized grain domains are the major characteristics in the ASB. Combined with the calculation of the adiabatic temperature rise, we speculated that development of the substructures within shear bands is mainly controlled by the dramatic change of temperature in ASB.

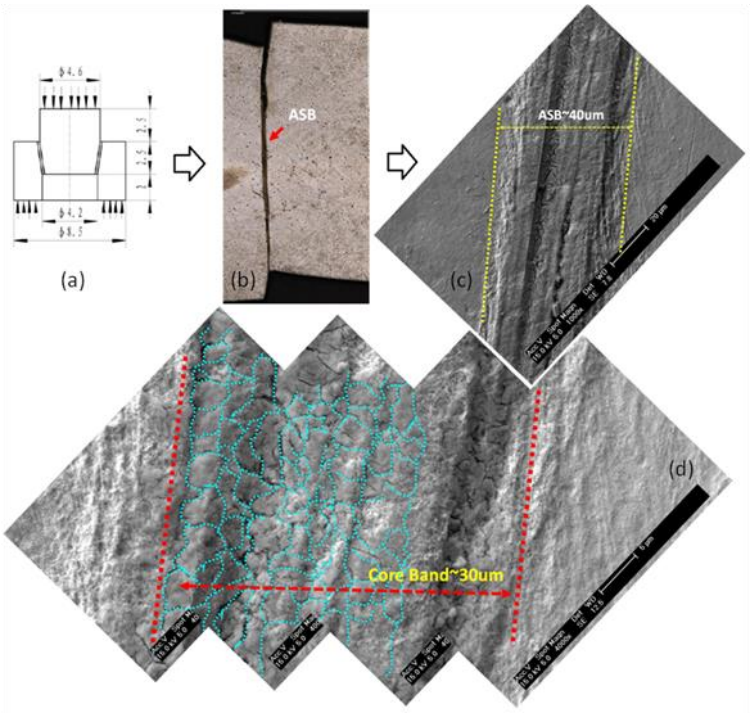


Fig. 1 (a)Configuration of the hat-shaped specimen.(b) OM micrographs of ASB in U-5.7Nb alloy.(c-d)SEM micrographs of ASB.ASB in U-5.7Nb alloy has a "sandwich" microstructure with the core area about 30um surrounded by the transition bands. A lot of microcracks, which have two different directions that coalesce to form a "net" to split out some equiaxed "broken grains", can be seen in the core area of ASB.

# The sources of plutonium around nuclear facilities in the South of France

**Laurent Pourcelot**,[1] **Beatrice Boulet**[2]

[1] *Institute for Radiological protection and Nuclear Safety-IRSN, CEN Cadarache PB3, 13115-St-Paul-lez-Durance, France, e-mail: laurent.pourcelot@irsn.fr*
[2] *Institute for Radiological protection and Nuclear Safety-IRSN, Bois des Râmes bat 501, 91400 Orsay, France*

Plutonium isotopes nowadays determined in soils and sediments allow to distinguish stratospheric or "global" fallout and tropospheric fallout emitted by above-ground nuclear weapons tests from the early 1950s through the mid-1970s. Thus stratospheric fallout exhibits elevated $^{240}Pu/^{239}Pu$ (0.180±0.005 in the northern hemisphere) as a consequence of the activation by neutrons whereas tropospheric fallout which involves low-yield nuclear devices shows much lower values [1]. Pu analyses have also been performed after accidental releases in the vicinity of Tomsk and Mayak (Russian Federation), Chernobyl and Fukushima. Further Pu isotopes measurements carried out at some sites in Finland [2, 3] and Poland [4] have highlighted the long range transport of airborne reactor particles released by the Chernobyl explosion. To date the less studied source of plutonium in the environment remain the releases from nuclear facilities, mostly because the released activity is usually low and a good precision is thus required to detect any deviation of the global fallout baseline isotopic ratio, whatever $^{240}Pu/^{239}Pu$ or $^{238}Pu/^{239+240}Pu$ ratio is considered.
Plutonium is found in reactors, in fuels reprocessing plants, fuel fabrication plants and research facilities where different fuels are developed and studied. The plutonium isotopic composition of each nuclear material is well-known to vary from a nuclear fuel to another and also according to neutrons irradiation flux. Thus in PWR $^{239}Pu$ massic content is about 50 and 35 % for $UO_x$ and $MO_x$, respectively [5, 6]. In the specific case of natural uranium-graphite reactor $^{239}Pu$ content reaches 80 %. As a consequence soils or sediments sampling around nuclear facilities followed by an accurate determination of the isotopic composition of Pu enable us to identify the source of the release and the fuel type. This hypothesis is made possible by assuming that the isotopic composition is kept preserved in soils and sediments. Among spars available studies carried out in France the influence of plutonium released by the former fuel reprocessing facility of Marcoule has been shown in bioindicators and soils surrounding the facility [7] as well as in downstream lagoon sediments [8]. Low $^{240}Pu/^{239}Pu$ ratios observed in soils and sediments taken around Malvési U-facility are the consequence of the releases when the facility purified uranium from spent fuel [9].
The present study deals with plutonium in soils and sediments taken near nuclear facilities in the south of France, in the frame of environmental studies. The activity of plutonium measured in soils and sediments is low (see Fig. 1) and thus does not pose any radiological issue since the inhalation or the ingestion of plutonium particles from soils or sediments is negligible. Therefore the proposed presentation is a comprehensive synthesis of plutonium available monitoring data from different nuclear facilities in France. Such synthesis of available Pu ratios contributes to the interpretation of any Pu ratios deviating from global fallout recorded by soils or sediments.

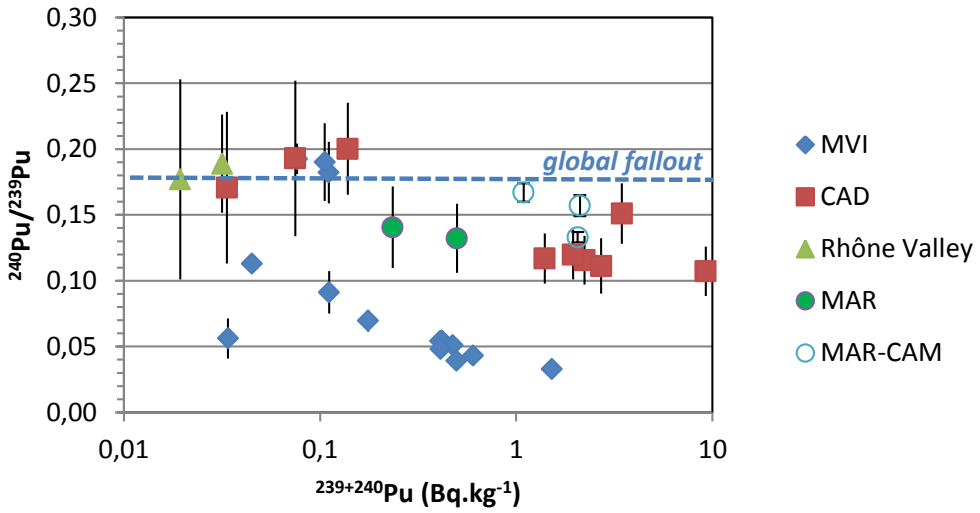


Fig. 1: Example of plutonium available data: $^{240}Pu/^{239}Pu$ with respect to $^{239+240}Pu$ activity recorded by soils/sediments in the vicinity of some nuclear facilities in the south of France, compared to the isotopic ratio of global fallout.

## References

[1] L.W. Cooper et al., *Marine Chemistry* **69**, 253-276 (2000).
[2] J. Paatero et al., *Journal of Radioanalytical and Nuclear Chemistry* **252**,407-412 (2002).
[3] S. Salminen-Paatero et al., *Journal of Environmental Radioactivity* **113**, 163-170 (2012).
[4] M.E. Ketterer et al., *Journal of Environmental Radioactivity* **73**, 183-201 (2004).
[5] Ph. Guetat et al., *CEA Report* ISSN0429-3460, 256 p. (2008).
[6] H. Yamana et al., *Radioactivity in the environment* A Kudo Editor **1C**, 31-46 (2001).
[7] C. Duffa et al., *Compte Rendu à l'Académie des Sciences* **332**, 275-281 (2001).
[8] J. Miralles et al., *The Science of the Total Environment* **320**,63-72 (2004).
[9] L. Pourcelot et al., *Journal of Environmental Monitoring* **13**, 355-361 (2011).

# A series of tetravalent Pu, Np, U and Th complexes of a salen type ligand

**Thomas Radoske[1], Peter Kaden[1], Olaf Walter[2], Roger Kloditz[1], Michael Patzschke[1], Thorsten Stumpf[1], Juliane März[1]**

[1] *Helmholtz-Zentrum Dresden-Rossendorf, Institute of Resource Ecology, Bautzner Landstraße 400, 01328 Dresden, Germany, j.maerz@hzdr.de*
[2] *European Commission, Directorate for Nuclear Safety and Security, Joint Research Centre, PO Box 2340, 76125 Karlsruhe, Germany*

Fundamental actinide (An) coordination chemistry is still rather scarcely explored though it can provide a deep insight into the bonding situation and bonding trends across the An series. Characteristic of actinides is their huge variety of possible oxidation states, typically ranging from +II to +VII for early An. A suitable approach to explore fundamental physical-chemical properties of actinides is to study series of isostructural An compounds in which the An possesses the same oxidation state.[1-3] Changes in e.g. the binding situation or magnetic effects among the An series allow insights into their unique electronic properties mainly originating from the 5*f*-electrons. The tetravalent actinides (An(IV)) are particularly suitable for this kind of systematic studies, as this is the largest accessible series within the early actinides.

Against this background, we performed the current study focusing on a systematic comparison of isostructural An(IV) complexes of Th, U, Np and Pu with a salen type ligand ($H_2L$).[4]

All syntheses and characterizations are conducted under inert, water-free nitrogen atmosphere. SC-XRD results prove that an isostructural complex series was achieved with a molecular unit where two ligands coordinate to the An tetradentately with all oxygen and nitrogen donor atoms. The resulting eightfold coordination environment exhibits a distorted square antiprismatic coordination geometry around the An center. Moreover, the relevant complexes are characterized in solution by NMR-spectroscopy displaying characteristic paramagnetic effects according to the unpaired *f*-electrons. Interestingly, the paramagnetic contributions to the $^{1}H$ and $^{13}C$ NMR chemical shifts reach their maximum with [$NpL_2$], and are drastically lower for [$PuL_2$]. The acquired experimental results are further supported by quantum chemical calculations to study the electronic structure of the complexes.

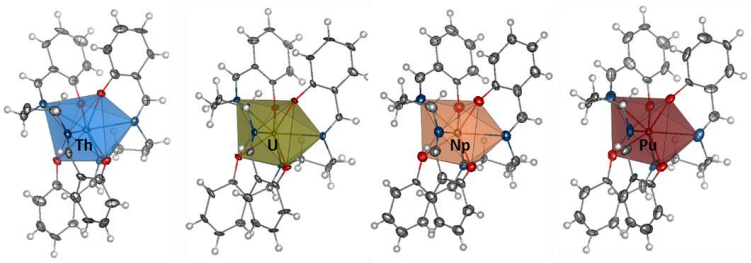


Fig. 1. Isostructural series of tetravalent actinide complexes [$ML_2$] with M = Th, U, Np, Pu.

## References

[1] A.J. Gaunt *et al.*, *Inorg. Chem.* **47**, 29-41 (2008).
[2] M.B. Jones *et al.*, *Chem. Sci.*, **4**, 1189-1203 (2013).
[3] S. G. Minasian *et al.*, *Inorg. Chem.*, **51**, 5728-5736 (2012).
[4] T. Radoske et al., publication in preparation.

# Controlled synthesis of actinide and mixed-metal *f*-element materials from organometallic precursors

**Joy H. Farnaby, James R. Hickson, Samuel J. Horsewill, Bradley Wilson, Jake McGuire, Claire Wilson, & Stephen Sproules**

*School of Chemistry, University of Glasgow, Glasgow, UK, e-mail: Joy.Farnaby@glasgow.ac.uk*

The amount and profile of research in molecular non-aqueous uranium chemistry has increased dramatically in the last 20 years. For no other single element in the periodic table have as many recent breakthroughs been reported: the first molecular uranium nitride, the first example of the $U^{2+}$ oxidation state, the reductive homologation at low temperature of the strongest bonds in nature and single molecule magnet behaviour. [1] However, in spite of their potential application in nuclear and materials science, there are no examples of molecule to material processes, which utilize organometallic precursors. Volatile complexes of uranium have been studied since the Manhattan project and recently have been used in chemical vapor deposition (CVD) or metal organic (MOCVD) processes, but without notable success. [2] Solution-based CVD processes such as Aerosol Assisted (AA) CVD have been developed because of their low cost, scalability and versatility. [3] The use of precursor solubility rather than volatility not only greatly increases the range of applicable compounds but makes the process compatible with *in situ* precursor synthesis and the deposition of ternary materials. There is much greater scope for the input of design at the precursor stage, including multi-metallic organometallics incompatible with current materials science. [4-6] Here we will present on: synthesis of organometallic precursors, deposition process and thin-film characterization.

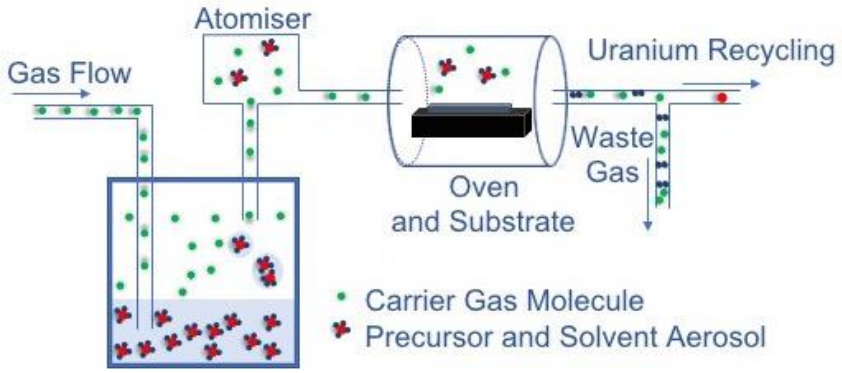


Fig. 1. Schematic of the AACVD process.

## References

[1] H. Nitsche, *Chem. Rev.* **113**, 855 (2013); M. B. Jones, *et al. Chem. Rev*. **113**, 1137 (2013); S. T. Liddle, *Angew. Chem. Int. Ed.* **54**, 8604 (2015).
[2] S. R. Daly and G. S. Girolami, *Inorganic Chemistry* **49**, 5157 (2010).
[3] C. E. Knapp and C. J. Carmalt, *Chem. Soc. Rev.* **45**, 1036 (2016).
[4] J. R. Hickson, S. J. Horsewill, J. McGuire, C. Wilson, S. Sproules and J. H. Farnaby, *Chem. Comm*. **54**, 11284 (2018)
[5] J. R. Hickson, S. J. Horsewill, C. Bamforth, J. McGuire, C. Wilson, S. Sproules and J. H. Farnaby, *Dalton Trans.* **47**, 10692 (2018)
[6] R. J. Kahan, J. H. Farnaby, N. Tsoureas, F. G. N. Cloke, P. B. Hitchcock, M. P. Coles, S. M. Roe and C. Wilson, *J. Organomet. Chem.* **857**, 110 (2018).

# Enantiopure Tetravalent Actinide Amidinates – Synthesis and Reactivity

**Sebastian Schöne,[1] Roger Kloditz[1], Juliane März[1], Peter Kaden[1], Michael Patzschke[1], Peter W. Roesky[2], Thorsten Stumpf[1]**

[1] *Helmholtz-Zentrum Dresden-Rossendorf, Institute of Ressource Ecology, Bautzner Landstraße 400, 01219 Dresden, Germany, e-mail: schoene.sebastian@hzdr.de*
[2] *Karlsruhe Institute of Technology (KIT), Institute for Inorganic Chemistry, 76131 Karlsruhe, Germany*

In contrast to the dominant trivalent state for the lanthanide series (Ln(III)), a wide variety of oxidation states (from II to VII) of actinides (An) makes their chemistry intricate but attractive. Especially the early An thorium (Th), uranium (U), neptunium (Np), and plutonium (Pu) form highly charged cations with the oxidation state +IV ($An^{4+}$), which are of particular interest for coordination chemistry due to their strong interaction with ligands.
The focus of our investigations lies in the comprehensive characterization of An(IV) complexes with ligands bearing soft donor atoms, such as nitrogen (N), both in the solid state and in solution. The present study focuses particularly on the interaction of An(IV) (Th, U, Np) with N-donor ligands of amidinate type, which could be considered as a simplified model of naturally occurring N-donor organic compounds.
Recently, the trivalent lanthanide complexes with the chiral benzamidine, (*S*,*S*)-*N*,*N*'-Bis-(1-phenylethyl)-benzamidine ((S)-HPEBA), have been successfully synthesized.[1,2] Mono- and bis-amidinate complexes of the later lanthanides (Er, Yb, Lu) were obtained using a salt metathesis approach. Only for the larger samarium(III) a homoleptic tris-amidinate was accessible.
We have extended this approach to the tetravalent An, and successfully synthesized the first transuranic amidinate complexes. Moreover, we have obtained the first enantiopure amidinate complexes of An(IV) [AnCl((S)-PEBA)$_3$] (An = Th, U, and Np) as well as the analogous Ce(IV) compound, a chemical analog of An(IV). The tris-amidinate complexes have been structurally characterized in solid state and in solution showing a comparable complex geometry.
Due to the presence of a $Cl^-$ ligand in the An coordination sphere, it could be speculated that the complex should be reactive. Thus, the reactivity of the complexes has been demonstrated by successful reduction with potassium graphite to homoleptic trivalent actinide amidinates [An((S)-PEBA)$_3$] (An = U, Np).

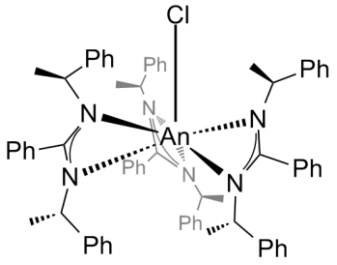


Fig. 1. Molecular structure of [AnCl((S)-PEBA)$_3$] (An = Th, U, Np, (Ce)).

## References

[1] P. Benndorf et al. *Chem. Commun*. **47**, 2574–2576 (2011).
[2] P. Benndorf et al. *Chem. Eur. J.* **18**, 14454–14463 (2012).

# The Inverse Trans Influence in U(IV/V) complexes

**Luisa Köhler,[1] Michael Patzschke[1], Juliane März[1], Thorsten Stumpf[1]**

[1] *Helmholtz-Zentrum Dresden-Rossendorf, Bautzner Landstraße 400, 01328 Dresden, Germany, e-mail: l.koehler@hzdr.de*

The inverse trans influence (ITI) is an effect well-known to occur in high valent U(V/VI) complexes. It appears as a shortening of the M–L bond in trans position to a strongly donating ligand. The effect can be explained by electron density donation from the strong ligand to the metal center, which fills up the electron hole formed through electron density transfer from semi-core 6*p* to vacant 5*f* orbitals.[1,2] This results in the observed contraction and strengthening of the bond trans to the donating ligand.
To compare the ITI in $U^{IV}$ and $U^{V}$ complexes, the U compounds $[U^{IV}(L^1)_2(TMSA)Cl_3]$ **1** ($L^1$ = $^{i}Pr_2Im$, TMSA = $(N(SiMe_3)_2)^-$) and $[U^{V}(TMSI)Cl_5](L^1H)_2$ **2** (TMSI = $NSiMe_3^-$) were synthesized from $U^{IV}$starting material in the presence of $^{i}$PrIm. In the case of **1** the metal center is surrounded by three chloro-, two carbene and one TMSA ligand, whereas **2** exhibits five chloro- and one TMSI ligand, thus generating an dianion, whose charge is compensated by the protonated carbene (Fig. 1). In **1**, the U–Cl bond, located trans to the TMSA ligand, is remarkably shorter (0.02 Å) than the other U–Cl bonds. This indicates the existence of an ITI, induced by TMSA. Based on the higher valent $U^{V}$ cation and stronger donating TMSI ligand, a similar or stronger effect should also be observed in **2**. Surprisingly, this could not be confirmed by the experimental data. The U–Cl bond lying trans to the TMSI ligand is not the shortest U–Cl bond (2.68 Å compared to 2.66 Å for U–$Cl_{1/2}$), but is in the same range as the other chloro ligands.

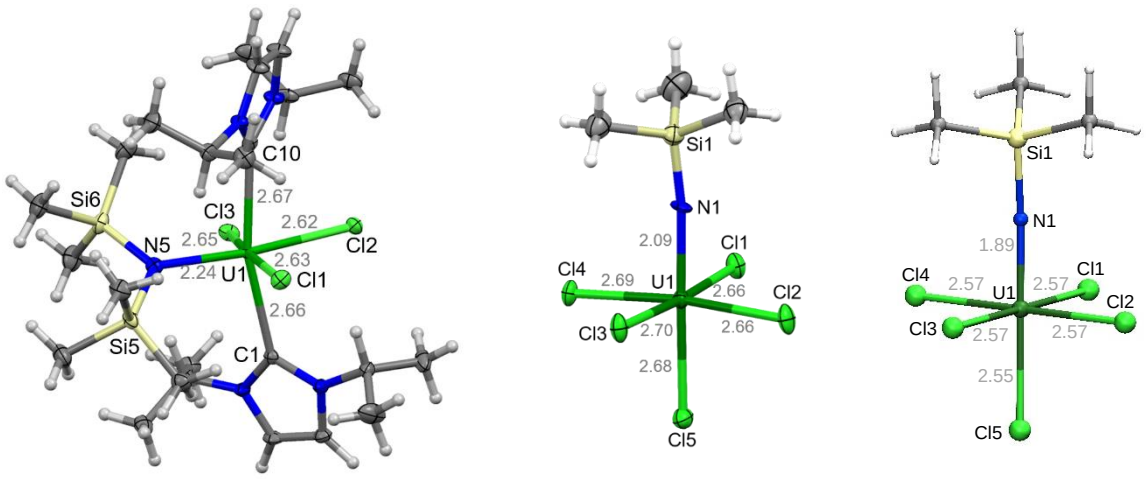


Fig. 1. Molecular structure of $[U^{IV}(L^1)_2(TMSA)Cl_3]$ **1** (left), of the experimental (middle) and optimized (right) $[U^{V}(TMSI)Cl_5]^{2-}$complex dianion structure in **2**, imidazolium counter ions omitted. Color code: carbon (C, gray), chlorine (Cl, lime green), hydrogen (H, white), nitrogen (N, blue), silicon (Si, yellow), and uranium (U, green).

The absence of a notable ITI can be attributed to intermolecular interactions in the crystal structure of **2**. Structure optimization of the molecular $U^{V}$ complex dianion (Fig. 1, right) by DFT yield a U–$Cl_5$ bond length of 2.55 Å, shorter than any other U–Cl bond by 0.02 Å. The difference between experiment and theory results from a great number of electrostatic interactions and hydrogen bonding between the complex dianion and the carbene counterions

in **2**. Similar intermolecular interactions are not present in the crystal structure of **1**, which is why the ITI could be observed for this compound.
The results demonstrate that the ITI affects complex structures for both, $U^{IV}$ and $U^{V}$ compounds, but additional effects, such as the intermolecular network observed in the structure of **2** can surpass its relatively small structural contribution.

## References

[1] M. Gregson, E. Lu, D. P. Mills, F. Tuna, E. J. L. McInnes, C. Hennig, A. C. Scheinost, J. McMaster, W. Lewis, A. J. Blake, et al., *Nat. Commun.* **8**, 14137 (2017).
[2] B. Kosog, H. S. La Pierre, F. W. Heinemann, S. T. Liddle, K. Meyer, *J. Am. Chem. Soc.* **134**, 5284–5289 (2012).

# Mechanochemistry of low valent uranium

**Markus Zegke,[1] Sophia Eimermacher[1], Khan Lê[1] and Mathias Wickleder[1]**

[1] *Institut für Anorganische Chemie, Universität zu Köln, Greinstraße 6, 50939 Köln, Germany, e-mail: m.zegke@uni-koeln.de*

The synthesis low valent actinoides oftentimes involves harsh reaction conditions, dry solvents and long reaction times of up to a month, and may still need further means of purification, such as celite filtration or other time-consuming methods. This has made the studies of such materials inherently difficult.
Here we present a simple method of mechanochemical synthesis of low valent inorganic and organometallic uranium compounds using an oscillating ball mill. The materials can be synthesised within 30 to 300 min in good to very good yields. The finely ground, homogenous, dry and solvent-free material can be easily sublimed to obtain single crystalline samples, and gram quantities can be synthesised within a few hours.
Conclusively, we have established a method for a quick and easy synthesis of actinoid starting materials that does not need any solvents, reduces the reaction times from months to days, produces dry and single crystalline material and proceeds in very good yields.

# Synthesis of actinides-based hybrids nanomaterials using bottom up approach

**Elisa Re, Jérôme Maynadie, Daniel Meyer, Xavier Le Goff**

*Institut de Chimie Séparative de Marcoule, UMR 5257 CEA/CNRS/UM/ENSCM, Site de Marcoule – Bât. 426, BP 1717130207, Bagnols / Cèze cedex, France*

Over the past two decades, nanoscience and nanotechnology have attracted increasing attention of the scientist community and industry. As a consequence of nanoscale, this type of materials exhibit size- and shape-dependent properties. Indeed, the physical and chemical properties show a lot of difference between the bulk and the nanoparticles (electronic, magnetic, optical, catalytic…). In 1993, Murray et al. have reported a surfactant-assisted method in organic medium enable to produce highly monodisperse nanocrystals [1]. Since, scientists have devoted a significant effort on the improvement of this synthetic method for the production of size- and shape-controlled nano-objects witch can be envisaged as novel building blocks. These parameters are crucial for the organization of nano-objects in 2D or 3D architectures and for the study of their intrinsic and collective properties.

This project aims to elaborate and characterize new nanostructured micrometric objects using two bottom-up approaches. The first one, called "one-pot", is based on simultaneous growth and self-assembly of nanoparticles using a bridging organic ligand. The second one need two steps: the first step consists in nanoparticles synthesis and the second one involves nanoparticle surface modification by reactive molecules able to promote self-assembling by formation of covalent bridges (Click Chemistry) or by electrostatic interactions.

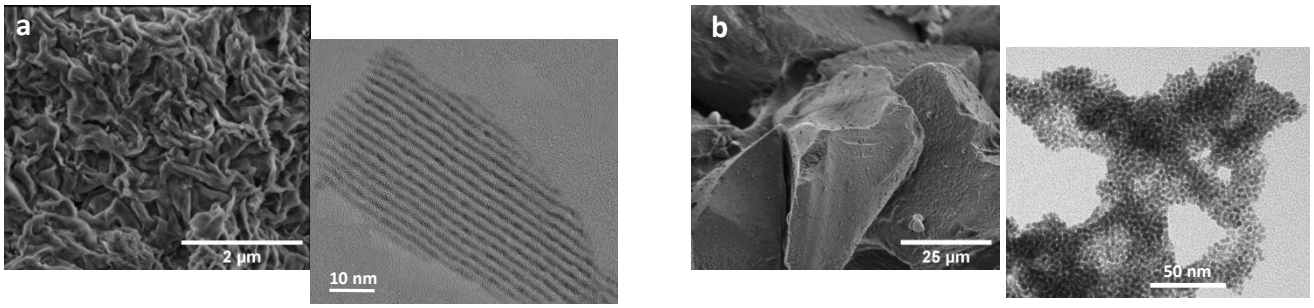


Fig 1: a) SEM and TEM images of uranium oxide hybrid nanomaterial synthetized by ***one pot synthesis***. b) SEM and TEM images of uranium oxide hybrid nanomaterial synthetized by ***self-assembly synthesis***

Using the first synthesis method, hybrid nanomaterial was produced as highly organized sheets presenting a lamellar structure as we can see on Fig. 1 a). The distance between sheets can be controlled by temperature and the inter-lamellar distance can be modulated by the nature of the organic linker. The self-assembly synthesis was used to obtain 3D nanostructured hybrid materials present on Fig. 1 b). The first part of this work has been done on uranium oxide. The next goal for this work is to assemble mixed actinide nanoparticles with platinoid nanoparticles in order to produce model materials.

[1] C. B. Murray, D. J. Norris, et M. G. Bawendi, *J. Am. Chem. Soc.*, **115** (19), 8706‑8715 (1993).

# Anisotropic low-temperature thermodynamic and magnetotransport properties of single crystalline $UCoSi_2$

**Daniel Gnida, Maria Szlawska, Piotr Wiśniewski, Dariusz Kaczorowski**

*Institute of Low Temperature and Structure Research, Polish Academy of Sciences, P.O. Box 1410, 50 – 950 Wroclaw, Poland, e-mail: D.Gnida@intibs.pl*

$UCoSi_2$ belongs to the family of ternary uranium silicides $UTSi_2$ ($T$ = Fe, Co, Ni, Pt) crystallizing with an orthorhombic crystal structure of the $CeNiSi_2$-type [1]. Recently, it was found for $UCoSi_2$ that its specific heat divided by temperature is proportional to –logT between 2 and 10 K, which could be considered as a non-Fermi liquid behavior [2]. Taking into account that gradual suppression of ferromagnetism in the solid solution $UNi_{1-x}Co_xSi_2$ ($0 < x < 1$) occurs in the vicinity of $x \approx 1$, it was suggested that the ground state properties of $UCoSi_2$ can be related to the closeness to quantum critical point governed by the ferromagnetic spin fluctuations [2].

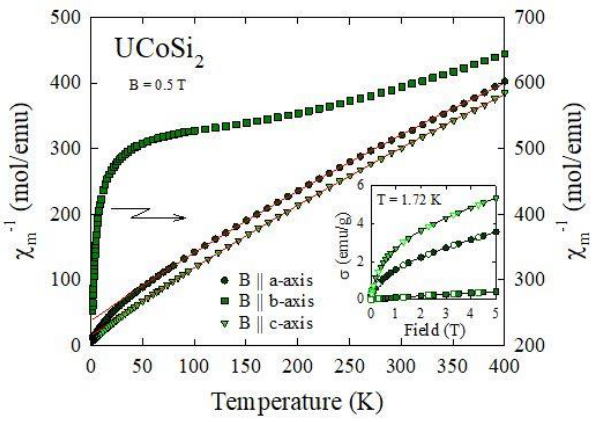


Fig.1. Temperature dependencies of the inverse magnetic susceptibility of single-crystalline $UCoSi_2$. Inset: the magnetization measured at 1.72 K as a function of magnetic field.

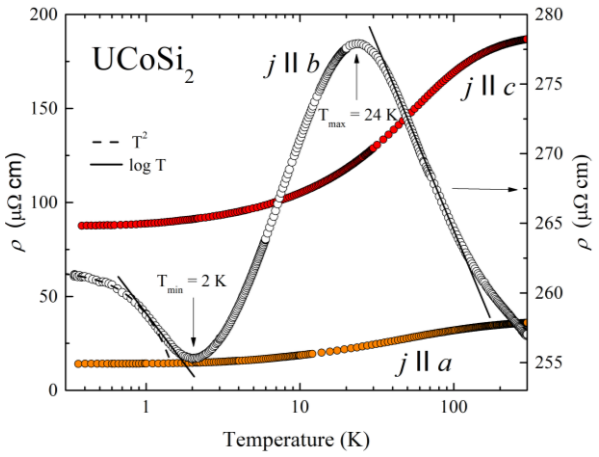


Fig.2. Temperature dependencies of the electrical resistivity of single-crystalline $UCoSi_2$.

To clarify the actual nature of the anomalous specific heat behavior in $UCoSi_2$ we investigated the low temperature properties of single crystals grown in a tetra-arc furnace using Czochralski method. Magnetic susceptibility ($\chi$), magnetization ($\sigma$) and electrical resistivity ($\rho$) measurements were carried out in three principal crystallographic direction of the orthorhombic unit cell. The results revealed that $UCoSi_2$ exhibits strongly anisotropic properties. As displayed in Fig. 1, $\chi^{-1}$ measured along the $a$ and $c$ axes changes with temperature in a manner describable above 30 K by modified Curie-Weiss (MCW) law. In contrast, $\chi^{-1}(T)$ measured along the $b$- axis does not follow the MCW relation and shows a broad hump-like feature near 50 K. Uniaxial magnetic anisotropy of $UCoSi_2$ is also evident in the magnetization data taken at 1.7 K (see the inset to Fig. 1). In a field of 5 T, the ratios $\sigma_a/\sigma_b$ and $\sigma_c/\sigma_b$ achieve very high values of 13 and 8, respectively.

As shown in Fig. 2, the electrical transport in $UCoSi_2$ is also highly anisotropic. The $b$-axis component of the electrical resistivity tensor is markedly different from the resistivity measured along the crystallographic directions $a$ and $c$. The temperature variation $\rho_b(T)$ shows logT

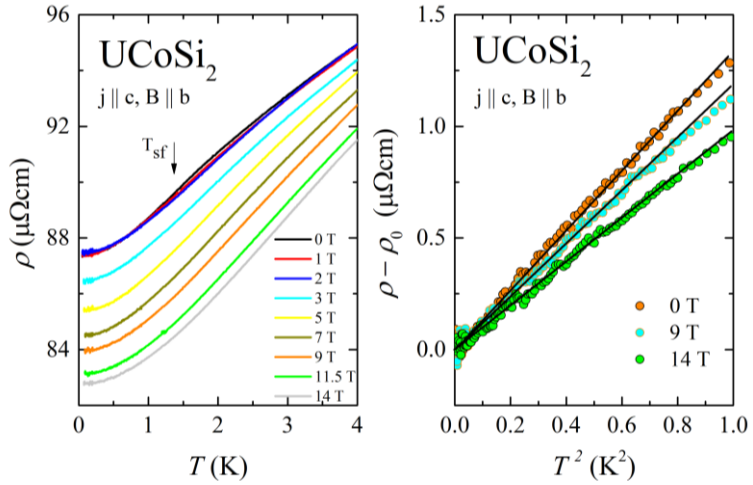


Fig.3. Low-temperature variations of the electrical resistivity $\rho_c(T)$ of single-crystalline $UCoSi_2$ measured in different magnetic fields B || b-axis (left panel). The right panel shows the $\rho_c(T)$ data taken in B = 0, 9 and 14 T plotted as a function of $T^2$.

slopes above $T_{max} \approx 24$ K and below $T_{min} \approx 2$ K, reminiscent of Kondo lattices. At the lowest temperatures, $\rho_b(T)$ is of Fermi liquid type. The crossover temperature from logT to $T^2$ dependencies defines the Kondo energy scale $T_K \approx 1$ K.

While the overall behavior of the *b*-axis resistivity may point to fairly localized nature of the 5f electrons in $UCoSi_2$, the temperature variations of the *c* and *a* components of the resistivity tensor are reminiscent of spin fluctuation systems, like $UAl_2$ [3], $UPt_3$ [4] or Coles alloys [5]. As can be inferred from Fig. 3, $\rho_c(T)$ exhibits a knee at $T_{sf} = 1.4$ K that can be considered as the spin fluctuation temperature. Remarkably, the value of $T_{sf}$ is similar to that of $T_K$ derived from $\rho_b(T)$. At lower temperatures, $\rho_c$ is proportional to $AT^2$, as expected for scattering conduction electrons on spin fluctuations. The coefficient A decreases in strong magnetic fields, however the $T^2$ behavior is preserved even in 14 T.

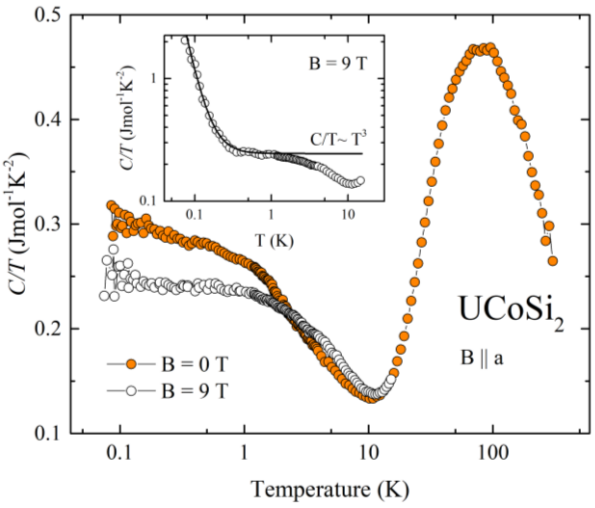


Fig.4. Temperature dependencies of the specific heat over temperature ratio of single-crystalline $UCoSi_2$ measured in zero field and in a field of 9 T applied along the *a*-axis. The 9 T data were corrected for the nuclear specific heat contribution in a manner shown in the inset.

The specific heat over temperature ratio of $UCoSi_2$ (see Fig. 4) shows at low temperatures an upturn that can be attributed to an interplay of Kondo effect and spin fluctuations. At T = 0.07 K, C/T achieves as large value as 0.3 $Jmol^{-1}K^{-2}$. In a magnetic field of 9 T, the upturn in C/T(T) decreases and forms a plateau below 2 K characteristic of a Fermi liquid. This behavior is in full agreement with the low-temperature magnetotransport data.

## References

[1] D. Kaczorowski, *Solid State Commun.* **99**, 949 (1996).
[2] A. Pikul, D. Kaczorowski, *Phys. Rev. B* **85**, 045113 (2012)
[3] R.J. Trainor, M.B. Brodsky, H.V. Culbert, *Phys. Rev. Lett.* **34**,1019 (1975)
[4] G. R. Stewart, Z. Fisk, J.O. Willis,and J. L. Smith, *Phys. Rev. Lett.* **52**, 679 (1984)
[5] N Rivier and V Zlatic, *J. Phys. F: Met. Phys.* **2** L99 (1972)

# Magnetic and related properties of the ternary germanides $UT_{1-x}Ge_2$ (T = Fe, Ni, Os)

**Mathieu Pasturel[1], Maria Szlawska[2], Adam P. Pikul[2], Antonio P. Gonçalves[3], H. Noël[1], Dariusz Kaczorowski[2]**

*[1] Univ Rennes, CNRS, Institut des Sciences Chimiques de Rennes - UMR6226, 35042 Rennes, France*
*[2]Institute of Low Temperature and Structure Research, Polish Academy of Sciences, P Nr 1410, 50-590 Wrocław 2, Poland, e-mail: A.Pikul@intibs.pl*
*[3] C[2]TN, Instituto Superior Técnico, Universidade de Lisboa, Campus Tecnológico e Nuclear, Estrada Nacional 10, 2695-066 Bobadela LRS, Portugal*

In the course of our search for novel uranium-based germanides we have recently synthesized and characterized a new compound $URu_{0.29}Ge_2$, crystalizing in a monoclinic structure of its own type (C2/c space group, lattice parameters: $a$ = 4.098(1) Å, $b$ = 15.936(3) Å, $c$ = 4.045(1) Å and $\beta$ = 90.091(2)°), derived from the $CeNiSi_2$-type structure. Physical properties measurements carried out on a polycrystalline sample revealed that the compound orders ferromagnetically below the Curie temperature $T_C$ of about 63 K. The phase transition manifests itself as distinct anomalies in temperature variations of thermodynamic as well as transport properties. In the electrical resistivity the onset of the ferromagnetic state is associated with a broad hump just below $T_C$, followed by a small upturn in $\rho(T)$ at the lowest temperatures. The hump hints at non-trivial magnetic structure of the system, while the upturn has been interpreted as resulting from atomic disorder inherently present in the system [1].

All those findings motivated us to look for other representatives of the $UT_{1-x}Ge_2$ family. In this contribution we present structural and physical properties of three phases with Fe [2], Ni [3,4], poorly described in the literature, and Os – reported here for the first time. X-ray powder diffraction and energy dispersive spectroscopy confirmed that these compounds possess the $UFe_{0.45}Ge_2$, $UNi_{0.45}Ge_2$ and $UOs_{0.25}Ge_2$ compositions and crystallize with the orthorhombic $CeNiSi_2$- (Fe, Ni) or $URu_{0.29}Ge_2$-type (Os) structures. The physical properties of these phases were studied by means of DC magnetization, AC magnetic susceptibility, specific heat and electrical resistivity measurements, performed on polycrystalline samples in wide ranges of temperature (down to 2 K) and magnetic field (up to 9 T).

As can be inferred from the preliminary data, $UFe_{0.45}Ge_2$ exhibits a transition into a spin-glass-like state at $T_f$ of about 37 K. Spin freezing in this material manifests itself as a frequency-dependent maximum in the AC magnetic susceptibility and smeared anomaly in the specific heat. The compound shows an enhanced Sommerfeld coefficient and large electrical resistivity, which can be attributed to the structural disorder. Upon applying magnetic field, the spin-glass state rapidly (below 0.1 T) evolves into a long-range ferromagnetic order.

The compounds $UNi_{0.45}Ge_2$ and $UOs_{0.25}Ge_2$ were found to order antiferromagnetically below 47 K and ferromagnetically below 54 K, respectively. In both materials, the magnetic phase transitions give rise to distinct anomalies in all the temperature characteristics measured. Interestingly, $UNi_{0.45}Ge_2$ exhibits a rapid drop of the resistivity in high magnetic fields, associated with a distinct magnetic hysteresis. We tentatively ascribe this behavior to a field-induced first-order metamagnetic phase transition.

Further experimental studies on the novel $UT_{1-x}Ge_2$ compounds are presently under way.

## References

[1] M. Pasturel *et al*., *Intermetallics* **95**, 19 (2018).
[2] M. S. Henriques *et al.*, *J. Alloys Compd.*, **639**, 224 (2015).
[3] L. G. Aksel'rud, in *Book of abstracts of the International Conference on Crystal Chemistry of Intermetallic Compounds*, Lviv, Ukrain (1995).
[4] Z. Molčanová *et al.*, *Acta Phys. Pol. A*, 131, 994 (2017).

# New Insights into Actinide High Pressure Science: Unraveling Pressured Induced Bond Expansion and Implications for Structural Chemistry

**Gabriel L. Murphy,[1] Evgeny V. Alekseev[1], Philip Kegler[1], Brendan J. Kennedy[2], Zhaoming Zhang[3] and Helen Maynard-Casely[3]**

[1] *Institute of Energy and Climate Research, Forschungszentrum Jülich GmbH, 52428 Jülich, Germany*
[2] *School of Chemistry, The University of Sydney, Sydney, NSW 2006, Australia*
[3] *Australian Nuclear Science and Technology Organisation, Lucas Heights, NSW 2234, Australia*

As a part of our interest in examining actinides under extreme conditions we have investigated a variety of uranium oxides exposed to *in situ* and *ex situ* high pressure conditions. We demonstrate using a combination of *in situ* neutron and synchrotron X-ray powder diffraction when polymorphs of $SrUO_4$ are exposed to elevated pressures they can undergo anomalous bond expansion caused by pressure induced electron delocalization associated with charge transfer from the uranyl $U^{6+}$ moiety (See Fig. 1.) [1]. As some theoretical studies have suggested [2], this demonstrates, for the first time, the inapplicability of Badgers rule to uranyl, and by extension, actinyl bearing materials. This has consequences for the interpretation and validity of previously reported [3] and future spectroscopic data arising from high pressure studies of actinides among other measurement methods. Conversely this new insight allows us to better understand the chemical reactivity and structure property relationships that can occur between actinide materials exposed to high pressure environments. A pertinent demonstration of this is in our *ex situ* structural investigation of the Ni-U-O system of oxides [4] using single crystal X-ray diffraction and X-ray absorption spectroscopy. Under ambient pressure conditions the oxides $NiU_2O_6$ and $NiU_3O_{10}$ can be accessed through high temperature methods both forming 3D framework structures based on interconnecting $UO_{6/7}$ polyhedra. Application of high pressure allows two polymorphs of the formula $NiUO_4$ to be obtained. Intrinsic to these structures is the occurrence of 1D $UO_6$ and $NiO_6$ rutile like chains. Their formation can be understood on the basis of the $Ni^{2+}$ cation being of insufficient size for either polymorph to form under ambient pressure conditions, where, instead $UO_6$ distortion occurs via substantial elongation of bonds to allow structure formation under high pressure conditions. An elegant second example can be observed in the $(Cr,Fe)U_2O_6$ structural system [5] which form 2D layered structures based on independent $(Cr,Fe)O_6$ and $UO_6$ layers. However the application of pressure allows aliovalent substitution to occur on the $(Cr,Fe)O_6$ layer through the inclusion of $Pt^{4+}$ for $Fe^{3+}$ which further causes reduction in the $UO_6$ layers to occur with further structural distortion. These investigations demonstrate profound new insight into the behaviour of actinides under pressure salient for both fundamental science and also applied nuclear waste form materials, particularly those within deep geological environments.

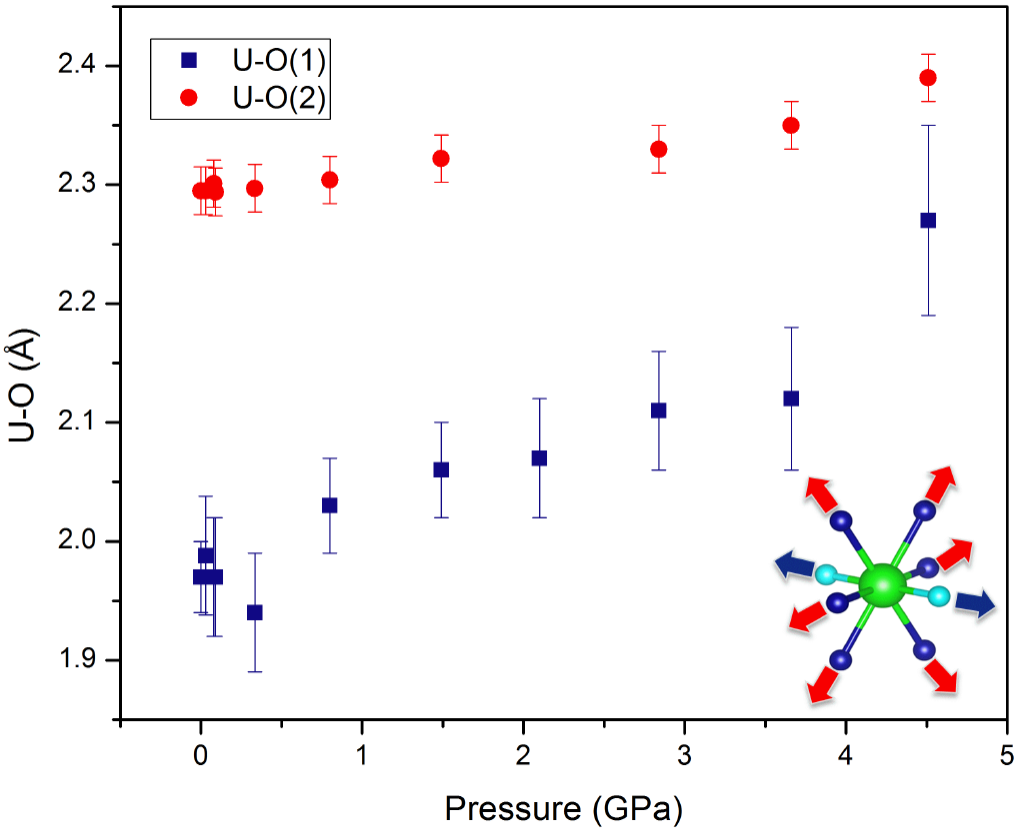


Fig. 1. Uranium-Oxygen bond lengths in the $UO_8$ polyhedra in α-$SrUO_4$ from ambient towards 5 GPa. Note the exceptional expansion of the uranyl U-O(1) bond length with increasing pressure.

## References

[1] Murphy, G. L.; et al. *In Situ* High Pressure Diffraction Studies of $SrUO_4$: Bond Expansion with Increasing Pressure and Violating Badger's Rule. *In preparation.*
[2] Osman, H. et al. Structure and bonding in crystalline cesium uranyl tetrachloride under pressure *Physical Chemistry Chemical Physics* ***58*** (1), pp 228–233 (2019).
[3] Warcheza, E. et al. High-Pressure Studies of Cesium Uranyl Chloride *Inorganic Chemistry* ***58*** (1), pp 228–233 (2019).
[4] Murphy, G. L.; et al. High-pressure synthesis, structural, and spectroscopic studies of the Ni–U–O system. *Inorganic Chemistry* **57** (21), 13847-13858 (2018).
[5] Murphy, G. L.; et al. Layer modification and redox mixing in the $(Cr_{1-x}Pt_x)FeUO_6$ *In preparation.*

# Particle Size vs. Local Environment Relationship for $ThO_2$ and $PuO_2$

**Laura Bonato,[1] Matthieu Virot,[1] Elodie Dalodière,[1] Thomas Dumas,[2] Adel Mesbah,[1] Oliver Dieste Blanco,[3] Thierry Wiss,[3] Damien Prieur,[4] André Rossberg,[4] Laurent Venault,[2] Philippe Moisy,[2] Sergey I. Nikitenko[1]**

*[1] Université de Montpellier, Institut de Chimie Séparative de Marcoule (ICSM), UMR 5257, CEA-CNRS-UM-ENSCM, Site de Marcoule BP17171, 30207 Bagnols sur Cèze, France. e-mail: matthieu.virot@cea.fr*
*.[2] French Nuclear and Alternative Energies Commission (CEA) Nuclear Energy Division, Department of Mining and Fuel Recycling Processes (DMRC), Site de Marcoule BP17171, 30207 Bagnols sur Cèze, France.*
*[3] European Commission, Joint Research Centre (JRC), Postfach 2340, 76125 Karlsruhe, Germany.*
*[4] Helmholtz-Zentrum Dresden - Rossendorf, Institute of Resource Ecology, Bautzner Landstraße 400, 01328 Dresden, Germany*

Nanomaterials have attracted considerable interest in recent interdisciplinary research for their technological applications related to the nanometric size of the building blocks composing the solids (ex: crystallite or atomic and molecular groups).[1,2] Nanostructured materials can be defined as solid samples exhibiting a microstructure the characteristic length scale of which is roughly ranging between 1 and 10 nm.[1] The controlled microstructure of materials at the atomic level offers new physical and chemical properties in comparison to similar bulk materials already applied, for instance, in catalysis, synthesis of luminescent materials, preparation of cosmetic and solar creams, preparation of solar cells, etc.[3,4] Such paradigm has been attributed to the increased surface-to-volume ratio of the shrinking particle size which increase the number of surface and interface atoms generating stress, stain, and structural perturbations.[2] In actinide chemistry, the synthesis and characterization of nanomaterials is very scarce but is of growing interest due to the contribution of actinide nanomaterials in environment (ex: migration of actinides) and industry (ex: high burn up structures). Recently, we observed the nanostructuration of $PuO_2$ and noticed its outstanding reactivity under ultrasound irradiation which stirred up our curiosity concerning the local environment of this oxide at the nanoscale.[5]

In this work, we investigate the synthesis and relevant characterization of nanostructured $PuO_2$ and $ThO_2$. Th can be considered as a good surrogate for Pu because both elements exhibit close ionic radii, their oxide crystallize in the fluorite Fm-3m structure, and they both exist at the (+IV) oxidation state. More precisely, Th only exists at the +IV oxidation state thus avoiding misinterpretations related to the potential contribution of other oxidation states in the crystalline structure. The synthesis studies allowed us to select the nanostructuration conditions for the various oxides and a careful characterization and correlation with AFM, HR-TEM, Raman spectroscopy, XRD and XAS techniques allowed us to probe the local disorder for the various oxides as a function of the particle size. Particularly, EXAFS investigations clearly show a linear decrease of the coordination number for An-O and An-An spheres with the shrinking particle sizes. The crystalline nature of the particles (HR-TEM, XRD) suggest that these observation are correlated to the increasing surface contribution of these particles. These new results raise the question of the physico-chemical properties of oxide nanomaterials crystallizing in the fluorite structure which are materials of paramount importance for engineering applications such as nuclear energy, solid oxide fuel cells, catalysis, or sensors.

## References

[1] H. Gleiter, *Acta Mater*. **48**,1-29 (2000).
[2] M. Fernandez-Garcia et al., *Chem. Rev.* **104**, 4063-4104 (2004).
[3] J.-M. Teulon, *Nanomaterials* **9**, 1-29 (2019).
[4] W. J. Stark et al., *Chem. Soc. Rev.* 44, 5793-5805 (2015).
[5] E. Dalodière et al., *Sci. Reports* 43514 (2017).

# In situ X-ray diffraction studies of $UO_2$ oxidation and phase transition into $U_3O_8$

**Jacek Wąsik[1,2]*, Joseph Sutcliffe[2], Neil Fox[3], Ross Springell[2]**

[1] *Bristol Centre for Functional Nanomaterials, University of Bristol, Bristol BS8 1FD, UK, e-mail: jacek.wasik@bristol.ac.uk*
[2] *School of Physics, University of Bristol, Tyndall Avenue, Bristol BS8 1TL, UK*
[3] *School of Chemistry, University of Bristol, Cantock's Close, Bristol BS8 1TS, UK*

The University of Bristol hosts one of the world's only physical vapour deposition systems that is dedicated to the synthesis of nuclear-related materials. The possibility of growing samples with Angstrom precision significantly reduces levels of radioactivity. This makes samples safe to work with and to transport within and outside the university. Another advantage offered by this system is the capability of growing single crystals with a specific orientation, or polycrystalline samples with controlled grain sizes. The thin-film approach to actinide materials gives a great opportunity for a better understanding of their bulk equivalents, without the need for special radiation protection infrastructure.
Uranium dioxide is the most common nuclear fuel. The microstructure of this nuclear fuel has an important influence on its properties. Recent synchrotron studies of uranium dioxide single crystal thin films showed that the crystal orientation has a strong impact on the dissolution of those thin films [1]. The (111) oriented film was found to be significantly more corrosion resistant in comparison to (001) and (110) films.
Oxidation of uranium dioxide into triuranium octoxide at temperatures below 400°C fallows a two-step reaction: $UO_2$->$U_4O_9$/$U_3O_7$->$U_3O_8$ [2]. In this study polycrystalline uranium dioxide thin films have been grown to investigate the influence of the crystallographic orientation on the oxidation rate by in situ XRD studies.

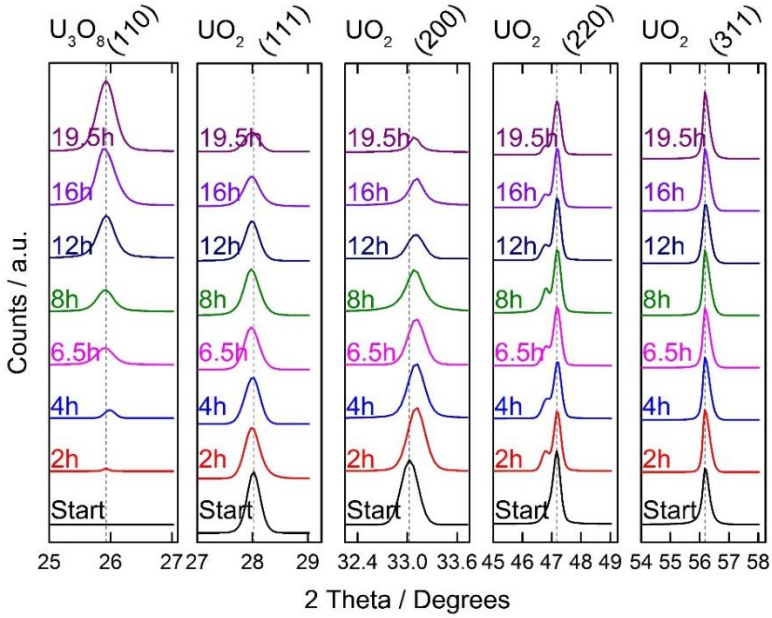


Fig. 1. Changes in XRD patterns of thin film sample after oxidation at 300° in 200mbar of oxygen atmosphere.

## References

[1] S. Rennie et al. Corrosion Science **145**, 162–169 (2018).
[2] R.J. McEachern et al. Nuclear Materials **254**, 87 (1998).

# The orbital to spin moment ratio in $UGe_2$ under pressure: part I experiment

**F. Wilhelm,[1] J.-P. Sanchez[2], D. Braithwaite[2], J.-P. Brison[2], D. Aoki[2,3], A. B. Shick[4] and A. Rogalev[1]**

*[1]European Synchrotron Facility (ESRF), B.P. 220, F- 38043 Grenoble cedex, France, e-mail: wilhelm@esrf.fr*
*[2]Univ. Grenoble Alpes, Commissariat à l'Energie Atomique et aux Energies Alternatives (CEA), Institut Nanosciences et Cryogénie (INAC)- PHELIQS, F- 38000 Grenoble, France*
*[3]Institute for Materials Research, Tohoku University, Oarai, Ibaraki 311-1313, Japan*
*[4]Institute of Physics, ASCR, Na Slovance 2, CZ-18221 Prague, Czech Republic*

The discovery that ferromagnetism and superconductivity could coexist sparked a wave of scientific interest at the beginning of the millennium [1], yet there are still few materials that display this unique behaviour. The most commonly studied, is the compound $UGe_2$, which has pressure-temperature and magnetic field-temperature phase diagrams, rich with unusual physical phenomena [2].
At ambient pressure, $UGe_2$ is a ferromagnet with a Curie temperature of ~53 K. Below 12 kbar (at 2.3K), it is in a so-called ferromagnetic phase 2 (FM2). A very interesting feature of this material is that a second ferromagnetic phase transition FM1 appears as a jump in the magnetization above ~12 kbar. This magnetic moment versus pressure change has been interpreted by Sandeman, Lonzarich, and Schofield [3] as a first-order Stonerlike phase transition in spin-only magnetization due to a sharp double-peak density of states (DOS) very near the Fermi level. Above this ~12 kbar pressure, the transition FM1→FM2 can be induced by a magnetic field for a fixed pressure.
We have carried out X-ray magnetic circular dichroism (XMCD) measurements under high pressure on $UGe_2$ single crystal at the ESRF beamline ID12. It is well established that XMCD at the U $M_{4,5}$-edges provides accurate quantitatively measurements of the U 5*f* orbital to spin magnetic moment ratio. To perform this challenging experiment, we have used a specific diamond anvil cell which combines a fully perforated anvil and a 30 µm thin plate of diamond through which the total fluorescence yield signal from the sample is collected in backscattering. The incident X-ray beam was focused on the sample using parabolic Be refractive lenses with typical beam size of few microns vertically and few tens of microns horizontally. We have measured the XMCD spectra at the U $M_{4,5}$-edges in both FM1 and FM2 phase of $UGe_2$ by tuning the pressure at around ~14 kbar at 2.7 K. By just varying the magnetic field, we were able record good quality XMCD at the U $M_{4,5}$-edges in the FM1 phase (1 T) and in the FM2 phase (4 T). We found that the orbital-to-spin moment ratio of the U 5*f* magnetic moments is different for both FM1 and FM2 phases and decreases as a function of the applied pressure [4].

## References

[1] S. S. Saxena *et al.* Nature **406**, 587 (2000)
[2] C. Pfleiderer and A. D. Huxley, Phys. Rev. Lett. **89**, 147005 (2002)
[3] K. Sandeman et al., Phys. Rev. Lett. **90**, 167005 (2003).
[4] F. Wilhelm, J.–P. Sanchez *et al.*, unpublished (2018).

# Broadening of the XPS Spectra in Heavy Metal Oxides

**Paul S. Bagus[1], Connie J. Nelin[2], Sophie Rennie[3], Gerard H. Lander[3], Ross Springell[3]**

*[1] Department of Chemistry, University of North Texas, Denton, TX 76203-5017, USA, Paul.Bagus@unt.edu*
*[2] Consultant, Austin, TX 78730, USA*
*[3] School of Physics, University of Bristol, Tyndall Avenue, Bristol BS8 1TL, UK*

It is common to assume that the broadening of X-ray Photoelectron Spectra, XPS, data arises mainly from experimental resolution. If the experimental resolution could be refined, for example using synchrotron radiation, then the limitation to the broadening of the XPS would be the lifetime of the core-holes, where estimates of these lifetimes are available for most atoms [1]. From our measurements of $UO_2$ at the Diamond synchrotron (where the instrumental resolution is 0.3 eV), we find broadening to ~1.3 eV, which is comparable to those obtained with conventional, monochromatized laboratory Al and Mg X-ray sources [2-3] where the instrumental resolution is not as good as with synchrotron radiation. However, it is known that there are other sources of XPS broadening. One source of broadening arises due to unresolved final state multiplets from angular momentum coupling of the core hole with valence open shell electrons (Ref. [4] and references therein) and from many body effects between the bonding and anti-bonding valence shell electrons. [5-7] Another source of broadening is vibrational excitations, or Franck-Condon broadening, which is known to be important for lighter metal oxides [8-10] leading to broadenings of ~1 eV. In the present work, the role of these excitations for $UO_2$ is examined from theoretical cluster model studies of the electronic structure, see Ref. [6] and references therein, and compared with our high-resolution synchrotron XPS measurements.

## References

[1] J. L. Campbell and T. Papp, "Widths of the atomic K - N7 Levels", *Atomic Data and Nuclear Data Tables* **77**, 1 (2001).
[2] J. E. Stubbs *et al*, "$UO_2$ Oxidative Corrosion by Nonclassical Diffusion", *Phys. Rev. Lett.* **114**, 246103 (2015).
[3] T. Gouder, R. Eloirdi, and R. Caciuffo, "Direct observation of pure pentavalent uranium in U2O5 thin films by high resolution photoemission spectroscopy", *Scientific Reports* **8**, 8306 (2018).
[4] P. S. Bagus, E. S. Ilton, and C. J. Nelin, "Extracting Chemical Information From XPS Spectra: A Perspective", *Catal. Lett.* **148**, 1785 (2018).
[5] P. S. Bagus *et al*, "Covalent Bonding In Heavy Metal Oxides", *J. Chem. Phys.* **146**, 134706 (2017).
[6] P. S. Bagus, E. S. Ilton, and C. J. Nelin, "The Interpretation of XPS Spectra: Insights Into Materials Properties", *Surf. Sci. Rep.* **68**, 273 (2013).
[7] P. S. Bagus, C. J. Nelin, and E. S. Ilton, "Theoretical modeling of the uranium 4f XPS for U(VI) and U(IV) oxides", *J. Chem. Phys.* **139**, 244704 (2013).
[8] M. Iwan and C. Kunz, "Investigation of the phonon broadening of core levels in NaCl", *Phys. Lett. A* **60A**, 345 (1977).
[9] C. J. Nelin *et al*, "Analysis of the Broadening of X-ray Photoelectron Spectroscopy Peaks for Ionic Crystals", *Angew. Chem. Int. Ed.* **50**, 10174 (2011).
[10] P. H. Citrin, P. Eisenberger, and D. R. Hamann, "Phonon broadening of X-ray photoemission linewidths", *Phys. Rev. Lett.* **33**, 965 (1974).

# Graphene derived uranium carbide for isotopes production targets

**Stefano Corradetti[1], Lisa Biasetto[2], Sara Carturan[1,3], Rachel Eloirdi[4], Pedro Amador-Celdran[4], Dragos Staicu[5], Oliver Dieste Blanco[5], Alberto Andrighetto[1]**

*[1] INFN-Laboratori Nazionali di Legnaro, Viale dell'Università 2, 35020, Legnaro (PD), Italy. e-mail: stefano.corradetti@lnl.infn.it*
*[2] Università di Padova, Dipartimento di Tecnica e Gestione dei Sistemi Industriali, Stradella San Nicola 3, 36100, Vicenza, Italy.*
*[3] Università di Padova, Dipartimento di Fisica e Astronomia, Via Marzolo 8, I-35131, Padova, Italy.*
*[4] European Commission, Joint Research Centre, Directorate G for Nuclear Safety and Security, Unit G.I.5, Advanced Nuclear Knowledge unit, Postfach 2340, 76215, Karlsruhe, Germany.*
*[5] European Commission, Joint Research Centre, Postfach 2340, 76215, Karlsruhe, Germany.*

Actinide-based targets are nowadays commonly used as sources of radioactive isotopes in ISOL (Isotope Separation On-Line) facilities such as SPES [1]. The design of a proper ISOL target is strictly related to the obtainment of porous refractory materials, which are capable to work under extreme conditions (temperatures up to 2000 °C in high vacuum) with a high release efficiency. Moreover, heat dissipation is one of the aspects to be considered when developing efficient targets capable of working under heat-induced stresses. For these reasons, actinide carbides such as uranium carbide are the most used materials for this application; they are often mixed with an excess of carbon in the form of graphite or pyrolytic carbon in order to tailor the thermal properties of the produced targets.
The work here presented describes the use of graphene as a carbon source for the obtainment of carbon-dispersed uranium carbide by the carbothermal reduction of uranium oxide. This material (referred to as $UC_x$-graphene in Fig. 1) possesses higher thermal diffusivity and conductivity with respect to the standard one obtained using graphite ($UC_x$-graphite), as shown in Fig.2 [2]. The synthesis and characterization of the material, performed at JRC-Karslruhe in the ActusLab framework (AUL #176), as well as a preliminary activity carried out at INFN-LNL using lanthanum carbide [3], will be presented.

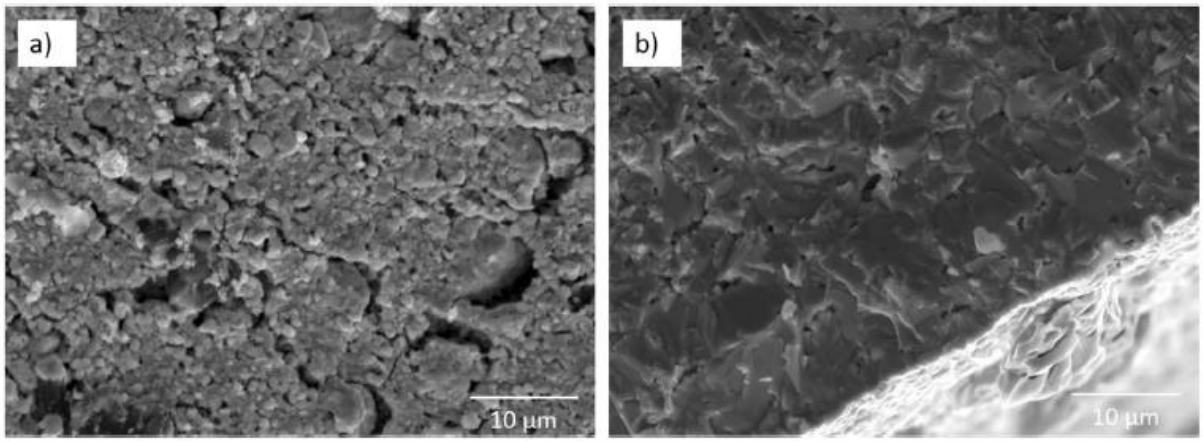


Fig. 1. SEM images of the cross-section of $UC_x$-graphite (a) and $UC_x$-graphene.

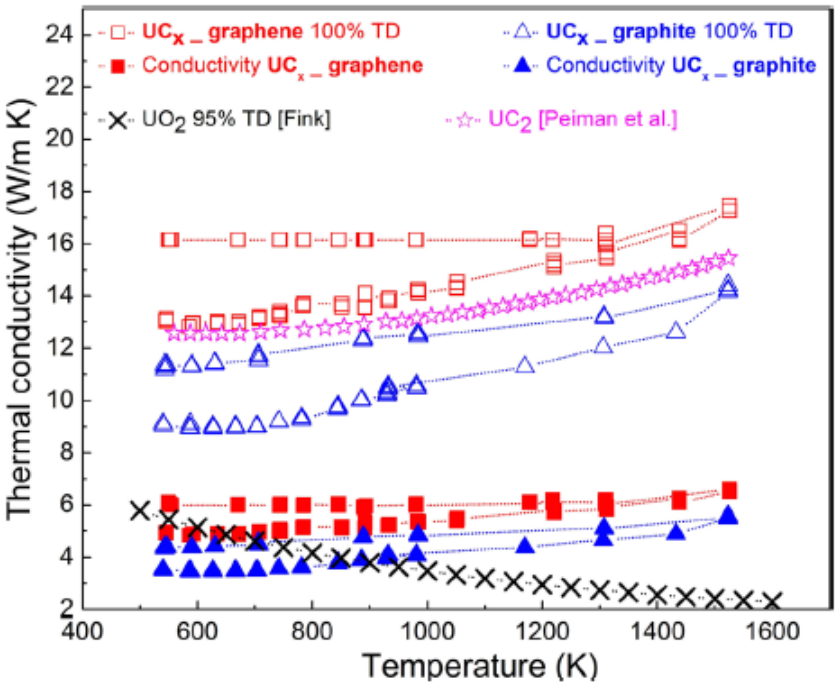


Fig. 2. Thermal conductivity measurement of $UC_x$-graphene and $UC_x$-graphite.

## References

[1] A. Monetti *et al.*, *Eur. Phys. J. A* **51**, 128 (2015).
[2] L. Biasetto *et al.*, *Scientific Reports* **8**, 8272 (2018).
[3] S. Corradetti *et al.*, *Ceram. Int.* **43**, 10824 (2017).

# Detection of Actinides/Lanthanides in Solutions by Time Resolved Laser Spectroscopy

**Igor Izosimov**

*Joint Institute for Nuclear Research, Dubna, 141980, Russia, e-mail: izosimov@jinr.ru*

Using short laser pulses for excitation of molecules and ions in liquids and time resolution (TR) for registration of luminescence (TRLIF) and chemiluminescence (TRLIC) produced by actinide and lanthanide ions one can efficiently separate target signals from short-lived background luminescence [1-4]. Selective excitation of detectable molecules and multi-step excitation schemes of luminescence/chemilumunescence can additionally decrease the intensity of background radiation.

Pu, Np, and some U compounds do not produce direct luminescence in solutions, but when excited by laser radiation, they can induce chemiluminescence of chemiluminogen (luminol in our experiments). The details of multi-step excitation of luminescence/chemiluminescence in solutions are considered. It is shown that a multi-step scheme of luminescence/chemilumines-cence excitation increase both the sensitivity and selectivity of detection of substances. Uranyl (or other elements and molecules) has a different circulation period in blood and in urine. Compare concentrations of the uranyl (or other elements and molecules) in blood plasma and in urine one can estimate the time when the uranyl (or other elements and molecules) was got into organism.

Results of the experiments on Eu, Sm, U, and Pu detection in different solutions are presented.

## References

[1] I.N. Izosimov, *Phys. Part. Nucl.*, **38**, 203 (2007).
[2] I.N. Izosimov, N.G. Firsin, N.G. Gorshkov and S.N. Nekhoroshkov, *Hyperfine Interact.*, **227**, 281(2014).
[3] I.N. Izosimov, *Journal of Rad. and Nucl. Chem.*, **304**, 211(2015).
[4] I.N. Izosimov, *Procedia Chemistry*, **21**, 473(2016).

# Effect of background electrolyte composition on the formation of Th(IV) nanoparticles on the muscovite (001) basal plane

**Moritz Schmidt,[1] C. Qiu,[1,†] S. Hellebrandt,[1,‡] P. J. Eng,[2] S. Skanthakumar,[3] M. Steppert,[4] and L. Soderholm[3]**

*[1] Helmholtz-Zentrum Dresden-Rossendorf, Bautzner Landstraße 400, 01328 Dresden, Germany, e-mail: moritz.schmidt@hzdr.de*
*[2] Center for Advanced Radiation Sources, University of Chicago, Chicago, IL, U.S.A.;*
*[3] Chemical Sciences and Engineering Division, Argonne National Laboratory, Argonne, IL, U.S.A.*
*[4] Institute of Radioecology and Radiation Protection, Leibniz University Hannover, Hannover, Germany.*
*[†] Present address: University of Kiel, Kiel, Germany; [‡] Present address: Lawrence Livermore National Laboratory, Livermore, CA, U.S.A.*

Reliable long-term predictions regarding the safety of a nuclear waste disposal facility must be based on a sound understanding of the fundamental processes controlling radionuclide mobility in a subsurface environment. In particular, reactions at the water/mineral interface must be characterized on the molecular level.[1] Several actinides (An) show a tendency to form An-oxo-nanoparticles[2], which may be enhanced in the presence of mineral surfaces and even drive redox reactions.[3-6] As these reaction may, both, enhance and reduce the mobility of the actinides, it is of utmost importance to understand their mechanism and which parameters control the nanoparticle formation in environmental systems.

Recently, we have reported an unusual variability in the reactivity of $Th^{IV}$ on the basal plane of muscovite mica dependent on the composition of the background electrolyte.[7] In this study, based on surface X-ray diffraction [SXD; crystal truncation rod diffraction (CTR) and resonant anomalous X-ray reflectivity (RAXR)] and alpha spectrometry, it was observed that $Th^{IV}$ sorption from $NaClO_4$ solution was significantly lower [< d.l. (~0.04 $Th^{IV}$ per area of the muscovite unit cell $A_{UC}$)] than from NaCl solution ($\theta_{NaCl}$ = 0.4 Th/$A_{UC}$) under otherwise identical conditions.[8] The study also revealed that the adsorbed quantity of $Th^{IV}$ was significantly higher in $LiClO_4$ medium ($\theta_{LiClO4}$ = 4.9 Th/$A_{UC}$), than in $NaClO_4$ with $KClO_4$ intermediate between Li and Na ($\theta_{KClO4}$ ~ 0.1 Th/$A_{UC}$). In the case of $LiClO_4$ it could be shown by RAXR, that sorption occurs in the form of small particles a few nm in size.

Here, we present a study using SXD in combination with alpha spectrometry and atomic force microscopy (AFM) aiming to identify the basis of the previously observed, unexpected effects. To probe whether anion and cation effect occur independently, $Th^{IV}$ sorption was studied in the presence of LiCl and KCl ([Th] = 0.1 mM, pH = 3.3, I = 0.1 M). $Th^{IV}$ uptake is strongest in the presence of LiCl ($\theta_{LiCl}$ = 8.8 Th/$A_{UC}$), while sorption in the presence of KCl is weaker ($\theta_{KCl}$ = 3.6 Th/$A_{UC}$) but still exceeds the surface occupancy previously found in NaCl media.[8] For all cations $Th^{IV}$ sorption is stronger when $Cl^-$ is the counterion compared to $ClO_4^-$, confirming that the cation effect is indeed independent of the background electrolyte's anion. The influence of aqueous speciation on the sorption processes was determined using electro-spray-ionization time-of-flight mass spectrometry (ESI-TOF-MS), which finds a speciation dominated by the $Th^{IV}$ aquo ion in all media, indicating that any electrolyte effects must occur at the water/mineral interface. We investigated the influence of the presence of oligomers on the sorption process, by repeating experiments at higher initial [Th] = 3.0 mM. As expected $Th^{IV}$ sorption is significantly increased. $Th^{IV}$ adsorbs at a preferential height of ~6.5 Å, which can be identified as the preferred size of Th-nanochains on the mica basal plane by AFM (Fig. 1). Uptake from LiCl media is still larger than from NaCl, but only by

~32% compared to 2100% at the lower $Th^{IV}$ concentration. This suggests that the electrolyte cation influences the formation or aggregation of $Th^{IV}$ oligomers at the interface, and its influence is diminished when these are initially present.

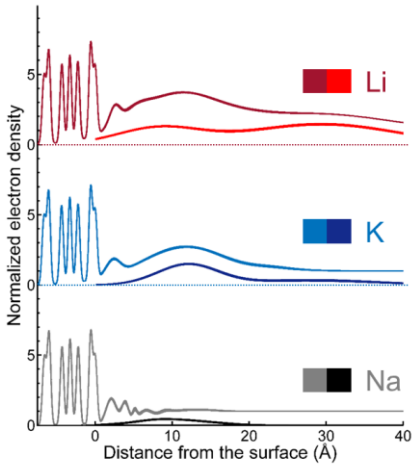


Fig. 1. Total electron density and $Th^{IV}$ electron density as a function of distance from the mineral surface determined by SXD upon sorption from NaCl, KCl, and LiCl, respectively. Upper curves (grey, light blue, dark red) are total electron densities determined by CTR, lower curves (black, dark blue, light red) are $Th^{IV}$ electron density distributions from RAXR.

## References

[1] H. Geckeis, *et al.*, *Chem. Rev.*, ***113***, 1016 (2013).
[2] K. E. Knope, *et al.*, *Chem. Rev.*, ***113***, 944 (2012).
[3] S. Hellebrandt, *et al.*, *Langmuir*, ***32***, 10473 (2016).
[4] A. E. Hixon, *et al.*, *Environmental Science: Processes & Impacts*, ***20***, 1306 (2018).
[5] M. Schmidt, *et al.*, *Env. Sci. Tech.*, ***47***, 14178 (2013).
[6] C. Walther, *et al.*, *Chem. Rev.*, ***113***, 995 (2013).
[7] M. Schmidt, *et al.*, *Geochim. Cosmochim. Acta*, ***165***, 280 (2015).
[8] M. Schmidt, *et al.*, *Geochim. Cosmochim. Acta*, ***88***, 66 (2012).

# Exploring excited state potential energy profile and luminescence properties of uranyl complexes by TRLFS and *ab initio* methods

**Hanna Oher,[1,2] Florent Réal[1], Thomas Vercouter[2], Valérie Vallet[1]**

[1] *Univ. Lille, CNRS, UMR 8523 - PhLAM, F-59000 Lille, France, e-mail: hanna.oher.etu@univ-lille.fr*
[2] *DEN – SEARS, CEA, Université Paris-Saclay, F-91191 Gif sur Yvette, France*

Uranyl complexes have been the subject of many research works for fundamental chemistry of actinides, environmental issues, or nuclear fuel cycle processes. The formation of various uranyl complexes, with organic and inorganic ligands in solution must be characterized for a better understanding of uranium speciation. Because uranyl-ligand interactions and symmetry of the complexes affect the electronic structure of U(VI) and thus its luminescence properties, time-resolved laser induced fluorescence spectroscopy (TRLFS) is one of the major techniques for analysis, with high sensitivity and selectivity to this element.
However, most of the relevant systems have complex chemical composition in solution and the identification of each species from spectroscopic data remains a tricky issue. Nowadays, combination of experimental and theoretical methods of investigation became quite effective and progressive. In our study, the balance of highly sensitive and selective to heavy metals methods such as TRLFS and *ab initio* based interpretation allows a better description of the complexation data.
Luminescence spectra of uranyl complexes in solution show in general a narrow energetical range about 6000 $cm^{-1}$ and we can identify a single electronic transition between the initial and target states with the vibrationally resolved band[1].

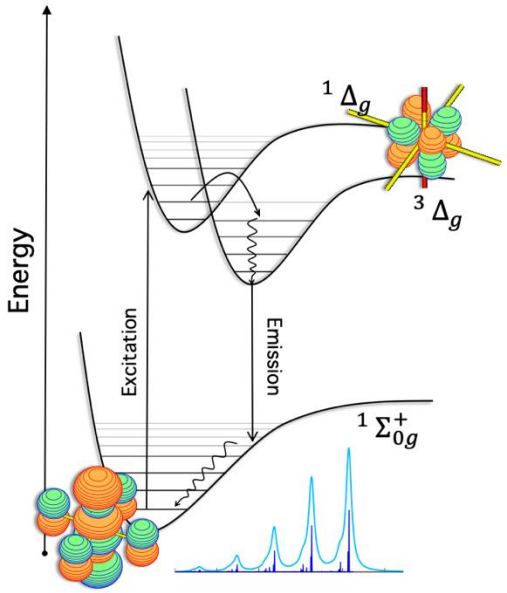


Fig. 1. Energy transfer in $UO_2Cl_4^{2-}$ between the ground and excited states after the photoexcitation, and simulated luminescence spectrum.

The main challenge consists in exploring a computationally cheap, fast and effective theoretical approach, in a relativistic context, to characterize the main spectral parameters and first excited state of symmetrical uranyl compounds (*i.e.* $UO_2X_4^{2-}$, where X=F, Cl, Br, I) with different organic counter ions after the photo-excitation and compute with high accuracy vibronic progression observed in experiments (Fig. 1). The most important steps are the

ground and excited state geometry optimization followed by normal modes calculation and application of Franck-Condon principle. The validation of results performs on each step by experimental data available in literature.
The time-dependent density functional theory (TD-DFT) with hybrid functionals is one of the most popular methods for electronic structure modelling of actinide's complexes with organic counter ions. This method is computationally not to expensive compare to the reference wave-function methods and known to be effective in computation of structural parameters. However, TD-DFT shows a limited capability at predicting the correct ordering of close-lying excitations in actinide complexes, a requirement in this framework. Thanks to previous benchmarks [2], it has been shown that the exact exchange from the range-separated hybrid CAM-B3LYP is able to reconcile the flaw in determination of excitation and emission energies.
As a benchmark system, to check the accuracy of the theoretical pathway appliance, the bare uranyl $UO_2^{2+}$ was selected because of extensive amount of structural and spectroscopic data available [3]. A good agreement was found between our and previously obtained theoretical data (structural parameters, orbitals nature, excitation energies) [4], the final luminescence spectrum is in remarkable agreement with our TRLFS measurements. In the framework of this conference I will explore in more details each steps of the theoretical pathway applied to uranyl-halide complexes together with obtained spectroscopic parameters and final theoretical luminescence spectrum.

## References

[1] J. Visnak and L. Sobec, EPJ Web of Conferences **128**, 02002 (2016).
[2] P. Tecmer et al., *J. Phys. Chem. A* **116**, 7397 (2012).
[3] A. Kovacs et al., *Chem. Rev*. **115**, 1725 (2015).
[4] F. Réal et al., J. Chem. Phys. **127**, 214302 (2007).

# Thorium and Uranium Endohedral Metallofullerenes: Theoretical Characterization of Oxidation States and Interactions Inside Fullerenes

**Roser Morales-Martínez[1], Antonio Rodríguez-Fortea[1], Ning Chen[2], Luis Echegoyen[3], Josep M. Poblet[1]**

*[1] Departament de Química Física i Inorgànica, Universitat Rovira i Virgili, c/Marcel·lí Domingo 1, 43007 Tarragona, Spain, e-mail: roser.morales@urv.cat*
*[2] Laboratory of Advanced Optoelectronic Materials, College of Chemistry, Chemical Engineering and Materials Science, Soochow University, Suzhou, Jiangsu 215123, PR China*
*[3] Department of Chemistry, University of Texas at El Paso, 500 W University Avenue, El Paso, Texas 79968, United States*

The chemical properties of U and Th are different since they have access to distinct oxidation states. Hence, whereas U(IV) and U(VI) are common oxidation states for U, the most common for Th is 4+. Inside a fullerene, the oxidation state of 6+ is not accessible and 5+ is rather difficult to stabilize.

Soon after the discovery of $C_{60}$ in 1985[1], the formation of La@$C_{60}$ was detected in mass spectra experiments.[2] The spherical shape of fullerenes allow encapsulating metal atoms but also small clusters such as $Sc_3N$, $Sc_2C_2$, etc. These systems are known as endohedral metallofullerenes (EMFs) and are stabilized by a formal charge transfer from the metal or cluster to the fullerene cage. Since the isolation and characterization of the third most abundant fullerene $Sc_3N@C_{80}$,[3] after $C_{60}$ and $C_{70}$, a large number of EMFs have been synthesized and characterized, the majority of them encapsulating group I-IV ions or lanthanides. In general, the captured fullerenes fulfil the isolated pentagon rule (IPR), but several non-IPR cages have been captured thanks to cluster-fullerene interactions.[4]

In contrast actinide EMFs has been less developed and only recently the groups of Echegoyen (UTEP) and Chen (Soochow Univ.) have been able to isolate and characterize several mono-actinide fullerenes. Here, we report recent computational studies on a series of uranium and thorium EMFs carried out in narrow collaboration with the experimental groups of Echegoyen and Chen. We have recently reported the full characterization of the first actinide EMF, Th@$C_{3v}$(8)-$C_{82}$, which is the first mono-EMF with a formal transfer of four electrons from the thorium atom to the fullerene cage, *i.e.* $Th^{4+}@C_{3v}(8)\text{-}C_{82}^{4-}$.[5]

Up to now, the oxidation state of an encapsulated metal is always observed to be the same, regardless of the cage size. For the first time, we have found a dependence of the oxidation state of uranium depending on the hosting fullerene isomer. DFT calculations, together with experimental results, revealed that uranium is trivalent in the case of U@$C_{2v}$(9)-$C_{82}$, while it is tetravalent for U@$D_{3h}$-$C_{74}$ and U@$C_2$(5)-$C_{82}$. Moreover, we have observed the formation of a U(V) after the first oxidation of U@$D_{3h}$-$C_{74}$ (Fig. 1).[6]

The nature of actinide-actinide bonds has attracted considerable attention for a long time, especially since recent theoretical studies have suggested that triple and up to quintuple bonds should be potentially possible.[7] $U_2@I_h(7)\text{-}C_{80}$ is the first isolated and fully characterized dimetallic uranium EMF.[8] The crystal structure revealed the U−U bond distance within the range of 3.46−3.79 Å. Computational studies suggest a strong metal-carbon cage interaction together with a rather weak U-U coupling. On the other hand, our investigations have shown that cage selection occurs through thermodynamic control at high temperatures. So the selected cages do not necessarily coincide with the most stable ones at room temperature, allowing to capture non-IPR fullerenes in which Th and U strongly interact with a pentalene unit (2 fused pentagons).[9] Although the actinide-carbon interactions are dominated by ionic

forces, calculations suggest that in the case of $U^{4+}$ the degree of covalence is higher than for $Th^{4+}$.

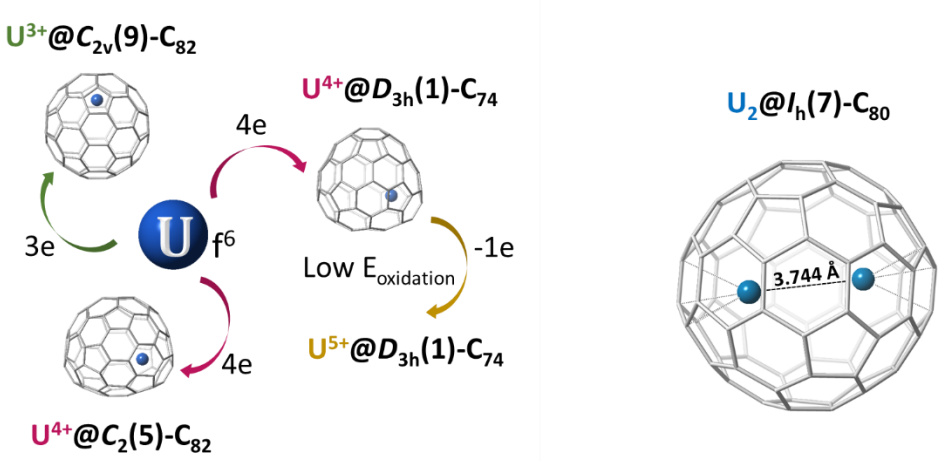


Fig. 1. Schematic representation of the different oxidation states of uranium inside different fullerene isomers (left) and computed structure for $U_2@C_{80}$ (right).

## References

[1] H. W. Kroto, J. R. Heath, S. C. O'Brien, R. F. Curl, R. E. Smalley, *Nature* **318**, 162 (1985).
[2] J. R. Heath, S. C. O'Brien, Q. Zhang, Y. Liu, R. F. Curl, F. K. Tittel, R. E. Smalley, *J. Am. Chem. Soc.* **107**, 7779 (1985).
[3] S. Stevenson, G. Rice, T. Glass, K. Harich, F. Cromer, M. R. Jordan, J. Craft, E. Hadju, R. Bible, M. M. Olmstead, K. Maitra, A. J. Fisher, A. L. Balch, H. C. Dorn, *Nature* **401**, 55 (1999).
[4] A. A. Popov, S. Yang, L. Dunsch, *Chem. Rev.* **113**, 5989 (2013).
[5] Y. Wang, R. Morales-Martínez, X. Zhang, W. Yang, Y. Wang, A. Rodríguez-Fortea, J. M. Poblet, L. Feng, S. Wang, N. Chen, *J. Am. Chem. Soc.* **139**, 5110 (2017).
[6] W. Cai, R. Morales-Martínez, X. Zhang, D. Najera, E. L. Romero, A. Metta-Magaña, A. Rodríguez-Fortea, S. Fortier, N. Chen, J. M. Poblet, L. Echegoyen, *Chem. Sci.* **8**, 5282 (2017).
[7] L. Gagliardi, B. O. Roos, *Nature* **433**, 848 (2005).
[8] X. Zhang, Y. Wang, R. Morales-Martínez, J. Zhong, C. de Graaf, A. Rodríguez-Fortea, J. M. Poblet, L. Echegoyen, L. Feng, N. Chen, *J. Am. Chem. Soc.* **140**, 3907 (2018).
[9] W. Cai, L. Abella, J. Zhuang, X. Zhang, L. Feng, Y. Wang, R. Morales-Martínez, R. Esper, M. Boero, A. Metta-Magaña, A. Rodríguez-Fortea, J. M. Poblet, L. Echegoyen, N. Chen, *J. Am. Chem. Soc.* **140**, 18039 (2018).

# $U_{1-x}Pu_xO_{2\pm\delta}$ fuel precursor synthesis through advanced thermal denitration in presence of organic additive

**Martin Leblanc[1,2], Gilles Leturcq[1], Eléonore Welcomme[1], Xavier Deschanels[2] and Thibaud Delahaye[3]**

*1 Laboratoire d'études des Procédés de Conversion des Actinides – LPCA – CEA Marcoule, CEA ; Nuclear Energy Division, Research Department on Mining and Fuel Recycling Processes Service – DEN\MAR\DMRC\SMFA\LPCA – F30207 Bagnols-sur-Cèze, France*
*martin.leblanc@cea.fr*
*2 Insitut de Chimie Séparative de Marcoule, ICSM UMR5257, Centre de Marcoule, F-30207 Bagnols/Ceze, France*
*3 Direction – DIR – CEA Marcoule, CEA ; Nuclear Energy Division, – DEN\MAR\DIR – F30207 Bagnols-sur-Cèze, France*

## Introduction

Within the U and Pu recycling process from spent nuclear fuels, the conversion of purified U and Pu solution onto oxide powder is a key step at the interface between the separation / purification processes and the fabrication of uranium-plutonium oxide fuels called MOx ("Mixed Oxides"). In order to simplify the industrial process, conversion must be able to integrate fluxes with the minimum of adjustments while leading to oxides or mixtures of oxides adapted to a direct shaping of fuel pellets. In the framework of Pu multi-recycling, new conversion routes have to be developed to suit new needs: increase of the quantity of synthetized oxides, reduction of dust generation, no redox adjustments of feed actinide solutions, simplified effluent management, no proliferation risks. To meet these future requirements, CEA is developing a "direct" conversion route based on advanced thermal denitration to obtain mixed actinide oxide $U_{1-x}Pu_xO_{2\pm\delta}$.

## Synthesis process

This synthesis method is based on the NPG (nitrate polyacrylamide gel) route developed for non-radioactive materials [1]]. Several adjustments of this synthesis path were performed prior its application to the production of $U_{1-x}Pu_xO_{2\pm\delta}$ (x = 0, 0.20, 0.25, 0.50 and 0.75) batches. For each sample uranium nitrate ($UO_2(NO_3)_2$) was dissolved in a solution of nitric acid containing Pu at the stoichiometry of the targeted oxide. In parallel, a mixture of mainly acrylic acid and N, N'-methylene bis (acrylamide) was prepared and then added to the actinide nitrate solution and stirred. Once homogeneous, the resulting solution was heated up to 100°C and supplemented with some radical initiator to quickly allow complete polymerization into a gel. A xerogel was then formed by dehydration of the polymeric gel. Oxidative calcination of as-obtained xerogel was then performed at 800°C in reconstituted air for 2h followed by a second calcination under $Ar/H_2$-5% up to 800°C for 2h. Batches of 0.5 g were synthetized except for $U_{0.80}Pu_{0.20}O_{2\pm\delta}$ for whom a scale up was attempted to produce 15 g.

## Results

Xerogel conversion at 800°C in reconstituted air produced intimate mixtures of $U_3O_8$ and $PuO_2$. After the second calcination, performed under $Ar/H_2$-5% at 800°C for 2h, single-phase oxides were obtained as confirmed by XRD analyses showing the presence of a single fluorite structure (Fm-3m) for the samples $U_{1-x}Pu_xO_{2\pm\delta}$ (x = 0 to 0.75) (Figure 1a), exhibiting a

morphology suitable for a pellet shaping by uniaxial pressing and sintering (Figure1b).

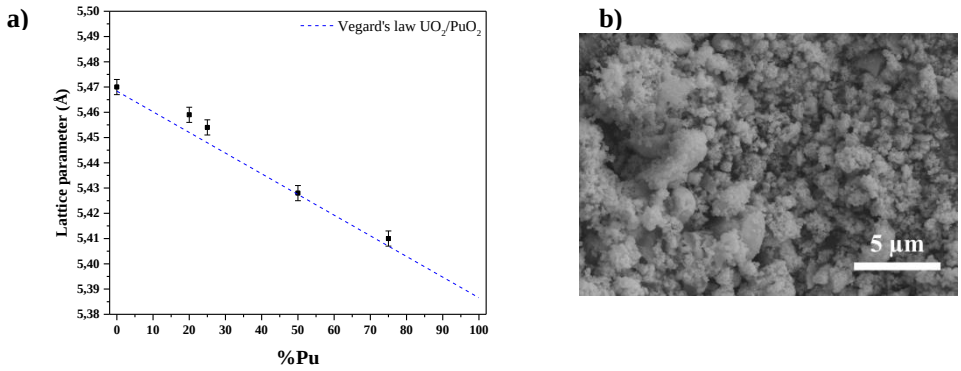


*Figure 1: a) Evolution of the lattice parameter a with Pu content in $U_{1-x}Pu_xO_{2\pm\delta}$ solid solution, measured by XRD and compared with Vegard's law. b) Microstructure of the $U_{1-x}Pu_xO_{2\pm\delta}$ powder (x=0.50)*

For $U_{0.80}Pu_{0.20}O_{2\pm\delta}$, the amount synthesized allowed the fabrication of a pellet. In this objective, the powder was pressed under 500 MPa in a three part die, no grinding step was used prior to the pelletization. The green density reached was 70% of the theoretical density (TD). The green pellet was then sintered in a dilatometer under $Ar/H_2$-4% with 1200 ppm of $H_2O$ and the axial shrinkage was recorded as function of temperature (Figure 2a). The maximum shrinkage rate is observed at 1455°C. The pellet was then maintained at 1700°C for 2h. At the end of this process, the density of the pellet reached 94±2% of TD and exhibited oxygen to metal ratio of 2.00. Visually the pellet did not show any cracks (Figure 2b).

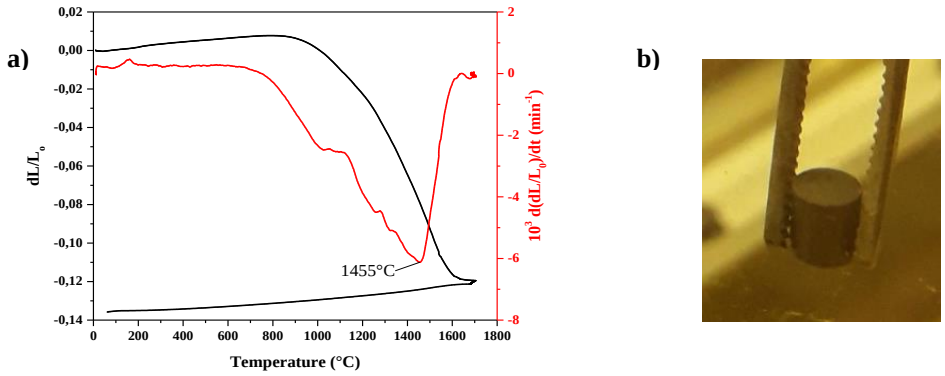


*Figure 2 : a) Dilatometric curve and evolution of the shrinkage rate of the co-converted $U_{0.80}Pu_{0.2}O_{2\pm\delta}$ compound at 2 K min$^{-1}$ under $Ar/H_2$-4%. b) Photograph of the pellet after sintering.*

## Conclusion

The main objective of this work was to explore the possibility to synthetize and sinter mixed U/Pu oxides by "advanced thermal denitration in the presence of organic additives". Feasibility is demonstrated here by the successful synthesis of $U_{1-x}Pu_xO_{2\pm\delta}$, whatever Pu content. The direct sintering of the obtained powder without milling step before shaping is possible. Therefore a significant breakthrough in the methods currently used for MOx fabrication is demonstrated. Indeed, this new process allows the synthesis of mixed oxides from solutions resulting from reprocessing without any redox adjustment (*i.e.* using U(VI)/Pu(IV) nitrate solution) and does not require any filtration and grinding steps, limiting highly contaminant dust generation.

## References

[1] Goupil, G., et al. "Selection and study of basic layered cobaltites as mixed ionic–electronic conductors for proton conducting fuel cells." Solid State Ionics **263**, 15-22 (2014).

# Peculiarities of the U-Fe-Sb system

**M.S. Henriques[1,2], I.C. Santos[1], L.C.J. Pereira[1], E.B. Lopes[1], J.C. Waerenborgh[1], N. Zahurakova[3], V.Kontul'[3], A. Džubinská[5], S. Il'kovič[3], I. Curlik[3], M. Reiffers[3], J. Rusz[4], A.P. Gonçalves,[1]**

*[1] C2TN, Instituto Superior Técnico, Universidade de Lisboa, Campus Tecnológico e Nuclear, Estrada Nacional 10, 2695-066 Bobadela LRS, Portugal, e-mail:apg@ctn.tecnico.ulisboa.pt*
*[2]Institute of Physics, Academy of Sciences of the Czech Republic, Na Slovance 2, 182 21 Prague, Czech Republic*
*[3]Faculty of Humanities and Natural Sciences, Prešov University, SK-081 16 Prešov, Slovakia*
*[4]Department of Physics and Astronomy, Uppsala University, Box 516, 75120 Uppsala, Sweden*
*[5]Faculty of Sciences, P. J. Safarik University, Park Angelinum 9, 041 54 Kosice, Slovakia*

The identification of new compounds, with specific and unusual properties, is vital for the advance of solid state sciences. This is particularly relevant in the case of uranium based compounds, where a vast number of ground states are found due to the dual nature of 5*f* electrons. Albeit the improvements on theoretical calculations, the best and most effective way to discover new compounds is still the experimental study of phase diagrams. In this communication we present our studies on the U-Fe-Sb system, where such procedure was successfully applied.

At the beginning of this work, the three binary systems (U-Fe, Fe-Sb and U-Sb) were reported up to the temperatures of the liquid phases in all the composition range. Eight binary solid phases were previously described in these systems, being all of them stable at 700ºC: two compounds ($UFe_2$ and $U_6Fe$) in U-Fe, one compound ($FeSb_2$) and a solid solution (ε-FeSb) in Fe-Sb and four compounds ($U_5Sb_4$, $U_3Sb_4$, USb and $USb_2$) in the U-Sb system. From the presence of binary solid phases in all systems and their relatively large number we could expect the existence of a significant number of ternary phases, but only one ternary compound, $UFeSb_2$, was briefly described in the literature [1]. The ground states of the uranium binary compounds were also reported before [2], ranging from superconductors ($U_6Fe$, $T_c$ = 3.7 K) to ferromagnets ($UFe_2$, $T_C$ = 162 K; $U_5Sb_4$, $T_C$ = 86 K; $U_3Sb_4$, $T_C$ = 146 K) and antiferromagnets (USb, $T_N$ = 213 K; $USb_2$, $T_N$ = 206 K). The ternary compound, $UFeSb_2$, was not studied in detail, due to the presence of impurity phases, but the possibility of being a ferromagnet was discussed [1].

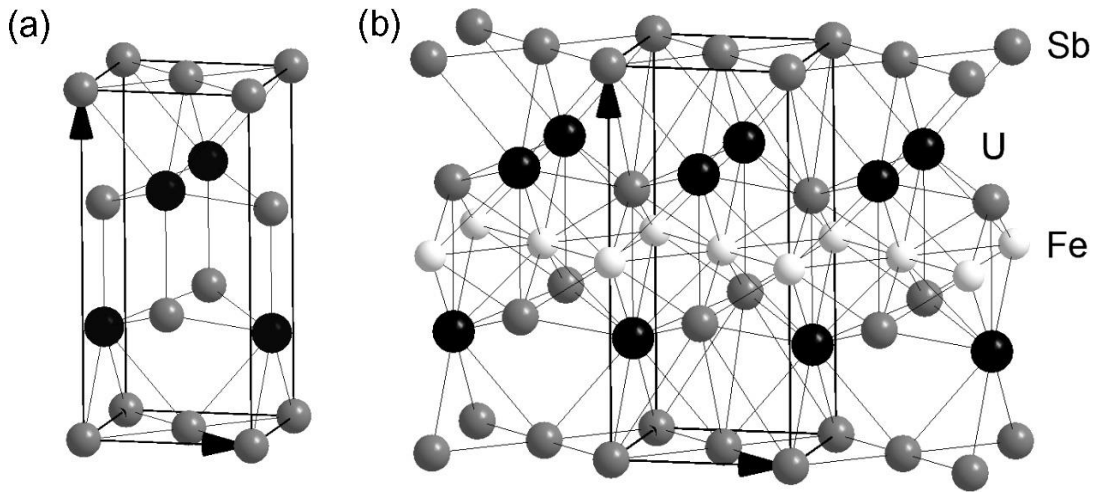


Fig. 1. Unit cells of (a) USb2 and (b) UFeSb2, emphasizing the relation between both structures.

Our study of the U-Fe-Sb ternary system at two temperatures, 700ºC and 750ºC [3], allowed the identification of another ternary solid phase, $U_3Fe_{3-x}Sb_4$, and the recognition of "$UFeSb_2$" as a solid solution, $UFe_{1-x}Sb_2$. Moreover, it also permitted the establishment of the ternary phase fields at those temperatures, which showed the equilibrium of $UFe_{1-x}Sb_2$ with a liquid Sb-based phase. This is expected to allow the growth of $UFe_{1-x}Sb_2$ single crystals by the flux method. However, in the case of $U_3Fe_{3-x}Sb_4$ only equilibriums with solid phases were found.
The $UFe_{1-x}Sb_2$ phase can be seen as derived from the $USb_2$ tetragonal compound by the (partial or complete) intercalation of an iron layer (Fig. 1). Different iron occupations leads to changes in the U-U nearest distances, anticipating substantial band structure modifications and the possibility of different ground states when compared with $USb_2$.
The study of ternary phases started with the preparation and characterization of polycrystalline $UFeSb_2$ materials. They show a ferromagnetic-type transition at $T_C$ = 31(1) K, with small magnetization saturation. The crystal structure refinement point to large U-(nearest neighbor) and very short Fe-Sb distances, which suggest the possibility of a significant magnetic moment on uranium and the iron magnetic moment collapse. Mössbauer spectroscopy results corroborate with this picture, indicating that iron is not associated to any long range magnetic ordering or standard spin-glass behavior.
Single crystals of $UFe_{0.7}Sb_2$ were grown by the self-flux method. Their study indicated anomalies consistent with the onset of antiferromagnetic order at $T_N$ = 26 K that changes to a ferromagnetic state at $T_C$ = 21 K, confirming the sensitivity of the ground state to the stoichiometry. Electronic structure first principles calculations show an unusually steep local minimum in the density of states at the Fermi level, which might be viewed as key to understand the properties of $UFe_{0.7}Sb_2$.
A $U_3Fe_3Sb_4$ polycrystalline sample was prepared by arc melting, followed by annealing. It crystallizes in the cubic $Y_3Au_3Sb_4$-type structure, showing a ferromagnetic-type behavior below $T_C$ = 110(2) K. However, and as in the case of the $UFe_{1-x}Sb_2$ phase, Fe-Sb distances are very short, which, together with the Mössbauer spectroscopy results, indicate no iron contribution to magnetism in this compound.
In conclusion, the two ternary phases existing in the U-Fe-Sb system have uranium based magnetic ground states, with negligible contribution from the iron atoms. However, in the case of $UFe_{1-x}Sb_2$ the U-U and U-(nearest neighbor) distances and the electronic band structure strongly depend on the iron content.

## References

[1] D. Kaczorowski et al., *Phys. Rev. B* **58**, 9227 (1998).
[2] V. Sechovsky and L. Havela, Intermetallic Compounds of Actinides in: the Handbook on Ferromagnetic Materials, Elsevier Science Publishers, Amsterdam, **Vol. 4** (1988).
[3] M.S. Henriques et al., *Solid State Phenomena* **194**, 21 (2013).

# Investigation of structure and oxidation kinetics of uranium surface after pulsed laser nitriding

**Yanzhi Zhang, Jianwei Qin, Yongbin Zhang, Zhilei Chen, Yin Hu, Kezhao Liu**

*Institute of Materials, China Academy of Engineering Physics, Mianyang 621907, China, e-mail: zhangyanzhi@caep.cn*

In order to study the effect of pulsed laser nitriding on uranium, the crystal structure and oxidation kinetics of nitride layer were investigated using in-situ X-ray diffraction and reactor chamber. The experimental results indicate that the crystal structure of nitride is affected by the scanning speed of pulsed laser remarkably. The UN is the sole nitride at lower scanning speed; the mix structure of UN and $U_2N_3$ will achieve at higher scanning speed. The Rietveld refinement method and single-peak fitting were used to analyze the XRD data and obtain the oxidation kinetics of UN later in air. The oxidation kinetics of uranium is slow in the extreme when the surface is covered with a layer of UN. The oxidation kinetics and oxidation mechanism of nitride are analyzed and discussed in this work.

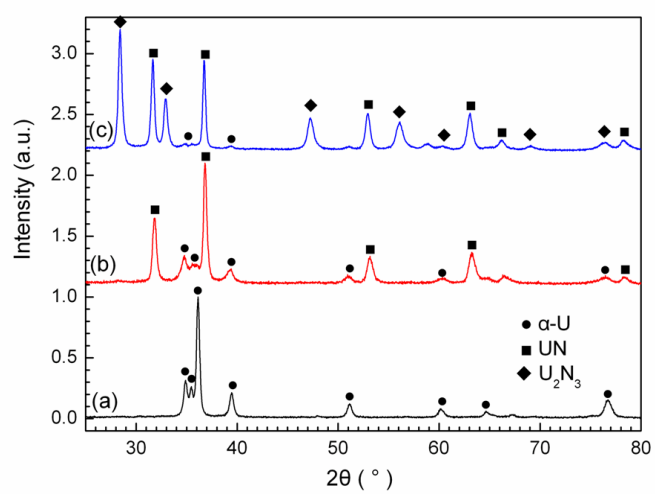


Fig. 1. XRD patterns of sample (a) before and after pulsed laser nitriding at (b) faster scanning and (c) lower scanning

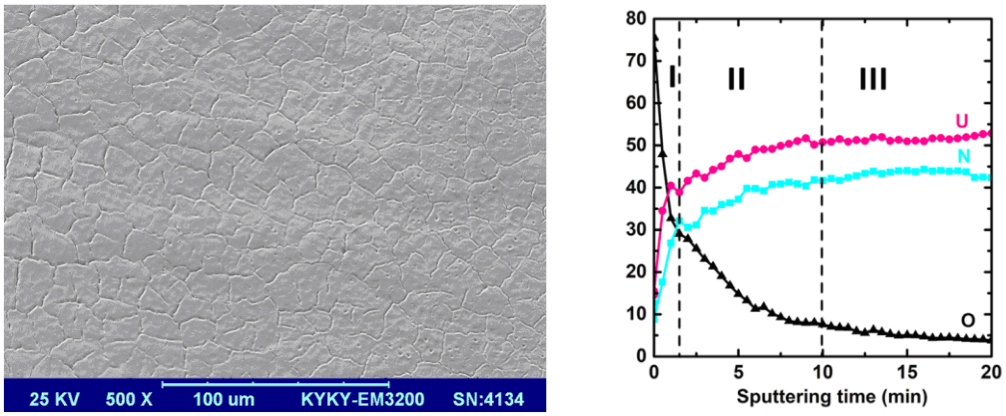


Fig. 2. A typical (a) SEM image and (b) AES depth profiles of nitriding sample

# Iridium 5*d*-electron driven superconductivity in $ThIr_3$

**Debarchan Das[1], Karolina Górnicka[2], Konrad Wochowski[1], Sylwia Gołąb[3], Bartłomiej Więdlocha[3], Tomasz Klimczuk[2], Dariusz Kaczorowski[1]**

[1]*Institute of Low Temperature and Structure Research, Polish Academy of Sciences, P.O.Box 1410, 50-590 Wrocław 2, Poland ; e-mail: D.Kaczorowski@intibs.pl*
[2]*Faculty of Applied Physics and Mathematics, Gdansk University of Technology, ul. Narutowicza 11/12, 80-233 Gdańsk, Poland*
[3]*Faculty of Physics and Applied Computer Science, AGH University of Science and Technology, Aleja Mickiewicza 30, 30-059 Kraków, Poland*

Since the seminal discovery of heavy-fermion superconductivity in $CeCu_2Si_2$ [1], exploration of superconducting properties of *f*-electron intermetallics has become one of the most intriguing topics in the condensed matter physics. Among the vast number of existing Ce-based materials a few compounds have been found to exhibit superconducting ground state of unconventional nature, like, for example, members of a homologous series $Ce_nT_mIn_{3n+2m}$, where $T$ = Co, Rh, Ir, Pd or Pt (e.g. $CeCoIn_5$, $Ce_2PdIn_8$, $Ce_3PtIn_{11}$), which crystallize in tetragonal structures build of n layers of $CeIn_3$ ($AuCu_3$ type) and m layers of $TIn_2$ ($HgTe_2$ type) units [2-5].

Lately, another homologous series has attracted much attention, namely $RE_{2m+n}T_{4m+5n}$, where RE stands for early rare earth metal (La – Gd), $T$ is a transition metal Ir or Rh, and m and n represent the numbers of $MgCu_2$ and $CaCu_5$ type blocks, respectively [6]. The compounds $LaIr_3$ and $CeIr_3$, which are terminal members of the series (m = n = 1), crystallize with a rhombohedral centrosymmetric structure (space group *R*-3*m*) of the $PuNi_3$ type, and they have been established to exhibit superconductivity below $T_c$ = 3.3 K and 2.5 K, respectively [7-9].

Most recently, we have succeeded in synthesizing the first actinoid-based superconducting representative of the $RE_{2m+n}T_{4m+5n}$ family, viz. $ThIr_3$. The bulk nature of the superconducting state in this material is evident from the prominent anomalies at $T_c$ = 4.4 K in its thermodynamic (magnetic susceptibility, heat capacity) and electrical transport characteristics. The value of $\Delta C/\gamma T_c$ (where $\Delta C$ is the heat capacity jump at $T_c$, $\gamma$ is the Sommerfeld coefficient) is equal to about 1.45, which is almost equal to that expected for a BCS superconductor. Our analysis of the experimental data revealed that $ThIr_3$ is a moderately coupled type-II superconductor (electron-phonon coupling constant $\lambda_{e-p}$ = 0.74, Ginzburg-Landau parameter $\kappa$ = 33). The lower critical field $H_{c1}(0)$ equals 7.7 mT, while the upper critical field $H_{c2}(0)$ is about 4.7 T (dirty limit), i.e. smaller than the Pauli limiting field $H_{c2}^{p}(0) = 1.85T_c = 8.2$ T. Our calculations indicated a multi-band character of the Fermi surface with the dominating contribution to the density of states at the Fermi level coming from 5*d* states of Ir atoms. Similar scenario of 5*d*-electron driven superconductivity has been observed also for $LaIr_3$ and $CeIr_3$ [9,10].

## References

[1] F. Steglich et al., *Phys. Rev. Lett.* **43**, 1892 (1979).
[2] C Petrovic et al., *J. Phys.: Condens. Matter* **13**, L337 (2001).
[3] D. Kaczorowski et al., *Phys. Rev. Lett.* **103**, 027003 (2009).
[4] J. Prokleška et al., *Phys. Rev. B* **92**, 161114 (2015);
[5] D. Das et al., *Sci. Rep.* **8**, 16703 (2018).
[6] O. Sologub et al., *J. Alloys Compd.* **373**, L5 (2004).
[7] N. Haldolaarachchige et al., *J. Phys.: Condens. Matter* **29**, 475602 (2017).
[8] Y. J. Sato et al., *J. Phys. Soc. Japan* **87**, 053704 (2018).
[9] K. Górnicka et al., *Supercond. Sci. Technol.* **32**, 025008 (2019).
[10] M. Hakimi M and J.G. Huber, Physica B+C 135, 434 (1985).

# Preliminary resistivity results on $U_2Ni_2Sn$ single crystals

**I. Halevy[1,2], A. Kolomiets[1,3], S. Mašková[1], A.V. Andreev[4], L. Havela[1]**

[1]*Department of Condensed Matter Physics, Charles University, 12116 Prague, the Czech Republic*
[2]*Department of Physics, IAEC-NRCN, Beer-Sheva 84190 Israel*
[3]*Department of Physics, Lviv Polytechnic National University, 79013 Lviv, Ukraine*
[4]*Institute of Physics, Academy of Sciences, 18221 Prague, the Czech Republic*

$U_2Ni_2Sn$ is a member of a large family of intermetallic compounds with the tetragonal $Mo_2FeB_2$ crystal structure, which has been studied intensively over the past years [1-3]. It orders antiferromagnetically at 25 K with a propagation vector $q$ = (0, 0, 1/2). Magnetization, magneto-acoustic, and neutron-diffraction experiments on a single crystal provide evidence that the uranium moments align parallel to the *c*-axis with the anisotropy energy of ≈170 K, indicating that $U_2Ni_2Sn$ can be classified as an Ising system. This behavior is rather exceptional, majority of the isostructural uranium ternaries have U moments confined into the basal plane.

Last results [1] are actually at variance with previous studies on polycrystals, which indicated different magnetic structure, and which were incompatible with the 5*f*-5*f* two-ion anisotropy model dominant in most of U band systems. High-field magnetization studies [1] exhibit a weak linear response for fields along the basal plane up to the highest field applied (60 T), while the *c*-axis magnetization curve exhibits three metamagnetic transitions at approximately 30, 39 and 50 T.

Few single crystals of $U_2Ni_2Sn$ were grown by the Czochralski method from a stoichiometric mixture of the pure elements (99.9% U, 99.99% Ni and 99.9999% Sn) in a tri-arc furnace with a water-cooled copper crucible under protective argon atmosphere. A tungsten rod was used as a seed. The pulling speed was 10 mm/h. We cut two different single crystal pieces for resistivity measurements with orientation of [001] and [110], respectively. The small size of crystals was chosen to be compatible with high-pressure study envisaged.

The four-point technique, as shown in Fig. 1, was used to measure the resistivity. 25 µm Au wire was used as leads for the measurement.


Fig. 1. Single crystals of $U_2Ni_2Sn$ mounted for the resistivity measurement in the [001] (left) and [110] (right) direction.

So far we measured the resistivity as function of temperature on the closed cycle refrigerator in the temperature range of 5-300 K.

Although the primary goal is the high pressure study (as $U_2Ni_2Sn$ is an itinerant antiferromagnet, we expect fast suppression of magnetic order with pressure), already the ambient pressure data (see below) yield an interesting insight.

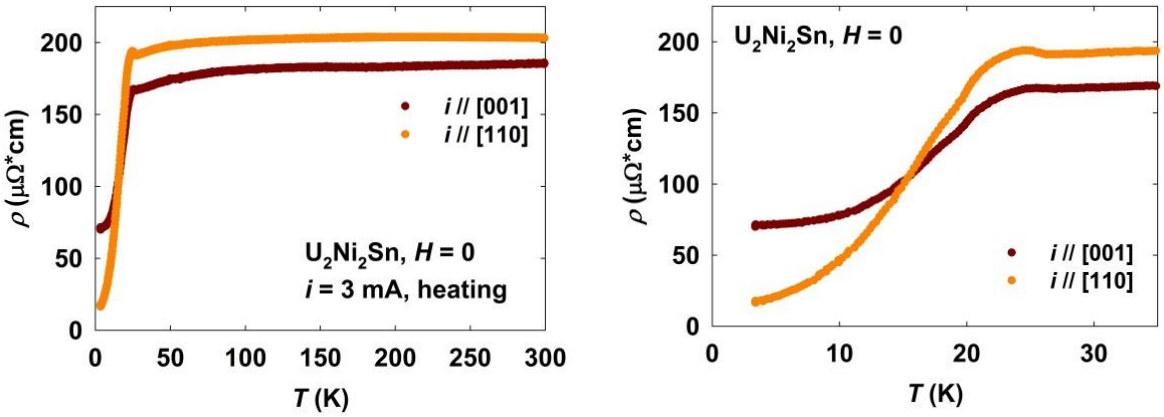


Fig. 2. The temperature dependence of resistivity of $U_2Ni_2Sn$ single crystal with i // [110] and i // [110] (left). The right panel shows the low-temperature detail.

The first finding is that single crystal resistivity has better RRR value, reaching 10 for $i$ // [110] and 3 for the [001] direction. The polycrystal value is about 3 [2]. None of the two directions exhibits the negative resistivity slope, $d\rho/dT < 0$, found for the polycrystal, and $\rho(T)$ shows merely a saturation. The magnetic propagation vector implies an influence of magnetic superzone gapping for [001], which can explain much higher residual resistivity in this direction. There is AF coupling between the U moments within the same basal-plane sheet, but it all happens within one unit cell, accommodating 4 U atoms.

Further differences are revealed by a numerical analysis. Fitting for $i$ // [110] indicates the quadratic dependence, compatible with the high uniaxial anisotropy, not permitting a population of magnons with energy lower than the anisotropy gap. On the other hand, $i$ // [001] exhibits an additional gap excitation term, $\rho = \rho_0 + AT^2 + C * exp\left(-\frac{\Delta}{T}\right)$ with $\Delta$ = 40-60 K, i.e. much smaller than the anisotropy gap 170 K. Such exchange gap has to be identified as a spin gap, suggesting an easy spin flipping along $c$.

The measurements under external pressure are in progress.

## References

[1] S. Mašková, A.V. Andreev, Y. Skourski, S. Yasin, D.I. Gorbunov, S. Zherlitsyn, H. Nakotte, K. Kothapalli, F. Nasreen, C. Cupp, H.B. Cao, A. Kolomiets, L. Havela, *Physical Review B.* (accepted 2019).

[2] K. Kindo, T. Fukushima, T. Kumada, F.R. de Boer, H. Nakotte, K. Prokes, L. Havela, V. Sechovsky, A. Seret, J.M. Winand, J.C. Spirlet ,J. Rebizant, *Journal of Magnetism and Magnetic Materials* **140-144** 1369 (1995).

[3] R.P. Pinto, M.M. Amado, M.E. Braga, M.A. Salgueiro, J.B. Sousa, B. Chevalier, D. Laffargue, J. Etourneau, *Journal of Magnetism and Magnetic Materials* **157/158** 698 (1996).

# Spectroscopy Study of the Intermediate Surface Oxide $U_2O_5$

**T. Gouder, R. Eloirdi and R. Caciuffo**

*European Commission, Joint Research Centre (JRC), Herrmann-von-Helmholtz-Platz 1, 76344 Eggenstein-Leopoldshafen, Germany*

Oxidation properties of uranium have a great influence on the stability of nuclear waste. U(VI) has a 1000 times higher solubility in water than U(IV), and so the dissolution of $UO_2$ based spent fuel nuclear waste and release of contained radionuclide strongly depends on the oxidation state of the surface. Incorporation of oxygen into surface of $UO_2$ has thus been a subject of research for many years. Unfortunately the formation of off-stoichiometric phases ($UO_{2+x}$) by corrosion is hard to differentiate from non-completed reaction (thermodynamic versus kinetic effects). The strong composition gradient between surface corrosion layers and the unreacted bulk may lead to a heterogeneous system, containing more than one uranium oxidation state. Replacing bulk samples by thin films allows creating homogeneous systems reaching equilibrium condition fast.

We present the use of thin films to study the electronic structure and reactivity of $U_2O_5$, containing uranium at the oxidation state (V), which is an intermediate between U(IV) and U(VI). Films had a thickness between 2 and 50 monolayers. While it is well known that oxidation of $UO_2$ leads to mixed valence compounds ($U_4O_9$, $U_3O_8$) containing U(V), the U(V) oxide has never been observed as pure compound by surface spectroscopies. This may be due to its low stability and the its easy transformation into $UO_2$ or $UO_3$, two more stable oxides. We will present electron spectroscopy (XPS, UPS and BIS) and Electron Energy Loss (ELS) studies of the oxide and compare them to the neighbouring oxides ($UO_2$ and $UO_3$). $U_2O_5$ has been produced by exposing $UO_2$ to atomic oxygen and $UO_3$ to atomic hydrogen. The reactions mimic corrosion and reduction reactions which may occur in nuclear waste repositories.

$U_2O_5$ is very sensitive to reduction, and short sputtering reduces it already to $UO_2$. It is thus hard to observe it on conventionally sputter cleaned surfaces. On the other side, because it occurs in a region with easily modifiable oxygen composition, most bulk studies simply missed it and saw instead mixed valence compounds such as $U_3O_8$ ($U^{5+}/U^{6+}$ mixture) or $U_4O_9$ ($U^{5+}/U^{4+}$ mixture) whose differentiation can be hardly done without high resolution photoelectron spectroscopy.

Determination of the oxidation states was based on the characteristic U-4f core level satellites, separated from the main lines by 6, 8 and both 4 and 10 eV for U(IV), U(V) and U(VI), respectively (Fig. 1). We managed producing films which showed exclusively a single 8 eV satellite, indicating the presence of pure U(V), within the uncertainty of the XPS. U(V) formation was confirmed by the intensity evolution of the U*5f* valence emissions (Fig. 2): the U*5f*/U*4f* ratio decreased by about 50% from $UO_2$ and $U_2O_5$, which is consistent with the $5f^2$ ($UO_2$) and $5f^1$ ($U_2O_5$) initial state configurations. Also the linewidth of the XPS *5f* valence band spectra decreases from $UO_2$, with the $5f^1$ final state multiplet configuration, to $U_2O_5$, with a $5f^0$ final state singlet. Spectra of U-5d show a multiplet structure due to interaction with the $5f^1$ state. In $UO_3$ this interaction is missing and the U-5d line is significantly narrower.

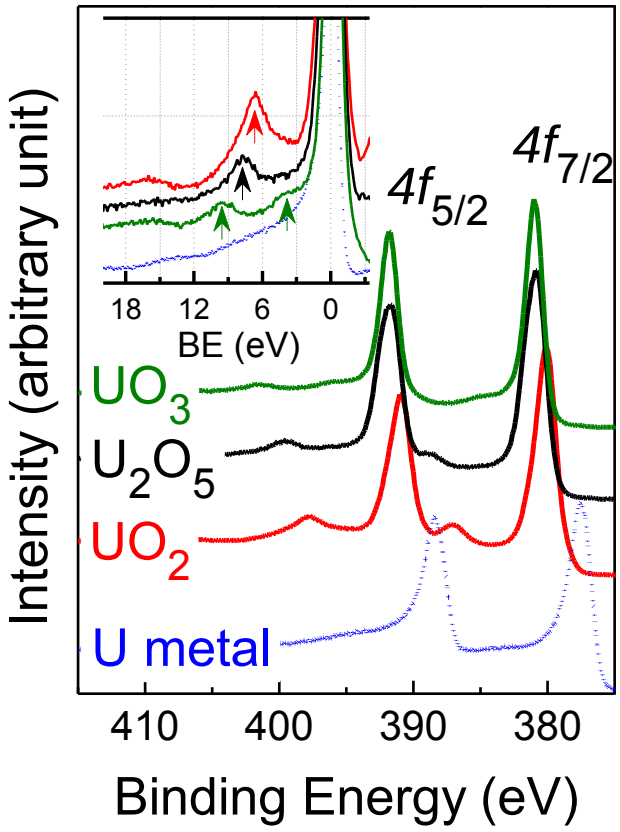


Fig. 1 U4f spectra of $UO_2$, $U_2O_5$ and $UO_3$ and compared to U metal. The inset shows the shift of the satellite when the main lines ($f_{5/2}$) are superimposed

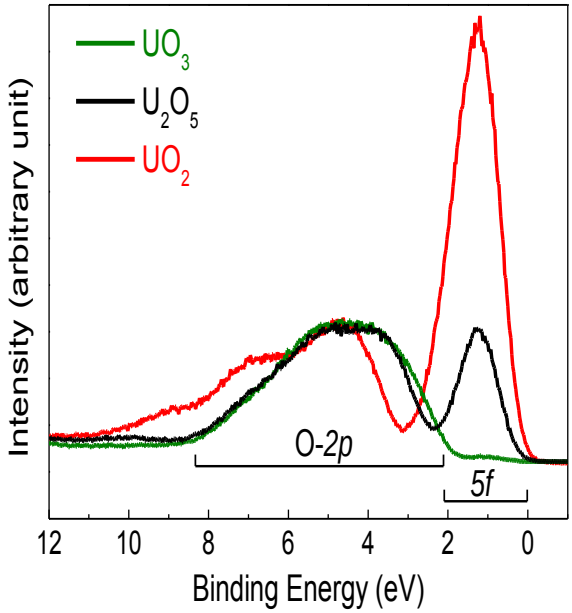


Fig. 2 Valence band spectra of $UO_2$, $U_2O_5$ and $UO_3$. With increasing oxidation state of U, the intensity of the U5f line is reduced-

# Electron spectroscopy study and magnetism of $UH_3$ and $UH_2$ thin films

**Ladislav Havela,[1] Evgeniya Tereshina-Chitrova[1], Mykhaylo Paukov[1], Milan Dopita[1], Lukas Horak[1], Martin Divis[1], Ilja Turek[1], Dominik Legut[2], Lukáš Kývala[2], Thomas Gouder[3], Alice Seibert[3], Frank Huber[3]**

*[1]Faculty of Mathematics and Physics, Charles University, Ke Karlovu 5, 12116 Prague, Czech Republic, e-mail: havela@mag.mff.cuni.cz*
*[2]IT4Innovations Center, VSB-Technical University of Ostrava, CZ-70833 Ostrava, Czech Republic*
*[3]European Commission, Joint Research Centre (JRC), Directorate for Nuclear Safety and Security, Postfach 2340, D-76125 Karlsruhe, Germany*

Uranium is known to form with hydrogen two different hydrides of the $UH_3$ stoichiometry. The transient form, α-$UH_3$, represented as *bcc* uranium filled with H atoms, is fast converted to the stable form β-$UH_3$, which is also cubic, with U atoms occupying two different crystallographic positions. Both are ferromagnets with the Curie temperature close to 165 K. Recently we found that *fcc* hydride, presumably $UH_2$, can be formed in the thin film form [1]. In all three U hydrides, H ions are located within practically identical U tetrahedra, with the U-H distances 232-233 pm. Only the arrangement of the tetrahedra is different.

**α-$UH_3$** $d_{U\text{-}H}$ = 233 pm, $d_{U\text{-}U}$ = 360 pm

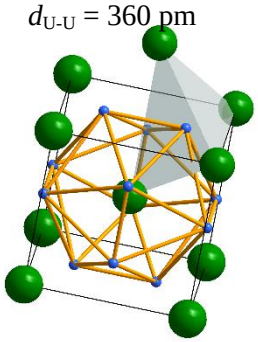

**β-$UH_3$** $d_{U\text{-}H}$ = 232 pm, $d_{U\text{-}U}$ = 331 pm

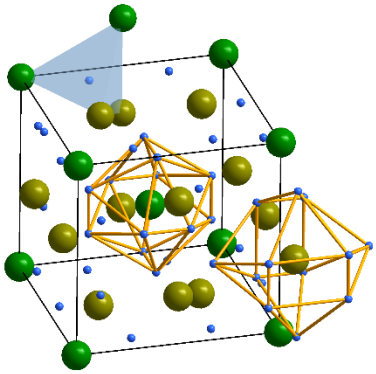

**$UH_2$** $d_{U\text{-}H}$ = 232 pm, $d_{U\text{-}U}$ = 378 pm

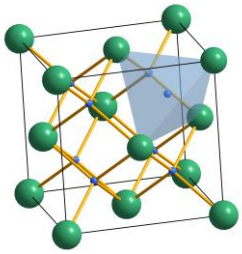

Magnetic properties of all three materials are rather similar, they are ferromagnets with $T_C$ = 165 K (both $UH_3$) or 120 K ($UH_2$). The highest U-U spacing in $UH_2$, 378 pm, together with lower $T_C$ means that higher U-U spacing does not promote the 5*f* magnetism in this case. The U-H interaction, which may withdraw the 5*f* states from the 5*f*-6*d* hybridization with strong 6*d*-1*s* hybridization, may be actually the prominent mechanism, responsible for high $T_C$ for short U-U spacings (331 pm in β-$UH_3$). Hence, despite short U-U spacing, important influence of electron-electron correlations can be expected.

Our XPS, UPS and BIS spectra of $UH_2$ and β-$UH_3$ (the latter prepared also with Mo alloying) are rather similar. As example we show the U-4*f* spectra and valence-band XPS spectra. The spectra of $UH_2$ are in all cases between U metal and $UH_3$, but much closer to the $UH_3$ case. The U-4*f* lines (see both left panels below) exhibit between the U metal and U hydrides only very small (0.2 eV) shift towards higher binding energies (BE), but the $4f_{5/2}$ and $4f_{7/2}$ lines broaden and develop a satellite at ≈ 4 eV higher BE. The small shift can be due to the fact that the 5*f* occupancy remains close to $n_f$ = 3 even in the hydride. The charge transfer towards the hydrogen states affects (as to ab initio calculations) mainly the 6*d* and 7*s* states [2]. Those couple stronger to the more extended U-5*d* states. Indeed, the shift of respective 5d

states is about 0.5 eV (see the lower right panel). Even more extended 6*p* states (not shown here) shift by 1.5 eV. The valence-band spectra (upper right panel) are well reproduced by ab-initio calculations on a global scale. However, high-resolution UPS shows the 5*f* states up to the Fermi level, while GGA+U calculations have the DOS around 0.5 eV BE. Pure GGA on the other hand have the 5*f* states up to $E_F$ but miss the experimental satellite at 0.5 eV.

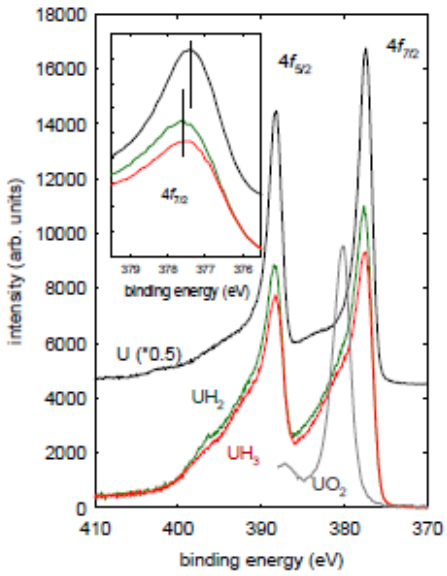


Comparison of U-4*f* spectra in U metal, $UH_2$ and $UH_3$ with $UO_2$ in various representations (up and down).

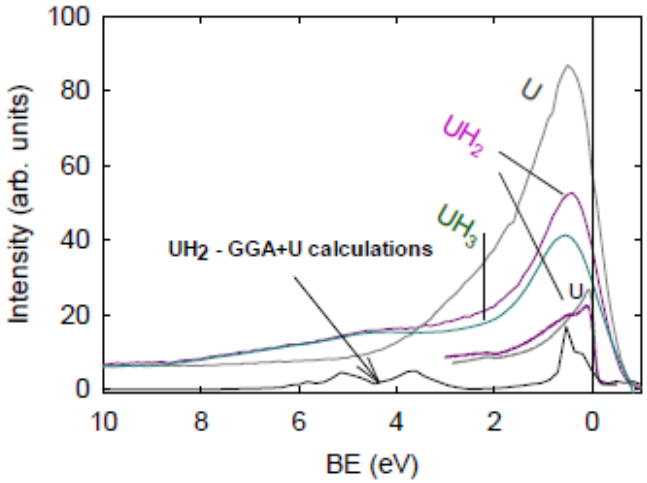


Valence band XPS (1486.6 eV) and UPS (40.81 eV) for U and $UH_2$ together with total DOS from GGA+U calculations.

Comparison of U-5*d* spectra in U metal and $UH_3$.

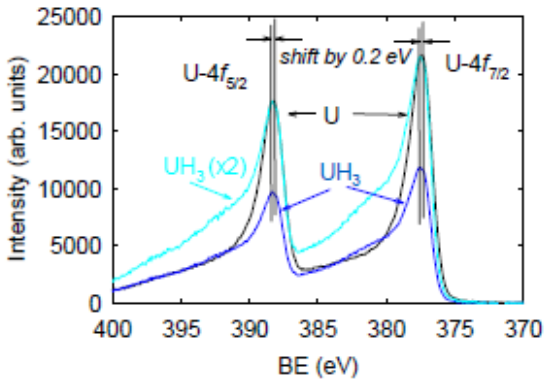


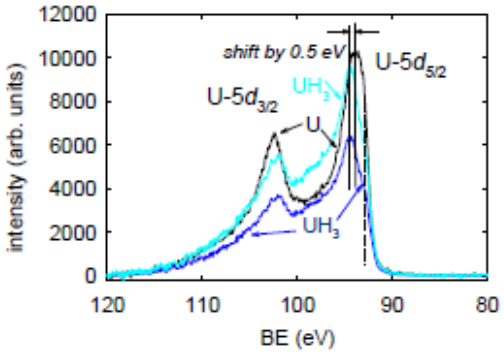


*This work was supported by the Czech Science Foundation under the grant No. 18-02344S. The work at JRC Karlsruhe was supported by the Actuslab project under contract with the European Commission. Part of the work was supported by the project "Nanomaterials centre for advanced applications", project No. CZ.02.1.01/0.0/0.0/15_003/0000485, financed by ERDF.*

## References

[1] L. Havela et al., Inorg. Chem. **57**, 14727 (2018).
[2] I. Tkach et al. Phys.Rev. **B 91**, 115116 (2015).

# Thermodynamic properties of UMo alloys from first-principles

**Aloïs Castellano, Johann Bouchet, François Bottin, Boris Dorado**

*CEA, DAM, DIF, F-91297 Arpajon, France, e-mail: alois.castellano@cea.fr*

UMo alloys appear to be the most promising nuclear fuels for the conversion of highly enriched fuels that are currently used in research reactor cores, such as U3$Si_2$, UAl alloys, or $U_3O_8$. These alloys have been selected because of their high uranium density, as well as their cubic crystal structure that guarantee isotropic swelling under irradiation. It is therefore crucial that we get some basic understanding of their thermal properties via the determination of phonon spectra and density of states. However, while a lot of work has been dedicated to the electronic structure of UMo with respect to the Mo content, there is little data related to the phonon dispersion curves.

In this work, we run ab initio molecular dynamics and we use TDEP method [1-3] in order to calculate the phonon spectra of UMo alloys over the whole range of Mo concentrations. We compare the results with those of pure bcc uranium and molybdenum, as well with experimental results [4] in order to get a consistent and comprehensive picture of UMo thermodynamic properties. We show how the interplay between the addition of Mo and the temperature stabilizes the uranium bcc structure and we calculate a number of thermal properties derived from the phonon density of states, such as Gibbs free energies, phonon and electron thermal conductivities, Grüneisen parameters, expansion coefficients, etc.

## References

[1] O. Helmann et al., Phys. Rev. **B 87**, 104111 (2013)
[2] J. Bouchet et al., Phys. Rev. **B 95**, 054113 (2017)
[3] B. Dorado et al., Phys. Rev. **B 95**, 104303 (2017)
[4] D. Chaney, R. Springell, G.H. Lander, private commucation

# Electronic Structure and Magnetism of $UGa_2$ Using LDA+DMFT Method

**Banhi Chatterjee** and **Jindřich Kolorenč**

*Institute of Physics, Czech Academy of Sciences, Na Slovance 2, 182 21 Praha, Czech Republic*
*e-mail: kolorenc@fzu.cz*

The debate whether uranium 5f electrons are closer to being localized or delocalized in $UGa_2$ does not appear fully concluded yet, and one can even find (at least seemingly) incompatible spectroscopic observations of the uranium 5f electrons in the literature (Fig. 1) [1,2]. The present state of the theoretical understanding of the $UGa_2$ electronic structure is not satisfactory either. For instance, the magnetic moments at the uranium atoms are severely underestimated by the band theory (LDA), and although the correlated band theory (LDA+U) makes the moments larger, the increase is still not large enough to match the experiment [3,4].

We attempt to gain more insight into the electronic structure of $UGa_2$ by means of LDA+DMFT calculations using exact diagonalization as the impurity solver [5]. One of the properties we focus on is the M-edge x-ray absorption spectrum that reflects the unoccupied uranium 5f density of states. Figure 2 shows the computed spectrum and compares it with a recent high-resolution measurement [6]. The experiment detects a shoulder at the high-energy side of the absorption line which LDA does not see at all. The LDA+DMFT adds an extra feature at these higher energies and links it with (localized) 5f atomic multiplets. The intensity of this feature is overestimated which we interpret as a sign that our impurity solver is probably biased and pushes the 5f electrons too much toward localization. The results shown in Fig. 2 were computed in the paramagnetic phase, the investigation of the ferromagnetic phase is in progress.

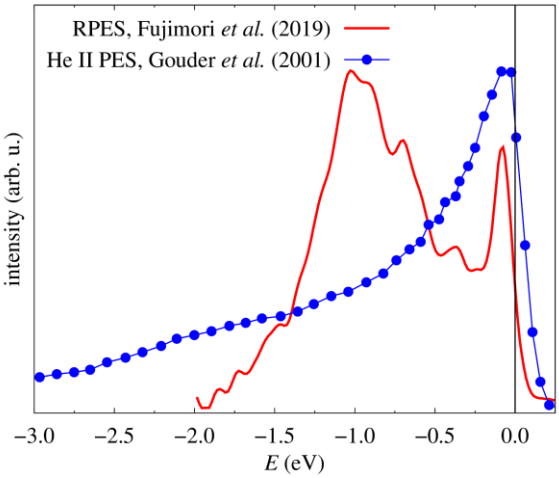


**Fig. 1.** Two estimates of the occupied uranium 5f density of states in $UGa_2$. One uses U 4d – 5f resonant photoemission (data adopted from [1]) and the other regular photoemission at the He II line (data adopted from [2]). Apparently, some assumptions made when interpreting these experiments cannot be fulfilled.

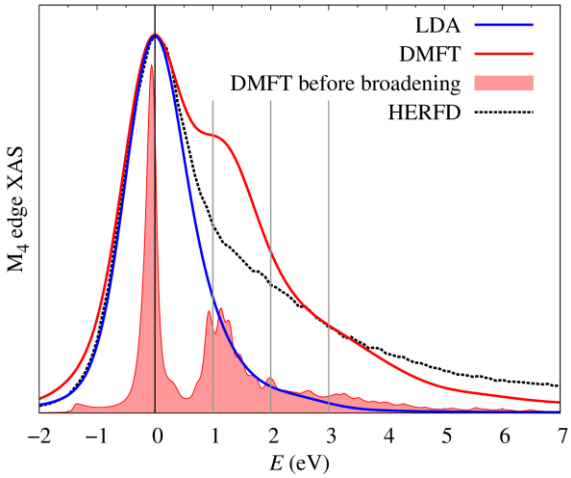


**Fig. 2.** X-ray absorption at the uranium $M_4$ edge. High-resolution experiment [6] is compared to LDA calculation (which entirely misses the high-energy shoulder) and to LDA+DMFT calculation (which does see the shoulder but with a too high intensity – likely due to overestimated tendency to localization).

*This work was supported by the Czech Science Foundation under the grant No. 18-02344S.*

## References

[1] S.-i. Fujimori *et al.*, *Phys. Rev. B* **99**, 035109 (2019).
[2] T. Gouder *et al.*, *J. Alloys Compd.* **314**, 7 (2001).
[3] M. Diviš *et al.*, *Phys. Rev. B* **53**, 9658 (1996).
[4] A. V. Andreev *et al.*, *Sov. Phys. JETP* **48**, 1187 (1978).
[5] J. Kolorenč *et al.*, *Phys. Rev. B* **92**, 085125 (2015).
[6] K. Kvashnina, L. Havela, *private communication*

# Lattice dynamics and thermodynamic stability of $UH_2$ and $UH_3$ from first principles

**L. Kývala[1], L. Havela[2], and D. Legut[1]**

*[1]IT4Innovations & Nanotechnology Center, VSB-Technical University of Ostrava,17.listopadu 2172/15 , CZ-70800 Ostrava, Czech Republic, e-mail: dominik.legut@vsb.cz*
*[2] Faculty of Mathematics and Physics, Charles University, Ke Karlovu 5, 12116 Prague, Czech Republic*

Uranium metal is known to form two different hydrides with the same $UH_3$ stoichiometry. Although the other 5*f*-elements as Pu, Np or Th exist in dihydride form, $UH_2$ was not reported for very long time. Hovewer, recent work [1] shows that fcc uranium dihydride can exist, if is synthetized as a thin film. We investigate electronic structure, mechanical and magnetic properties, lattice dynamics and thermodynamic stability of *fcc* uranium dihydride within density function theory, as implemented in the VASP package. Magnetic order and anisotropy are discussed both in substantial compressive residual stress and in relaxed structure. Comparison $UH_2$ with $UH_3$ corresponds to the question why $UH_2$ can be stabilized as thin film and not in a bulk form. This work was supported by CSF grant No. 17-27790S.

## References

[1] L. Havela, M. Paukov, M. Dopita, L. Horák, D. Drozdenko, M. Diviš, I. Turek, D. Legut, L. Kyvala, T. Gouder, A. Seibert, and F. Huber, *Inorg. Chem.* **57**, 14727 (2018).

# Resonant x-ray diffraction of uranium nitride epitaxial films

**E. Lawrence Bright[1], R. Springell[1], D. G. Porter[2], and G. H. Lander[1]**

*[1]School of Physics, University of Bristol, Tyndall Avenue, Bristol, BS8 1TL, UK*
*[2]Diamond Light Source, Harwell Science & Innovation Campus, Didcot, Oxon OX11 0DE, UK*

Epitaxial films have been produced at Bristol of both UN and $U_2N_3$ [1]. We have now examined 70 and 200 nm films of the respective films with the I16 diffractometer at the Diamond Light Source using X-ray energies tuned to the U $M_4$ energy of 3.725 keV.

The crystal structure of UN is cubic *fcc* NaCl-type and the magnetic structure is known as type-I [2]. This has tetragonal symmetry, but there is no reliable observation of the formally allowed tetragonal lattice distortion in UN, with the experimental evidence being contradictory [3, 4, 5]. We have observed magnetic scattering at the expected $q$ = 1 positions in the UN film with $T_N$ ~ 48 K, some 6 K below the value found for the bulk material. All three domains are populated despite the small tetragonality of the film from locking with the substrate. We then performed a series of measurements with 15 keV X-rays to examine the temperature dependence of the lattice parameters. The expansion of the lattice below $T_N$ on cooling measured by earlier work is confirmed [3, 5, 6]. *No* tetragonal distortion occurs, but complicated strain effects occur below $T_N$ and will be discussed.

$U_2N_3$ is a well-known cubic (bixbyite structure $a_o$ = 10.68 Å) compound in the U-N phase diagram and no single crystals have previously been synthesized. The compositions and their magnetic susceptibility were investigated in 1975 [7], and antiferromagnetism occurs at 90 K in the stoichiometric material. We have not found any report of the magnetic configuration. Resonant X-rays show that the magnetic structure has $q$ = 1 and $T_N$ = 75 K. The magnetic structure resembles that of $Yb_2O_3$ [8]. To determine such a structure through RXS measurements, where the *absolute* intensities are required, is difficult, especially as there are *two* different uranium sites in the structure.

We have also observed "anisotropic resonant scattering" [9] at certain reflections (both allowed and forbidden) in this material. This suggests that at the $U_1$ site (point symmetry $C_{3i}$) the 5*f* electron distribution is *anisotropic* and does not have a local inversion center, thus implying that the 5*f* states, of at least $U_1$, are involved in covalent bonding in this material. The reflections from this effect are independent of temperature and have an energy dependence that exhibits a pure *f"* component of the scattering factor.

## References

[1] E. Lawrence Bright *et al.*, Thin solid films **661**, 71 (2018).
[2] N. A. Curry, Proc. Phys. Soc. **86**, 1193 (1965).
[3] J. A. C. Marples *et al.*, J. Phys. C: Solid State Phys., **8**, 708 (1975).
[4] J. Rossat-Mignod *et al.* Physica B **102,** 237 (1980).
[5] H. W. Knott *et al.*, Phys. Rev. B **21**, 4159 (1980).
[6] K. Shrestha *et al.*, Scientific Reports **7**, 6642 (2017).
[7] R. Troc, J. Solid State Chemistry, **13**, 14 (1975).
[8] R. Moon *et al.*, Phys. Rev. **176** 722 (1968).
[9] J. Kokubun and V.E. Dmitrienko, Eur. Phys. J. Special Topics **208**, 39 (2012).

# Tuning the uranium ferromagnetic superconductors with hydrostatic and uniaxial pressure

**Daniel Braithwaite[1], Dai Aoki[1,2], Jean-Pascal Brison[1], Jacques Flouquet[1], Georg Knebel[1], Ai Nakamura[1,2], Alexandre Pourret[1].**

*[1]Université Grenoble Alpes and CEA, INAC-PHELIQS, F-38000 Grenoble, France*
*[2]Institute for Materials Research, Tohoku University, Oarai, Ibaraki 311-1313, Japan*

The microscopic co-existence of superconductivity and ferromagnetism is established in three uranium based heavy-fermion systems: $UGe_2$, URhGe and UCoGe. This coexistence strongly suggests an unusual superconducting state, with triplet pairing, where the Pauli limiting mechanism is not active and the Cooper pairs can survive in the strong exchange field. Hydrostatic pressure is a powerful method to tune and understand unconventional superconductivity in many systems, often by driving them close to the threshold of a magnetic instability. Indeed in the first discovered ferromagnetic superconductor $UGe_2$, superconductivity appears only under pressure. In UCoGe, like in $UGe_2$, hydrostatic pressure suppresses the ferromagnetic order. In both theses systems we have studied the rich phase diagram of the ferromagnetic and superconducting phases versus pressure, temperature and magnetic field. However in URhGe, hydrostatic pressure increases the Curie temperature, driving the system further away from its instability. We demonstrate that in URhGe, uniaxial stress can act as negative pressure leading to a decrease of the Curie temperature and to a strong increase of the superconducting critical temperatures at zero field and under field [1]. The driving force for the enhancement of pairing mechanism under uniaxial stress, even in zero magnetic field, seems to be the increase of the *b*-axis susceptibility, moving the system away from the Ising-type limit. This mechanism is predicted by microscopic theories of anisotropic ferromagnetic superconductors, as arising from an enhanced coupling of the spin-polarized bands by transverse fluctuations.

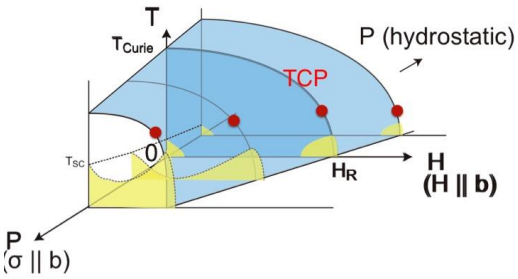


Figure 1. Comparison in URhGe of the opposite effects : Hydrostatic pressure which enhances $T_{Curie}$ and suppresses superconductivity, driving the low and high field superconducting pockets apart. Uniaxial stress along the b-axis suppresses $T_{Curie}$ and strongly enhances superconductivity, reuniting the two superconducting pockets.

## References

[1] D. Braithwaite et al. Phys. Rev. Lett. **120**, 037001 (2018)

# Structure and magnetic properties of uranium-vanadium hydrides

**Oleksandra Koloskova[1], Volodymyr Buturlim[1], Peter Minárik[1], Mykhaylo Paukov[1,2], Ladislav Havela[1]**

[1] *Charles University, Faculty of Mathematics and Physics, Ke Karlovu 5, 12116 Prague 2, Czech Republic, koloskova.alexandra@gmail.com*
[2] *Immanuil Kant Baltic Federal University, STP"Fabrica", Gaidara 6, 236029 Kaliningrad, Russia*

Uranium hydride $UH_3$ is the first known material with ferromagnetism based purely on the 5*f* electronic states [1] with the Curie temperature around 165 K for both existing modifications, a transient α-$UH_3$ and a stable β-$UH_3$ forms. The structure and properties of the initial hydride can be altered by the use of fast-cooled U-T alloys as precursors for obtaining hydrides, which incorporate the transition metal T atoms. In particular, the hydrides with modified structure and composition exhibit either a stable crystalline α-$UH_3$ hydride type or nanocrystalline β-$UH_3$. Moreover, all the studied $(UH_3)_{1-x}T_x$ hydrides show higher $T_C$ values, exceeding 200 K in the case of Mo alloying, with a maximum corresponding to 12-15 at.% of alloying element. A reason for such general increase has been so far unclear, we can speculate about an effect of electronic states of alloying elements or an impact of crystal structure.

Vanadium was chosen for the new set of studies. Physical properties (especially low temperature ones) of U-V alloys and corresponding hydrides have not been investigated yet. Only phase composition, microstructure and elastic properties have been reported. Vanadium exhibits the phase diagram with uranium similar to U-Pt. There a specific situation is encountered, with limited solubility of Pt in the *bcc* phase in equilibrium phase diagram and much higher Pt concentration accommodated as metastable in rapidly cooled alloys [2].

The analysis of XRD and TEM data for the previously synthesized $UH_3$-Mo and $UH_3$-Zr hydrides revealed that the hydrogenation process results in the homogenization of the structure even if the precursor had a multi-phase structure [2]. The U-V alloys need, similar to other U-T systems, high hydrogen pressures (50-100 bar for 5 days) to saturate the system with hydrogen at room temperature. The same time range is not sufficient for the minimum pressure of 9 bar $H_2$ to complete the process. Unlike other U-T hydrides, the crystal structure is regular β-$UH_3$, only for high V concentrations (20%) the grain size decreases, reaching nanocrystallinity. Lattice parameters slightly decrease with the increase of V concentration ($a$ = 6.6444 Å, 6.6616 Å , 6.6429 Å, 6.6416 Å for pure $UH_3$, 10%, 15%, 20% V concentrations, respectively).

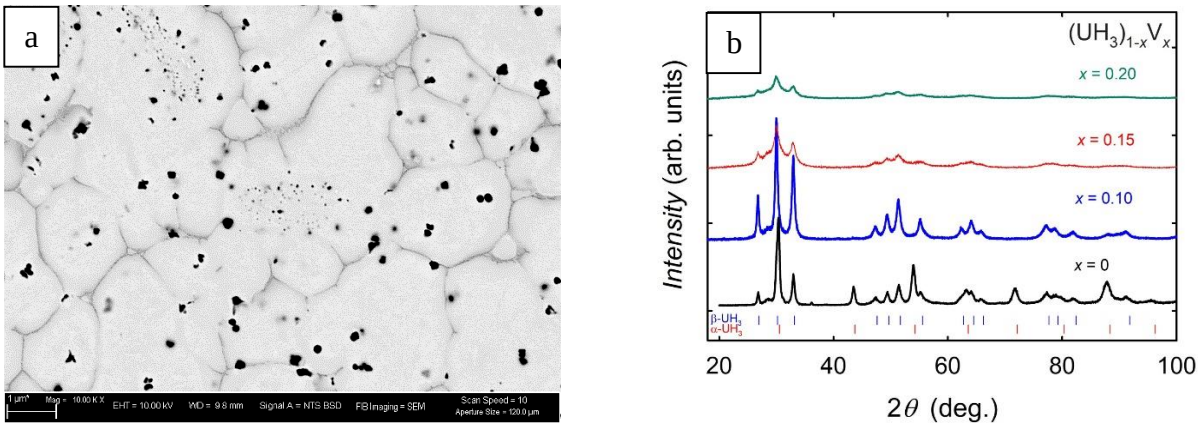


Fig. 1. SEM micrograph for $(UH_3)_{0.85}V_{0.15}$ (a) and X-ray diffraction pattern of the $(UH_3)_{1-x}V_x$ hydrides (b).

The SEM study of the hydride material showed a tendency to segregate excessive V in small clusters (≈ 100-250 nm), preventing to have more than ≈15% V dissolved in the uranium hydride phase. Pilot magnetization study of the $UH_3$-V samples indicated $T_C$ values increasing to ≈ 190 K for 15 at.% V, followed by a saturation. If the additional studies will prove that, we can conclude that the increase of $T_C$ has nothing to do with modification of the type of crystal structure.

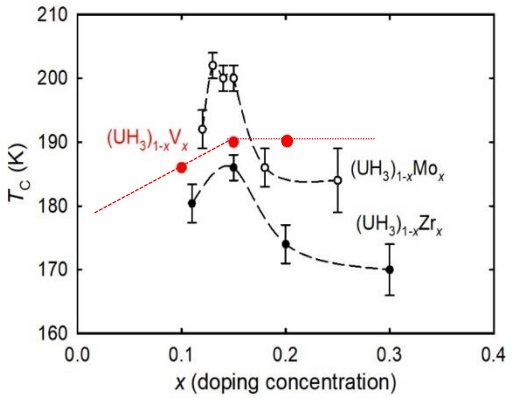


Fig. 2. Concentration dependence of the Curie temperature in the series $(UH_3)_{1-x}$(Zr-Mo-V)$_x$.

Basic magnetic (temperature and field dependences of the magnetization) data on the hydrides will be presented, as well as study of their microstructure. The results obtained for the newly synthesized samples will be compared to those received for Mo and Zr alloyed hydrides.

*This work was supported by the Czech Science Foundation under the grant No. 18-02344S and by the Czech Ministry of Education under the COST project scheme, project No. LTC18024.*

## References

[1] N.-T.H. Kim-Ngan et al., *J.Nucl.Mater.* **479**, 287 (2016).
[2] L. Havela et al., *J.Mag.Mag.Mater.* **400**, 130 (2016).

# Poster Presentations

# Magnetism of $Nd_{3-x}U_xRu_4Al_{12}$ intermetallic compounds

**A.V. Andreev,[1] D.I. Gorbunov[2], J. Šebek[1]**

[1] *Institute of Physics, Academy of Sciences, 18221 Prague, Czech Republic*
*e-mail: a.andreev@seznam.cz*
[2] *Hochfeld-Magnetlabor (HLD-EMFL), Dresden-Rossendorf, D-01328 Dresden, Germany*

The ternary intermetallic compounds $R_3Ru_4Al_{12}$ ($R$ – rare-earth element or U) crystallize in a hexagonal crystal structure of $Gd_3Ru_4Al_{12}$ type (space group $P6_3/mmc$), where the $R$ atoms form a distorted kagome lattice parallel to the basal plane. They attract attention for two reasons. First, the crystal structure leads to unequal exchange and crystal-electric-field interactions for atoms occupying the same crystallographic position and, when magnetic moments are coupled antiferromagnetically, gives rise to geometrical frustration. Second, $R_3Ru_4Al_{12}$ allow a comparison between the single-ion and two-ion mechanisms of magnetic anisotropy. It was found that $Nd_3Ru_4Al_{12}$ is a ferromagnet and displays uniaxial anisotropy [1], whereas its actinide analog, $U_3Ru_4Al_{12}$, is an antiferromagnet and shows planar anisotropy [2]. Therefore, the single-ion and two-ion mechanisms lead to distinct anisotropies. In the present work, we prepared $Nd_{3-x}U_xRu_4Al_{12}$ single crystals ($x$ = 0, 1, 2, 3) in order to study the evolution of their magnetic properties.

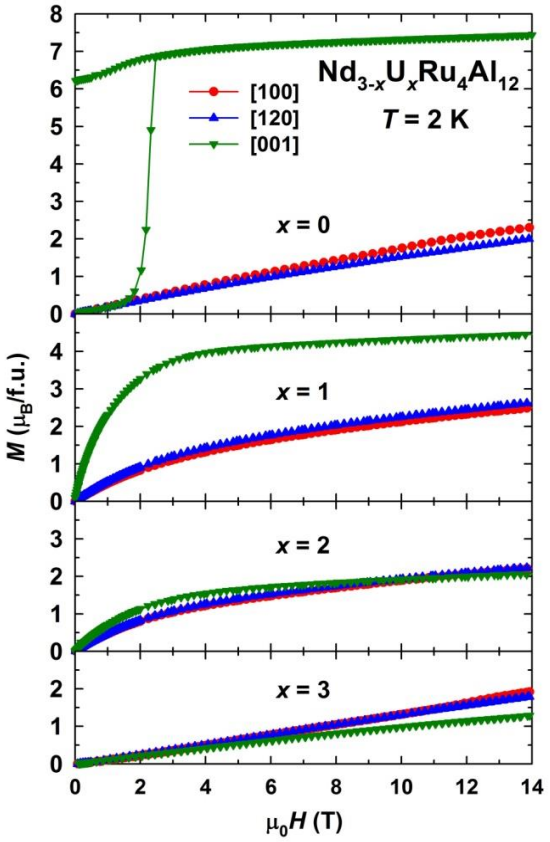


Fig. 1. Magnetization curves along the principal crystallographic axes of $Nd_{3-x}U_xRu_4Al_{12}$ single crystals at 2 K.

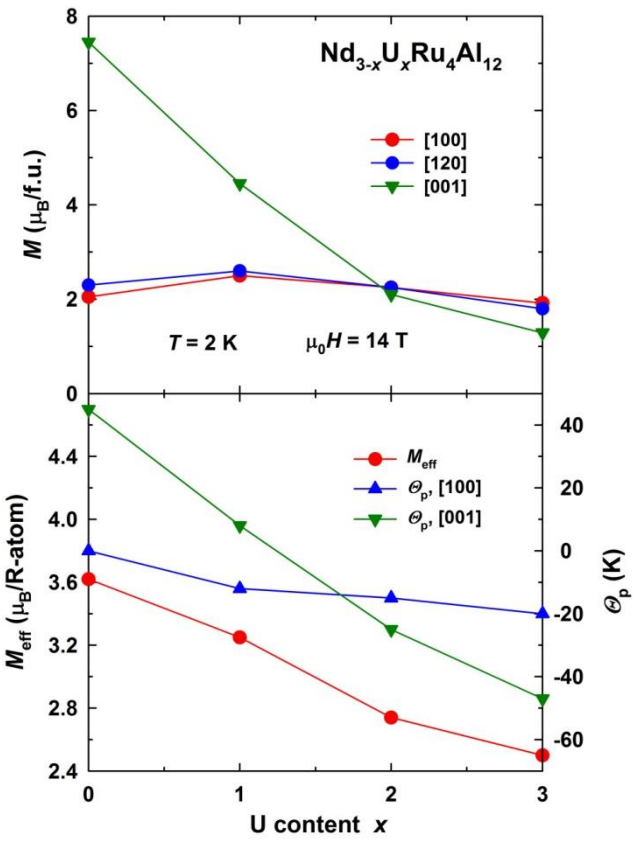


Fig. 2. Concentration dependence of the magnetization, $M$, in 14 T at 2 K, effective magnetic moment, $M_{eff}$, and paramagnetic Curie temperature, $\Theta_p$.

The crystals were grown by the modified Czochralski method from an 8 g stoichiometric mixture of the pure elements (99.9% U, 99.99% Ru and 99.999% Al) in a tri-arc furnace with a water-cooled copper crucible under protective argon atmosphere. A tungsten rod was used as a seed. The pulling speed was 10 mm/h. Back-scattered Laue patterns showed good quality of the single crystals.

The lattice of $Nd_{3-x}U_xRu_4Al_{12}$ shrinks with $x$ anisotropically (by 0.4% in basal plane and by 2.1% along the [001] axis) with a volume effect of 2.8% in accordance with a smaller atomic radius of U than of Nd.

Magnetization curves (Fig. 1) show that $Nd_3Ru_4Al_{12}$ is a ferromagnet (below Curie temperature $T_C$ = 39 K) with easy axis [001]. A strong uniaxial magnetic anisotropy (the first anisotropy constant is 3 MJ $m^{-3}$ at 2 K) leads to a large magnetic hysteresis ($\mu_0 H_c$ = 2 T at 2 K) of narrow domain walls. The anisotropy within the basal plane is not large, nevertheless, it is non-negligible, the [120] axis is the hardest magnetization axis. For $x \geq 1$, $Nd_{3-x}U_xRu_4Al_{12}$ do not show spontaneous magnetization, therefore, they are not ferromagnets. For the materials with $x$ = 1 and 2, we did not find any anomaly in the magnetic susceptibility as a function of temperature. Therefore, $Nd_2URu_4Al_{12}$ and $NdU_2Ru_4Al_{12}$ are likely paramagnets (at least above 2 K). The U substitution for Nd affects also the magnetic anisotropy. For $x$ = 1, the strong uniaxial anisotropy is still observed, whereas the compound with $x$ = 2 is close to magnetically isotropic below 14 T. Finally, the magnetization becomes larger in the basal plane than along the [001] axis at $x$ = 3, confirming a basal-plane arrangement of its antiferromagnetic structure.

Figure 2 shows concentration dependence of magnetization in 14 T. Whereas along the [001] axis the magnetization decreases strongly with increasing U content, in the basal plane it is almost concentration-independent. Lower panel of Fig. 2 presents the results of a Curie-Weiss treatment of temperature dependences of the magnetic susceptibility. The effective magnetic moment, $M_{eff}$, per $R$ atom is 3.6 $\mu_B$ at $x$ = 0, which well corresponds to the moment of single-ion $R^{3+}$ ions both for Nd and U. With increasing $x$, $M_{eff}$ decreases to 2.5 $\mu_B$. The difference in the paramagnetic Curie temperatures, $\Theta_p$, between the [100] axis and the basal plane is 45 K at $x$ = 0, which confirms the strong uniaxial anisotropy seen from magnetization curves. At $x$ = 3, this difference is -28 K. The anisotropy is of the easy-plane type and is weaker in magnitude than for $x$ = 0. A change of the anisotropy type occurs in the vicinity of $x$ = 2, in accordance with our $M$ vs. $H$ data (Fig. 1).

## References

[1] R. Troc, M. Pasturel, O. Tougait, A.P. Sazonov, A. Gukasov, C. Sulkowski, H. Noel, Phys. Rev. B **85**, 064412 (2012).

[2] D.I. Gorbunov, M. S. Henriques, A.V. Andreev, V. Eigner, A. Gukasov, X. Fabreges, Y. Skourski, V. Petricek, J. Wosnitza, Phys. Rev. B **93**, 024407 (2016).

# X-ray diffraction study of dislocations in uranium

**A.E. Shestakov, I.V. Artamonov**

*Russian Federal Nuclear Center - Zababakhin All-Russia Research Institute of Technical Physics (RFNC-VNIITF), Vasilieva str. 13 p.b. 245, 456770, Snezhinsk, Russia, a.e.shestakov@vniitf.ru*

X-ray diffraction patterns of samples loaded at high deformation rates (>$10^3 s^{-1}$) are observed to have diffraction peaks that are broader than the initial ones. This can be caused by the crystalline lattice microstrain or the coherent scattering region refinement down to <0.1μm. The angular dependence analysis determines how each of these two factors influences peak broadening. The X-ray diffraction method based on the Williamson-Hall procedure was proposed to measure the crystalline lattice microstrain in uranium and it was methodically checked.

In metals after plastic deformation, microstrain is induced by chaotically distributed dislocations. Correlation between the dislocations density ($\rho$) and the lattice microstrain amount ($\varepsilon$) can be written as $\rho = K \cdot \varepsilon^2$. In order to find the coefficient *K*, microstrain of the uranium lattice was measured in a series of experiments involving samples with the known dislocations density determined through transmission electronic microscopy (TEM). Figure 1 shows the experimental data and the extrapolational right line.

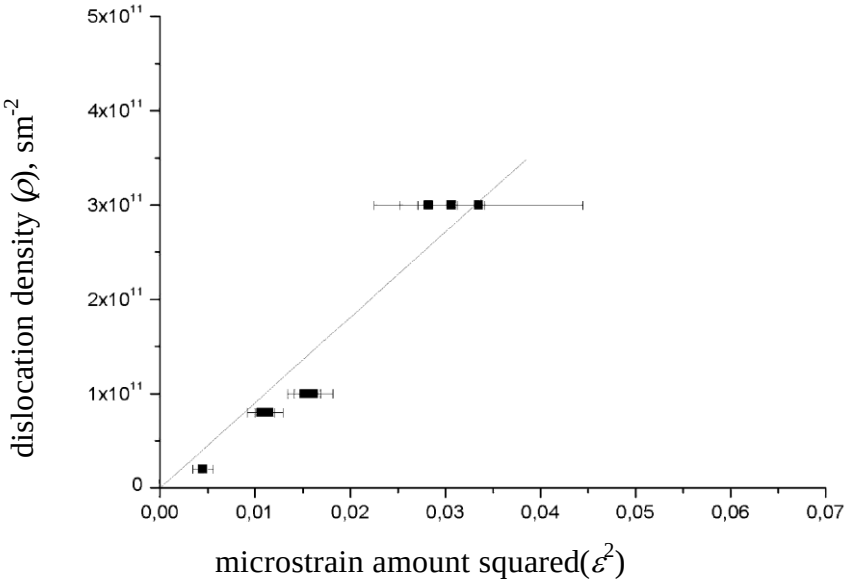


Fig. 1. TEM-data on the dislocations density and the lattice microstrain measured by diffraction peaks broadening. Solid line – is the linear extrapolation.

The dislocations density was measured on uranium samples after their low-rate deformation. We obtained dependences for the dislocation density in uranium after its deformation up to 60% at the room temperature and after its follow-on annealing at temperatures up to 850˚C.

The dislocation density over the cross-section of the uranium spherical shell recovered after shock-wave loading was measured (Figure 2).

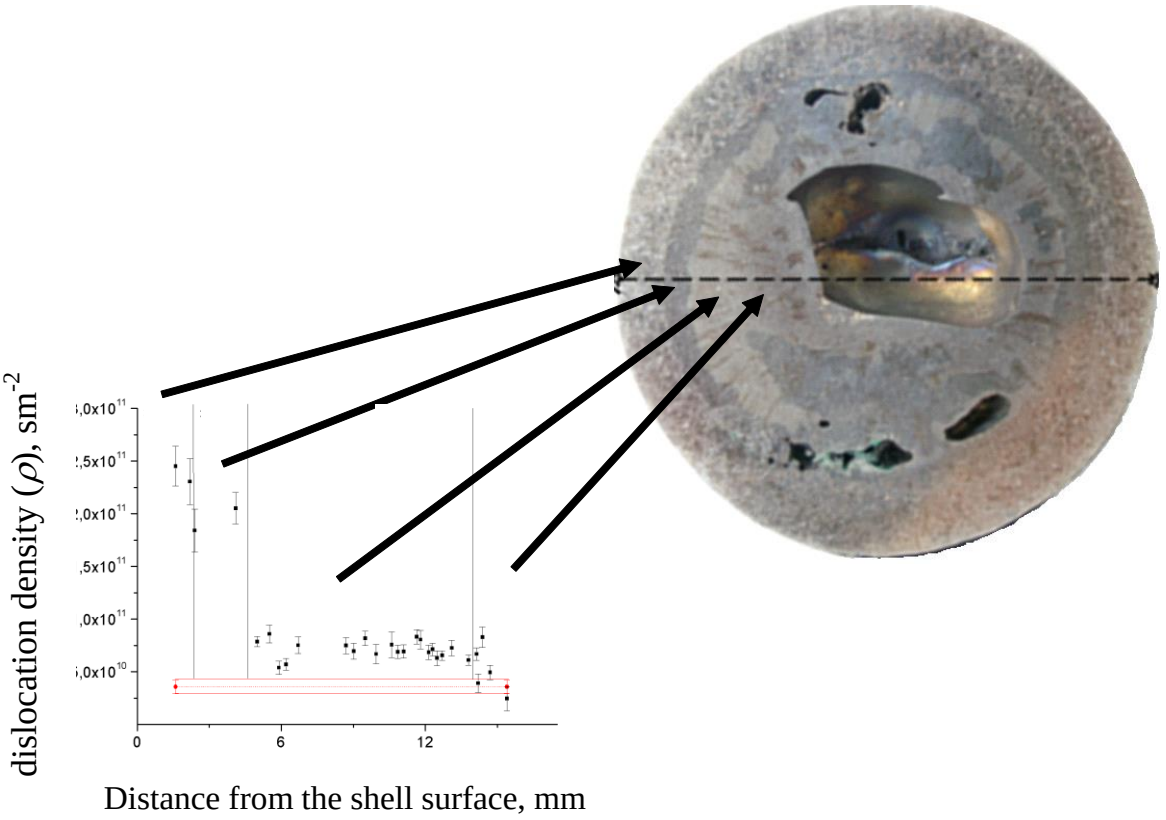


Fig. 2. Dislocations density versus distance from the surface and zonal structure of the shell

Light microscopy demonstrated agreement between the dislocations density amount dependence on the coordinate and the zonal structure of the recovered shell.

# Experimental separation of americium-241 from aged MOX-fuel

**A.O. Makarov, A.S. Kornilov, O.S. Dmitrieva, K.O. Scherbakova**

*Joint-stock Company "State scientific center – Research Institute of Atomic Reactors", Russia, Ulyanovsk region, Dimitrovgrad, Zapadnoye Shosse 9, 433510, e-mail: osdmitrieva@niiar.ru*

The formation of long-lived actinides (americium, neptunium, curium) and their accumulation in spent nuclear fuel is one of the main problem to the sustainable development of nuclear energy. Therefore, one of the processes for the treatment of such products discussed and verified at the moment is transmutation - burning in fast neutron reactors with the aim of minimizing their number. Consider various options: the inclusion of long-lived actinides in the composition of nuclear materials (for example, mixtures of uranium and plutonium nitrides), when recycled - repeated use in a nuclear reactor with a fast spectrum or separate burning, for example, americium hydride [1]. As a consequence, the uptime of americium for the manufacture of experimental fuels with the inclusion of americium or various compositions with americium is relevant.

In the JSC "SSC RIAR" accumulated significant reserves of plutonium dioxide of energy origin and waste from the production of MOX-fuel. Plutonium-241, contained in MOX-fuel and in long-term waste from the production of MOX-fuel, largely has beta decayed to isotopically pure americium-241, which makes them a valuable raw material for producing americium-241.

To accomplish the task, was developed a method, based on the precipitation of uranium and plutonium formiates and the subsequent selective precipitation of americium oxalate. To assess the suitability of the proposed method, mathematical modeling of chemical equilibria in the "americium – plutonium – oxalic acid" system was carried out, which showed the possibility of selective separation of americium from a mixture of uranium and plutonium. A fundamental verification of the applicability of the data obtained on real long-term waste from the production of MOX-fuel has been carried out.

The MOX-fuel was dissolved in hot 10 M nitric acid with the addition of hydrofluoric acid. The obtained nitrate solution of MOX-fuel was denitrated by adding 23 M formic acid with an excess up to the precipitation of uranium and plutonium formiates. The precipitates obtained were filtered, and the resulting filtrate was used to precipitate americium oxalate by adding oxalic acid and ammonium acetate to the solution. The precipitate of americium oxalate was washed on a filter, dried, separated from the filter, and then calcined at 800 ° C in air to obtain americium dioxide.

To determine the purity of the obtained americium oxide for the residual plutonium content, α-radiometry was used using data on the isotopic composition of the plutonium used. To exclude the influence of the plutonium-238 isotope in americium oxide, the content of americium-241 was also additionally determined by γ-spectrometry. To determine the phase composition of the powder, the obtained americium oxide was analyzed by the X-ray diffraction method.

It was determined that the resulting preparation is americium dioxide, with an americium-241 content of more than 88.0 wt.% and the content of plutonium and cationic impurities less than 1.0 wt.%.

## References

[1] Catherine Campbellet al., The Separation of $^{241}$Am from Aged Plutonium Dioxide for Use in Radioisotope Power Systems Using the AMPPEX Process, *Procedia Chemistry*, **140-147, 21** (2016).

# Influence of Mo and B doping on the structure and properties of $U_6Fe$-based alloys prepared by splat cooling

**N.-T.H. Kim-Ngan[1], M. Paukov[2], V. Buturlim[2], L. Havela[2]**

[1] *Institute of Physics, Pedagogical University, 30-084 Krakow, Poland, E-mail: hoakimngan.nhu-tarnawska@up.krakow.pl*
[2] *Faculty of Mathematics and Physics, Charles University, Ke Karlovu 5, 12116 Prague, Czech Republic*

To explore possible modifications of U superconductor $U_6Fe$, we investigated structure and properties of $U_6Fe$ (or $U_{85.7}Fe_{14.3}$), $U_{90}Fe_{10}$, $U_{85}Fe_{14}Mo_1$ (or $(U_6Fe)_{0.95}Mo_{0.05}$), $U_{85}Fe_{10}Mo_5$, $U_{85}Fe_{14}B_1$ and $U_{85}Fe_{10}B_5$, all prepared by splat-cooling, i.e. with a cooling rate of $10^6$K/s. The XRD pattern of $U_6Fe$ splat reveals a normal crystalline state similar to its precursor alloy, having the body-centered tetragonal structure, with the room temperature lattice parameters $a$ = 10.297 Å, $c$ = 5.197 Å. Increasing the U concentration to $U_{0.90}Fe_{0.10}$ leads to a segregation of the α-U phase. Doping with B with a smaller atomic radius than that of Fe can be apparently adopted within the crystal structure of $U_6Fe$. Doping with a small amount of Mo (with a larger ionic radius ($r_{Mo}$ = 140 pm compared with $r_{Fe}$ = 126 pm) leads to a formation of the bcc γ-U phase. The XRD data analysis of $U_{85}Fe_{14}Mo_1$ yields 72% $U_6Fe$, 23% α-U and a small amount of γ-U, whereas increase the Mo content in $U_{85}Fe_{10}Mo_5$ leads to a significant change of the phase composition. The two dominant phases are $U_6Fe$ (78%, with the lattice parameters $a$ = 10.309Å, $c$ = 5.236Å) and γ-U (20%, $a$ = 3.540 Å), while the contribution of α-U is negligible.

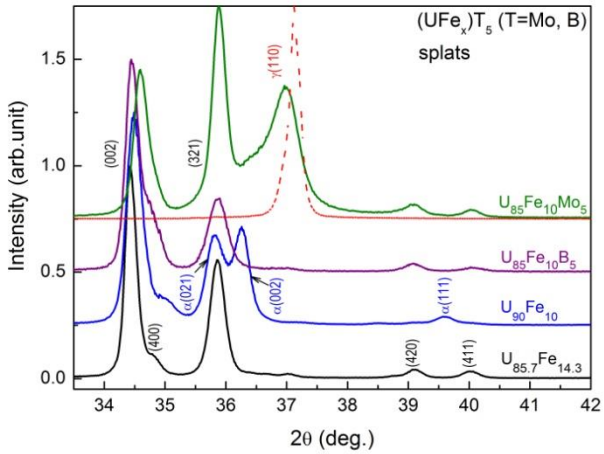


Fig.1. Comparison of the low-angle XRD patterns of $U_6Fe$ (or $U_{85.7}Fe_{14.3}$), $U_{90}Fe_{10}$, $U_{85}Fe_{10}B_5$ and $U_{85}Fe_{10}Mo_5$ prepared by the splat-cooling technique. The reflections of the body-centered tetragonal structure of $U_6Fe$ and α-U are indicated respectively by black and blue color. The red-color dashed line shows the strongest γ(110) reflection obtained for $U_{85}Mo_{15}$ splat-cooled alloy stabilized in the cubic γ-U structure [1].

Alloying with Mo has a dramatic impact on superconducting properties of $U_6Fe$. It leads to a pronounced decrease of $T_c$. For $U_{85}Fe_{14}Mo_1$ (corresponding to $(U_6Fe)_{0.95}Mo_{0.05}$), the superconducting phase transition seen as a sharp drop in the electrical resistivity gives $T_c$ = 2.85 K with the transition width $\Delta\rho$ = 0.20 K). The estimated Sommerfeld coefficient of electronic specific heat $\gamma_e$ = 100 mJ/mol K$^2$ gives about 17.5 mJ/mol U K$^2$. The λ-type peak at $T_c$ in the specific heat is broadened and reduced, the experimental specific jump is below the theoretical weak-coupling BCS value ($\Delta C_{BCS}$=1.43*$\gamma_e$*$T_c$ = 0.41 J/mol K). One can compare

with the $U_{85}Mo_{15}$ splat consisting of the pure *bcc* γ-U, in which the pronounced λ-type peak appears in the specific heat and the experimental specific-heat jump is in a good agreement with that estimated from BCS theory ($T_c$ =2.11 K, $\gamma_e$ = 16 mJ/mol K$^2$, $\Delta C_{BCS}$ = 48.28 mJ/mol K) [1]. At present it cannot be concluded whether the effect is due to a small Mo involvement into the $U_6Fe$ phase or Mo forms the alloy with U, leaving an excess of Fe in the 6-1 Phase. In any case, the superconductivity has to be related to the 6-1 phase, so far none of the *bcc* phases has $T_c$ higher than 2.11 K.

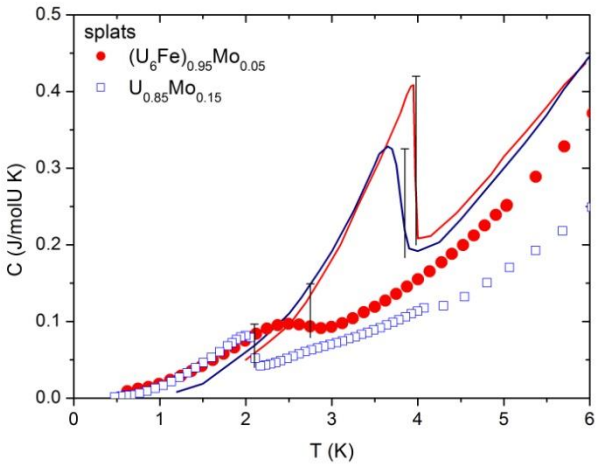


Fig. 2. The specific heat around the superconducting phase transition in $U_{85}Fe_{14}Mo_1$ and $U_{85}Mo_{15}$ splats. For a comparison with $U_6Fe$ single crystal (red line, $T_c$ = 3.95 K, $\gamma_e$ =154 mJ/mol K$^2$ [2]) and polycrystal (blue line, $T_c$ =3.8 K, $\gamma_e$ =155 mJ/mol K$^2$ [3]), it was plotted as per mol Uranium. The vertical black lines show the theoretical BCS jumps.

Like most of the investigated U-based splats, the ($U_6Fe$)-Mo splats absorb a large amount of hydrogen. $(UH_3)_{85}Fe_{10}Mo_5$ (the hydride of $(U_6Fe)_{0.95}Mo_{0.05}$) was found to be a mixture of α-$UH_3$ (28%) and β-$UH_3$ (72%) [4], both being ferromagnetic with $T_C$ = 160-170 K.

## References

[1] N.-T.H. Kim-Ngan, I. Tkach, S. Mašková, A.P. Goncalves, L. Havela, *J. Alloys and Comp.* **580**, 223 (2013).
[2] W.G. Whitley, PhD thesis (2016), https://www.era.lib.ed.ac.uk/handle/1842/22031
[3] L. E. DeLong, J. G. Huber, K. N. Yang, M. B. Maple, *Phys. Rev. Lett.* **51**, 312 (1983).
[4] M. Paukov, L. Havela, N.-T.H. Kim-Ngan, V. Buturlim, I. Tkach, D. Drozdenko, S. Mašková, S. Sowa, Z. Molčanová, M. Mihálik, M. Krupska, *J. of Science: Advanced Materials and Devices* **1**, 185 (2016).

# Coordination of Uranyl Ions by Hydroxybisphosphonates

**Chris H. Sala,[1] Gerrit Scharper[1], Felix Hennersdorf[1], Giuseppe Zanoni[2], Jan J. Weigand[1]**

*[1]Technische Universität Dresden, Faculty of Chemistry and Food Chemistry, Inorganic Molecular Chemistry, 01062 Dresden, Germany, e-mail: chris.sala@tu-dresden.de*
*[2]University of Pavia, Department of Chemistry, Viale Taramelli 10, 27100 Pavia, Italy.*

A class of compounds termed 1-hydroxy-1,1-bisphosphonates (HBP) has been successfully applied in the treatment various metabolic bone diseases.[1] Their high affinity for bone material might feature the potential to bind uranyl species, which are also accumulated in bones, and thus, limit their bioavailability. An *in-vivo* study with rats being injected uranyl nitrate showed an increase of the survival rate from 50% to 100%, if concomitantly being treated with 1-hydroxyethan-1,1-diphosphonic acid (HEDP) [2].
A comprehensive analytical study focused on uranyl-HEDP complexes suggests, that the predominant species in solution feature a $UO_2^{2+}$ to HEDP ratio of 1:1 and 1:2, respectively (Fig.1) [3]. Despite a library of differently substituted HBPs is available, studies have never been extended.
In this contribution, we report the synthesis of several substituted HBP ligands (Fig. 1), which we have used for the coordination of $UO_2(X)_2$, X = $CH_3COO^-$, $NO_3^-$ salts. UV/VIS studies indicate the formation complexes with an $UO_2^{2+}$ to HBP ratio of 2:1 under the chosen conditions. Different functional groups in the HBP's backbone allow post synthetic modifications such as binding to solid support, highlighting their potential application as uranium ion scavengers.

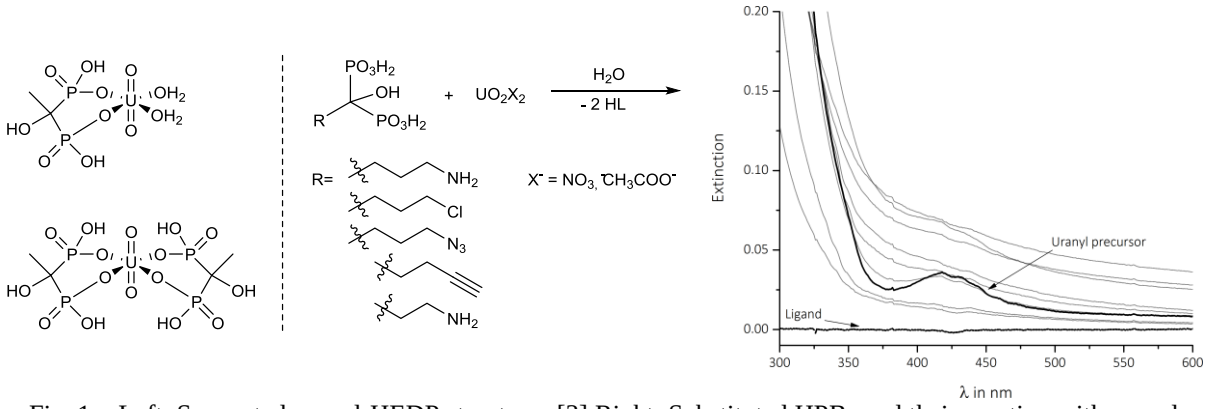


Fig. 1.: Left: Suggested uranyl-HEDP structures.[3] Right: Substituted HPBs and their reaction with uranyl compounds.

Acknowledgement: With the support of the German Federal Ministry of Education and Research (FENABIUM project 02NUK046A) and Fondazione Cariplo – Regione Lombardia grant (Sottomisura A – 2015).

## References

[1] R. Graham, G. Russell, *Bone* **49**, 2 (2011).
[1] A.M. Ubius *et al*., *Health Phys.* **66**, 540 (1993).
[2] C. Jacopin *et al*., *Inorg. Chem.* **42**, 5015 (2003).

# Structure and Properties of Reactively Deposited Uranium Hydride Coatings Studied by the X-ray Scattering Methods

**Milan Dopita[1], Lukáš Horák[1], Mykhaylo Paukov[1], Evgenia Tereshina-Chitrova[1], Ladislav Havela[1]**

[1] *Department of Condensed Matter Physics, Faculty of Mathematics and Physics, Charles University, Ke Karlovu 5, 12116, Prague 2, Czech Republic, e-mail: dopita@gmail.com*

A series of Uranium hydride coatings was prepared using a reactive sputtering method. The samples were sputtered with different Mo doping levels as well as at different hydrogen pressure and various substrate temperature. Fused silica and Si single-crystals were used as substrates for deposited coatings. The structure and the real structure (i.e. the deviations of the structure from the ideal 3D crystal periodicity) of the samples were investigated using the x-ray scattering methods. The x-ray reflectivity yielded the information on the coatings thickness, roughness and electron density. The key results of our work were the determination of the phase composition and its evolution, the description of the coherently diffracting domains size – the crystallite size and defects distributions, the description of the residual stress, strains and preferred orientation of crystallites - textures and their depth profiles in the coatings.

The sample sputtered on the fused silica substrates crystallized in the β-$UH_3$ structure (stable uranium hydride phase) with the stress free lattice parameter $a$ = 0.6703 ± 0.0004 nm. The coating exhibited strong *00l* preferred orientation of crystallites and compressive residual stress $\sigma$ = -5.1 ± 0.1 GPa. Additionally, the coating revealed a bimodal distribution of crystallite sizes with two components having the mean crystallite size $D_1$ = 200 nm and $D_2$ = 3.6 nm with volume fractions of 60:40, respectively, and huge microstrain in both components. Contrary, the coating sputtered on cooled Si single-crystal substrate showed totally different behaviour. It did not form nor the stable β-$UH_3$ neither the meta-stable α-$UH_3$ structure. The measured diffraction pattern revealed the fluorite fcc structure, analogous to e.g. $PuH_2$. This is highly interesting result, since to our best knowledge such form of uranium hydride has not been so far reported in the literature. The polycrystalline coating exhibited tilted *hhh* texture, stress free lattice parameter $a$ = 0.53598 ± 0.00014 nm, compressive residual stress $\sigma$ = -1.54 ± 0.09 GPa and mean crystallite size of 82 nm. Besides, the coating contains pronounced microstrain caused by the crystal lattice defects and significant fraction of the stacking faults. The results of the x-ray scattering studies were correlated with data obtained from HRTEM. Additionally, the possibility of formation of uranium hydride with fcc fluorite structure was confirmed by the ab-initio theoretical calculations (LDA+U).

*This work was supported by the project "Nanomaterials centre for advanced applications", Project No. CZ.02.1.01/0.0/0.0/15_003/0000485, financed by ERDF.*

## References

[1] L. Havela et al., *Inorganic Chem.*, **57 (23)** 14727 (2018).
[2] L. Havela et al., *Physical Review B*, **95**, 235112 (2017).
[3] Z. Matěj et al., *Powder Diffraction*, **29**, 35-41 (2014).

# P.Mo7

WITHDRAWN

# Epitaxial layers of $UO_2$ studied by x-ray scattering methods

**L. Horák,[1] E. A. Tereshina-Chitrova[1,2], Z. Bao[3], L. Havela[1], T. Gouder[3], R. Caciuffo[3]**

[1] *Faculty of Mathematics and Physics, Charles University, 12116 Prague, Czech Republic, e-mail: horak@karlov.mff.cuni.cz*
[2] *Institute of Physics, Czech Academy of Sciences, 18121 Prague*
[3] *European Commission, Joint Research Centre (JRC), DE-76125 Karlsruhe, Germany*

Uranium dioxide is the major nuclear fuel component of fission power reactors. The production of uranium-based films has advantage over bulk materials studies as it allows performing advanced physics and chemistry experiments on small amounts of radioactive material. It was shown however that the use of particular substrates for the $UO_2$ thin films production plays crucial role in the magnetic properties formation. Bao et at. [1] showed that the $LaAlO_3$-based films do not order magnetically throughout the thickness of $UO_2$, and there exists a magnetically dead layer at the interface with the substrate [1]. The quality of the films produced using $CaF_2$ substrates is substantially better ($UO_2$ has a $CaF_2$ crystal structure with a lattice mismatch of 0.1%) and $CaF_2$-based $UO_2$ films are fully magnetically ordered [1].
Generally, the identical crystal structure, lattice orientation and very small lattice mismatch of substrate and epitaxial layer result in the overlapped diffraction maxima in the reciprocal space. Therefore, the lattice parameters cannot be straightforwardly determined from the observed peak positions.
We have studied $UO_2$ epitaxial layers in the set of $UO_2/Fe_3O_4$ bi-layers grown on the $CaF_2$ substrates. The samples were prepared by reactive sputtering from metallic U and Fe targets. The samples were covered by a Mg capping layer. The correct stoichiometry of each deposited layer was confirmed by an in-situ X-ray Photoelectron Spectroscopy (XPS). The x-ray reflectometry (XRR) and x-ray diffraction (XRD) measurements were performed with Rigaku SmartLab diffractometer equipped with a 9kW rotating anode. The primary beam was monochromatized and parallelized by a parabolic x-ray mirror and a 2-bounce Ge(220) monochromator. Reflectivity curves and XRD $\theta$-$2\theta$ scans were measured with two receiving slits in front of the detector and the XRD reciprocal space map (RSM) measurements were performed with a HyPix-3000 in the 1D mode (medium resolution). From the XRR data we determined the thickness of individual layers and roughness of the corresponding interfaces. All samples were found to be laterally homogeneous and flat.
We have measured $\theta$-$2\theta$ scans as demonstrated in Fig. 1(*a*) from which it followed that $UO_2$ layers grow in the [100] direction while $Fe_3O_4$ have a [111] out-of plane orientation, and basal planes of the hexagonal Mg capping layer are parallel to the surface. Additionally, we observed thickness fringes around $UO_2$ reflections indicating single crystalline nature of the layer (see Fig. 1(*b*)).
In order to obtain lattice parameters and a relaxation state of the $UO_2$ layers we performed RSM measurements in the vicinity of $CaF_2$ symmetric 400, 200 and asymmetric 422 reflections (see Fig. 2(*a*)-(*c*)). From the symmetric RSMs we were able to obtain an out-of-plane lattice parameter and the thickness of the single crystal layers, precise values can be determined by simulation based on the kinematic theory of diffraction (Fig. 2(*e*)). On the other hand, the strain in the layer (i.e, fully strained or relaxed state) can be clearly seen in the asymmetric RSMs (see Fig. 2(*c*)). The in-plane lattice parameter was determined from the intensity distribution in the asymmetric RSM around the 422 $CaF_2$ reflection.

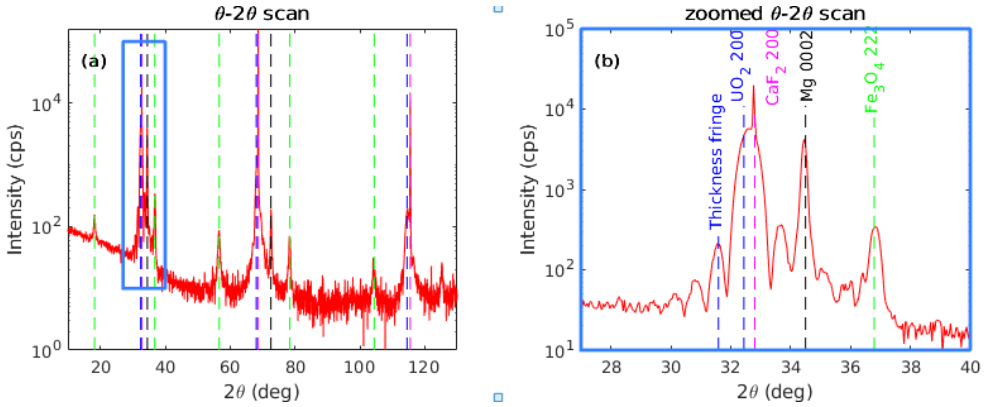


Fig. 1. (*a*) Typical $\theta$-$2\theta$ scan for the $CaF_2$(substrate)/$UO_2$/$Fe_3O_4$/Mg sample. Only Bragg reflections $CaF_2$ *h*00, $UO_2$ *h*00, $Fe_3O_4$ *hhh* and Mg 000*l* are visible revealing the lattice orientation for all layers. Panel (*b*) shows the zoomed area in the vicinity of the reflection $CaF_2$ 200.

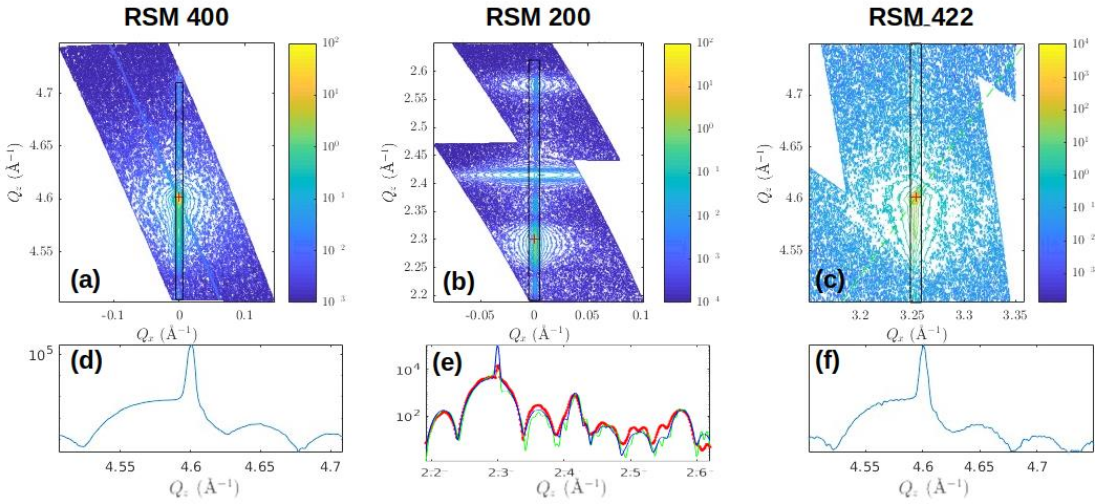


Fig. 2. Reciprocal space maps in the vicinity of the $CaF_2$ 400, 200 and 422 Bragg reflections are shown in panels (*a*), (*b*) and (*c*). For further detailed analysis, the diffracted intensity in the areas denoted by the black rectangles in (*a*)-(*c*) was integrated along $Q_x$ in order to get intensity distribution along the Crystal Truncation Rods (CTR) plotted in panels (*d*)-(*f*), respectively. Experimental data (blue) in panel (*e*) are fitted with 2 different simulations: coherently (red) and incoherently summed diffraction signals (green) calculated from optimized values of lattice parameters and thicknesses. The Bragg reflection $UO_2$ 422 with the identical $Q_x$ coordinate to $CaF_2$ 422 indicates the fully strained (pseudomorphic) state of the layer.

Our results show that the lateral strain in $UO_2$ homogeneous epitaxial layer decreases with the increasing layer thickness and it approaches a certain residual value given most probably by the different thermal expansions of the substrate and the layer during the post-growth cooling. Therefore, the $UO_2$ unit cell in the thicker layers is not completely relaxed (i.e. is not cubic) and it is tetragonally distorted. This study stresses out the importance of x-ray reciprocal space mapping in the vicinity of the $CaF_2$ Bragg reflections since it is allows us to obtain accurate lattice parameters of the $UO_2$ thin layers and their epitaxial relation and the crystal quality.

The samples were prepared in the framework of the TALISMAN project of the European Commission Joint Research Centre, Karlsruhe. We also acknowledge support of Czech Science Foundation, project #18-02344S, and "Nano-materials Centre for Advanced Applications," Project No.CZ.02.1.01/0.0/0.0/15_003/0000485, financed by ERDF

## Reference

[1] Z. Bao et al., *Phys. Rev. B* **88**, 134426 (2013).

# Actinide dioxide nanocrystals via low temperature oxalate decomposition in hot compressed water

**Olaf Walter,[1] Karin Popa[1], Marco Cologna[1], Oliver Dieste[1]**

[1] *European Commission, DG Joint Research Centre, G.I.5, P.O. Box 2340, 76125 Karlsruhe, Germany, e-mail: olaf.walter@ec.europa.eu*

Nanocrystals (NC's) represent fundamental building blocks in nanoscience and nanotechnology because of their size and shape dependent properties and have attracted high interest. Much has been published on nanomaterials with stable elements, less is published on actinide nanoparticles, and then practically all on actinide dioxides ($AnO_2$).
The synthesis of NC's in hot compressed water under hydrothermal conditions or in other solvents is today well known and established. The production of NC's in continuous flow reactors is applied successfully. However, only our reports exist for the synthesis of $AnO_2$ NC's under hydrothermal decomposition of the corresponding oxalates $An(oxalate)_2*nH_2O$ and the characterisation of the obtained NC's in the literature up to now [1-5] even if nanocrystalline $AnO_2$ is already our research objective since several years [6-13].
In this contribution a brief overview over our research will be presented on highly crystalline $AnO_2$ NC's obtained via hydrothermal decomposition of the $An(oxalate)_2*nH_2O$ in hot compressed water at temperatures below 250°C.

## References

[1] O. Walter, K. Popa, O. Dieste Blanco, *Open Chem.*, **14**, 170 (2016).
[2] L. Balice, D. Bouëxière, M. Cologna, A. Cambriani, J.-F. Vigier, E. De Bona, D.G. Sorarù, C. Kübel, O. Walter, K. Popa, *J. Nucl. Mater.*, **498**, 307 (2018).
[3] K. Popa, O. Walter, O. Dieste Blanco, A. Guiot, D. Bouëxière, J.-Y. Colle, L. Martel, M. Naji, D. Manara, *Cryst. Eng. Comm.*, **20**, 4614 (2018).
[4] D. Bouëxière, K. Popa, O. Walter, M. Cologna, *RSC Advances*, **9**, 6542 (2019).
[5] E. De Bona, O. Walter, H. Störmer, T. Wiss, G. Baldinozzi, M. Cologna, K. Popa, *J. Am. Ceram. Soc.* (2019), https://doi.org/10.1111/jace.16375
[6] R. Jovani-Abril, R. Eloirdi, D. Bouëxière, R. Malmbeck, J. Spino, *J. Mater. Sci.*, **46**, 5 (2011).
[7] D. Hudry, C. Apostolidis, O. Walter, T. Gouder, E. Courtois, C. Kübel, D. Meyer, *Chem. Eur. J.*, **18**, 8283 (2012).
[8] D. Hudry, C. Apostolidis, O. Walter, T. Gouder, A. Janssen, E. Courtois, C. Kübel, D. Meyer, *RSC Advances*, **3**, 18271 (2013).
[9] D. Hudry, C. Apostolidis, O. Walter, T. Gouder, E. Courtois, C. Kübel, D. Meyer, *Chem. Eur. J.*, **19**, 5297 (2013).
[10] D. Hudry, C. Apostolidis, O. Walter, A. Janßen, D. Manara, J. C. Griveau, E. Colineau, T. Vitova, T. Prüßmann, D. Wang, C. Kübel, D. Meyer, *Chem. Eur. J.*, **20**, 10431 (2014).
[11] D. Hudry, J.-C. Griveau, C. Apostolidis, O. Walter, E. Colineau, G. Rasmussen, D. Wang, V. S. K. Chakravadhaluna, E. Courtois, C. Kübel, D. Meyer, *Nano Research*, **7**, 119, (2014).
[12] R. Jovani-Abril, M. Gibilaro, A. Janßen, R. Eloirdi, J. Somers, J. Spino, R. Malmbeck, *J. Mater. Sci.*, **477**, 298 (2016).
[13] V. Tyrpekl, J.F. Vigier, D. Manara, T. Wiss, O. Dieste Blanco, J. Somers, *J. Nucl. Mater.*, **460**, 200 (2015).

# The Actinide User Laboratory: JRC Open Access in Karlsruhe

**Eric Colineau, Roberto Caciuffo**

*European Commission, Joint Research Centre (JRC), Directorate for Nuclear Safety and Security, Postfach 2340, D-76125 Karlsruhe, Germany, e-mail: JRC-ACTUSLAB-KARLSRUHE@ec.europa.eu*

Safety precautions at Universities in Europe have almost excluded the possibility of working beyond uranium in the periodic table. Only a few facilities are available worldwide where actinide materials can be safely investigated. Among these, a prominent position is occupied by the laboratories operated by the Joint Research Centre (JRC) of the European Commission. With JRC's unique facilities being opened [1] to the academic community on the basis of peer-reviewed proposals, Europe's researchers can still be at the cutting edge of this vital field.

The "Actinide User Laboratory" (ActUsLab) is a pioneer User Access to Research Infrastructures program, that delivered over 1400 Access Units (Operating Days) to more than 160 Users from Member States since 2002, a considerable amount when considering the limited size of the PAMEC (Properties of Actinide Materials under Extreme Conditions) laboratory. Recently, the FMR (Fuels and Materials Research) laboratory officially joined the ActUsLab program. Some examples of facilities are shown in Fig.1.

PAMEC [2] is an ensemble of state-of-the-art installations designed for basic research on behaviour and properties of actinide materials under extreme conditions of temperature, pressure, external magnetic field and chemical environment. The PAMEC Laboratory includes sample preparation (arc-melting, metal flux, furnace, sputter deposition, solution chemistry), sample characterization (powder and single crystal X-ray diffraction), surface science (film deposition, photoelectron spectroscopies, LEED, HREELS, TPD), physical properties measurements (SQUID magnetometry, specific heat, Seebeck effect, electrical resistivity, magic-angle-spinning nuclear magnetic resonance, Mössbauer spectroscopy). By exploring materials properties in a wide range of temperature, pressure, and magnetic field, studies performed at the JRC are helping in bringing the actinide knowledge to a "material-by-design" level.

FMR [3] provides the scientific basis for the objective assessment and modelling of the safety related behaviour of nuclear materials, with emphasis on nuclear fuels, under normal and off-normal operating conditions. The main activities covered by the FMR laboratory involve the synthesis and characterisation of actinide-containing materials (including plutonium and minor actinides). Standard and advanced techniques for sample synthesis, materials characterization and property determination are employed. These include sol-gel precipitation, powder blending and pressing, conventional or spark plasma sintering, encapsulation techniques, X-ray diffraction, vibrational spectroscopy (Raman and infra-red), electron microscopy (scanning and transmission) and focused ion beam, drop and differential scanning calorimetry, Knudsen cell effusion mass spectrometry, electro-motive force analysis, dilatometry, indentation, laser flash methods for the measurement of thermal properties, laser melting, etc.

The JRC team is made up of multi-lingual scientists from several EU countries, with a diverse range of expertise, including chemistry, physics and actinide science. The team is comprised of specialists in a number of different techniques, and is therefore able to provide a multi-disciplinary approach to support research and development studies in the fields of actinide science.

The JRC offers access to its nuclear facilities to researchers and scientists from EU Member States, candidate countries (on the conditions established in the relevant agreement or decision) and countries associated to the Euratom Research Programme.

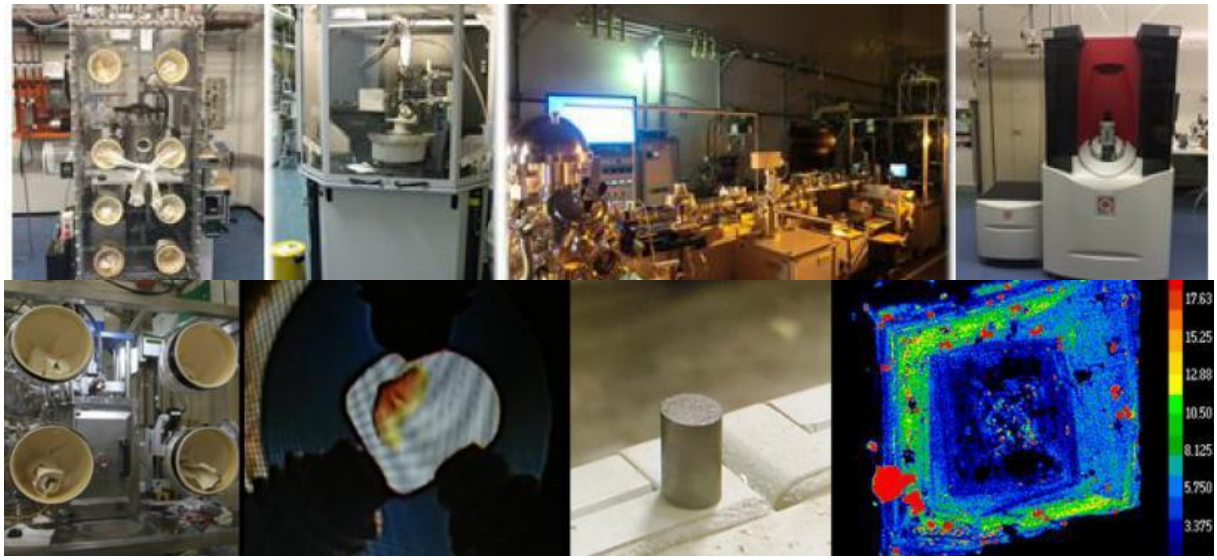


Fig. 1. Examples of PAMEC (upper panel) and FMR (lower panel) facilities at JRC-Karlsruhe.

## Acknowledgements

We are grateful to Krisztina Varga for her crucial administrative support to the programme and to the staff of PAMEC and FMR for their instrumental scientific and technical support to Users. We also thank the support Units of JRC-Karlsruhe for making the access possible (security and medical clearances, radioprotection training…).

## References

[1] https://ec.europa.eu/jrc/en/research-facility/open-access
[2] https://ec.europa.eu/jrc/en/research-facility/properties-actinide-materials-under-extreme-conditions-pamec-laboratory
[2] https://ec.europa.eu/jrc/en/research-facility/fuel-and-materials-research-fmr-laboratory

# $YbPd_2In$: a promising metallic material for adiabatic demagnetization cooling

**Mauro Giovannini[1], Federica Gastaldo[1], Andrea Džubinska[2], Marian Reiffers[3], Slavo Gabani[4], Gabriel Pristas[4], Ivan Čurlik[3], J.G. Sereni[5]**

[1] *Dept. of Chemistry, University of Genova, Via Dodecaneso 31, I-16146 Genoa, Italy*
[2] *Faculty of Natural Sciences, P. J. Šafárik University, SK-040 01 Košice, Slovakia*
[3] *Faculty of Humanities and Natural Sciences, Prešov University, SK-081 16 Prešov, Slovakia*
[4] *Slovak Academy of Sciences, Košice, Institute of Experimental Physics, Slovakia*
[5] *Low Temperature Division, CAB-CNEA, 8400 San Carlos de Bariloche, Argentina*

Today there is a critical shortage of $^3$He due to an increasing demand and to a reduced supply [1]. Therefore it is necessary to find good alternatives to the use of this isotope. Since for cooling below 1 K $^3$He is currently used, this crisis affects also solid state physicists. Refrigeration by adiabatic demagnetization of paramagnetic salts is a $^3$He-free alternative method to reach temperatures significantly below 1 K. However, the utilization of these insulating materials as refrigerants suffers from substantial drawbacks such as poor thermal conductance which makes it difficult to achieve thermal equilibrium within the salt and deterioration of the salt due to dehydration [2]. For this reason, very recently metallic compounds have been proposed as good alternative materials to paramagnetic salts in adiabatic demagnetization [3,4].

In this work we report experimental results on crystal structure, magnetic, thermodynamic and transport properties of the new cubic Heusler indide $YbPd_2In$. From the fitting of the magnetic susceptibility a stable trivalent $Yb^{3+}$ ($\mu_{eff}$= 4.5 $\mu_B$) state is deduced [5]. The compound is characterized by very weak magnetic interactions and by the absence of a significant Kondo effect as suggested by the very low value of $\theta_p$ = -9 K and the thermal dependence of the resistivity [5]. At low temperatures, for temperature decreasing, the magnetic specific heat divided by temperature $C_m/T$ first increases steeply with a $\sim 1/T^2$ dependence within more than one decade of temperature, and then a maximum occurs at around $T_m$ = 250 mK reaching the record value of about 30 J/mol K$^2$. This anomaly is shifted to lower temperatures by applying a magnetic field, and it becomes sharper indicating a gradual switch from second order to first order transition. The resulting associated thermomagnetic effect, which drastically shifts the entropy to higher temperatures by the application of magnetic field, makes $YbPd_2In$ a promising candidate for adiabatic demagnetization cooling.

## References

[1] R.T. Kouzes, J.H. Ely, "Status summary of $^3$He and neutron detection alternatives for homeland security" (Report PNNL-19360, Pacific Northwest National Laboratory, 2010).
[2] "Matter and Methods at Low Temperatures" by Frank Pobell, Springer –Verlag (1991).
[3] D. Jang at al. Nature Comm. **6**, 8680 (2015).
[4] Y. Tokiwa et al. Sci. Adv. **2**, e1600835 (2016).
[5] F. Gastaldo et al. arXiv:1711.02335v1 (2017).

# Development of In-situ Remote Dismantling System For Reactor Vessel (RV) in Nuclear Power Plant

**Kwang-soo Park, Hae-woong Kim, Hee-dong Sohn, Han-sol Im, Chang-sig Kong**

*Doosan Heavy Industries & Construction, 22 Doosan-Volvo-ro Seongsan-gu, 51711 Changwon, republic of Korea, kwangsoo.park@doosan.com*

Kori unit 1 nuclear power plant (NPP) was permanently shut down in 2017. The activated Reactor Vessel (RV) in reactor cavity will be planned to be dismantled after 2023. Kori unit 1 is the first NPP which will be dismantled in Korea. So, to prepare for the decommissioning market, we need to develop the dismantling technology. This study is one of the fields that Doosan is carrying out as in-situ remote dismantling system for RV in Kori unit 1.

In order to develop the dismantling system, we review the several scenarios after that scenario using a thermal cutting method was selected. On the basis of the scenario, we develop the customized thermal cutting head. The reason why the cutting head was developed, the maximum thickness of the reactor to be cut is 480 mm and there are restrictions on the working space. Also cutting test was performed to find the conditions for cutting thickness of 480mm.

The developed Kori unit 1 RV dismantling scenario is basically to cut by raising the RV in the air environment using the thermal cutting method. This method is a proven technology [1]. Based on the dismantling scenario, we have developed a device for using in actual dismantling work. The device is in-situ remote dismantling system. This system consists of ventilation equipment & tent, gantry type manipulator & robot and rail. Also the robot has thermal cutting head. The reason why gantry type manipulator was developed, the bottom head also will be cut and segmented for disposal.

Table. 1. The result of thermal cutting test

| Items | 300 T | 500 T |
|---|---|---|
| Horizontal Cutting Speed (mm/min) | 170 – 230 | 50 – 100 |
| Vertical Cutting Speed (mm/min) | 100 – 130 | 30 – 60 |

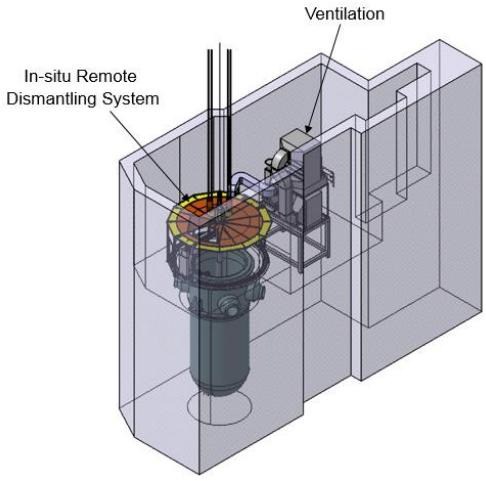


Fig. 1. The In-situ Remote Dismantling System

## References

[1] Stefan Datig, "Experience in the Decommissioning of the ZION Nuclear Power Plant in the USA, ICOND, (2018).

## Acknowledgement

This research was supported by a grant from Energy Technology Development Program Funded by Ministry of Trade, Industry and Energy of Korean Government

# Crystal structure, magnetism and electrical resistivity of the $\beta$-$UH_3$ and *fcc* $UH_2$ thin films

**E. A. Tereshina-Chitrova,[1,2] L. Havela[1], M. Paukov[1], L. Horak[1], M. Dopita[1], T. Gouder[3], A. Seibert[3], F. Huber[3]**

[1]*Faculty of Mathematics and Physics, Charles University, 12116 Prague, Czech Republic*
[2]*Institute of Physics, Czech Academy of Sciences, 18121 Prague, Czech Republic, e-mail: teresh@fzu.cz*
[3]*European Commission, Joint Research Centre (JRC), Postfach 2340, DE-76125 Karlsruhe, Germany*

Uranium trihydride, $UH_3$, was the first observed ferromagnet purely on the basis of an actinide element. Recently, a new type of uranium binary hydride, $UH_2$, with the $CaF_2$ crystal structure, was synthesized in a thin-film form [1]. In this work, we conducted a study of the crystal structure, magnetic and related electronic properties of the uranium hydrides thin film samples prepared by reactive sputter deposition. The films were obtained at temperatures from -170 to +30 $^{o}$C using various substrates. The basic in situ diagnostics was performed using photoelectron spectroscopy (XPS) with a monochromated Al–$K_\alpha$ radiation and SPECS PHOIBOS 150 MCD-9 electron energy analyzer. The crystal structure was studied by X-ray diffraction on a Rigaku SmartLab diffractometer equipped with 9 kW cooper rotating anode X-ray source (CuK$\alpha$ radiation $\lambda$= 0.15418 nm), using the parallel beam geometry with incidence angle of the primary beam $\omega$= 1.5°. Temperature and field dependencies of magnetization were measured using a PPMS installation (Quantum Design, USA) equipped with a Vibrating Sample Magnetometer. Resistivity was measured using a van der Pauw technique on a PPMS installation.

We successfully prepared uranium hydride films of two different types, either β-$UH_3$ or $UH_2$. Among all variable parameters, the ion current value seems to be responsible for formation of individual species. For smaller currents, $UH_3$ was typically formed, while $UH_2$ was formed for higher currents, i.e. higher deposition rates, for nearly constant partial pressure of $H_2$ in the sputter gas. In both cases a transition metal (*T* = Mo) can be embedded in the hydride, similar to bulk hydrides formed from U-*T* alloys.

Magnetization study showed that $UH_2$ and β-$UH_3$ (with Mo) are ferromagnets with the Curie temperature $T_C \approx$ 120 K and 165 K, respectively. The samples exhibited very wide magnetic hysteresis loops at low temperatures, which indicated strong magnetocrystalline anisotropy of the hydride films. Besides magnetization, we studied also the temperature dependence of electrical resistivity. Fig. 1 shows one example, a $U_{0.74}Mo_{0.26}$-H film deposited on fused silica substrate at room temperature, with the β-$UH_3$ structure, lattice parameter $a$ = 0.6703 ± 0.0004 nm, which is somewhat higher

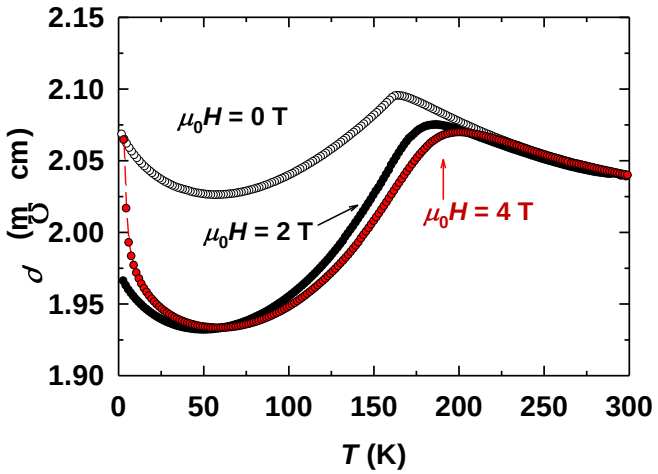


Fig. 1. Temperature dependencies of electrical resistivity of the $U_{0.74}Mo_{0.26}$-H film (β-$UH_3$) measured by van der Pauw method in various fields applied along the sample surface.

than the bulk value $a$ = 0.6644 nm. $\rho(T)$ exhibits a pronounced cusp at $T_C$, interrupting the net negative resistivity slope, attributed to fluctuating magnetic moments in the paramagnetic state and static disordered moments in the ordered state, which can be affected, however, by magnetic field. Similarity with the bulk material with lower Mo concentration [2] indicated that Mo can be randomly distributed in the hydride films, as well, and that $T_C$ decreases after reaching a maximum over 200 K for 15% Mo.

$UH_2$ obtained using Si substrates was found to have the lattice parameter $a$ = 0.5359 ± 0.0001 nm, i.e. close to that in known Np (0.5343 nm) and Pu (0.5359 nm) iso-types. The grains size in the $UH_2$ film is 50-100 nm. Fig. 2 shows the temperature dependence of resistivity of the $UH_2$-type film. The cusp at $T_C$ divides resistivity into the paramagnetic and ferromagnetic part, both with a negative slope in zero magnetic field. While the paramagnetic resistivities are practically field-independent, the negative slope in the ordered state can be removed by magnetic field, indicating that the static disordered moments below $T_C$ can be aligned by magnetic field.

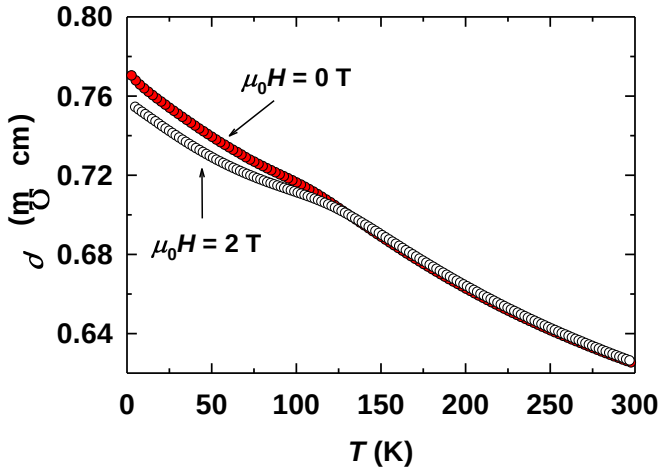


Fig. 2. Temperature dependencies of electrical resistivity of the $UH_2$-type film (Mo/$UH_2$/Mo) measured by van der Pauw method in 0 and 2 T field applied along the sample surface.

Finally, at low temperatures, -170 °C, the hydride layers $(UH_3)_{0.62}Mo_{0.38}$ with the mean crystallite size of 1.5 nm were grown. The crystal structure study showed that its properties are similar to the bulk splat $(UH_3)_{0.85}Mo_{0.15}$ [2]. The sample has a stress-free lattice parameter $a$ = 0.6725 ± 0.0008 nm. The Curie temperature of the $(UH_3)_{0.62}Mo_{0.38}$ thin film determined from the temperature dependence of magnetization is ≈ 145 K. Lower $T_C$ of $(UH_3)_{0.62}Mo_{0.38}$ as compared to β-$UH_3$ with Mo shown above (composition $U_{0.74}Mo_{0.26}$-H) is due to the higher content of Mo in the former sample.

*This work was supported by the Czech Science Foundation under the grant No. 18-02344S. The work at JRC Karlsruhe was supported by the Actuslab project under contract with the European Commission. Part of the work was supported by the project "Nanomaterials centre for advanced applications", project No. CZ.02.1.01/0.0/0.0/15_003/0000485, financed by ERDF.*

## References

[1] L. Havela *et al.*, *Inorganic Chem.*, **57 (23)** 14727 (2018).
[2] I. Tkach *et al.*, *Phys. Rev. B* **88**, 060407(R) (2013).

# Study of uranium oxides fluorination using aqueous hydrofluoric acid in ionic liquid [Emim][$NTf_2$]

**Florian Joly[1], Mehdi Arab[3], Bertrand Morel[3], Christophe Volkringer[1,2]**

[1] *UCCS UMR 8181, Cité Scientifique, 59655, Villeneuve d'Ascq, FRANCE e-mail: florian.joly@univ-lille.fr, christophe.volkringer@univ-lille.fr*
[2] *Institut universitaire de France, 75005 Paris, FRANCE*
[3] *Orano, Place Jean Millier, 92400 Courbevoie, FRANCE*

Ionic liquids have met an increasing interest over the last twenty years. These salts which have a melting point below 100°C are often presented as alternative for classical solvents because of their low vapor pressure and adaptable properties through the cation and anion choice.

Use of ionic liquid in the field of uranium fuel cycle has been studied mainly for liquid/liquid extractions and electrodeposition. To the best of our knowledge, only two works have reported the synthesis of uranium fluorides using ionic liquids: one from $UF_5$ [1], the other from uranium oxides ($UO_2$ or $UO_3$) [2]. Both used an uncommon ionic liquid [Emim][$F(HF)_{2.3}$] whose anion stabilizes hydrofluoric acid by exchange between its two forms. However, synthesis of this ionic liquid requires the use of anhydrous HF which is highly corrosive and not commonly found in laboratories.

Our work deals with preparation of uranium fluoride from a solution of 48% aqueous hydrofluoric acid combined with a commercially available ionic liquid [Emim][$NTf_2$]. $UO_2$ and $UO_3$ were used as uranium sources to study the influence of uranium oxidation state on the synthesis.

Our results show that in the absence of other reactant, no transformation of the initial oxide is observed, even after several days. To solubilize uranium in the ionic liquid and improve reactivity toward hydrofluoric acid, we studied the addition of three molecules (H2O, HNO3, HCOOH).

Using nitric acid, we found that uranium dissolution in the ionic liquid was dependent on the $HNO_3$/U ratio. However, all ratio lead to the precipitation of a predominant unknown phase in mixture with $UF_4.2H_2O$ and unreacted $UO_2$.With water, solubility of uranium was only observed in the aqueous phase where both oxidation state of uranium (IV and VI) could be observed by UV-visible spectroscopy. These samples also lead to the precipitation of $UF_4.2H_2O$ in mixture with unreacted $UO_2$ and an unknown phase. Similar results were obtained with formic acid: uranium is found in the aqueous phase as U(VI) , but never in the ionic liquid.

This presentation will detail the results obtained with the three different complexing molecules using PXRD, UV-visible spectroscopy and ICP-OES measurement. A mechanism for the formation of uranium fluoride in the ionic liquid will be also proposed.

## References

[1] T. Kanatani et al., *Chemistry Letters* **38**, *714* (2009).
[2] C.A. Zarzana et al., *Journal of the American Society for Mass Spectrometry* **29**, *1963* (2018).
[3] I. Billard et al., *Dalton Transactions* **2**, *4214* (2007).

# Single Crystal X-ray Structure Analysis of $UNi_4B$

**Chihiro Tabata,[1] Hajime Sagayama[2,3], Hiraku Saito[4], Hironori Nakao[2,3], and Hiroshi Amitsuka[5]**

[1]*Institute for Integrated Radiation and Nuclear Science, Kyoto University, Kumatori 590-0494, Japan, e-mail: tabata.chihiro.3z@kyoto-u.ac.jp*
[2]*Photon Factory, Institute of Materials Structure Science, KEK, Tsukuba 305-0801, Japan*
[3]*Condensed Matter Research Center, Institute of Materials Structure Science, KEK, Tsukuba 305-0801, Japan*
[4]*KENS, Institute of Materials Structure Science, KEK, Tokai 319-1106, Japan*
[5]*Graduate School of Science, Hokkaido University, Sapporo 060-0810, Japan*

The phenomena that magnetism couples with ferroelctricity, which is called the magnetoelectric (ME) effect, has been attracting much interest in condensed matter physics. A recent theoretical study proposes that the ME effect can arise not only in insulating materials but also in metals where the magnetic moments order in vortex-like arrangements, referred to as toroidal order [1]. $UNi_4B$ is the first example of toroidal ordering metal that is confirmed experimentally to exhibit magnetization induced by electric current [2]. Still, the observed direction dependence of current-induced magnetization is not fully understood by the proposed theory. One of problems that hinder understanding of this phenomenon is an existence of two controversial reports of the crystal structure of this compound: the hexagonal (*P*6/*mmm*) [3] and orthorhombic (*Cmcm*) [4] structures. This motivated us to perform the crystal structure analysis using a high-energy synchrotron X-ray.

The X-ray diffraction of single crystalline $UNi_4B$ was measured at the beamline PF-AR NE1A in Photon Factory. The obtained diffraction patterns strongly suggest the orthorhombic unit cell, whose lattice constants are: $a$ = 6.922(4) Å, $b$ = 14.773 (2) Å, $c$ = 17.04 (1) Å, which is the same as the structure of *Cmcm* in the literature [4]. The observed reflection conditions indicate possible space groups as follows: *Cmcm* ($D_{2h}^{17}$, no. 63), *Cmc*2$_1$ ($C_{2v}^{12}$, no. 36), and *C*2*cm* ($C_{2v}^{16}$, no. 40). The direct method and the least-squares refinement give very similar structures for each of these space groups, which have distorted triangular lattices formed by U atoms, without local inversion symmetry at each U site (see Fig. 1). Although the differences of reliability factors (*R*-factors) of the refinements among these space groups are no more than 0.5 %, *Cmcm* is suggested as the most likely space group with the fewest refined parameters and the lowest *R*-factor. Nevertheless, the refined crystal structure, not only of *Cmcm* but also of the other two space groups, cannot explain the magnetization induced by electric current along the [100] direction. The crystal structure below $T_N$ = 20 K should be closely examined as well.

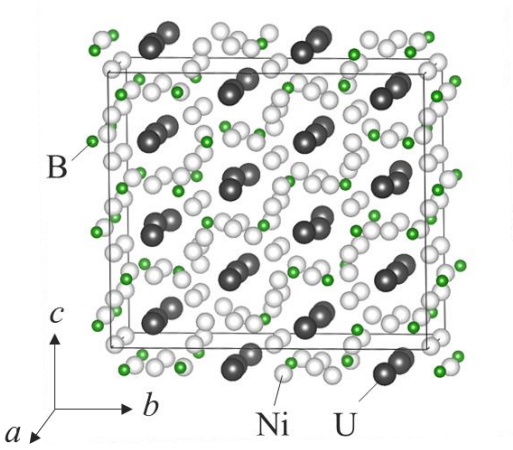


Fig. 1. Crystal structure of $UNi_4B$ suggested by the least-squares refinement, assuming the space group of *Cmcm*.

## References

[1] S. Hayami, H. Kusunose, and Y. Motome, Phys. Rev. B **90**, 024432 (2014). [2] H. Saito *et al.*, J. Phys. Soc. Jpn. **87**, 033702 (2018). [3] S. A. M. Mentink *et al.*, Physica B **186-188**, 270 (1993). [4] Y. Haga, *et al*., Physica B **403**, 900 (2008).

# Large enhancement of the electron mass in the U-Ti hydrides

**Volodymyr Buturlim[1], Ladislav Havela[1], Oleksandra Koloskova[1], Daria Drozdenko[1], Milan Dopita[1], Peter Minarik[1], Silvie Mašková[1], Michal Falkowski[1]**

*[1]Charles University, Faculty of Mathematics and Physics, Ke Karlovu 5, 12116 Prague, Czech Republic, email: buturlim@mag.mff.cuni.cz*

Interaction of different metals with hydrogen very often leads to a pronounced lattice expansion. Such negative chemical pressure is an efficient way in which the 5*f* states localization in actinides can be tuned, as real hydrogen bonding effects may be secondary.
Uranium has a low corrosion resistance against hydrogen atmosphere. $\alpha$-U interacts with hydrogen even at $H_2$ pressures in the millibar range. Pressures need to hydrogenate *bcc* U-T alloys are much higher, typically $p \geq 4$ bar (T- transition metal). Crystal structure of the obtained hydrides depends on T. U-Mo alloying leads to formation of nano-crystalline $\beta$-$UH_3$ hydride, while Zr stabilizes the $\alpha$-$UH_3$ phase. Alloying with Ti is still different. Hydrogenation of the *bcc*-U-Ti alloys at room temperature results in a mixture of the nano-crystalline $\beta$-$UH_3$ and $\alpha$-$UH_3$. On the other hand, at high temperatures (973 K) hydrogen stabilizes a hydride which has the cubic Laves phase structure, yielding $UTi_2H_x$.
Such Uranium hydrides have diverse ground state properties. β-$UH_3$ is the first discovered U ferromagnet with $T_C \approx 165$ K. T doping does not lead to significant changes of the magnetic properties. $T_C$ can increase, e.g $(UH_3)_{0.87}Mo_{0.13}$ reaches 203 K[1]. It can be perhaps related to the fact that the shortest U-U links in the hydride are disrupted due to presence of Mo, therefore it develops an isolation of the U atoms in the *6c* positions supporting ferromagnetism [2].
$(UH_3)_{1-x}Ti_x$ hydrides reach $T_C = 192$ K. Magnetic properties of α-$UH_3$ are similar to β-$UH_3$.
Approx. 60% volume expansion not only induces magnetism out of weakly paramagnetic U and its alloys. The 5*f* band narrowing affects also the Sommerfeld coefficient $\gamma$ of electronic specific heat. $\gamma \approx 10$ mJ/mol $K^2$ is more than trippled in the hydrides. Nano-crystalline $\beta$-$UH_3$ hydrides with Mo and Ti present similar increase to approx. 30 mJ/mol $K^2$.
The hydrides with the cubic Laves phase structure behave differently. We synthesized two different types, $UTi_2H_6$ is ferromagnet wtth $T_C = 54$ K, $UTi_2H_5$ is just at the verge of magnetic order. In such regime, non-Fermi liquid behavior can be expected. Indeed, it can be classified as mid-weight heavy fermion system. $C_p/T$ vs $T$ exhibits a pronounced increase. Below $T$ = 10 K it can be fitted with a weakly interacting spin fluctuation term ($f(T) = a\ T^{1/2}$) added to $C_p/T = \gamma + \beta T^2$. We obtain $\gamma = 256$ mJ/mol $K^2$ [3]. Such materials have a strong resemblance to spin fluctuator $UAl_2$ [4], however $\gamma$ is even higher. The fingerprint of spin fluctuations was found also in all transport studies (electrical resistivity, heat conductivity, Seebeck effect), which could be studied due to the monolithic form of the hydride obtained. Unfortunately $UTi_2H_6$ is a fine powder and such studies were not possible.
Increase of the Ti concentration leads to further increase of the Sommerfeld coefficient, for the hydride with 80 at. % of Ti $\gamma$=345.2 mJ/mol U $K^2$. In contrast to $U_{0.34}Ti_{0.66}H_x$ the $C_p/T$ of $U_{0.20}Ti_{0.80}H_x$ is better described by the non-interacting spin fluctuation term ($f(T)=T^2\ ln\ T$). The hydrides also demonstrate different field response of $C_p$. The anomaly is easier suppressed for the hydride with higher Ti concentration, it supports the idea that U-U interaction becomes weaker. In many Laves compounds partial substitution of one of the elements is possible, in other words, it can be either $A_xB'_{1-x}B_2$ or $A(B_xA'_{x-1})_2$. $UFe_2$, for instance, shows variations of the stoichiometry composition which subsequently lead to the change of the Curie temperature[5]. Therefore, the scenario where Ti substitute U atoms looks

quite realistic. Regarding to the atomic sizes, U and Ti do not differ very much, $r_U/r_{Ti}$=1.06. The value lies on the verge of values observed for the existing Laves phases (in the general formula $AB_2$ the $r_A/r_B$ ranges between 1.05 and 1.70). It explains the reason why the interstitial hydrogen atoms are required for the stabilization of the structure (the phase diagram of the U-Ti system does not have $UTi_2$). The atomic disorder influences the transport properties.
Detailed analysis of the physical properties will be presented.

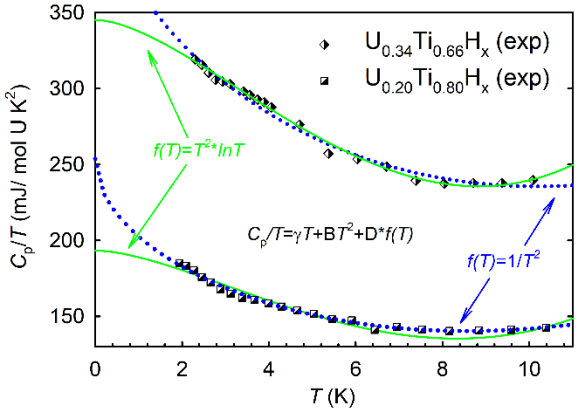


Fig. 1. Comparison of the $C_p/T$ vs $T$ data for the U-Ti hydrides with the Laves phase structure. The dotted line corresponds to the fit performed with the non-interacting spin fluctuation term ($f(T)=T^2\ ln\ T$), while the solid line represents the weakly interacting spin fluctuation term ($f(T)=T^{1/2}$)

*This work was supported by the Czech Science Foundation under the grant No. 18-02344S.*

## References

[1] L. Havela, I. Tkach, M. Paukov, Z. Matej, D. Drozdenko, A. V. Andreev, N.-T.H. Kim-Ngan, Structure and properties of hydrides of γ-U alloys, *J. Alloys Compd.* **645** 190 (2015).
[2] M. Paukov, L. Havela, N.-T.H. Kim-Ngan, V. Buturlim, I. Tkach, D. Drozdenko, S. Mašková, S. Sowa, Z. Molcanova, M. Mihalik, M. Krupska, Variations of magnetic properties of $UH_3$ with modified structure and composition, *J. Sci. Adv. Mater. Devices.* **1** 185 (2016).
[3] G.R. Stewart, Non-fermi-liquid behavior in d-and f-electron metals, *Rev. Mod. Phys.* **4** 7379 (2001).
[4] R.J. Trainor, M.B. Brodsky, H. V. Culbert, Specific Heat of the Spin-Fluctuation System $UAl_2$, *Phys. Rev. Lett.* **34** 1019 (1975).
[5] A.P. Gonçalves, M.S. Henriques, J.C. Waerenborgh, L.C.J. Pereira, E.B. Lopes, M. Almeida, S. Mašková, L. Havela, A. Shick, Z. Arnold, D. Berthebaud, O. Tougait, H. Noël, Peculiarities of U-based Laves phases, IOP Conf. *Ser. Mater. Sci. Eng*. **9** 012090 (2010).

# Novel phase and phase equilibria at 1000 K in the U-Ag-Ge ternary system

**Stéphanie Fryars, Francis Gouttefangeas, Thierry Guizouarn, Mathieu Pasturel**

*Univ Rennes, CNRS, ISCR - UMR6226, ScanMAT – UMS2001, 35042 Rennes, France*
*e-mail: stephanie.fryars@univ-rennes1.fr*

Investigating binary and ternary uranium germanium systems is a wide playground to discover new compounds with unusual physicochemical behaviour. Among their most intriguing properties, the coexistence of ferromagnetic ordering and superconductivity in $UGe_2$ [1], URhGe [2] and UCoGe [3] rises many questions about its nature.

In the course of our investigation of ternary U-T-Ge (T = transition metal) phase diagrams to discover new phases with unusual properties, we underwent the screening of the U-Ag-Ge isothermal section at 1000 K. Due to the miscibility gap in the liquid state within the U-Ag binary system, the sample syntheses sound difficult. However, we show that the addition of germanium strongly help to overpass this problem.

Our work evidences the formation of a new phase, namely $U_3Ag_{1-y}Ge_{4+y}$, of tetragonal $U_3Al_{2-x}Ge_{3+x}$ [4,5] structure-type [space group I4/mcm (140), cell parameters: a = 7.725(1) Å, *c* = 11.104(1) Å] where U-atoms occupy *4a* and *8h* Wyckoff positions, Ge a *16l* one and a mixture of Ag and Ge the *4c* one. To the best of our knowledge, this germanide is the second ternary phase, after $UAgSb_2$ [6], reported based on uranium and silver.

The scanning electron microscopy coupled to energy dispersive spectroscopy (SEM-EDS) analyses on a sample with 3U-1Ag-4Ge starting composition show the presence of $U_3Ag_{0.3}Ge_{4.7}$ as majority phase and UGe and Ag as impurities. X-ray diffraction (XRD) analysis on this sample confirms the presence of $U_3Ag_{0.3}Ge_{4.7}$ with Ag (~ 10%), UGe (~ 30%) and additional $UGe_2$ (~ 10%).

However, preliminary magnetic measurements on this composition show 4 transitions:

- a very tiny one around 90 K may be attributed to undetected $UGe_{1.57}$;
- a sharper one at about 50 K comes from $UGe_2$;
- we attribute the main 18 K one to $U_3Ag_{0.3}Ge_{4.7}$ as long as this temperature is close to the Curie temperature of the Ge-richest border of the $U_3Al_{2-x}Ge_{3+x}$ solid solution [5];
- the fourth transition at about 130 K is more difficult to assign. It could be related to a structural transition.

Regarding phase equilibria, the U-Ag-Ge isothermal section mainly shows equilibrium lines running from the U-Ge binary axis towards Ag corner. Differential thermal analyses show phase transformations at around 600°C in a large area of the section.

The crystallographic details of the new germanide as well as the phase equilibria, determined by means of SEM-EDS and powder XRD will be presented together with preliminary results of magnetic, electrical and specific heat measurements on the new phase.

## References

[1] S. S. Saxena *et al., Nature* **406**, 587 (2000).
[2] D. Aoki *et al., Nature* **413**, 613 (2001).
[3] N. T. Huy *et al., Phys. Rev. Lett.* **99**, 067006 (2007).
[4] F. Weitzer *et al., J. Solid State Chem.*, **111**, 267 (1994).
[5] C. Moussa *et al., J. Solid State Chem*. **243**, 168 (2016).
[6] M. Brylak *et al., J. Solid State Chem*. **115**, 305 (1995).

# Hardness and damage of the U-Fe-Ge alloy sphere under explosive loading

**D.A. Belyaev, A.S. Aleksandrov. Yu.N. Zuev, E.A. Kozlov, S.A. Lekomtsev, A.S. Nedosviti, I.L. Svyatov, E.A. Levi**

*Russian Federal Nuclear Center- Zababakhin All-Russia Research Institute of Technical Physics, Snezhinsk, Chelyabinsk region, 456770, Russia, e-mail: bad1331@gmail.com*

The paper presents the metallography analysis results for the structural state of the three-phase U-Fe-Ge alloy sphere (Figure 1) recovered under the symmetrical explosive loading by converging shock waves (Figure 2). The sphere initial geometry and the loading conditions are identical to that of the unalloyed plutonium sphere studied in [1]. The analysis was carried out using light microscopy and scanning electron microscopy, microhardness testing combined with digital mapping of the observed physical magnitudes [2].

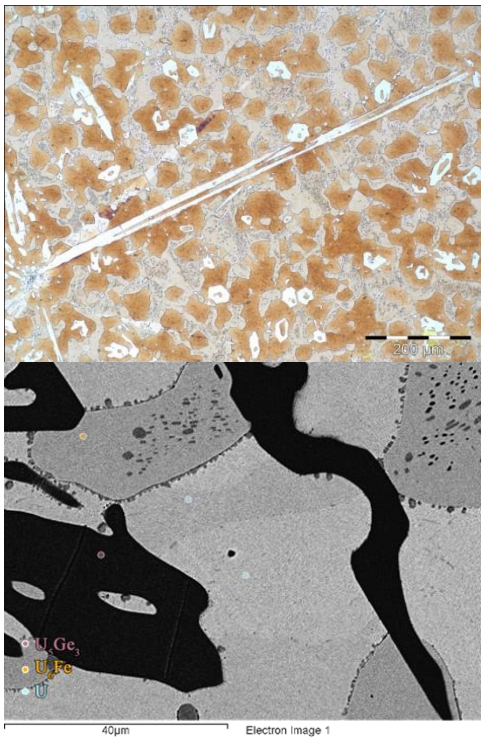


Fig. 1. Three-phase microstructure of the alloy U-Fe-Ge

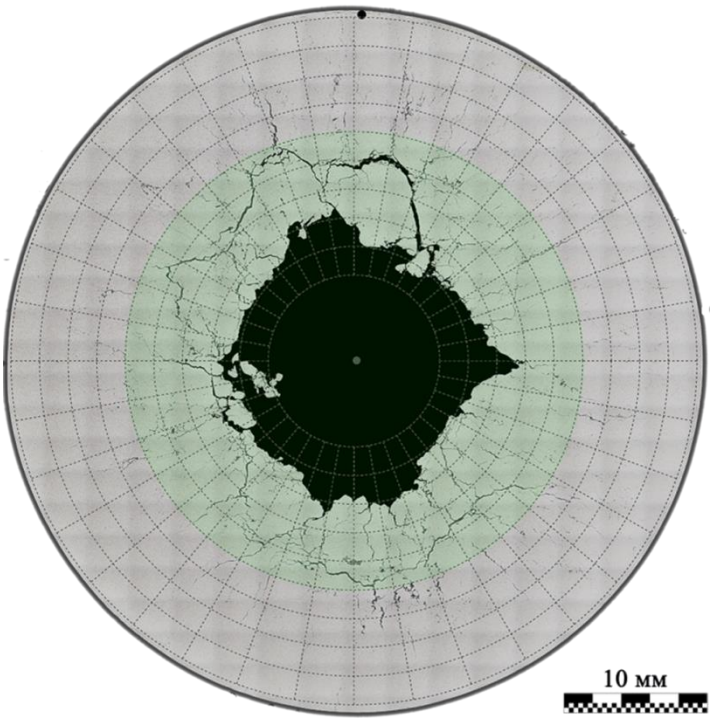


Fig. 2. Damage in the meridional section of the sphere due to the explosive loading

Statistic and spatial distributions of damage, microhardness and hardness in the meridional section of the sphere, as well as changes in the microstructructural state were obtained and analyzed. The material fracture behavior was determined and the pattern of its localization along the radius was identified.

## References

[1] Kozlov E.A., B.V. Litvinov, L.V. Timofeeva. *Structural and phase transformations, spall and shear fractures in the sphere of unalloyed plutonium under explosive loading.* Litvinov B.V. Selected works. — (2014). http://elib.biblioatom.ru

[2] D.A. Belyaev, Yu.N. Zuev, A.V. Lukin, I.L. Svyatov. *Application of the colour mapping technique in the metallography analysis of the samples under dynamic loading*. Industrial laboratory. Material diagnostics**.** #6, **V. 82,** P. 40-43 (2016).

# Low-Temperature Electronic and Magnetic Properties of $UIr_2Ge_2$ Single Crystal

**Yusuke Suzuki[1], Fusako Kon,[1] Akinari Koriki[1], Masataka Yamamoto[1], Ryoya Murata[1], Hiroyuki Hidaka[1], Tatsuya Yanagisawa[1], Hiroshi Amitsuka[1], Chihiro Tabata[2], Hironori Nakao[3], Yusei Shimizu[4], Yoshiya Homma[4], Fuminori Honda[4], Li Dexin[4], Ai Nakamura[4], and Dai Aoki[4]**

*[1]Graduate School of Science, Hokkaido University, N10W8 Kita-ku, Sapporo 080-0810, Japan*
*e-mail: amiami@phys.sci.hokudai.ac.jp*
*[2]Institute for Integrated Radiation and Nuclear Science, Kyoto University, 2 Asashiro-Nishi, Kumatori, Sennan-gun, Osaka 590-0494, Japan*
*[3]IMSS CMRC, KEK, 1-1 Oho, Tsukuba, Ibaraki 305-0801, Japan,*
*[4]International Research Center for Nuclear Materials Science, IMR Tohoku University, 2145-2, Narita-cho, Oarai, Ibaraki 311-1313, Japan*

We have grown a $UIr_2Ge_2$ single crystal using Czochralski method with a tetra-arc furnace, and investigated physical properties by performing electrical resistivity, specific heat and magnetization measurements in the temperature range from 2 K to 300 K under magnetic fields up to 14 T. The study of Lloret *et al*. (1987) showed that quenched polycrystals crystalize in the $CaBe_2Ge_2$ type tetragonal structure (No. 129, $P4/nmm$, $D_{4h}^{17}$), while it changes in orthorhombic (No. 49, $Pmmm$, $D_{2h}^{1}$) by annealing at 800 °C [1]. They also reported that the magnetic susceptibility shows a cusp anomaly at ~ 19 K for the quenched samples, while at ~ 33 K for the annealed ones. One year later, Menovsky reported the conditions and the results of a single-crystal growth of this system, where the grown crystals were found to have the $CaBe_2Ge_2$ type structure [2]. Including his article, however, no detailed studies on physical properties of single-crystalline $UIr_2Ge_2$ have been reported thus far. The single-crystalline sample grown in the present study has also been found to have the $CaBe_2Ge_2$ type tetragonal structure, which is however unchanged by annealing at 800 °C contrary to the previous reports on polycrystals [1]. We have revealed that magnetic response is strongly anisotropic with the tetragonal *c* axis as the easy direction. Magnetic susceptibility shows a sharp cusp anomaly at ~ 19 K, suggesting the occurrence of an antiferromagnetic (AF) order at this temperature. Magnetization processes for fields along the *c* direction show a metamagnetic-like nonlinear increase below this temperature, indicating the termination of the AF order. The critical field for the AF order is estimated to be ~ 4 T at 2 K, which is seemingly very weak if compared with the ordering temperature. Specific heat shows an enhancement of the electronic specific heat coefficient of ~ 98 $mJ/K^2mol$ even in the AF ordered state. Electrical resistivity shows a logarithmic increase in a wide temperature range below room temperature, suggesting the existence of Kondo effects, while the Kondo coherence behavior does not appear even when the temperature goes down to 2 K. We will discuss, in detail, the possible ground state and the relevant electronic correlations of this system.

## References

[1] B. Lloret *et al*., J. Magn. Magn. Mater. **67**, 232 (1987).
[2] A.A. Menovsky, J. Magn. Magn. Mater. **76 & 77**, 631 (1988).

# Neutronic Parameters and CPS (Control and Protection System) Worth Calculation of Thermal Research Reactor Using MCNPX code

**H. Shamoradifar [1], B. Teimuri[2], P. Parvaresh[1], S. Mohammadi[1]**

[1] *Department of Nuclear Physics, Payame Noor University, Tehran, Iran*
[2] *Nuclear Science and Technology Research Institute, Atomic Energy Organization of Iran*

## Introduction

One of the main attributes of reactor core design is finding the best distribution of the core control and protection system. Nuclear reactors have several distinct types of control and protection elements, such as control rods, shimming rods and emergency rods. Each of these elements performs a separate task in a control procedure. The distribution of these elements in the core contributes to their worth and expense, therefore finding the best location and distribution of the control protection system (CPS) elements is very important from the view point of nuclear reactor design and safety. This research presents a neutronic parameter and CPS worth calculation of heavy water research reactor using MCNP.

## 1. Control and Protection System (CPS) Related Calculations

### 1.1 Infinite Multiplication Factor

Reactor single cell multiplication factor has been studied with the help of uniform lattice configuration (single cell calculations). Reactor single cell model consists of a fuel channel plus the heavy water (D2O) coolant and moderator environment with an axial extension of 1m. The grid spacers of the fuel pin bundle are homogenized within the coolant. The gap between the fuel and the zircaloy cladding is considered.
The results of the single cell multiplication factor together with their standard deviation are summarized in table 1 .In general, calculations were done by MCNPX2.6 are statistical in nature, therefore for getting a better accuracy and precision, calculation has been repeated five times.

| Code And Cross-Section File | $K_{inf.}$ ± S.D. | $\overline{K_{inf.}}$ ± S.D. |
|---|---|---|
| MCNP + ENDF/ ENDF/B-VII | 1.16636 ± 0.00024<br>1.16639 ± 0.00023<br>1.16624 ± 0.00024<br>1.16607 ± 0.00023<br>1.16608 ± 0.00023 | 1.16623 ± 0.00010 |

## 2. Neutron Spectrum

The spectrum characteristic at the center of reactor core is illustrated in Fig. In this figure the spectrum has been normalized by the flux density in the 0 to 0.009 eV energy bin. The shape in the fast-neutron region is basically a fission spectrum at the higher energies, but degraded by scattering in the moderator as evident for energies below 2 MeV. The fast region joins the intermediate (epithermal, resonance, or 1/E) region at roughly 0.5 MeV. As indicated, the intermediate spectrum is very close to:

$$f(E)d(E) = f_0 \frac{d(E)}{E}$$

This means there is an equal flux density in each logarithmic energy interval. The quantity is proportional to the fast neutron source density and inversely proportional to the slowing-down power of the moderator. The shape of the spectrum in the thermal region is approximately Maxwellian, degrading into the 1/E tail. Because of the absorption and other effects, the spectrum is slightly harder, i.e., contains a greater proportion of higher energy neutrons, than Maxwellian at the temperature of the moderator. The hardening effect, has caused the most probable energy of the thermal neutrons to be near 0.03 eV

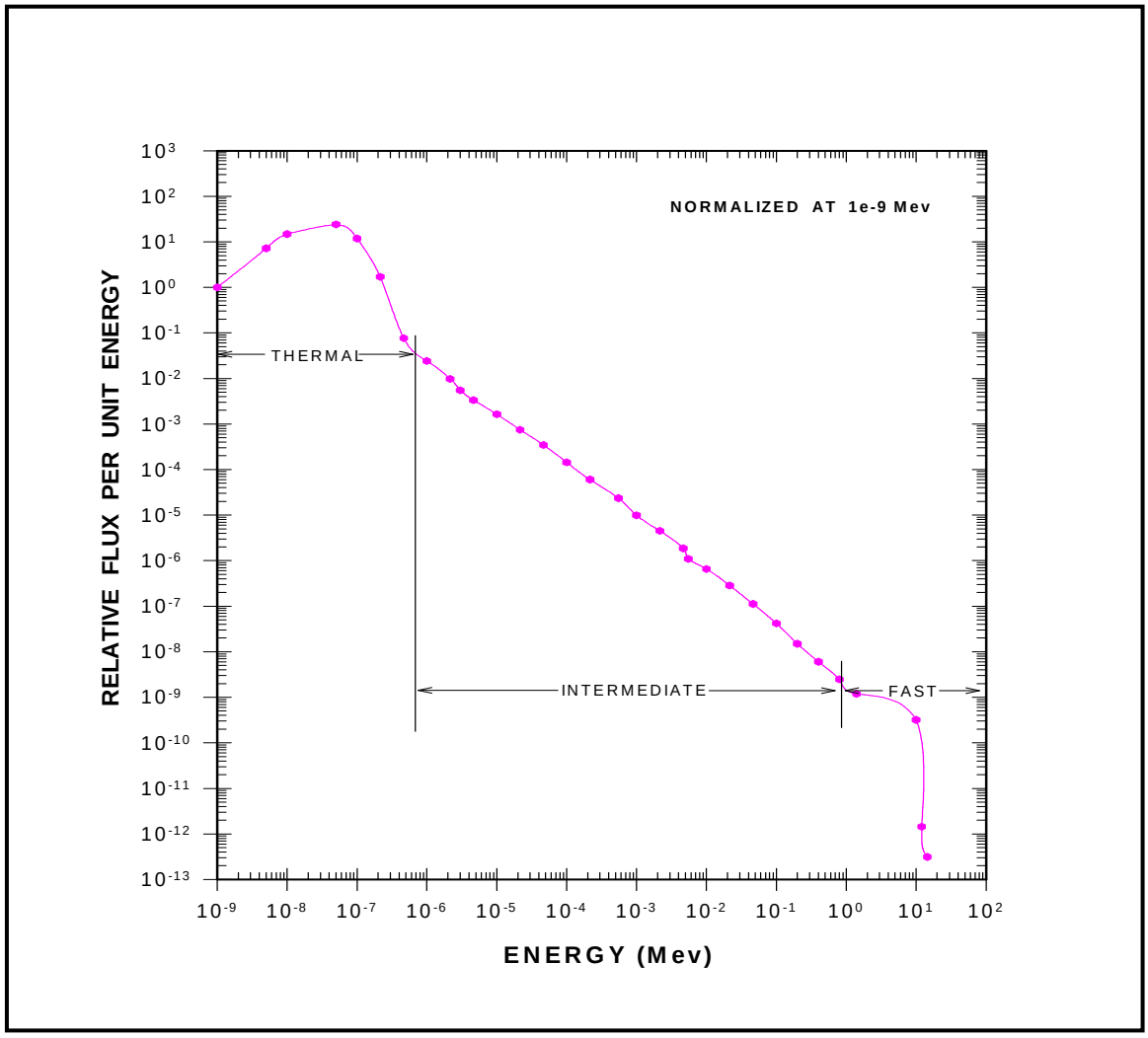


## Conclusion

The obtained computational data showed that when all the emergency rods are fully inserted in the core, or when all the emergency channels are filled by light water, the negative imposed reactivity is more than the clean core excess reactivity (5% ΔK/K) plus 1%. Therefore, the emergency system satisfies the nuclear safety regulations.

### References

[1] J. S. Hendricks, G.W. McKinney, M.L. Fensin, M. R. James, R.C. Johns, J. W. Durkee, J. P. Finch, D. B. Pelowitz, L. S. Waters, M. W. Johnson" MCNPX 2.6.0 Extensions' Los Alamos National Laboratory, LA-UR-08-2216, APRIL 11 (2008).

[2] J. Willy and S.Inc, "Experimental Reactor Physics ",(1976).

# Prof. Dr. Robert Troć
(1935 – 2019)

Robert Troć, professor emeritus at the Trzebiatowski Institute of Low Temperature and Structure Research (ILT&SR) of the Polish Academy of Sciences in Wrocław, passed away on March 15, 2019 at the age of almost 84. Robert was an outstanding scientist, a world-renowned expert in the field of physics and chemistry of 5*f*-electron materials, especially uranium-bearing systems. He was a pioneer in Poland of experimental research carried out down to liquid helium temperatures in strong magnetic fields. He discovered numerous chemical compounds based on uranium and deeply characterized their low-temperature magnetic and electrical transport properties.


Robert decorated with JdA medal
(Karpacz, March 27, 2017)

Robert Troć obtained his doctoral degree in chemistry in 1966 for his study on magnetism in uranium pnictides and chalcogenides, supervised by Prof. Włodzimierz Trzebiatowski. In 1974, he accomplished his habilitation, and in 1983, he received his scientific title of professor of chemistry. In years 1972-2005, Robert headed Magnetic Research Department at ILT&SR. Between 1976 and 1983, he was the chair of doctoral school at ILT&SR. For many years, he served as an elected member of the Scientific Council of ILT&SR. He was a member of the Polish Chemical Society and the Polish Physical Society.

For over 50 years, Robert continued his investigations on magnetic and related properties of actinide compounds using self-build and commercial equipment. In his research he exploited also neutron diffraction and inelastic neutron scattering techniques. His scientific interests focused at Kondo and heavy-fermion systems, non-collinear and frustrated magnetism, magnetic fluctuations, metamagnetic transitions, crystal field effects, and rattling in cage-type compounds. In recent years, his favorite concept was dual behavior of 5*f* electrons, that he applied for example to describing coexistence of local ferromagnetism and superconductivity in pressurized $UGe_2$. Often, Robert explored scenarios of mixed valence and/or spin-glass freezing to clarify complex properties of various uranium compounds.

Robert was a declared advocate of broad international cooperation. Himself he conducted his research at a few foreign laboratories (e.g., Argonne National Laboratory, Centre d'Études Nucléaires in Grenoble, University of Rennes), and many others visited. He co-organized several important conferences, including Intern. Conf. on the Electronic Structure of Actinides (Wrocław, 1976), Intern. Conf. on Magnetism (Warsaw, 1994), 50$^{th}$ Anniversary of the First 5*f*-Electron Ferromagnet Discovery (Wrocław, 2002). In 1996, he chaired 26$^{èmes}$ Journées des Actinides in Szklarska Poręba.

Robert was a tireless mentor of young scientists, supervisor and teacher of three generations of physicists and chemists. He promoted 5 doctors, two of whom became full professors. He was also a lauder for two honorary professors of ILT&SR: Gerry Lander (2002) and Bernard Coqblin (2009).

Robert co-authored over 300 papers in peer-reviewed scientific journals (i.a., 29 in Physical Review B), which were cited until now over 2300 times by other authors. In addition to original articles, Robert co-authored several review articles and book chapters (e.g., in Handbook on the Physics and Chemistry of the Actinides, eds. G.H. Lander and A.J. Freeman). His remarkable achievement was compilation of as many as 6 volumes of the Landolt-Börnstein encyclopedia on magnetic and related properties of actinide elements and actinide oxides, pnictides and chalcogenides. In 1994, Robert served as a guest editor of the proceedings of the Intern. Conf. on Magnetism, published in Journal of Magnetism and Magnetic Materials.

For his outstanding scientific accomplishments, Robert was decorated with Knight's Cross of the Order of Polonia Restituta and with Silver Cross of Merit, both granted by the Polish Council of State, and then honored with Officer's Cross of the Order of Polonia Restituta, conferred by the President of Poland. In recognition of his enormous scientific activity, he also received several awards from authorities of the Polish Academy of Sciences. In 2017, Robert was awarded by the Journées des Actinides community with life-time research award.

We have lost an eminent scientist, collaborator and mentor, a good man and close friend to many of us. For years, Robert will remain in our memories.

*Compiled by Dariusz Kaczorowski and Małgorzata Samsel-Czekała*

# LIST OF PARTICIPANTS

| | | | |
|---|---|---|---|
| Amadon | Bernard | CEA, DAM, DIF | France |
| Amidani | Lucia | ROBL - HZDR | France |
| Amitsuka | Hiroshi | Graduate School of Science, Hokkaido University | Japan |
| Andreev | Alexander | Institute of Physics, Czech Academy of Sciences | Czech Republic |
| Bagus | Paul S. | University of North Texas | United States |
| Belyaev | Dmitry | Russian Federal Nuclear Center- Zababakhin All-Russia Research Institute of Technical Physics | Russian Federation |
| Ben David | Roey | Israel Atomic Energy Commission (IAEC) | Israel |
| Bonato | Laura | ICSM Marcoule | France |
| Braithwaite | Daniel | Univ. Grenoble Alpes and CEA | France |
| Buturlim | Volodymyr | Charles University | Czech Republic |
| Caciuffo | Roberto | European Commission, Joint Research Centre | Germany |
| Castellano | Aloïs | CEA | France |
| Chaney | Daniel | University of Bristol | United Kingdom |
| Chen | Ning | College of Chemistry, Chemical Engineering and Material Sciences, Soochow University | China |
| Colineau | Eric | European Commission, Joint Research Centre | Germany |
| Corradetti | Stefano | INFN-LNL | Italy |
| Dopita | Milan | Charles University | Czech Republic |
| Dorado | Boris | CEA | France |
| Dumas | Thomas | CEA | France |
| Farnaby | Joy | University of Glasgow | United Kingdom |
| Fryars | Stéphanie | Université de Rennes 1 | France |
| Gatti | Flavio | INFN (Istituto Nazionale Fisica Nucleare) | Italy |
| Giovannini | Mauro | INFN (Istituto Nazionale Fisica Nucleare) | Italy |
| Gnida | Daniel | Institute of Low Temperature and Structure Research, Polish Academy of Sciences | Poland |
| Gouder | Thomas | European Commission, Joint Research Centre | Germany |
| Griveau | Jean-Christophe | European Commission, Joint Research Centre | Germany |
| Halevy | Itzhak | NRCN | Israel |
| Havela | Ladislav | Charles University | Czech Republic |
| Hibert | Nicolas | CEA Marcoule | France |
| Holdsworth | Alistair | University of Manchester | United Kingdom |
| Horák | Lukáš | Faculty of Mathematics and Physics, Charles University | Czech Republic |
| Huang | He | China Academy of Engineering Physics | China |
| Im | Hansol | Doosan Heavy Industries & Construction | South Korea |
| Izosimov | Igor | Joint Institute for Nuclear Research | Russian Federation |
| Joly | Florian | Université de Lille | France |
| Kaczorowski | Dariusz | Institute of Low Temperature and Structure Research, Polish Academy of Sciences | Poland |
| Karavaev | Alexey | Russian Federal Nuclear Center Zababakhin Institute of Technical Physics (RFNC-VNIITF) | Russian Federation |
| Kim-Ngan | Hoa Nhu-Tarnawska | Institute of Physics, Pedagogical University | Poland |

| | | | |
|---|---|---|---|
| Kloditz | Roger | Helmholtz-Zentrum Dresden-Rossendorf | Germany |
| Köhler | Luisa | Helmholtz-Zentrum Dresden-Rossendorf | Germany |
| Kolorenc | Jindrich | Institute of Physics, Czech Academy of Sciences | Czech Republic |
| Koloskova | Oleksandra | Charles University | Czech Republic |
| Kon | Fusako | Graduate School of Science, Hokkaido University | Japan |
| Lander | Gerard | ILL, Grenoble | France |
| Lawrence Bright | Eleanor | University of Bristol | United Kingdom |
| Leblanc | Martin | CEA | France |
| Legut | Dominik | VSB - Technical University of Ostrava | Czech Republic |
| Lin | Jian | Shanghai Institute of Applied Physics, Chinese Academy of Sciences | China |
| Lu | Haiyan | Institute of Materials, China Academy of Engineering Physics | China |
| Luo | Lizhu | Institute of Materials, China Academy of Engineering Physics | China |
| März | Juliane | Helmholtz-Zentrum Dresden-Rossendorf | Germany |
| Maiwald | Martin | Heidelberg University Institute of Physical-Chemistry | Germany |
| Makarov | Artem | Joint-stock Company State scientific center Research Institute of Atomic Reactors | Russian Federation |
| Martel | Laura | European Commission, Joint Research Centre | Germany |
| Mašková | Silvie | Charles University | Czech Republic |
| Mineev | Vladimir | CEA | France |
| Morales-Martínez | Roser | Universitat Rovira i Virgili | Spain |
| Murphy | Gabriel | Institute of Energy and Climate Research (IEK-6), Forschungszentrum Jülich GmbH | Germany |
| Oher | Hanna | CEA-Saclay | France |
| O'Sullivan | Sarah | University of Sheffield | United Kingdom |
| Paolasini | Luigi | ESRF | France |
| Park | Kwang soo | Doosan Heavy Industries & Construction | South Korea |
| Pasturel | Mathieu | Institut des Sciences Chimiques de Rennes | France |
| Pereira Gonçalves | Antonio | Instituto Superior Técnico | Portugal |
| Pikul | Adam | Institute of Low Temperature and Structure Research, Polish Academy of Sciences | Poland |
| Pourcelot | Laurent | IRSN | France |
| Re | Elisa | Institut de Chimie Séparative de Marcoule | France |
| Sala | Chris | Technische Universität Dresden | Germany |
| Schmidt | Moritz | Helmholtz-Zentrum Dresden-Rossendorf | Germany |
| Schöne | Sebastian | Helmholtz-Zentrum Dresden-Rossendorf | Germany |
| Sechovsky | Stepan | Charles University | Czech Republic |
| Shamoradifar | Hadi | Payam-e Noor university | Iran |
| Shestakov | Alexander | Russian Federal Nuclear Center, Zababakhin All-Russian Research Institute of Technical Physics | Russian Federation |
| Shick | Alexander | Institute of Physics CAS, Prague | Czech Republic |
| Soldi | Luca | CEA Saclay | France |
| Svanidze | Eteri | MPI CPfS | Germany |
| Tabata | Chihiro | Kyoto University | Japan |
| Tereshina-Chitrova | Evgenia | Charles University in Prague | Czech Republic |
| Tcepilov | Aleksandr | RFNC-VNIITF | Russian Federation |

| | | | |
|---|---|---|---|
| Tougait | Olivier | Université de Lille | France |
| Virot | François | IRSN | France |
| Virot | Matthieu | ICSM Marcoule | France |
| Vitova | Tonya | Karlsruhe Institute of Technology (KIT), Institute for Nuclear Waste Disposal (INE) | Germany |
| Walker | Helen | ISIS Neutron and Muon Source | United Kingdom |
| Walter | Olaf | European Commission, Joint Research Centre | Germany |
| Wąsik | Jacek | University of Bristol | United Kingdom |
| Wilhelm | Fabrice | ESRF | France |
| Yu | Huilong | Institute of Materials China Academy of Engineering Physics | China |
| Zegke | Markus | University of Cologne | Germany |
| Zeng | Rongguang | Institute of Materials, China Academy of Engineering Physics | China |
| Zhang | Yanzhi | Institute of Materials, China Academy of Engineering Physics | China |
| Zhao | Yawen | Institute of Materials, China Academy of Engineering Physics | China |

# LIST OF AUTHORS